5-2019

Hydrodeoxygenation of Pinyon-Juniper Catalytic Pyrolysis Oil

Hossein Jahromi
Utah State University

HYDRODEOXYGENATION OF PINYON-JUNIPER CATALYTIC PYROLYSIS OIL

by

Hossein Jahromi

A dissertation submitted in partial fulfillment
of the requirements for the degree

of

DOCTOR OF PHILOSOPHY

in

Biological Engineering

Approved:

_____	_____
Foster A. Agblevor, Ph.D. Major Professor	Ronald C. Sims, Ph.D. Committee Member
_____	_____
Jixun Zhan, Ph.D. Committee Member	Anhong Zhou, Ph.D. Committee Member
_____	_____
Tianbiao Liu, Ph.D. Committee Member	Laurens H. Smith, Ph.D. Interim Vice President for Research and Dean of the School of Graduate Studies

UTAH STATE UNIVERSITY
Logan, Utah

2018

ABSTRACT

Hydrodeoxygenation of Pinyon-Juniper Catalytic Pyrolysis Oil

by

Hossein Jahromi, Doctor of Philosophy

Utah State University, 2018

Major Professor: Dr. Foster Agblevor
Department: Biological Engineering

Catalytic hydrodeoxygenation (HDO) of pyrolysis oil (bio-oil) is one of the most effective technologies to improve physico-chemical properties of bio-oil such as high acidity, poor stability, and low energy density. However, development of HDO catalysts has been a challenging task during past decades. Red mud (RM) which is an alkaline waste from alumina industry, was used to prepare a new multifunctional RM-supported nickel catalyst (Ni/RM) for the HDO of pinyon-juniper (PJ) catalytic pyrolysis oil. The Ni/RM catalyst was characterized by inductively coupled plasma atomic emission spectrometry (ICP-AES), X-ray diffraction analysis (XRD), scanning electron microscopy (SEM), BET specific surface area, and temperature programmed reduction (TPR). The catalytic activity of Ni/RM was compared with that of commercial Ni/SiO_2-Al_2O_3 in three major HDO processes; HDO of the organic phase pyrolysis oil, HDO of the aqueous phase pyrolysis oil, and HDO of bio-oil model compounds.

HDO of the organic fraction of PJ bio-oil using Ni/RM produced more liquid (HDO oil), less gas, and less coke as compared to the commercial catalyst. Also less hydrogen was consumed in the case of Ni/RM. HDO of the aqueous phase pyrolysis oil

using Ni/RM produced liquid hydrocarbons, whereas the commercial catalyst gasified the organics compound in the aqueous phase pyrolysis oil and did not produce liquid hydrocarbon. HDO studies of bio-oil model compounds showed that the formation of hydrocarbons using Ni/RM was due to the cross-reactions of HDO intermediates (such as anisole, furans, aldehydes, and ketones) on the RM support. RM (in reduced form) catalyzed ketonization and carbonyl alkylation reactions. Furthermore, the selectivity to BTX using Ni/RM was higher than the commercial catalyst after HDO of guaiacol model compound.

Coke formation, oxidation, and formation of nickel iron oxide contributed to the deactivation of Ni/RM during HDO process. After complete deactivation, the catalytic activity of Ni/RM was entirely restored by burning off the coke and activation by reduction using a reducing gas mixture of 10% H_2 and 90% N_2, however, the regeneration of the commercial Ni/SiO_2-Al_2O_3 was not possible following the same procedure and the catalyst did not show HDO activity after regeneration/reduction.

(288 pages)

PUBLIC ABSTRACT

Hydrodeoxygenation of Pinyon-Juniper Catalytic Pyrolysis Oil

Hossein Jahromi

Catalytic hydrodeoxygenation (HDO), is an effective process to convert oxygenated compounds to hydrocarbons. This process is widely used for improving the negative properties of biomass-derived pyrolysis oils (bio-oils) such as high acidity, poor stability, and low heating value. During this process oxygen is removed from the bio-oil in the form of water, thus the liquid product of HDO process consists of aqueous phase and hydrocarbon phase that can be easily separated. Synthesis of efficient HDO catalyst has been a major challenge in the field of bio-oil upgrading. Red mud, which is an alkaline waste from alumina industry was used to develop a new red mud-supported nickel catalyst (Ni/RM) for the HDO of pinyon-juniper catalytic pyrolysis oil. The new catalyst was more effective than the commercial Ni/silica-alumina catalyst for the HDO of organic phase pyrolysis oil, the aqueous phase pyrolysis oil, and bio-oil model compounds. Less hydrogen was consumed in the case of Ni/RM and more liquid hydrocarbon yield was obtained compared to the commercial catalyst. In addition to HDO reactions, the Ni/RM catalyst catalyzed ketonization and carbonyl alkylation reactions that was important to produce liquid hydrocarbon from low molecular weight oxygenated compounds. Unlike the commercial catalyst, Ni/RM was regenerable by burning off the deposited coke and activation by reduction using hydrogen.

ACKNOWLEDGMENTS

I would like to thank my major professor, Dr. Foster Agblevor for his support, guidance, mentoring throughout the years, giving me the opportunity to pursue my graduate studies at Utah State University, and his patience as I worked my way from the initial proposal writing to this final document. I could not have done it without him. My heartfelt gratitude to Dr. Ronald Sims, Dr. Jixun Zhan, Dr. Anhong Zhou, and Dr. Tianbiao Liu for serving on my committee. I am grateful to Dr. Charles Miller and Dr. Jagath Kaluarachchi for their assistance, support, and advice during difficult times.

Particular thanks to my previous colleagues; Dr. Oleksandr Hietsoi, Dr. Sedat Beis, Kyle Christian, Brandon Sargent, and Garrett Smith; I appreciate your diverse roles with regards to my work. I gratefully acknowledge Dr. Fen-Ann Shen at the Microscopy Core Facility at Utah State University for her assistants in SEM imaging of my samples.

To my loving mom and dad (Fatemeh and Ali) and my wonderful brother (Reza), thank you for all your sacrifices. It was impossible to complete this chapter of life without your encouragements, supports, and patience.

To Nafzigers: Alanna, Seth, Gaia, Mark & Cleo; you have been my first friends and my best people in the United States and you always will be, thanks for all your cares. Last but not least, I would like to thank my friends, Clint Rickson, Martin Schroeder, Nicolas Clark, Brandon Handy, Cristian Ballack, Jordan Ogata, and Angela Akude for their love, care, and all the wonderful time we had together during my graduate studies.

Hossein Jahromi

CONTENTS

Page

LIST OF TABLES

LIST OF FIGURES

CHAPTER 1

1. INTRODUCTION

1. Format of dissertation

Chapter 1 of this dissertation is an introduction to the research, covering concepts of pyrolysis, hydrodeoxygenation (HDO), and catalyst development. Chapter 2 contains a general literature review covering catalytic conversion of lignocellulosic biomass into hydrocarbons, bio-oil upgrading techniques, HDO studies, and catalytic applications of red mud. Chapter 3 is an article published in the journal *Energy* [1] on HDO of pinyon-juniper (PJ) catalytic pyrolysis oil including parametric studies. Chapter 4 is an article published in journal *Applied Catalysis A: General* [2]. It covers the performance of a new red mud-supported nickel (Ni/RM) catalyst versus commercial Ni/SiO_2-Al_2O_3 for HDO of guaiacol model compound. Chapter 5 is an article published in journal *Applied Catalysis B: Environmental* [3] demonstrating the use of Ni/RM catalyst for upgrading of PJ pyrolysis oil via hydrodeoxygenation. Chapter 6 includes two manuscripts published in peer reviewed journals. This chapter covers synthesis of liquid hydrocarbons from low molecular weight oxygenates categorized under furfural-based compounds [4], and guaiacol-based compounds [5]. Chapter 7 is a manuscript published in journal *Industrial & Engineering Chemistry Research* [6]. It covers the application of Ni/RM catalyst for HDO of aqueous phase PJ pyrolysis oil to produce liquid hydrocarbons. Chapter 8 is a summary of this dissertation. The appendices include supplementary data, copyright permissions, and the author's curriculum vitae.

2. Overview

Considerable attention has been focused on the development of alternative fuels since the shortage of petroleum resources began with the global energy crisis in the 1970s and the potential global climate change reported. Pyrolysis is effective potential technology for conversion of biomass into liquid fuels. Compared to competing technologies such as fermentation and gasification, pyrolysis has low capital and operating cost advantages [7-9]. In addition, conventional fast pyrolysis oil (bio-oil) has environmental advantages when compared to fossil fuels because, when combusted, bio-oil produces less pollution than fossil fuels, specifically, negligible quantities of NO_x and SO_x emission, and it is considered to be CO_2 neutral [10]. Unlike fossil fuel, biomass takes carbon out of the atmosphere while it is growing, and returns it when it is burnt. This results in a close carbon cycle with no net increase in atmospheric CO_2 levels.

Bio-oils have some negative properties such as high acidity, low energy density, poor stability, and immiscibility with petroleum products. These properties limit the application of bio-oils as direct transportation fuels [11-14]. Oxygenated compounds including, aldehydes, ketones, and carboxylic acids are responsible for the negative characteristics of pyrolysis oils [15-17], thus, removal of oxygen is necessary to improve the fuel properties of bio-oils.

Hydrodeoxygenation (HDO) is a catalytic process of removing oxygenated compounds from a molecule usually in the form of water. Traditional HDO catalysts such as supported Co, Ni, Mo and supported noble metal catalysts (e.g. Pt, Ru, and Pd) have been widely studied for upgrading of bio-oils via HDO process. Catalyst deactivation,

especially due to coke deposition has always been a major problem [18, 19], hence, development of a robust HDO catalyst is a challenging task.

3. Research objectives

Yathavan and Agblevor successfully demonstrated that catalytic pyrolysis of pinyon-juniper (PJ) can be used to produce liquid products [20], the fuel properties of the oil were better than conventional bio-oils. The aqueous phase PJ catalytic pyrolysis oil contained about 15% organic compounds, but were less acidic than conventional bio-oils. The water-soluble organics can potentially cause corrosion of processing equipment, require wastewater treatment, and a potential source of carbon loss for the biomass conversion processes. The primary goal of this research is to produce liquid hydrocarbons via HDO of the liquid products of PJ catalytic pyrolysis. To this end, the following specific objectives were addressed:

- HDO of PJ catalytic pyrolysis oil to liquid hydrocarbons using commercial Ni/SiO_2-Al_2O3 catalyst.
- Development of a new Ni/RM HDO catalyst.
- HDO of PJ catalytic pyrolysis oil to liquid hydrocarbons using Ni/RM.
- HDO of Aqueous Phase Pinyon Juniper Catalytic Pyrolysis Oil (APPJCPO) to liquid hydrocarbons using Ni/RM catalyst.
- Synthesis of liquid hydrocarbons from low molecular weight oxygenated compounds that are found in aqueous phase pyrolysis oils.
- Understanding the reaction pathways and cross-interactions of bio-oil model compounds during HDO process using Ni/RM.
- Understanding the deactivation mechanisms of Ni/RM during HDO.

4. Engineering significance

Hydrodeoxygenation of bio-oil is one of the most effective methods to improve the quality of bio-oil including energy content, viscosity, stability, acidity, and H/C ratio. However, high amounts of hydrogen consumption is a major inevitable challenge that increases the cost of operation. Therefore, one potential way of reducing the cost of HDO is sustainable development of cheaper catalysts for this process. A practical catalyst for HDO should improve hydrogenation and deoxygenation versus (hydro)cracking and coke formation. Moreover, regenerability, lifetime, and stability of the catalyst are essential to make the catalyst competitive with commercial catalysts.

Ni/SiO_2-Al_2O_3 is a commercial HDO catalyst that is available on the market at 65% Ni supported on Silica-Alumina. Unlike traditional HDO (CoMo/Al_2O_3 and NiMo/Al_2O_3) catalysts, this catalyst does not require any pre-treatment such as sulfidation and it can be used as received. Also this catalyst is much cheaper than typical noble metal catalysts that are widely used for HDO reactions. However, high amounts of gas yield from HDO processes and catalyst regenerability, are severe issues that, to some extents, make the application of Ni/SiO_2-Al_2O_3 more challenging.

Red mud, which is a waste from alumina industry was used as support material for preparation of a new HDO nickel catalyst (Ni/RM). HDO experiments were carried out at three levels; HDO of the organic phase pyrolysis oil, HDO of the aqueous phase pyrolysis oil, and HDO of bio-oil model compounds. Development of Ni/RM catalyst addressed several major problems of the commercial Ni/SiO_2-Al_2O_3. In general, less hydrogen consumption, less coke formation, and less gasification of hydrocarbons

compared to the commercial catalyst was achieved using Ni/RM. The new catalyst was more active for deoxygenation than hydrogenation reactions. Furthermore, production of liquid hydrocarbons from low molecular weight oxygenates was achieved using Ni/RM while the commercial catalyst gasified those compounds. In addition to HDO reactions, Ni/RM catalyzed carbonyl alkylation and ketonization reactions, which play critical roles in the production of liquid hydrocarbon via HDO of aqueous phase pyrolysis oil. Finally, in contrast to the commercial catalyst, Ni/RM was regenerable by burning off the coke and activation by reduction in hydrogen.

5. References

[1] Jahromi H, Agblevor FA. Upgrading of pinyon-juniper catalytic pyrolysis oil via hydrodeoxygenation. Energy 2017;141:2186–95.

[2] Jahromi H, Agblevor FA. Hydrotreating of guaiacol: A comparative study of Red mud-supported nickel and commercial Ni/SiO2-Al2O3catalysts. Appl Catal A Gen 2018;558:109–21.

[3] Jahromi H, Agblevor FA. Hydrodeoxygenation of pinyon-juniper catalytic pyrolysis oil using red mud-supported nickel catalysts. Applied Catal B, Environ 2018;236:1–12.

[4] Agblevor FA, Jahromi H. Aqueous phase synthesis of hydrocarbons from furfural reactions with low molecular weight biomass oxygenates. Energy & Fuels 2018:32:8552-8562.

[5] Agblevor FA, Jahromi H. Aqueous phase synthesis of hydrocarbons from reactions of guaiacol and low molecular weight oxygenates. ChemCatChem 2018. ChemCatChem 10.1002/cctc.201800982

[6] Jahromi H, Agblevor FA. Hydrodeoxygenation of aqueous-phase catalytic pyrolysis oil to liquid hydrocarbons using multifunctional nickel catalyst. Industrial & Engineering chemistry Research 2018: 57: 13257-13268.

[7] Lin Y-C, Huber GW. The critical role of heterogeneous catalysis in lignocellulosic biomass conversion. Energy Environ Sci 2009;2:68–80.

[8] Anex RP, Aden A, Kazi FK, Fortman J, Swanson RM, Wright MM, et al. Techno-economic comparison of biomass-to-transportation fuels via pyrolysis, gasification, and biochemical pathways. Fuel 2010;89:S29–35.

[9] Bridgwater A V. Review of fast pyrolysis of biomass and product upgrading. Biomass and Bioenergy 2012;38:68–94.

[10] Tanneru SK, Steele PH. Pretreating bio-oil to increase yield and reduce char during hydrodeoxygenation to produce hydrocarbons. Fuel 2014;133:326–31.

[11] Cheng S, Wei L, Alsowij MR, Corbin F, Julson J, Boakye E, Raynie D. In situ hydrodeoxygenation upgrading of pine sawdust bio-oil to hydrocarbon biofuel using Pd/C catalyst. J Energy Inst 2018;91:163–71.

[12] Ahmadi S, Reyhanitash E, Yuan Z, Rohani S, Xu C. Upgrading of fast pyrolysis oil via catalytic hydrodeoxygenation: Effects of type of solvents. Renew Energy 2017;114:376–82.

[13] Guo C, Rao KTV, Yuan Z, He S, Rohani S, Xu C. Hydrodeoxygenation of fast pyrolysis oil with novel activated carbon-supported NiP and CoP catalysts. Chem Eng Sci 2018;178:248–59.

[14] Arun N, Sharma R V., Dalai AK. Green diesel synthesis by hydrodeoxygenation of bio-based feedstocks: Strategies for catalyst design and development. Renew Sustain Energy Rev 2015;48:240–55.

[15] Cheng T, Han Y, Zhang Y, Xu C. Molecular composition of oxygenated compounds in fast pyrolysis bio-oil and its supercritical fluid extracts. Fuel 2016;172:49–57.

[16] Chen W, Luo Z, Yu C, Li G, Yang Y, Zhang H. Upgrading of bio-oil in supercritical ethanol: Catalysts screening, solvent recovery and catalyst stability study. J Supercrit Fluids 2014;95:387–93.

[17] Cheng S, Wei L, Julson J, Muthukumarappan K, Kharel PR, Cao Y, et al. Hydrodeoxygenation upgrading of pine sawdust bio-oil using zinc metal with zero valency. J Taiwan Inst Chem Eng 2017;74:146–53.

[18] Kay Lup AN, Abnisa F, Wan Daud WMA, Aroua MK. A review on reactivity and stability of heterogeneous metal catalysts for deoxygenation of bio-oil model compounds. J Ind Eng Chem 2017;56:1–34.

[19] Pourzolfaghar H, Abnisa F, Wan Duad WMA, W, Aroua MK. Atmospheric hydrodeoxygenation of bio-oil oxygenated model compounds: A review. J Anal Appl Pyrolysis 2018;133:117–27.

[20] Yathavan BK, Agblevor FA. Catalytic pyrolysis of pinyon-juniper using red mud and HZSM-5. Energy and Fuels 2013;27:6858–65.

CHAPTER 2

2. ABBREVIATED LITERATURE SURVEY

This chapter is a brief literature survey that covers basic concepts and general information on lignocellulosic biomass, pyrolysis, upgrading techniques, and hydrodeoxygenation catalysts. As this dissertation is multiple-papers style, more in-depth literature review is provided in next chapters.

1. Conversion of lignocellulosic biomass components into hydrocarbons

1.1. Cellulose

Cellulose is a glucan formed by polymerization of glucose monomer through highly stable β-1,4-glycosidic bonds, accompanied with strong inter-molecular hydrogen bonds. Cellulose accounts for more than 40 wt. %, as the dominant component of lignocellulosic biomass [1,2]. In order to produce alkanes, cellulose must be depolymerized and deoxygenated. Cellulose can also be converted to value-added chemicals through dehydration, hydrogenation, and hydrogenolysis over different catalysts [3,4]. Because of the process complication and high cost of multistep processes, conversion of cellulose to liquid fuels is difficult to accomplish. A few representative studies for the production of sustainable hydrocarbons from cellulose were reported [5–7].

1.2.Hemicellulose

Hemicellulose is one of the most abundant polysaccharides, which is mainly composed of pentoses. Hemicellulose, accounts for 15-30 wt. % of the lignocellulosic biomass, can be used as a cheap and large amount of available feed material for the high value-added chemicals and alkanes production [8–10]. The C_5 sugars (mostly xylose) derived from hemicellulose have a great potential in the production of several platform chemicals such as levulinic acid. Recently were numerous researches focused on the catalytic transformation of hemicellulose, starting from the hydrolysis to pentose, followed by dehydration to furfural or hydrogenation to xylitol [11,12], meanwhile the production of pentane from furfural has also been reported [13] which is a new and sustainable path for the efficient use of raw biomass.

1.3. Lignin

Lignins are phenol-based biopolymers with a fraction of 10-25 wt. % in lignocellulosic biomass and have a high energy density compared to cellulose and hemicellulose [14]. These complex polymers form key structural materials in the support tissues of vascular plants. Lignins are mainly important in the formation of cell walls, especially in wood and bark, because they provide stiffness. The decomposed building blocks of lignin are a mixture of phenolic compounds, such as phenol, guaiacol, syringol and derivatives, which are not suitable for fuel applications. Previous studies on the HDO reaction of lignin were mainly concentrated on the conversion of lignin derivatives, such as phenol, guaiacol and syringol to cycloalkanes or aromatics [14,15]. Important model compound studies have been carried out for establishing proper conditions to efficiently convert lignin to hydrocarbons. Additionally, one crucial step for the selective breaking

of the C-O bonds in aryl ethers of phenolic dimers has attracted wide spread attention, because it could offer a deeper understanding for the decomposition of lignin [16–18]. Considering different problems such as complex steps and costly production of liquid hydrocarbons from the raw lignin, more attractive transformation pathways for direct conversion of lignin into desired products should receive more attention.

2. Bio-oil characteristics and common upgrading techniques

Pyrolysis oil (bio-oil) can be produced from fast pyrolysis of biomass with yields up to 75 wt. % [19]. The structure of three major polymeric components, cellulose, hemicellulose, and lignin, are well-represented by the bio-oil components in the case of lignocellulosic biomass-derived pyrolysis oil. Bio-oil is a complicated mixture comprising more than 300 organic compounds including phenolics (phenol, catechol, anisole, syringol, guaiacol, etc.), oxygenates (alcohols, acids, esters, aldehydes and ketones), hydrocarbons (aromatics, alkene), furans, sugars, high molecular species (lignin derived oligomers, lignin, hemicellulose and cellulose) and water [20,21].

Oxygen is the most challenging element, as bio-oils contain 10–40% oxygen. This influences the heating value, acidity, viscosity, polarity, and homogeneity of the bio-oil. The high water and oxygen contents contribute to the high polarity and therefore poor immiscibility of bio-oil with crude petroleum oil. Furthermore, the high oxygen content contributes to the low energy density of the fuel. Carboxylic acids are known as the main reasons for low pH of bio-oils that cause harsh conditions for equipment used for processing, transportation, and storage [22,23]. Therefore, upgrading the bio oil is essential to improve its properties for practical application as liquid fuel. Bio-oil upgrading techniques are briefly described in this section.

2.1. Hydrotreating

Hydrodeoxygenation (HDO) and hydro-cracking are two main processes that can be categorized under hydrotreating. Hydrotreating, which is a petroleum refinery term, for the nondestructive or simple hydrogenation process that is used for improving product quality without appreciable alteration of the boiling range. Hydrogenation has become the most common process in modern petroleum refineries. The catalysts commonly used for hydrotreating are sulfided $CoMo/Al_2O_3$ and $NiMo/Al_2O_3$ [24].

Hydro-cracking is less popular than hydrotreating because it requires more severe conditions such as higher temperature and hydrogen pressure, which is not economical and energy efficient. This process is performed by dual-function catalysts, in which silica–alumina (or zeolite) catalysts provide the cracking function, and platinum and tungsten oxide catalyze the reactions, or nickel provides the hydrogenation function. Hydro-cracking is an effective way to make a large amount of light product [25]. The wide range of products possible from hydro-cracking is the results of combining catalytic cracking reactions with hydrogenation and the variety of reactions that can occur.

2.2. Supercritical fluids (SCFs)

Supercritical fluids (SCFs) possess unique transport properties. They can effuse through solids like a gas and dissolve materials like a liquid. SFCs have the ability to dissolve materials not normally soluble in either liquid or gaseous phases of the solvent, thus to promote the gasification/liquefaction reactions. Water is the cheapest and most commonly used SCF in hydrothermal processing, however, application of water as the solvent has some drawbacks such as decreased yield of the water-insoluble oil products

and high viscosity of the bio-oil. To enhance the oil yields and qualities, the application of organic solvents (e.g. ethanol, butanol, acetone, n-hexanol, and 1,4-dioxane) has been investigated [26–28]. Although SCFs can be produced at relatively lower temperature and the process is environmentally friendly, some of these organic solvents are too expensive to make it economically feasible on a large scale.

2.3. Solvent addition/ Esterification

Polar solvents (e.g. methanol, ethanol, and furfural) have been used to homogenize, reduce the viscosity, and increase the heating value of bio-oils. The increase in heating value for bio-oils mixed with solvents occurs because the solvent has a higher heating value than that of most bio-oils. The solvent addition reduces the oil viscosity due to physical dilution, reducing the reaction rate by molecular dilution, and chemical reactions between the solvent and the oil components that prevent further polymerization. Most studies have directly added solvents after pyrolysis to decrease the viscosity and increase stability and heating value. However, several recent studies showed that reacting the oil with alcohols (such as ethanol) and acid catalysts (such as acetic acid) resulted in a better bio-oil quality. This process is referred to as catalytic esterification or esterification treatment in the literature [29–31].

2.4. Emulsification

Pyrolysis oils are not miscible with fossil fuels, but with the aid of surfactants they can be emulsified with diesel oil. One of the methods in using bio-oil as a combustion fuel in transportation or boilers is to produce an emulsion with other fuel sources. Upgrading of bio-oil via emulsification with diesel oil has been investigated by

many researchers [20,32–35]. Those emulsions were less corrosive and showed promising ignition characteristics, however, fuel properties such as heating value, cetane number and corrosivity were still disappointing. Overall, upgrading of bio-oil via emulsification provides a short-term approach to the utilization of bio-oil in diesel engines.

2.5. Steam reforming

The term ‘‘reforming’’ was initially used to define the thermal conversion of petroleum cuts to more volatile products. Reforming also refers to the conversion of hydrocarbon gases and vaporized organic compounds to hydrogen containing gases such as syngas, which is a mixture of carbon monoxide and hydrogen. Fast pyrolysis of biomass followed by catalytic steam reforming to obtain H_2 from bio-oil was presented as an effective way to upgrade biomass pyrolysis oils. Hydrogen production from reforming bio-oil has been extensively studied by many researchers [36–38], including the reactions in a fixed bed and a fluidized bed using commercial nickel catalysts.

3. Bio-oil upgrading via hydrodeoxygenation (HDO)

Most HDO studies have been carried out using NiMo and CoMo catalysts. Furthermore, noble metal catalysts (e.g. Pt/C, Ru/C, Pd/C, and Ru/TiO_2) have also been investigated and shown to result in higher levels of hydrodeoxygenation than the traditional HDO catalysts such as sulfided CoMo [39–41]. However, noble metal catalysts are relatively more costly than common HDO catalysts. The effect of catalyst support on HDO activity and stability of catalyst has also been examined. Ni and Ru

supported on silica gel, nano-spring (NS) silica, and Al_2O_3 have been investigated for HDO of phenol [42]. Silica based Ni catalysts performed better than alumina supported catalysts. The Ni(20%)-NS was the best performing Ni catalyst in terms of deoxygenation. Among the Ru based catalysts, the Ru-NS could accomplish nearly complete phenol conversion and deoxygenation [42].

One-ring aromatic compounds are also valuable platform chemicals. An investigation of production of aromatics via HDO of model bio-oil over Ni/SBA-15 and Co/SBA-15 has shown that Ni/SBA-15 catalyst showed higher catalytic performance compared to Co/SBA-15 catalyst for the hydrodeoxygenation of anisole. Co/SBA-15 could selectively hydrogenate the C-O bond and could act as the potential hydrodeoxygenation catalyst for aromatic compounds production from the bio-oils [43]. For selective production of aromatics, heterogeneous precious and transition metal catalysts (Ru, Pt, Ni, Cu, 2Pt1Ru, NiCu) supported on mesoporous alumina and carbon have been investigated. Base metal catalysts on carbon support showed improved reactivity and production of desired compounds to a greater extent than single-metal catalysts. For base metals, the effect of alumina was more pronounced than the effect of metal type, whereas carbon support enabled the positive synergy of NiCu combinations [44]. However, stability was a major problem for application of bimetallic base metal catalysts on carbon.

With this concept, one of the major challenges is to find a catalyst with a high activity for deoxygenation reaction and at the same time obtain a sufficient lifetime, as deposition of carbonaceous species has proven to be a severe issue [22].

Table 2.1 is a summary of several HDO studies that have been carried out using different types of catalysts.

Table 2. 1: Overview of catalysts investigated for HDO of bio-oil [22].

Catalyst	Setup	Feed	Time [h]	P [bar]	T [°C]	DOD [%]	O/C	H/C	Y_{oil} [wt%]
Co–MoS_2/Al_2O_3	Batch	Bio-oil	4	200	350	81	0.8	1.3	26
Co–MoS_2/Al_2O_3	Continuous	Bio-oil	4[a]	300	370	100	0.0	1.8	33
Ni–MoS_2/Al_2O_3	Batch	Bio-oil	4	200	350	74	0.1	1.5	28
Ni–MoS_2/Al_2O_3	Continuous	Bio-oil	0.5[a]	85	400	28	–	–	84
Pd/C	Batch	Bio-oil	4	200	350	85	0.7	1.6	65
Pd/C	Continuous	Bio-oil	4[b]	140	340	64	0.1	1.5	48
Pd/ZrO_2	Batch	Guaiacol	3	80	300	–	0.1	1.3	–
$Pt/Al_2O_3/SiO_2$	Continuous	Bio-oil	0.5[a]	85	400	45	–	–	81
Pt/ZrO_2	Batch	Guaiacol	3	80	300	–	0.2	1.5	–
Rh/ZrO_2	Batch	Guaiacol	3	80	300	–	0.0	1.2	–
Ru/Al_2O_3	Batch	Bio-oil	4	200	350	78	0.4	1.2	36
Ru/C	Continuous	Bio-oil	0.2[a]	230	350–400	73	0.1	1.5	38
Ru/C	Batch	Bio-oil	4	200	350	86	0.8	1.5	53
Ru/TiO_2	Batch	Bio-oil	4	200	350	77	1.0	1.7	67

[a] Calculated as the inverse of the WHSV.
[b] Calculated as the inverse of the LHSV.

The choice of support material is also a key factor in catalyst formulation for evaluating the HDO activity of different catalysts [45]. HDO reactions have been carried out using acidic support materials such as alumina, silica, and zirconia. Support materials such as calcia and magnesia are basic materials and usage of basic supports are scarce with respect to HDO reactions. The most common and traditional support is Al_2O_3 [46]. Alumina has been shown to have excellent crushing strength, high surface area, and good metal dispersion on the surface. However, Al_2O_3 has been shown to be unsuitable support in presence of large amounts of water since it converts to boemite (AlO(OH)) [46,47]. Lauent and Delmon (1994) showed that the formation of boemite resulted in the oxidation of nickel on Ni-MoS_2/γ-Al_2O_3 catalyst. These nickel oxides were HDO-inactive and could further block other Mo or Ni sites on the catalyst [47]. Also, catalyst deactivation due to coke formation was a main problem especially with the use of alumina support.

Other materials such as SiO_2, activated carbon, TiO_2, ZrO_2, Nb_2O_5, zeolites, and various metal oxides were used in HDO reactions [48]. Activated Carbon has been

reported to be a suitable support in the HDO of bio-oil and its model compounds [49–51]. The neutral nature of carbon is advantageous, because this provides a lower tendency for carbon formation compared to Al_2O_3 [50,51]. Also SiO_2 has been shown as a potential support for HDO as it is neutral in general , thus has a relatively low affinity for coke formation [52].

ZrO_2 and CeO_2 are also known as potential support materials for HDO catalysts. ZrO_2 has some acidic character, but considerably less than Al_2O_3 [53,54]. ZrO_2 and CeO_2 are thought to have the potential to activate oxy-compounds on their surface, and therefore increase activity. Thus, they seem attractive in the preparation of new HDO catalysts [45,53–55]. Table 2.2 shows the advantages and disadvantages of popular supports for HDO catalysts.

Table 2. 2: Supports for HDO catalysts [22,56].

Support	Pros	Cons
Alumina	Excellent crushing strength High surface area Active Lewis acid sites Good metal dispersion on the surface	Coke formation on acidic sites Poor tolerance to water
Mesoporous materials (HMS, SBA-15, …)	Large pores High tolerance to water More active acid sites	Less metal dispersion than alumina
Silica	Inert character Low affinity for carbon formation	Less active than alumina
Activated carbon	Low cost Low coke tendency Weak acidity High surface area	Weak interaction with supported phase High sintering problem Micropore blocking Poor crushing strength
Zirconia, Ceria, and Titania	High metal dispersion High sulfidability Low coke formation	Expensive
Magnesium oxide	Superior resistance to coke formation	Less surface area than alumina

Overall, two features should be taken into account in the choice of catalyst support. First, the tendency for carbon (coke) formation should be low, which to some extent is associated with the acidity (which should be low). Second, it should have the ability to activate oxy-compounds to provide sufficient activity. The latter is mostly important in the case of noble metal catalysts such as Rh, Pd, and Pt. Thereby, selection of a sufficient, cheaply available catalyst support can play a critical role in HDO process, scientifically and economically.

4. Catalytic applications of red mud

Developing catalysts from waste materials is an effective means of value addition to the waste and can potentially reduce the cost of the catalytic process. Red mud has received considerable attention in this regard. Red mud or red sludge is a by-product of

processing of bauxite (the most common ore of aluminum) that is generated in the industrial production of alumina. In 1821 Geologist Pierre Berthier discovered reddish clay rock deposits in southern France. The rock was named bauxite after Les Baux, the area where it was found. More than 68 years later, in 1889, Karl Josef Bayer, an Austrian chemist, invented the Bayer process for the production of alumina from bauxite [57]. Even more than a century later, the aluminum industries still widely rely on this process for alumina production [58]. The ore is washed, ground and dissolved in sodium hydroxide under heat and pressure. The resulting products are sodium aluminate liquor, that goes for further processing and a large quantity of un-dissolved solid waste called ‘red mud’ or ‘bauxite waste’. Depending on the type/grade of ore used, the amount of red mud generated per ton of alumina produced may vary from 0.3 tons for a high-grade ore to 2.5 tons for a low-grade ore [57].

Red mud consists of compounds originally present in the parent ore and those introduced during the Bayer process. The main chemical compositions of red mud are Fe_2O_3, Al_2O_3, SiO_2, CaO, Na_2O, TiO, K_2O and MgO and a number of minor constituents like Cr, V, S, Ni, Cu, Mn, Zn etc. Table 2.3 compares the composition of red mud in various locations [59].

Table 2. 3: Comparison of red mud composition in various areas [59].

Area	Composition wt%									
	SiO_2	Al_2O_3	Fe_2O_3	TiO_2	CaO	MgO	K_2O	Na_2O	L.O.I.	V_2O_5
Seydiehir Aluminium Plant, Konya, Turkey	2.50	14.10	38.30	–	4.10	–	–	–	–	–
Etibank Seydiehir Aluminium Plant, Konya, Turkey	15.74	20.39	36.94	4.98	2.23	–	–	10.10	8.19	0.05
Hindustan Aluminium Company (HINDALCO) (Renukoot, India)	9.64	17.28	38.80	18.80	–	–	–	6.86	7.34	–
Queensland Alumina Ltd. refinery, Gladstone, Australia	17.06	25.45	34.05	4.90	3.69	1.86	0.20	2.74	–	–
Bauxite ore refinery, Guinea	5.50	26.60	48.40	–	1.20	0.90	–	–	14.60	–
Alumina-aluminio of san Ciprian, lugo, Spain	6.10	20.10	31.80	22.60	4.78	0.20	0.03	4.70	–	–
Slurry pond from the Worsley Alumina, Australia	5.00	15.00	60.00	5.00	–	–	–	16.00	–	–
Aluminium de Grèce S.A.	6.96	15.65	45.58	7.07	14.84	–	0.07	3.26	–	–
Eurallumina alumina plant, Italy	9.58	17.19	30.45	8.61	7.77	0.86	0.30	12.06	12.38	–
Aluminum de Greece	6.80	19.95	40.80	5.80	12.60	0.20	0.14	2.70	10.54	–
Shandong Aluminium Corporation, Shandong, China	19.14	6.93	12.76	3.43	46.02	1.15	1.20	2.37	5.73	–
Hindalco industries LTD. Renukoot	3.00	48.00	16.50	8.50	0.50	–	–	–	–	–
Shandong Province, China	5.81	28.72	14.17	4.09	36.04	–	–	2.70	–	–
Greece	7.79	17.04	44.34	5.12	11.64	0.57	0.07	3.17	9.77	
Seydiehir Aluminium Plant, Konya, Turkey	12.08	23.29	35.73	4.08	2.81	0.76	0.28	7.40	8.66	–
Eurallumina (Porto Vesme, Cagliari, Italy)	11.60	20.00	35.20	9.20	6.70	0.40	–	7.50	7.30	–
Alpart factory and the Alcan Ewarton red mud pond. Jamaica	4.30	18.80	45.30	6.40	3.10	–	–	1.50	–	–
Etibank Seydisehir Aluminium Plant, Turkey	14.52 ± 0.37	18.71 ± 0.59	39.70 ± 0.67	4.90 ± 0.54	4.47 ± 0.56	–	–	8.82 ± 0.96	–	–
Aluminium Pechiney, Gardanne, France	4.98	15.00	26.62	15.76	22.21	0.95	0.02	1.02	12.10	–
Ajka Aluminum Industry, Hungary	9–15	16–18	33–48	4–6	0.5–3.5	0.3–1	–	8–12	–	0.2–0.3
Hindustan Aluminum Company (HINDALCO) Renukoot, India	8.50	20.10	31.88	21.20	2.99	–	–	6.00	–	–
Seydisehir Aluminium Inc., Turkey	13.50	20.20	35.04	4.00	5.30	0.33	0.39	9.40	8.44	–
ALCOA factory, San Cibrao (Northwest of Spain)	9.00	12.00	37.00	20.00	6.00	–	–	5.00	–	–
Korea Chemical Co.	22.90	23.70	16.60	6.70	6.70	–	–	11.60	–	–
Shandong Aluminium Factory, China	21.90	7.96	6.57	–	38.84	1.60	0.41	2.32	17.42	–
Greek red mud, Greece	9.20	15.60	42.50	5.90	19.70	–	–	2.40	–	–

Red mud has been investigated as catalyst for various applications, including pyrolysis of biomass [60], hydrogenation and liquefaction [61–63], hydrodechlorination reactions [64,65], and exhaust gas clean-up [66,67]. Red Mud has also been used as catalyst in other reactions such as degradation of poly vinyl chloride containing polymer mixture into fuel oil [68,69], conversion of waste oil and waste plastic to fuel [70], heavy crude oil hydrotreating [71], ammonia decomposition in presence of sulfur compounds [72], and nitrile synthesis from aldehydes and hydroxylamine [73].

5. Motivation

A new red mud-supported nickel catalyst was prepared for upgrading of pinyon-juniper catalytic pyrolysis oil via hydrodeoxygenation. The development of the new catalyst was based on the idea that promising catalysts for this process should be

supported on oxides of Al, Si, Zr, or Ti. On one hand, metal oxides are needed for the activation of oxy-groups in the oxygen-containing compounds in bio-crude oil and red mud contains these oxides as discussed earlier. On the other hand, a transition metal in its reduced state is required to activate dihydrogen. To achieve the latter goal, Ni was involved in catalyst preparation. It be recognized that the catalyst is likely to deactivate due to the coke formation; therefore the reaction temperature should not exceed 350–400 °C and the hydrogen pressure should be as high as 5.0–10.0 MPa. In addition, the oxides of other trace metals in red mud may undergo reduction and catalyze HDO reactions. In view of strong stability, sintering resistance, and poisoning resistance it was expected that red mud can serve as a suitable catalyst support for HDO process. Moreover, it could be potentially more cost-effective in comparison with other catalyst supports such as Al_2O_3, SiO_2, and TiO_2 which require complicated preparation procedures.

6. References

[1] Wyman CE, Dale BE, Elander RT, Holtzapple M, Ladisch MR, Lee YY. Coordinated development of leading biomass pretreatment technologies. Bioresour Technol 2005;96:1959–66.

[2] Alriols MG, Tejado A, Blanco M, Mondragon I, Labidi J. Agricultural palm oil tree residues as raw material for cellulose, lignin and hemicelluloses production by ethylene glycol pulping process. Chem Eng J 2009;148:106–14.

[3] Román-Leshkov Y, Chheda JN, Dumesic J a. Phase modifiers promote efficient production of hydroxymethylfurfural from fructose. Science (80-) 2006;312:1933–7.

[4] Nakagawa Y, Shinmi Y, Koso S, Tomishige K. Direct hydrogenolysis of glycerol into 1,3-propanediol over rhenium-modified iridium catalyst. J Catal 2010;272:191–4.

[5] Yin S, Mehrotra AK, Tan Z. Direct formation of gasoline hydrocarbons from cellulose by hydrothermal conversion with in situ hydrogen. Biomass and

Bioenergy 2012;47:228–39.

[6] Helder M, Strik DPBTB, Timmers RA, Raes SMT, Hamelers HVM, Buisman CJN. Resilience of roof-top Plant-Microbial Fuel Cells during Dutch winter. Biomass and Bioenergy 2013;51:1–7.

[7] Op de Beeck B, Dusselier M, Geboers J, Holsbeek J, Morré E, Oswald S, et al. Direct catalytic conversion of cellulose to liquid straight-chain alkanes. Energy Environ Sci 2015;8:230–40.

[8] Yi G, Zhang Y. One-pot selective conversion of hemicellulose (Xylan) to xylitol under mild conditions. ChemSusChem 2012;5:1383–7.

[9] Gürbüz EI, Gallo JMR, Alonso DM, Wettstein SG, Lim WY, Dumesic JA. Conversion of hemicellulose into furfural using solid acid catalysts in γ-valerolactone. Angew Chemie - Int Ed 2013;52:1270–4.

[10] Rissanen J V., Grénman H, Willför S, Murzin DY, Salmi T. Spruce hemicellulose for chemicals using aqueous extraction: Kinetics, mass transfer, and modeling. Ind Eng Chem Res 2014;53:6341–50.

[11] Hilpmann G, Becher N, Pahner FA, Kusema B, Mäki-Arvela P, Lange R, et al. Acid hydrolysis of xylan. Catal Today 2016;259:376–80.

[12] Matsagar BM, Dhepe PL. Brönsted acidic ionic liquid-catalyzed conversion of hemicellulose into sugars. Catal Sci Technol 2015;5:531–9.

[13] Liu S, Okuyama Y, Tamura M, Nakagawa Y, Imai A, Tomishige K. Selective transformation of hemicellulose (xylan) into n-pentane, pentanols or xylitol over a rhenium-modified iridium catalyst combined with acids. Green Chem 2016;18:165–75.

[14] Yan N, Yuan, Dykeman R, Kou Y, Dyson PJ. Hydrodeoxygenation of lignin-derived phenols into alkanes by using nanoparticle catalysts combined with Brensted acidic ionic liquids. Angew Chemie - Int Ed 2010;49:5549–53.

[15] Zhao C, He J, Lemonidou AA, Li X, Lercher JA. Aqueous-phase hydrodeoxygenation of bio-derived phenols to cycloalkanes. J Catal 2011;280:8–16.

[16] Zhao C, Lercher JA. Selective Hydrodeoxygenation of Lignin-Derived Phenolic Monomers and Dimers to Cycloalkanes on Pd/C and HZSM-5 Catalysts. ChemCatChem 2012;4:64–8.

[17] Chen CJ, Lee WS, Bhan A. Mo2C catalyzed vapor phase hydrodeoxygenation of lignin-derived phenolic compound mixtures to aromatics under ambient pressure.

Appl Catal A Gen 2016;510:42–8.

[18] Yoon JS, Lee T, Choi JW, Suh DJ, Lee K, Ha JM, et al. Layered MWW zeolite-supported Rh catalysts for the hydrodeoxygenation of lignin model compounds. Catal Today 2017;293–294:142–50.

[19] Gollakota ARK, Reddy M, Subramanyam MD, Kishore N. A review on the upgradation techniques of pyrolysis oil. Renew Sustain Energy Rev 2016;58:1543–68.

[20] Chiaramonti D, Bonini M, Fratini E, Tondi G, Gartner K, Bridgwater A V., et al. Development of emulsions from biomass pyrolysis liquid and diesel and their use in engines - Part 1: Emulsion production. Biomass and Bioenergy 2003;25:85–99.

[21] Wang H, Male J, Wang Y. Recent advances in hydrotreating of pyrolysis bio-oil and its oxygen-containing model compounds. ACS Catal 2013;3:1047–70.

[22] Mortensen PM, Grunwaldt JD, Jensen PA, Knudsen KG, Jensen AD. A review of catalytic upgrading of bio-oil to engine fuels. Appl Catal A Gen 2011;407:1–19.

[23] Graca I, Lopes JM, Cerqueira HS, Ribeiro MF. Bio-oils upgrading for second generation biofuels. Ind Eng Chem Res 2013;52:275–87.

[24] Nava R, Pawelec B, Castaño P, Álvarez-Galván MC, Loricera C V., Fierro JLG. Upgrading of bio-liquids on different mesoporous silica-supported CoMo catalysts. Appl Catal B Environ 2009;92:154–67.

[25] Czernik S, Bridgwater A V. Overview of applications of biomass fast pyrolysis oil. Energy and Fuels 2004;18:590–8.

[26] Xu C, Etcheverry T. Hydro-liquefaction of woody biomass in sub- and super-critical ethanol with iron-based catalysts. Fuel 2008;87:335–45.

[27] Liu Z, Zhang FS. Effects of various solvents on the liquefaction of biomass to produce fuels and chemical feedstocks. Energy Convers Manag 2008;49:3498–504.

[28] Remón J, Arauzo J, García L, Arcelus-Arrillaga P, Millan M, Suelves I, et al. Bio-oil upgrading in supercritical water using Ni-Co catalysts supported on carbon nanofibres. Fuel Process Technol 2016;154:178–87.

[29] Lu J, Guo S, Fu Y, Chang J. Catalytic upgrading of bio-oil by simultaneous esterification and alkylation with azeotropic water removal. Fuel Process Technol 2017;161:193–8.

[30] Zhang Q, Xu Y, Li Y, Wang T, Zhang Q, Ma L, et al. Investigation on the

esterification by using supercritical ethanol for bio-oil upgrading. Appl Energy 2015;160:633–40.

[31] Oasmaa A, Kuoppala E, Selin JF, Gust S, Solantausta Y. Fast pyrolysis of forestry residue and pine. 4. Improvement of the product quality by solvent addition. Energy and Fuels 2004;18:1578–83.

[32] Jiang X, Ellis N. Upgrading bio-oil through emulsification with biodiesel: Thermal stability. Energy and Fuels 2010;24:2699–706.

[33] Garcia-Perez M, Shen J, Wang XS, Li CZ. Production and fuel properties of fast pyrolysis oil/bio-diesel blends. Fuel Process Technol 2010;91:296–305.

[34] Lin BJ, Chen WH, Budzianowski WM, Hsieh CT, Lin PH. Emulsification analysis of bio-oil and diesel under various combinations of emulsifiers. Appl Energy 2016;178:746–57.

[35] Zhang M, Yewe-Siang Lee Shee We M, Wu H. Direct emulsification of crude glycerol and bio-oil without addition of surfactant via ultrasound and mechanical agitation. Fuel 2018;227:183–9.

[36] Nath K, Das D. Hydrogen from biomass. Curr Sci 2003;85:265–71.

[37] Czernik S, Evans R, French R. Hydrogen from biomass-production by steam reforming of biomass pyrolysis oil. Catal Today 2007;129:265–8.

[38] Arregi A, Lopez G, Amutio M, Artetxe M, Barbarias I, Bilbao J, et al. Role of operating conditions in the catalyst deactivation in the in-line steam reforming of volatiles from biomass fast pyrolysis. Fuel 2018;216:233–44.

[39] He Z, Wang X. Hydrodeoxygenation of model compounds and catalytic systems for pyrolysis bio-oils upgrading. Catal Sustain Energy 2012;1:28–52.

[40] Elkasabi Y, Mullen CA, Pighinelli ALMT, Boateng AA. Hydrodeoxygenation of fast-pyrolysis bio-oils from various feedstocks using carbon-supported catalysts. Fuel Process Technol 2014;123:11–8.

[41] Oh S, Hwang H, Seok H, Weon J. The effects of noble metal catalysts on the bio-oil quality during the hydrodeoxygenative upgrading process. FUEL 2015;153:535–43.

[42] Han Y, McIlroy DN, McDonald AG. Hydrodeoxygenation of pyrolysis oil for hydrocarbon production using nanospring based catalysts. J Anal Appl Pyrolysis 2016;117:94–105.

[43] Yang Y, Lv G, Deng L, Lu B, Li J, Zhang J, et al. Renewable aromatic production

through hydrodeoxygenation of model bio-oil over mesoporous Ni/SBA-15 and Co/SBA-15. Microporous Mesoporous Mater 2017;250:47–54.

[44] Elkasabi Y, Liu Q, Choi YS, Strahan G, Boateng AA, Regalbuto JR. Bio-oil hydrodeoxygenation catalysts produced using strong electrostatic adsorption q. Fuel 2017;207:510–21.

[45] Yakovlev VA, Khromova SA, Sherstyuk O V, Dundich VO, Ermakov DY, Novopashina VM, et al. Development of new catalytic systems for upgraded bio-fuels production from bio-crude-oil and biodiesel. Catal Today 2009;144:362–6.

[46] Elliott DC. Historical Developments in Hydroprocessing Bio-oils 2007:1792–815.

[47] Laurent E, Delmon B. Influence of water in the deactivation of a sulfided NiMo γ-Al2O3 catalyst during hydrodeoxygenation. J Catal 1994;146.

[48] Serrano-Ruiz JC, Braden DJ, West RM, Dumesic JA. Conversion of cellulose to hydrocarbon fuels by progressive removal of oxygen. Appl Catal B Environ 2010;100:184–9.

[49] Wildschut J, Mahfud FH, Venderbosch RH, Heeres HJ. Hydrotreatment of fast pyrolysis oil using heterogeneous noble-metal catalysts. Ind Eng Chem Res 2009;48:10324–34.

[50] Echeandia S, Arias PL, Barrio VL, Pawelec B, Fierro JLG. Synergy effect in the HDO of phenol over Ni-W catalysts supported on active carbon: Effect of tungsten precursors. Appl Catal B Environ 2010;101:1–12.

[51] Elliott DC, Hart TR. 73 Catalytic Hydroprocessing of Chemical Models for Bio-oil 2009:631–7.

[52] Zhao HY, Li D, Bui P, Oyama ST. Hydrodeoxygenation of guaiacol as model compound for pyrolysis oil on transition metal phosphide hydroprocessing catalysts. Appl Catal A Gen 2011;391:305–10.

[53] Wang W, Wu K, Liu P, Li L, Yang Y, Wang Y. Hydrodeoxygenation of p-Cresol over Pt/Al2O3Catalyst Promoted by ZrO2, CeO2, and CeO2-ZrO2. Ind Eng Chem Res 2016;55:7598–603.

[54] Bui VN, Laurenti D, Delichère P, Geantet C. Hydrodeoxygenation of guaiacol. Part II: Support effect for CoMoS catalysts on HDO activity and selectivity. Appl Catal B Environ 2011;101:246–55.

[55] Gutierrez A, Kaila RK, Honkela ML, Slioor R, Krause AOI. Hydrodeoxygenation of guaiacol on noble metal catalysts. Catal Today 2009;147:239–46.

[56] Arun N, Sharma R V., Dalai AK. Green diesel synthesis by hydrodeoxygenation of bio-based feedstocks: Strategies for catalyst design and development. Renew Sustain Energy Rev 2015;48:240–55.

[57] Aluminum leaders http://www.aluminiumleaders.com/history/industry history/ n.d.

[58] Agrawal A, Sahu KK, Pandey BD. Solid waste management in non-ferrous industries in India. Resour Conserv Recycl 2004;42:99–120.

[59] Sushil S, Batra VS. Catalytic applications of red mud, an aluminium industry waste: A review. Appl Catal B Environ 2008;81:64–77.

[60] Yathavan BK, Agblevor FA. Catalytic pyrolysis of pinyon-juniper using red mud and HZSM-5. Energy and Fuels 2013;27:6858–65.

[61] Klopries B, Hodek W, Bandermann F. Catalytic hydroliquefaction of biomass with red mud and CoOMoO3catalysts. Fuel 1990;69:448–55

[62] Pratt KC, Christoverson V. Hydrogenation of a model hydrogen-donor system using activated red mud catalyst. Fuel 1982; 61: 460-462.

[63] Alvarez J, Rosal R, Sastre H, Dõ F V. Characterization and deactivation studies of an activated sul ® ded red mud used as hydrogenation catalyst 1998;167:215–23.

[64] Ordóez S, Sastre H, Díez F V. Catalytic hydrodechlorination of tetrachloroethylene over red mud. J Hazard Mater 2001;81:103–14.

[65] Martino M, Rosal R, Sastre H, Diez F V. Hydrodechlorination of dichloromethane , trichloroethane , trichloroethylene and tetrachloroethylene over a sulfided Ni / Mo ± γ -alumina catalyst. Appl Catal. 1999; 20: 301-307.

[66] Paredes JR, Ordóñez S, Vega A, Díez F V. Catalytic combustion of methane over red mud-based catalysts. Appl Catal B Environ 2004;47:37–45.

[67] Djerad S, Crocoll M, Kureti S, Tifouti L, Weisweiler W. Effect of oxygen concentration on the NOx reduction with ammonia over V2O5-WO3/TiO2 catalyst. Catal Today 2006;113:208–14.

[68] Yanik J, Uddin MA, Ikeuchi K, Sakata Y. The catalytic effect of Red Mud on the degradation of poly (vinyl chloride) containing polymer mixture into fuel oil. Polym Degrad Stab 2001;73:335–46.

[69] Sinag A, Sungur M, Canel M. Effect of experimental conditions on the yields during the copyrolysis of Mustafa Kemal Pasa (MKP) lignite (Turkey) with low-density polyethylene. Energy and Fuels 2006;20:1609–13.

[70] Cakici AI, Yanik J, Ucar S, Karayildirim T, Anil H. Utilization of red mud as catalyst in conversion of waste oil and waste plastics to fuel. J Mater Cycles Waste Manag 2004;6:20–6.

[71] Iannibello A, Marengo S, Girelli A. Bauxite-based catalysts in heavy crude oil hydrotreating. Appl Catal 1982;3:261–72.

[72] Uemiya S, Uchida M, Moritomi H. Ammonia decomposition catalyst with resistance to coexisting sulfur compounds. Mater Trans 2005;46:2709–12.

[73] Khezri SH. Red mud catalyzed one-pot synthesis of nitriles from aldehydes and hydroxylamine hydrochloride under microwave irradiation. Arkivoc 2007;2007:162–70.

CHAPTER 3

3. UPGRADING OF PINYON-JUNIPER CATALYTIC PYROLYSIS OIL VIA HYDRODEOXYGENATION[1]

1. Abstract

This study involves the hydrodeoxygenation (HDO) of pinyon juniper (PJ) catalytic pyrolysis oil over Ni/SiO_2-Al_2O_3 catalyst in a batch reactor to convert it into hydrocarbon fuel. The influence of temperature (350-500 °C), reaction time (15-90 min), and initial hydrogen pressure (3.5-10 MPa), on hydrodeoxygenation of PJ pyrolysis oil was investigated. After hydrogenation was completed, gas, coke, and a liquid product of two immiscible phases (aqueous and organic), were obtained. Maximum HDO of bio-oil was achieved at 450 ° C while the initial hydrogen pressure was 7.0 MPa and the reaction time was 30 minutes. Under these conditions, the H/C and O/C atomic ratios changed from 1.29 and 0.29 respectively for bio-oil to 2.36 and 0.0 for HDO oil respectively. The higher heating value increased from 27.64 MJ/kg of bio-oil to 45.58 MJ/kg of upgraded oil. The water content of organic liquid product was less than 0.05 wt. % while it was 1.63 wt. % in the feed. The viscosity of upgraded oil was 1.26 cP compared to119 cP for the crude bio-oil.

2. Introduction

The global demand for energy is growing due to the development of society. Considering the limited supply of fossil fuels, the need for sustainable renewable fuels is increasing [1]. Fast pyrolysis technique has attracted the attention researchers in recent decades because of its potential to produce liquid fuels. Fast pyrolysis is a

[1] Published in Energy, 2017

thermochemical decomposition process that occurs in absence of oxidizing agents at elevated temperatures [2-5]. This process is effective in breaking down macromolecular structures into smaller organic compounds [3]. A number of studies on fast pyrolysis oils of different types of feedstock such as woody and proteinaceous biomass, grass, and animal waste have indicated the different properties of the final bio-oil [4-8]. However, their qualities were not suitable for direct refinery due to poor stability, high acidity, and low heating value [9-12].

The high oxygen and water content of bio-oil lowers its heating value. The pH of bio-oil is usually between 2-4 due to the presence of carboxylic acids [13, 14]. The acidic nature of bio-oil causes harsh conditions for the equipment used for transportation, storage, and processing. Another problem that is associated with bio-oil is stability during storage. The instability of bio-oil is attributed to presence of highly reactive organic compounds causing repolymerization. Moreover, organic acids, aldehydes, and ketones can react to form hemiacetals, acetals, and ethers respectively [15, 16]. Overall, the unfavorable properties of pyrolysis oils make it impossible to use as drop-in transportation fuels [17, 19].

Intensive studies have been carried out on upgrading of pyrolysis oils through different techniques such as esterification under supercritical ethanol, hydrogenation/hydrodeoxygenation (HDO), hydrocracking, emulsification, solvent addition, and steam reforming [17, 19, 20]. Among these techniques, catalytic hydrodeoxygenation of pyrolysis oil is one of the potential technologies to improve its fuel quality. In addition to hydrogenation of unsaturated compounds, the majority of

hydrogenation catalysts normally favor several other reactions simultaneously such as cracking, decarbonylation, decarboxylation, and hydrodeoxygenation [11, 20, 21].

Production of value-added hydrocarbons is one of the major goals of bio-oil upgrading. Aromatic compounds production via HDO indicates that the catalyst(s) deoxygenate the oil more efficiently with less hydrogenation, resulting in less hydrogen consumption. Moreover, one-ring aromatic compounds are valuable chemicals. An investigation of production of aromatics through HDO of model bio-oil over mesoporous Ni/SBA-15 and Co/SBA-15 has been shown that Ni/SBA-15 catalyst exhibit much higher catalytic performance as compared with Co/SBA-15 catalyst for the hydrodeoxygenation reaction performance of anisole. While the Ni/SBA-15 catalyst would lead to the appearance of partial hydrodeoxygenation products due to the hydrogenation ability of nickel active phase, Co/SBA-15 could selectively cause hydrogenolysis of the C-O bond and could act as the potential hydrodeoxygenation catalyst for aromatic production from the bio-oils [22]. In the case of bio-oil, it has been reported that a first stage HDO at temperatures up to 270 °C is required to convert highly reactive compounds such as aldehydes and ketones so that second stage HDO could be conducted at higher temperatures for complete removal of oxygen [23]. Most HDO studies have been performed using sulfided NiMo and CoMo as suitable catalysts. Moreover, noble metal catalysts such as Pt/C, Ru/C, Pd/C, and Ru/TiO_2 have also been tested and shown to result in higher levels of hydrodeoxygenation than the traditional HDO catalysts such as sulfided CoMo [24-26]. However, noble metal catalysts are relatively more expensive than common HDO catalysts. The influence of catalyst support on HDO activity and stability of catalyst has also been investigated. Ni and Ru supported on silica gel, nano-

spring (NS) silica, and Al_2O_3 have been tested for HDO of phenol as a model compound [27]. Silica supported Ni catalysts performed better than alumina support. The Ni(20%)-NS was the best performing Ni catalyst in terms of deoxygenation. Of the Ru based catalysts, the Ru-NS were the best performing, exhibiting nearly complete phenol conversion and deoxygenation [27].

Although various studies have been published on HDO of different types of biomass pyrolysis oils, the majority of previous research on bio-oil HDO was generally carried out to evaluate the effect of catalysts [28, 29] thus, parametric studies require more detailed investigations to find the optimum feedstock and operating conditions for bio-oil hydrotreating to obtain high quality hydrocarbons.

According to the U.S. Billion Ton update [30], biomass for bioenergy would come from a variety of sources such as agricultural crops (i.e. corn stover), herbaceous energy crops (i.e. switchgrass), forests (i.e. pine bark), and short rotation woody biomass (i.e. pine, hybrid poplar, and pinyon juniper (PJ)). PJ woodlands occupy about 30 million hectares in the western United States (including states of Arizona, California, Colorado, Idaho, Utah, Nevada, New Mexico, Oregon, and Wyoming). Domination of PJ woodlands decreases the herbaceous vegetation and increases bare lands, thus causes soil erosion and nutrition loss [4]. Studies have shown that expansion of PJ woodlands has reduced the amount of precipitation, increased soil erosion, and increase the potential of crown fires. Hence, land management agencies are aiming on reducing the population of PJ woodlands by bulldozing, chaining, hand cutting, mechanical removal, and prescribed fire [31-34]. Therefore, PJ can be a potential biomass feedstock for production of bio-oil.

The objective of this research is to study hydrogenation/deoxygenation of PJ catalytic pyrolysis oil over commercial Ni/SiO_2-Al_2O_3 catalyst. Unlike traditional HDO catalysts such as $CoMo/Al_2O_3$ and $NiMo/Al_2O_3$, this catalyst does not require pre-sulfidation. Furthermore, Ni/SiO_2-Al_2O_3 is cheaper than precious metal HDO catalysts such as Pt, Pd, and Ru [24, 26, 35]. In this study we discuss the effect of temperature, hydrogen pressure, and reaction time on the HDO of PJ pyrolysis oil.

3. Material and methods

3.1. Material

PJ biomass chips were supplied by the U.S. Bureau of Land Management. Red mud was used as catalyst for fast pyrolysis of biomass. The wet red mud was dried at room temperature and then ground and sieved to a particle size of 125−180 μm for fluidized-bed pyrolysis. The ground particles were calcined at 550 °C in a muffle furnace (Thermo Scientific, Inc., Waltham, MA) for 5 h before being used for the pyrolysis. The detailed characterization of the red mud has been reported by Yathavan and Agblevor [4]. Commercial Nickel on silica/alumina (~65 wt % loading Ni) catalyst powder, obtained from Sigma-Aldrich (St. Louis, MO, USA), was used (as received) in HDO experiments. High purity (99%) hydrogen (Airgas, PA, USA) was used for HDO experiments.

3.2. Pyrolysis if biomass

PJ chips ground to pass a 2-mm sieve, were used as a raw material for production of catalytic pyrolysis oil. Catalytic pyrolysis oil was produced at 450 ° C using a pilot scale fluidized bed reactor system, the details of which can be found elsewhere [36]. The

pyrolytic products were condensed to liquid using a series of two water-cooled condensers and an electrostatic precipitator (ESP). The oil product that was collected by ESP (operating at 30 kV) was used for HDO studies.

3.3. Hydrodeoxygenation of bio-oil

The bio-oil was subjected to HDO reactions in a Parr Series 4571 1000 mL autoclave reactor (Parr Instruments, Moline, IL, USA). The reactor can withstand a maximum pressure of 35 MPa at 500 ° C. A Parr 4848 controller was used to control the internal temperature and impeller speed. In a typical test, bio-oil (30 g) and catalyst (6 g) were loaded into the reactor. The reactor was first flushed with nitrogen three times and then flushed with hydrogen three times to purge the reactor. High purity hydrogen was supplied from a reservoir tank via a pressure regulator. The reactor was then pressurized with hydrogen (3.5, 5.2, 7, 8.6, or 10 MPa) and a gas sample was taken from a gas release valve from the gas sampling port for gas analysis when the reactor was at room temperature. The reactor was then heated to reaction temperature (350, 400, 450, or 500 °C) at heating rate of 10 °C/min using a heating mantle. The reaction time was recorded when the required temperature was reached. The stirrer speed was kept constant (~1000 rpm) in all experiments.

After the desired reaction time (15, 30, 60, or 90 minutes), the reactor was cooled to room temperature using the internal cooling coil and an external air fan simultaneously. A gas sample was collected in a tedlar bag for gas analysis when the reactor was cooled down to room temperature. Hydrogen consumption was measured using equation (1).

$$H_2\ consumption\ \left(\frac{moleH_2}{kg\ biooil}\right) = \left(n_{i_{H2}} - x_{f_{H2}}.n_{f_{tot}}\right) \times \frac{1}{30\ g\ biooil} \times \frac{1000\ g}{1\ kg} \qquad (1)$$

Where $n_{i_{H2}}$ is the initial number of mole of hydrogen, $x_{f_{H2}}$ is the final mole fraction of hydrogen, and $n_{f_{tot}}$ is the total number of mole of gas at the end of experiment.

After each experiment, the liquid products were collected in centrifuge test tubes and centrifuged for 30 minutes at g-force of 2147 to separate the resulting aqueous and organic phases and residual solids and catalyst. Both liquid phases were separated and weighed for mass balance computation. The solids (catalyst and coke) were collected and dried at 95 °C for 6 hours. The vessel and reactor parts were rinsed with methanol-toluene mixture (1:1 vol. ratio) to collect any remaining catalyst and oil. The solvent washings were filtered through Watman 42 ashless filter paper (GE Healthcare, UK) and dried at 95 °C. The weight of filter paper was recorded before and after filtration.

The total mass of gaseous product was calculated back using equation (2):

$$W_g = \sum_i x_i.MW_i.n_{tot} \qquad (2)$$

Where W_g is the total mass of gaseous product (g), x_i is the mole fraction of gas i, MW_i is the molecular weight of gas i (g/mole), and n_{tot} is the total number of moles of gas product. The yield of liquid, gas, and solid product were calculated using equations 3, 4, and 5 respectively.

$$Y_{liquid}(\%) = \frac{W_l}{W_f} \times 100 \qquad (3)$$

$$Y_{gas}(\%) = \frac{W_g}{W_f} \times 100 \quad (4)$$

$$Y_{coke}(\%) = \frac{(W_s - W_C)}{W_f} \times 100 \quad (5)$$

Where W_f is the mass of feed bio-oil and consumed hydrogen combined (g), W_l is the mass of liquid product (g), W_g is the mass of gas product (g), W_s is the weight of total solid residues (g), and W_c is the weight of catalyst (g).

An elemental carbon balance before and after each experiment was performed. In a blank experiment, without catalyst, 30 g of PJ bio-oil was charged into the reactor and the reactor was pressurized to 7 MPa with hydrogen. The bio-oil was allowed to react for 60 minutes at 450 ° C. All experiments were conducted in duplicate.

3.4. Characterization of PJ wood, catalytic pyrolysis oil, and upgraded oil

3.4.1. Physical properties

The moisture content of the PJ wood was determined according to standard method ASTM E1756- 08 [37]. The ash content of the PJ wood was determined according to ASTM E1755-01 method [38]. The water content of the crude bio-oil and hydrotreated oil were determined by Karl-Fisher titration method with Hydranal® - composite 5 solution. A Metrohm 701KF Titrino and 703 titration stand setup (Brinkmann Instruments, Riverview, FL, USA) were used for the volumetric Karl Fischer titration. The pH was measured using Mettler Toledo pH Meter and probe (Mettler−Toledo GmbH, Switzerland). The density and kinematic viscosity of the bio-oil and hydrogenated oil were measured at 40 °C using Anton Parr Stabinger viscometer svm 3000 (Ashland, VA, USA).

3.4.2. Chemical properties

The higher heating value (HHV) of PJ wood, bio-oil, and hydrotreated oil were determined using an IKA Model C2000 basic bomb calorimeter (Wilmington, NC, USA). The elemental composition of biomass, bio-oil, and hydrogenated oil were determined using ThermoFischer Scientific Flash 2000 organic elemental analyzer (ThermoFisher Scientific,Waltham, MA, USA). Fourier transform infrared spectroscopy (FTIR) over the range of 600 to 4000 nm was recorded using Avatar 360 FTIR instrument (ThermoFisher Scientific, Waltham, MA, USA). The ^{13}C NMR spectra were recorded on a JEOL 300 MHz NMR spectrometer (JEOL Ltd., Japan). In a 5-mm sample probe about 0.5 g of oil was dissolved in 1.5 g deuterated solvent. Dimethyl sulfoxide-d6 (DMSO-d_6) (Sigma-Aldrich, St. Louis, MO, USA) was used for catalytic pyrolysis oil and chloroform-d (Cambridge Isotope Laboratories, Inc., USA) was used for HDO oil. The observing frequency for the ^{13}C nucleus was 100.58 MHz, the pulse width was 10 μs, the acquisition time was 1.58 s, and the relaxation delay was 2 s. The spectra were obtained with 3000 scans and a sweep width of 20 kHz.

3.5. Gas analysis

Gas samples were collected in tedlar sampling bags from the sampling port installed on the reactor head and injected to a Varian 490- micro GC system (Aginelt Technology, Santa Clara, CA, USA). The micro GC was equipped with two modules: a 10 m Molsieve 5A (MS) column, and a 10 m porous polymer (PPU) column. Each module had a thermal conductivity detector. MS column was used to analyze hydrogen, methane, and carbon monoxide (CO), while carbon dioxide (CO_2) and C1−C5

hydrocarbons were analyzed on the PPU column. Argon and helium were used as carrier gases for MS column and PPU column respectively. Gas concentrations were calculated relative to calibration curves of three standard gas mixtures supplied from Scotty Specialty Gases (Fremont, CA, USA). Gas samples were analyzed for H_2, CO, CO_2, CH_4, C_2H_4, C_2H_6, C_3H_8, C_4H_{10}, and C_5H_{12}.

4. Results and discussion

4.1. Characterization of PJ wood and catalytic pyrolysis oil

The biomass was characterized on the basis of moisture, ash content, elemental composition, and higher heating value (HHV). The physicochemical properties of the PJ wood are shown in Table 3.1. The ESP-captured oil was used in HDO experiments. The ESP oil were characterized based on ash content, elemental composition, HHV, pH, water content, density, and dynamic viscosity. The yield of organic liquid after fast pyrolysis of biomass was about 30 % mass of fed PJ dry basis. The physicochemical properties of the raw bio-oil are shown in Table 3.1.

Table 3. 1: Characterization of Pinyon-Juniper biomass and bio-oil*

Properties	PJ biomass	Catalytic PJ bio-oil
Composition (wt%)		
Ash content	0.53 ± 0.06	0.00
Nitrogen	0.17 ±0.01	0.47 ± 0.04
Carbon	54.43 ± 0.11	66.88 ± 0.21
Hydrogen	6.27 ± 0.09	7.20 ± 0.07
Sulfur	0.00	0.00
Oxygen**	38.60 ± 0.12	25.42 ± 0.12
HHV (MJ/kg)	19.37 ± 0.11	27.64 ± 0.23
pH	NA***	3.46 ± 0.05
Water content (wt%)	6.65 ± 0.09	1.63 ± 0.08
Density (g/cm^3)	0.55 ± 0.03	1.16 ± 0.02
Dynamic viscosity (cP)	NA***	119 ± 5

* Error are the standard deviation of two measurements

** By difference
*** Not applicable

4.2. HDO experiments results

4.2.1. Influence of reaction temperature

4.2.1.1. Mass balance of HDO products

The HDO of bio-oil was performed in the temperature range of 350-500 °C. In all of the experiments the catalyst to feed mass ratio was 0.2, the reaction time was 60 minutes, and the initial hydrogen pressure was 7 MPa. The products yield distribution vs. temperature is shown in Fig. 3.1.

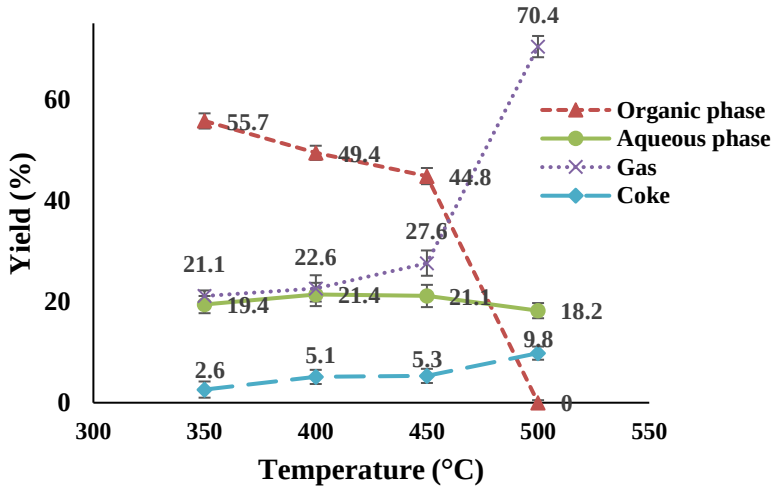

Fig. 3. 1: Effect of temperature on HDO product yield distributions. The H_2 initial pressure, and reaction time were 7 MPa, and 60 minutes respectively.

As expected the reaction temperature influenced the product yields. As the reaction temperature increased from 350 °C to 450 °C, the yield of organic phase decreased from 55.7% to 44.8% and the gas yield increased from 21.1% to 27.6%, while the yield of aqueous phase slightly increased from 19.4% to 21.1%. Also the coke yield

increased from 2.6% to 5.3% over the temperature range of 350-450 ℃. However, by increasing the temperature from 450 ℃ to 500 ℃, the organic liquid yield decreased dramatically from 44.8% to 0% while the gas yield increased considerably from 27.6% to 70.4%. This phenomena can be explained by complete cracking of bio-oil hydrocarbons into gas at 500 ℃. By increasing the temperature, the oil was converted to gas rather than increased hydrodeoxygenation of the oil [39]. By increasing the temperature from 450 to 500 ℃, the aqueous phase yield decreased slightly from 21.1% to 18.2%. This result is explained in section 3.2.1.2. The total mass balance and carbon balance of all HDO experiments at different reaction temperatures were between 98-99% (Table 3.2). (Pressure profile during HDO experiments at different temperatures is demonstrated in Fig. A.1 in Appendix A).

Table 3. 2: Total mass balance and carbon mass balance of HDO experiments at different temperatures

T(˚C)	Total mass balance (wt. %)					Carbon balance (wt. %)				
	Organic	**Aqueous**	**Gas**	**Coke**	**SUM**	**Organic**	**Aqueous**	**Gas**	**Coke**	**SUM**
350	55.7	19.4	21.1	2.6	**98.8**	72.7	2.1	20.1	3.8	**98.7**
400	49.4	21.4	22.6	5.1	**98.5**	68.8	0.5	21.5	7.4	**98.2**
450	44.8	21.1	27.6	5.3	**98.8**	68.8	0	22.1	7.8	**98.7**
500	0	18.2	70.4	9.8	**98.4**	0	0	84.3	14.4	**98.7**

4.2.1.2. Characterization of HDO products

Reaction temperature significantly influenced the physicochemical properties of HDO oil. Table 3.3 illustrate the properties of HDO oil and gas product analysis at

different temperatures. Increasing reaction temperature from 350 °C to 450 °C increased the hydrogen content of HDO oil from 10.42 wt.% to 16.41 wt.% while the oxygen content were remarkably reduced from 20.12 wt.% to 0 wt.%. This would indicate the increased hydrodeoxygenation of the oil over this temperature range. Hydrogen consumption increased gradually from 48 mol/kg to 57 mol/kg in this temperature range. The density of oil reduced by 10.23% from 0.88 g/cm^3 to 0.79 g/cm^3 while the temperature increased from 350°C to 450 °C. Also the dynamic viscosity decreased from 3.22 cP to 1.35 cP over this temperature range. The reduction in density and viscosity could be attributed to hydrocracking of high molecular weight compounds in the bio-oil during HDO [40]. The reduction in acidity can be due to conversion of carboxylic acids in the bio-oil during hydrodeoxygenation [10].

Table 3. 3: H_2 consumption, physicochemical properties of the liquid products, and gas product composition at different temperatures*

Properties	Reaction time and hydrogen initial pressure were 60 min and 7 MPa respectively			
	350 °C	400 °C	450 °C	500 °C
H_2 consumption (mol/kg bio-oil)	48 ± 8	50 ± 7	57 ± 3	91 ± 2
Aqueous phase				
Water content (wt%)	93.23 ± 0.10	97.26 ± 0.15	99.51 ± 0.15	99.17 ± 0.25
pH	5.11 ± 0.12	6.34 ± 0.17	6.85 ± 0.05	6.87 ± 0.34
HDO oil (organic phase)				
Elemental analysis (wt%)				
N	0.21 ± 0.02	0.13 ± 0.01	0.12 ± 0.01	NA
C	69.25 ± 0.85	75.12 ± 1.14	83.47 ± 1.09	NA
H	10.42 ± 0.75	12.54 ± 0.65	16.41 ± 0.43	NA
O	20.12 ± 0.05	12.21 ±0.06	0.00	NA
HHV (MJ/kg)	42.07 ± 0.67	42.57 ± 0.91	45.44 ± 0.84	NA
pH	5.72 ± 0.33	6.53 ± 0.21	NA	NA
Water content (wt%)	<DL**	<DL**	<DL**	NA
Density (g/ml)	0.88 ± 0.02	0.84 ± 0.02	0.79 ± 0.01	NA
Dynamic viscosity (cP)	3.22 ± 0.01	1.58 ± 0.01	1.35 ± 0.01	NA
Gas composition (mole %)				
H_2	0.00	0.00	0.00	11.75 ± 0.22
CO_2	1.33 ± 0.02	0.00	0.00	3.10 ± 0.05
CH_4	94.41 ± 0.23	87.22 ± 0.71	85.83 ± 0.42	84.72 ± 0.81
C_2H_4	2.73 ± 0.02	7.22 ± 0.10	9.02 ± 0.03	0.51 ± 0.01
C_3H_8	1.04 ± 0.01	3.52 ± 0.08	3.82 ± 0.01	0.01
C_4H_{10}	0.41 ± 0.01	1.57 ± 0.01	1.18 ± 0.01	0.01

C_5H_{12}	0.05	0.46 ± 0.01	0.15	0.00

** Errors are the standard deviation of two measurements
* The detection limit was 0.05%.

At 350 °C the major gas product was methane (94.41%) and small amounts of CO_2 and C_2-C_5 hydrocarbon gasses were formed (Table 3.3). When the temperature was increased from 350 °C to 450 °C, the amount of C_2-C_5 hydrocarbon gases increased indicating further cracking of the bio-oil compounds [39]. Also no CO_2 was detected at 400-450 °C. This would suggest the methanation of carbon dioxide over nickel (known as Sabatier reaction). This reaction takes place between 250 °C and 500 °C [41].

Increasing the reaction temperature from 450 °C to 500 °C resulted in high consumption of hydrogen (91 mol/kg). As previously mentioned (Fig. 3.1), overcracking of hydrocarbon molecules at 500 °C resulted in complete conversion of oil into gas products. The major gas component was methane (84.72%) at this temperature. This would suggest that at 500 °C hydrocracking of the bio-oil compounds result in production of methane that would confirm the high amount of hydrogen consumption. At this temperature, 3.10% CO_2 was detected in the gas product. Since methanation of CO_2 is a reversible reaction [41], this would explain the reduction of aqueous liquid yield from 21.1% to 18.2% by increasing the temperature from 450 °C to 500 °C (Fig. 3.1). At 500 °C overcracking of hydrocarbon compounds resulted in formation of high amounts of methane. Methane could then partially react with the water produced from HDO and form CO_2 and hydrogen (1).

$$CO_{2\,(g)} + 4\ H_{2\,(g)} \leftrightarrows CH_{4\,(g)} + 2\ H_2O_{\,(g)} \qquad (1)$$

4.2.2. Influence of hydrogen pressure

4.2.2.1. Mass balance of HDO products

A set of experiments was carried out in the range of 3.5-10 MPa of initial hydrogen pressure. In these experiments, reaction temperature and reaction time were kept constant at 450 °C and 60 minutes respectively. The data obtained on product yields distribution is shown in Fig. 3.2.

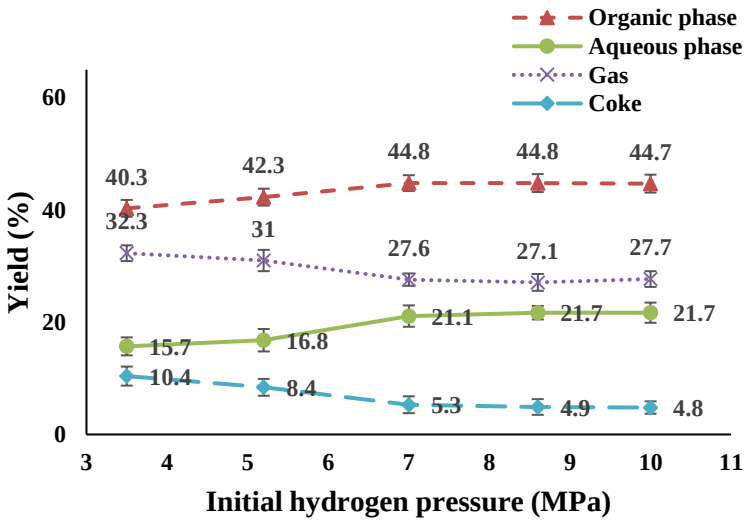

Fig. 3. 2: Effect of H_2 pressure on HDO product yield distributions. The temperature and reaction time were 450 °C and 60 minutes respectively.

Increasing hydrogen pressure from 3.5 MPa to 7 MPa increased the organic liquid yield from 40.3% to 44.8%. This could be due to increase in concentration of adsorbed hydrogen on catalyst surface and increase in the amount of dissolved H_2 in the oil, as hydrogen pressure was increased [23, 42]. Over this pressure range, the gas yield reduced from 32.3% to 27.6% and the coke yield decreased from 10.4% to 5.3%. This would suggest that higher levels of hydrogen pressure would help HDO reactions to predominate cracking and (re)polymerization reactions that produce gas and coke [43].

By increasing the initial hydrogen pressure from 3.5 MPa to 7 MPa, the yield of aqueous phase product increased from 15.7% to 21.1%. Since water is a product of HDO this would suggest that increasing the hydrogen pressure promotes the hydrodeoxygenation of bio-oil compounds.

Increasing the hydrogen pressure from 7 MPa to 10 MPa did not have a significant effect on product yields as is illustrated in Fig. 3.2. These results indicate that solubility of hydrogen in the oil and adsorbed hydrogen on the catalyst surface reached a maximum (saturated) value at 7 MPa [23, 43]. Thus, increasing hydrogen pressure to higher levels would not have significant effect on HDO, cracking, and condensation reactions. Table A.1 (in Appendix A) presents the total mass balance and carbon balance of all HDO experiments at different initial hydrogen pressures. Also for more information on pressure profile during HDO experiments at different hydrogen initial pressure refer to Fig. A.2 in Appendix A.

4.2.2.2. Characterization of HDO products

Tables A.2 (in Appendix A) shows the physicochemical properties of HDO oil and gas product analysis at different hydrogen pressures. By increasing H_2 pressure from 3.5 MPa to 7 MPa hydrogen content of HDO oil increased from 10.24 wt.% to 16.41 wt.% and its oxygen content considerably decreased from 18.23 wt.% to 0 wt.%. These results indicate that higher pressure of hydrogen favors higher level of both oil hydrogenation and deoxygenation. As previously mentioned, this could be due to the increased concentration of hydrogen in the liquid phase [23]. The water content of the HDO oil reduced from 1.07 wt.% to less than 0.05 wt.%. This could be due to the

movement of water from organic phase to aqueous phase as HDO reactions progress [44, 45]. The heating value increased from 42.72 MJ/kg to 45.44 MJ/kg. Like previous experiments the major gas product was methane and a small amount of C_2-C_5 hydrocarbon gases were produced in all experiments. The concentration of C_2-C_5 gases increased by increasing the hydrogen initial pressure. This would suggest that hydrocracking of the bio-oil compounds increased by increasing hydrogen pressure [46].

Increasing the pressure from 7 MPa to 10 MPa did not have a significant effect on the oil and gas composition. These results suggest that at hydrogen initial pressure of 7 MPa, dissolved hydrogen on the catalyst surface reached a maximum value and increasing the pressure to higher levels will not affect HDO reactions [24].

4.2.3. Influence of reaction time

4.2.3.1. Mass balance of HDO products

To examine the effect of reaction time on product yield distributions, HDO experiments were performed at four different reaction times. In all experiments the temperature and initial hydrogen pressure were kept at 450 °C and 7 MPa respectively. The reactor was maintained at 450 °C for 15, 30, 60, and 90 minutes and cooled down to room temperature afterwards. The yields of HDO products for these reaction times are illustrated in Fig. 3.3.

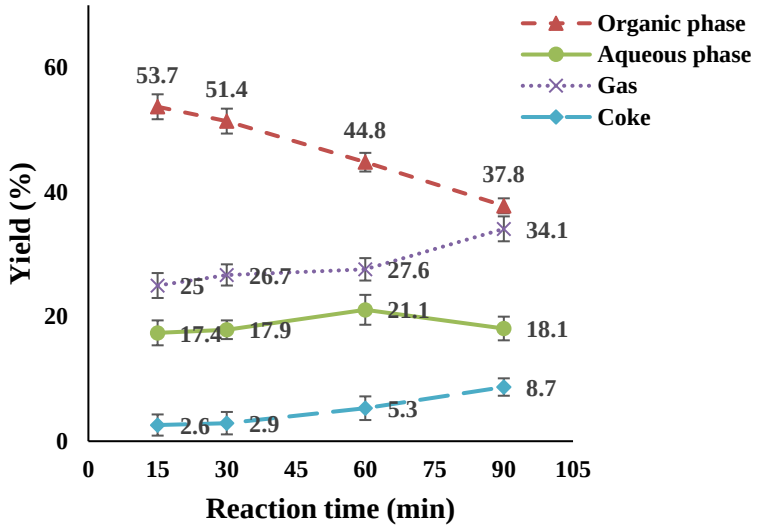

Fig. 3. 3: Effect of reaction time on HDO products yield distributions. The temperature and H_2 initial pressure were 450 °C and 7 MPa respectively.

Increasing the reaction time from 15 to 90 minutes significantly decreased the organic liquid yield from 53.7% to 37.8%. The gas yield increased from 25.8% to 34.1% over time. This result implies that the organic compounds in the oil phase were converted to gas by further cracking rather than increased HDO of the oil [39]. From 15 to 60 minutes, the aqueous liquid yield slightly increased from 17.4% to 21.1% that indicates the hydrodeoxygenation reaction progress that removes oxygen in the form of water. Then it slightly decreased to 18.1% as the reaction time increased to 90 minutes. The latter observation is explained in section 3.2.3.2. Increasing the reaction time from 15 to 90 minutes increased the coke yield from 2.6% to 8.7%. It suggests that side reactions such as repolymerization and recombination might have occurred over longer reaction times, resulting in coke formation [10]. (For detailed information on total mass balance and carbon balance of HDO experiments at different reaction times refer to Table A.3 in

Appendix A. Also more information about pressure profile during HDO experiments at different reaction time is provided in Fig. A.3 in Appendix A)

4.2.3.2. Characterization of HDO products

As shown in Table A.4 (Appendix A), increasing the reaction time from 15 to 30 minutes increased the hydrogen content from 13.27 wt.% to 16.42 wt.% and decreased the oxygen content from 8.11 wt.% to 0 wt.%. Hydrogen consumption was slightly increased from 46 mol/kg to 50 mol/kg. In this reaction time range water content, density, and dynamic viscosity slightly improved.

Increasing the reaction time from 30 minutes to 60 and 90 minutes did not have a significant effect on elemental composition of HDO oil, HHV, water content, density, and viscosity. However, H_2 consumption increased from 50 mol/kg to 57 mol/kg and 60 mol/kg respectively (Table A.4 in Appendix A).

In all experiments at different reaction times, the major gas product was methane. At reaction time of 90 minutes, 1.75% CO_2 was detected in gas products that could be formed from reverse methanation reaction as discussed before [41]. This would also explain the reduction of aqueous phase yield while the reaction time was increased from 60 to 90 minutes (Fig. 3.3).

These results suggest that 30 minutes reaction time was long enough for completion of HDO reactions and longer reaction time result in further hydrocracking of the organic components and conversion of organic compounds to gas phase as previously shown in Fig. 3.3.

4.3. FTIR and NMR analysis of organic liquid products

The FTIR spectra of the raw bio-oil and HDO oils at different temperatures are presented in Fig. 3.4. The absorbance peaks between 3050 and 3650 cm^{-1} were ascribed to –OH stretching vibration. This result indicated that phenolic compounds and alcohols were produced during catalytic pyrolysis of PJ biomass. These peaks were also ascribed to presence of water in the bio-oil. With the increase in temperature, these peaks gradually weakened or even disappeared in the HDO oil that could be due to phenolic or alcoholic hydroxyl cleavage, elimination, intramolecular dehydration, or hydrodeoxygenation of –OH groups. Furthermore, during HDO, water could possibly migrate to the aqueous phase. The peaks between 2840 and 3010 cm^{-1} and the two other bands at 1376 and 1453 cm^{-1} were caused by C–H stretching and deformation in methyl groups and the methylene groups, respectively. The peaks were intensified after HDO compared to the original bio-oil [47, 48]. The peaks at 1590-1610 cm^{-1} were attributed to in-ring C–C stretching. These peaks disappeared completely at 450 °C suggesting that the aromatics could possibly undergo cracking, or polymerization to form coke. The peak at 1670 cm^{-1} was ascribed to C=O stretching, which gradually disappeared with the increase of temperature. The appearance of typical carbonyl group C=O stretching vibrations at 1710 cm^{-1} showed that aldehydes, ketones, or carboxylic acids were only produced at 350 °C [49]. At higher temperatures the C–O stretching intensity of absorption band at 1033 and 1100 cm^{-1} faded away, which could be described as the deoxygenation of alcohols, phenols, or esters. Moreover, several bands that appeared between 740 and 830 cm^{-1} could be attributed to C–H out-of plane bending vibration from aromatics and their

derivatives disappeared gradually because of hydrogenation. These results indicated that the oxygenated groups (–OH, C=O, and C–O) were significantly removed in HDO oil.

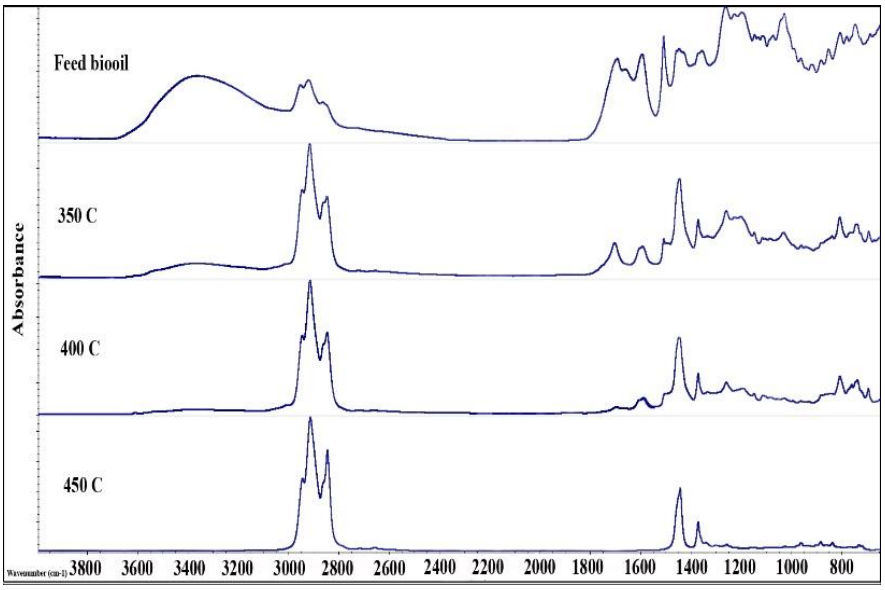

Fig. 3. 4: FTIR spectra of HDO oils obtained at different temperatures. H_2 initial pressure, and reaction time were 7 MPa and 60 minutes respectively.

In Fig. A.4 (provided in Appendix A), the FTIR spectra of the crude bio-oil and HDO oils at different hydrogen pressures are presented. The OH (carboxylic acids) stretching was decreased with the increase of pressure from 3.5 MPa to 7 MPa. CH (alkanes) aliphatic stretch increased considerably and CH bending stretch absorptions bands significantly decreased in this pressure range. The decrease in both OH and C=O stretch absorption bands and the increase in CH aliphatic stretch absorption band indicate that the carboxylic acids and other oxygenated chemical compounds were converted to hydrocarbons. At 5.2 MPa, the characteristic bands appeared between 740 and 830 cm^{-1} are ascribed to C–H out-of plane bending vibration from aromatics and their derivatives. The higher selectivity to the ring hydrogenation products at higher pressure is attributed

to the increased H_2 availability (i.e., high H_2 surface coverage) at higher pressures [40]. At 7 MPa these bands disappeared. Increasing hydrogen pressure from 7 MPa to 8.6 MPa and 10 MPa did not have significant effect on FTIR spectra of HDO oils. The results of FTIR are in good agreement with the physicochemical properties presented in Table A.2 (Appendix A).

Fig. A.5 (Appendix A) shows the FTIR spectra of the crude bio-oil and HDO oils obtained at different reaction times of 15, 30, 60, and 90 minutes. According to this figure, it is clear that the very broad OH stretching absorption peak present in the raw bio-oil completely disappears when the reaction time increased from 15 to 30 minutes. The CH aliphatic stretch absorption band at 2800-3050 cm^{-1} in the bio-oil dramatically increased at reaction time of 30 minutes. Also the C=O absorption band of carbonyl functional group and the C–O absorption band of ether and alcohol functional groups disappeared during 30 minutes HDO. The changes in FTIR spectrum of HDO oil absorption bands indicate that after 30 minutes reaction time at 450 °C in presence of 20% catalyst the carboxylic acids, aldehydes, and other oxygenated chemical compounds were converted to hydrocarbons. However the increase in reaction time from 30 minutes to 60 and 90 minutes did not have any significant effect on FTIR spectrum of HDO oil. As previously discussed, after reaction time of 30 minutes, hydrocracking of organic components causes the organic liquid to convert to gas phase. The results of FTIR at different reaction time were in good agreement with the properties of HDO oil (Table A.4).

The functional groups present in the crude bio-oil and HDO oils were characterized by semi-quantitative integration of ^{13}C NMR spectra. For comparison, a ^{13}C

NMR experiment was carried out on commercial gasoline as well. The ^{13}C NMR spectra of the raw bio-oil, two HDO oils obtained at different reaction temperature (400 °C and 450 °C), and commercial gasoline (regular grade) are shown in Fig. A.6 (Appendix A). The chemical shifts in the spectrum were assigned to different functional groups [50, 51]. The semi-quantitative analysis of the ^{13}C NMR functional groups are presented in Table 3.4. The crude bio-oil had high amounts of carbohydrate degradation products, alcohols, ethers, methoxylated phenols, carboxylic groups, aldehydes, and ketones.

Table 3. 4: Functional group distribution of crude bio-oil, commercial gasoline, and HDO oils from ^{13}C NMR spectral integration

Chemical shift region (ppm)	Dominant type of carbon	Percentage of carbon based on ^{13}C NMR analysis			
		Feed bio-oil	HDO oil-400 °C	Commercial gasoline	HDO oil-450 °C
0-28	saturated aliphatic groups	16.9	42.9	48.3	61.2
28-55	unsaturated aliphatic groups	10.6	16.7	13.3	38.8
55-95	alcohols, ethers, phenolic methoxys, anhydrosugars	13.1	0	1.7	0
95-165	aromatics, furans	56.7	40.4	36.7	0
165-180	organic (carboxylic) acids, esters	1.6	0	0	0
180-215	ketones, aldehydes	1.1	0	0	0

The characteristic peaks at the chemical shift of 0-28 ppm are assigned to saturated aliphatic carbon atoms. Clearly saturated aliphatics increased during HDO that could be due to hydrogenation of unsaturated aliphatics, HDO of alcohols, ethers, carboxylic acids, aldehydes, and ketones. Increasing the reaction temperature from 400 °C to 450 °C resulted in further increase in saturated aliphatic carbon atoms from 42.9% to 61.2% (Table 3.4). This would suggest that unsaturated compounds hydrogenate to saturated aliphatics.

The characteristic peaks at chemical shift of 95-165 ppm are assigned to aromatic carbon atoms, phenolic compounds, and furans. These carbon atoms decreased after HDO at 400 °C. With the increase in reaction temperature from 400 °C to 450 °C, unsaturated aliphatics increased from 16.7% to 38.8% and aromatic compounds disappeared. At 450 °C both saturated and unsaturated aliphatic increased from 42.9% and 16.7% (at 400 °C) to 61.2% and 38.8%. These results indicate that hydrogenation of unsaturated aliphatics took place at 450 °C causing an increase in saturated and unsaturated aliphatics. However hydrogenation of unsaturated aliphatics did not fully taken place. Longer reaction times might result in complete hydrogenation of unsaturated aliphatic carbon atoms, however, as previously mentioned, longer reaction times can cause hydrocracking of organic compound to gases that reduces the organic liquid yield.

The chemical shifts of 165-180 ppm are generally assigned to carboxylic acids and esters. After HDO process, these compounds were completely hydrodeoxygenated. This can explain the increase in aliphatic hydrocarbons during HDO process (Table 3.4).

Characteristic peaks positioned at the chemical shift of 180-215 ppm are assigned to carbon atoms of carbonyl groups contained in aldehydes and ketones whose content decreased from 1.1% in bio-oil to zero in HDO oil at 400 °C and 450 °C indicating that aldehydes and ketones fully deoxygenated to aliphatic hydrocarbons. Interestingly, HDO oil obtained at 400 °C had a very similar ^{13}C NMR spectra to that of commercial gasoline (Fig A.6 b and c, and Table 3.4).

Comparing to other bio-oils obtained from other feedstock, the catalytic PJ bio-oil used in this study had significantly less reactive groups of aldehydes, ketones, phenolics,

and carboxylic acid fractions that are responsible for instability of bio-oil [51, 52]. This could explain the accomplishment of HDO process in a single step.

No catalytic activity was seen in the case of blank experiments and the bio-oil polymerized (solidified) due to the presence of highly reactive compounds in bio-oil such as sugar derivatives and phenolic compounds [39, 53]. The reactor was not catalytically active and did not influence the experiment.

4.4. Evaluation of HDO

To accurately visualize and extrapolate trends from elemental analysis, the elemental composition was plotted in Van Krevelen-type diagrams. The molar O/C versus molar H/C ratios of the crude bio-oil and the HDO oils are illustrated in Figs. 3.5, 3.6, and 3.7 at different temperatures, initial hydrogen pressures, and reaction times respectively. Van-Krevelen diagrams drawn using elemental composition data reported in Tables 3.3, A.2, and A.4. These diagrams provide insight into the influences that process conditions have on the elemental composition of products [54]. According to Fig. 3.5, the O/C ratio of the oil decreased as a function of reaction temperature indicating deep deoxygenation occurs at higher temperatures. An increase in HDO process temperature resulted in an increase in H/C ratio from 1.81 at 350 °C to 2.36 at 450 °C. Fig. 3.5 shows that the ratio of H/C increased at lower temperatures while at higher temperatures O/C ratio decreased faster. This result suggests that hydrogenation reactions such as saturation of double bonds or alcohol formation from aldehydes and ketones may dominate at lower temperatures while HDO and dehydration reactions may be favored afterwards [45, 47].

This result was in a good agreement with ^{13}C NMR results that were discussed in section 3.3 (Table 3.4).

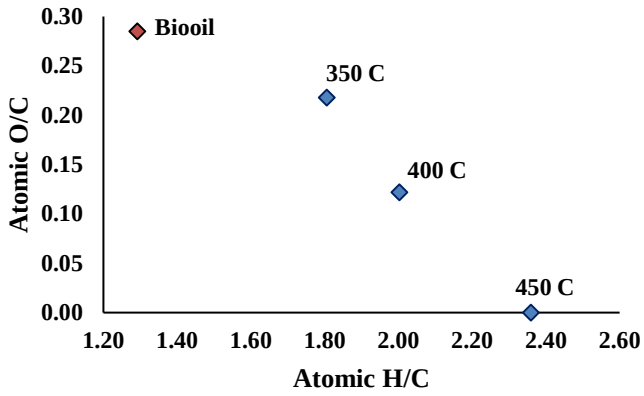

Fig. 3. 5: Van Krevelen diagram of the HDO oil products at different reaction temperatures. H_2 initial pressure, and reaction time were 7 MPa and 60 minutes respectively.

HDO process using initial hydrogen pressure of 3.5 MPa decreased the O/C ratio from 0.29 of original bio-oil to 0.19 of HDO oil. The H/C increased significantly from 1.29 of bio-oil to 1.73 of HDO oil. Increasing the hydrogen initial pressure from 3.5 MPa to 5.2 MPa caused a slight decrease in O/C ratio from 0.19 to 0.13 while H/C increased considerably from 1.73 to 2.19. With the increase in hydrogen pressure from 5.2 MPa to 7 MPa O/C ratio dropped significantly from 0.13 to 0.00 while H/C ratio slightly increased from 2.19 to 2.36. These results indicate that hydrogenation reactions take place at lower pressure since the increase in H/C ratio were more notable than the decrease in O/C. However as shown in Fig. 3.6, deoxygenation of chemical components require higher hydrogen pressures. Increasing hydrogen initial pressure from 7 MPa to 8.6 MPa and 10 MPa did not have a significant effect on H/C and O/C ratios suggesting

that 7 MPa of initial hydrogen pressure was sufficient to accomplish a complete HDO process.

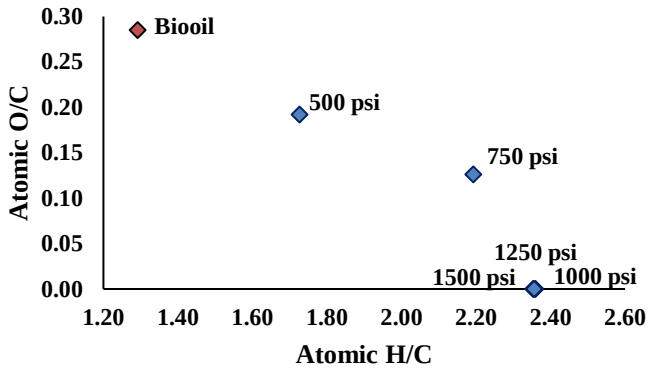

Fig. 3. 6: Van Krevelen diagram of the HDO oil products at different H_2 initial pressures. Temperature, and reaction time were 450 °C, and 60 minutes respectively.

As shown in Fig. 3.7, at reaction time of 15 minutes, the H/C ratio increased significantly to 2.03 compared to 1.29 of the original bio-oil. Also the O/C ratio decreased from 0.29 of bio-oil to 0.08 of HDO oil. With the increase in reaction time from 15 minutes to 30 minutes H/C and O/C ratios reached to 2.36 and 0.00 respectively. This result suggested that at 450 °C with catalyst loading of 20% and initial H_2 pressure of 7 MPa, HDO reactions took place rapidly in the first 15 minutes and slowed down in the second 15 minutes. At the reaction time of 60 and 90 minutes the H/C ratio remained constant at the value of 2.36. The O/C ratio was 0.00 at reaction times of 60 and 90 minutes. This can be explained by completion of HDO reactions in 30 minutes and further hydrocracking of components in organic liquid to gas phase at higher reaction times. These results were in a good agreement with yield distribution and FTIR results in sections 3.2.3 and 3.3.2 respectively.

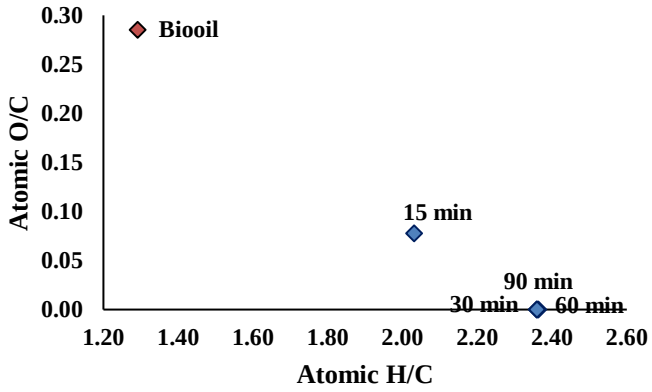

Fig. 3. 7: Van Krevelen diagram of the HDO oil products at different reaction times. Temperature, and H_2 initial pressures were 450 °C, and 7 MPa respectively.

5. Conclusion

A parametric hydrodeoxygenation study using commercial Ni/SiO_2-Al_2O_3 catalyst was carried out on pyrolysis oil derived from Pinyon Juniper. HDO experiments resulted in conversion of the bio-oil into two liquid phases (aqueous and organic), as well as gas and coke. The mass balance analysis of HDO experiments demonstrated that product yield distributions were considerably influenced by temperature, hydrogen pressure, and reaction time. High temperature lead to high catalytic activity for HDO. Hydration reactions mainly occurred at low temperature, while deoxygenation or cracking of oxygenated compounds were predominant at high temperature. With increasing reaction temperature from 350 °C to 450 °C the yield of upgraded oil decreased, but it was beneficial in improving the physicochemical properties. At low hydrogen pressure, hydrogenation dominated deoxygenation reactions. With increase in hydrogen initial pressure, deoxygenation reactions were favored, in addition to hydrogenation. The increase in reaction time led to the decrease in organic liquid yield, due to the formation

of gas-phase components and coke through cracking and polymerization respectively. The properties of HDO oils were significantly improved compared to the original bio-oil. This work provided a new alternative for production of liquid hydrocarbon from bio-oil.

Carbon loss due to coke and gas formation was a major challenge that reduced the yield of organic liquid product in HDO process. High amounts of hydrogen consumption during HDO operation was also another issue that adds to the cost of operation. Thus, it will be necessary to conduct a full economic optimization that incorporates the overall efficiency from pyrolysis to HDO, including the feedstock losses during pyrolysis. Future work should also investigate the rates of catalyst deactivation and coke formation, which could significantly alter the effectiveness of the process.

6. References

[1] Sorrel S, Speirs J, Rentley R, Brandt A, Miller R. Global oil depletion: A review of the evidence. Energy Pol 2010; 38:5290-5.

[2] Zhang S, Yan Y, Li T, Ren Z. Upgrading of liquid fuel from the pyrolysis of biomass. Biores Technol 2005; 96: 545-50.

[3] Lee JW, Hawkins B, Day DM, Reicosky DC. Sustainability: the capacity of smokeless biomass pyrolysis for energy production, global carbon capture and sequestration. Energy Environ Sci 2010;3:1695-705.

[4] Yathavan BK, Agblevor FA. Catalytic pyrolysis of pinyon juniper using red mud and HZSM- 5. Energy Fuels 2013; 27: 6858-65.

[5] C. A. Mullen, Boateng AA. Production and Analysis of Fast Pyrolysis Oils from Proteinaceous Biomass. Bioenergy Res 2011; 4: 303-11.

[6] Agblevor FA, Beis SH, Mante OD, Abdoulmoumine N. Fractional catalytic pyrolysis of hybrid poplar wood. Ind Eng Chem Res 2010;49:3533-8.

[7] Boateng AA, Daugaard DE, Goldberg NM, Hicks KB. Bench-Scale Fluidized-Bed Pyrolysis of Switchgrass for Bio-Oil Production. Indus Eng Chem Res 2007;46:1891-7.

[8] Schnitzer MI, Monreal CM, Facey GA, Fransham PBJ. The conversion of chicken manure to biooil by fast pyrolysis I. Analyses of chicken manure, biooils and char by ^{13}C and ^{1}H NMR and FTIR spectrophotometry. J Environ Sci Health B; 2007: 42 71-7.

[9] Agblevor FA, Mante OD, Mcclung R, Oyama ST. Co-processing of standard gas-oil and biocrude oil to hydrocarbon fuels. Biomass Bioenergy 2012;45:130-7.

[10] Kim TS, Oh Sh, Kim JY, Choi IG, Choi IW. Study on the hydrodeoxygenative upgrading of crude bio-oil produced from woody biomass by fast pyrolysis. Energy 2014; 68: 437-43.

[11] Mortensen PM, Grunwaldt JD, Jensen PA, Knudsen KG, Jensen AD. A review of catalytic upgrading of bio-oil to engine fuels. Appl Catal A: General 2011; 407: 1-19.

[12] Bridgwater AV, Czernik S, Piskorz J. Progress in thermochemical biomass conversion, Blachwell Wissenschafts-Verlag 2001; pp: 977-97.

[13] Oasmaa A, Elliott DC, Korhonen J. Acidity of biomass fast pyrolysis oils: state of the art for the end users. Energy Fuels 2010; 24: 6548-54.

[14] Mante OD, Agblevor FA. Storage stability of biocrude oils from fast pyrolysis of poultry litter. Waste manage 2012; 32: 67-76.

[15] Oasmaa A, Kuoppala E. Fast pyrolysis of forestry residue: 3. Storage stability of liquid. Energy fuels 2003; 17: 1075-84.

[16] Boucher ME, Chaala A, Pakdel H, Roy C. Bio-oils obtained by vacuum pyrolysis of softwood bark as a liquid fuel for gas turbines. Part II: Stability and ageing of bio-oil and its blends with methanol and a pyrolytic aqueous phase. Biomass Bioenergy 2000; 19: 351-61.

[17] Ahmadi Sh, Reyhanitash E, Yuan Z, Rohani S. Upgrading of fast pyrolysis oil via catalytic hydrodeoxygenation: Effects of type of solvents. Renewable Energy 2017; 114:376-382.

[18] Zhang Z, Bi P, Jiang P, Fan M, Deng Sh, Zhai Q, Li Q. Production of gasoline fraction from bio-oil under atmospheric conditions by an integrated catalytic transformation process. Energy 2015; 90: 1922-30.

[19] Lee H, Kim Y, Lee I, Joen J, Jung S, Chung JD, Choi WG, Park Y. Recent advances in the catalytic hydrodeoxygenation of bio-oil. Korean J Chem Eng. 2016; 33:3299-3315.

[20] Xiu Sh, Shahbazi A. Bio-oil production and upgrading research: A review. Renewable Sustainable Energy Rev 2012; 16: 4406-14.

[21] Choudhary TV, Phillips CB. Renewable fuels via catalytic hydrodeoxygenation. Appl Catal A: General 2011; 397: 1-12.

[22] Yang y, Lv G, Deng L, Lu B, Li J, Zhang J, Shi J, Du S. Renewable aromatic production through hydrodeoxygenation of model bio-oil over mesoporous Ni/SBA-15 and Co/SBA-15. Microporous and Mesoporous Materials 2017; 250:47-54.

[23] Joshi N, Lawal A. Hydrodeoxygenation of pyrolysis oil in a microreactor. Chem Eng Sci 2012; 74: 1-8.

[24] He Z, Wang X. Hydrodeoxygenation of model compounds and catalytic systems for pyrolysis bio-oils upgrading. Catal Sustain Energy 2013; 28-52.

[25] Elkasabi Y, Mullen ChA, Pighinelli LMT, Boateng AA. Hydrodeoxygenation of fast pyrolysis oils from various feedstocks using carbon-supported catalysts. Fuel Process Technol 2014: 123: 11-8.

[26] Oh Sh, Hwang H, Choi HS, Choi JW. The effect of noble metal catalysts on the bio-oil quality using the hydrodeoxygenative upgrading process. Fuel 2015; 153: 535- 43.

[27] Han Y, Mcllroy DN, McDonald AG. Hydrodeoxygenation of pyrolysis oil for hydrocarbon production using nanospring based catalysts. J Anal Appl Pyrolysis 2016; 117: 94-105.

[28] Elkasabi y, Liu Q, Choi YS, Strahan G, Boateng AA, Regalbuto JR. Bio-oil hydrodeoxygenation catalysts produced using strong electrostatic adsorption. Fuel 2017; 207:510-521.

[29] Li X, Chen G, Liu C, Ma W, Yan B, Zhang j. Hydrodeoxygenation of lignin-derived bio-oil using molecular sieves supported metal catalysts: A critical review. Ren Sust. En. Rev. 2017; 71:296-308.

[30] Perlak RD, Stokes BJ. U.S. Department of Energy, Oak Ridge National Laboratory, Oak Ridge, TN. 227 p. ORNL/TM-2011/224., 2011.

[31] Miller RF, Bates JD, Svejcar TJ, Pierson FB, Eddleman LE. Technical Bulletin 152; Corvallis Agricultural Experiment Station, Oregon State University, Corvallis, OR, 2005.

[32] Carrara PE, Carroll TR. The determination of erosion rates from exposed tree roots in the Piceance basin, Colorado. Earth Surf. Processes 1979; 4: 307−317.

[33] Ansley RJ, Wiedemann HT, Castellano MJ, Slosser JE. Herbaceous restoration of juniper Ddominated grasslands with chaining and fire. Rangel. Ecol. Manage. 2006; 59: 171−178.

[34] Baughman C, Forbis TA, Provencher L. Response of two sagebrush sites to low-disturbance, mechanical removal of Piñyon and Juniper. Invasive Plant Sci. Manage. 2010; 3:122−129.

[35] Lee EH, Park R, Kim H, Park SH, Jung S, Jeon j, Kim SC, Park Y. Hydrodeoxygenation of guaiacol over Pt loaded zeolitic materials. J Ind. Eng. Chem 2016; 37:18-21.

[36] Mante OD, Agblevor FA. Catalytic pyrolysis for the production of refinery-ready biocrude oils from six different biomass sources. Green Chem. 2014; 16:3364-3373.

[37] ASTM Standard E1756-08. In 2008 Annual Book of ASTM Standards, Vol. 11.05; American Society for Testing and Materials: West Conshohocken, PA, 2008.

[38] ASTM Standard E1755-01. In 2008 Annual Book of ASTM Standards, Vol. 11.05; American Society for Testing and Materials: West Conshohocken, PA, 2008.

[39] Hu X, Wang Y, Mourant D, Gunaman R, Lievens C, Chaiwat W, Gholizadeh M, Wu L, Li X, Li Ch. Polymerization on heating up of bio-oil: amodel compound study. AIChE 2013; 59: 888-900.

[40] Tanneru SK, Steele PH. Direct hydrocracking of oxidized bio-oil to hydrocarbons. Fuel 2015; 154: 268-74.

[41] Danaci S, Protasova L, Lefever J, Bedel L, Guiler R. Efficient CO_2 methanation over Ni/Al_2O_3 coated structured catalyst. Catal Today 2016; 273:234-43.

[42] Wan H, Chanudhari RV, Subramaniam B. Catalytic Hydroprocessing of p-cresol: Metal, solvent and mass transfer effect. Top Catal 2012; 55: 129- 139.

[43] Asphaug S. Catalytic hydrodeoxygenation of bio-oils with supported MoP-catalysts. TKP 4900 Thesis 2013; pp: 52-4.

[44] Shin EJ, Keane MA. Gas-phase hydrogenation/hydrogenolysis of phenol over supported nickel catalysts. Ind Eng Chem Res 2000;39:883-92.

[45] Gutierrez A, Kaila RK, Honkela ML, Slioor R, Krause AOI. Hydrodeoxygenation of guaiacol on noble metal catalysts. Catal Today 2009;147:239-46.

[46] Elliot DC, Hart TR, Neuenschwander GG, Rotness LJ, Zacher AH. Catalytic hydroprocessing of biomass fast pyrolysis bio-oil to produce hydrocarbon products. Environ Prog Sustain Energy 2009; 28: 441-9.

[47] Zhu Z, Rosendahl L, Toor SS, Yu D, Chen G. Hydrothermal liquefaction of barley straw to bio-crude oil: Effect of reaction temperature and aqueous phase recirculation. Appl Energy 2015; 137:183-92.

[48] Garcia T, Veses A, Lopez JM, Puertolas B, Perez-Ramirez J, Callen MS. Determining bio-oil composition via chemometric tools based on infrared spectroscopy. Sus Chem Eng 2017; 5:8710-8719.

[49] Durak H, Aysu T. Effects of catalysts and solvents on liquefaction of *Onopordum heteracanthum* for production of bio-oils. Bioresour Technol 2014; 166: 309-17.

[50] Mante OD, Agblevor FA, Oyama ST, McClung R. The effect of hydrothermal treatment of FCC catalysts and ZSM-5 additives in catalytic conversion of biomass. Appl Catal A: General 2012; 445: 312-20.

[51] Zhang X, Chen L, Kong W, Wang T, Zhang Q, Long J. Upgrading of bio-oil to boiler fuel by catalytic hydrotreatment and esterification in an efficient process. Energy 2015; 84:83-90.

[52] Strahan GD, Mullen CA, Boateng AA. Characterizing biomass fast pyrolysis oils by ^{13}C NMR and chemometric analysis. Energy Fuels 2011;25:5452-61.

[53] Kadarwati S, Oudenhoven S, Schagen M, Hu X, Garcia-Perez M, Kersten S, Li Ch, Westerhof R. Polymerization and cracking during the hydrotreatment of bio-oil and heavy fractions obtained by fractional condensation using Ru/C and $NiMo/Al_2O_3$ catalyst. J Anal Appl Pyrolysis 2016; 118: 136-143.

[54] Van Krevelen D. Graphical-statistical method for the study of structure and reaction process of coal. Fuel 1950;29:269-84.

CHAPTER 4

4. HYDRODEOXYGENATION OF GUAIACOL: A COMPARATIVE STUDY OF RED MUD-SUPPORTED NICKEL AND COMMERCIAL NI/SIO_2-AL_2O_3

(Applied Catalysis A: General, 2018)

1. Abstract

Upgrading of bio-oil through catalytic hydrotreating was investigated with guaiacol as a model compound. A nickel supported on red mud (Ni/RM) hydrotreating catalyst was developed and compared to the standard Ni/SiO_2-Al_2O_3 catalysts under similar experimental conditions. The Ni/RM catalyst was characterized by inductively coupled plasma atomic emission spectrometry (ICP-AES), X-ray diffraction analysis (XRD), scanning electron microscopy (SEM), BET specific surface area, and temperature programmed reduction (TPR). The effects of reaction temperature (300, 350, 400 °C) and initial hydrogen pressure (4.83 MPa (700 psi), 5.52 MPa (800 psi), and 6.21 MPa (900 psi)) on products distribution were investigated. The major products of hydrotreating process were catechol, anisole, phenol, cyclohexane, hexane, benzene, toluene, and xylene. Increasing the reaction temperature and hydrogen pressure improved HDO reactions. Complete HDO was achieved at reaction temperature of 400 °C and initial hydrogen pressure of 6.21 MPa (900 psi). Under these conditions, the selectivity to cyclohexane, benzene, toluene, and xylene over Ni/RM catalyst were 38.8, 24.5, 18.1, and 7.9% respectively, while these values were 62.2, 15.9, 8.4, and 4.5% respectively over Ni/SiO_2-Al_2O_3. Reaction network and the kinetics of guaiacol HDO were proposed according to analysis of the products. The Ni/RM catalyst was more effective for

deoxygenation reactions than hydrogenation while commercial Ni/SiO_2-Al_2O_3 was more effective for hydrogenation than deoxygenation. Thus, hydrogen consumption per gram of bio-oil was lower for the Ni/RM catalyst compared to the Ni/SiO_2-Al_2O_3. There was less hydrocracking and coke formation for the Ni/RM compared to the commercial catalyst and this resulted in higher liquid yield for the new catalyst.

2. Introduction

Biofuels are emerging as a promising substitute to fossil fuels, as they are renewable and contribute to lower CO_2 emissions [1-4]. Fast pyrolysis is an attractive thermochemical conversion process to generate alternative liquid fuels from biomaterials [5, 6]. These pyrolysis oils (crude bio-oils) are multicomponent mixtures of a large number of oxygenated compounds. However, the high oxygen content of crude bio-oils, usually 20 to 50 wt. %, results in a low heating value, poor stability, poor volatility, high viscosity and corrosiveness [7-12]. Therefore, oxygen removal from bio-oils is necessary for further application as liquid fuels.

Noble metal [13-16] and transition metal sulfide [17-20] catalysts have been studied for this purpose. Noble metals are relatively costly and they catalyze hydrogenation of aromatic rings [21, 22], which is undesirable in fuel production. Noble metal catalysts suffer from deactivation due to oxidation or hydrolysis of the active phase unless a sulfiding agent is added [1, 23-25] which increases the risk of product contamination. Thus, it is vital to find alternative catalysts for HDO applications in bio-oil upgrading.

Red mud (RM) is a caustic by-product of processing of bauxite that is generated in the industrial production of alumina using the Bayer process [26]. There are many problems with managing RM slurry including costly maintenance of RM ponds, risk of caustic pollutants for all living organisms, and leakage of alkaline contaminants into groundwater resources [26, 27]. The main chemical components of RM are Fe_2O_3, Al_2O_3, SiO_2, CaO, Na_2O, and a number of minor metal oxides of Cr, V, S, Ni, Cu, Mn, Zn, Mg etc. [27]. RM has been tested as catalyst for various applications, including pyrolysis of biomass [28, 29], hydrogenation and liquefaction of coal and biomass [30-35], hydrodechlorination and desulfurization reactions [36-38], methanogenesis reaction [39] and exhaust gas clean-up [40, 41]. The RM conversion into a value added product such as heterogeneous catalyst will be a desirable technology for the final fate of the residue.

Bio-oil is a complicated mixture of more than two hundred compounds such as aromatics, aliphatics, aldehydes, ketones, and ethers. Therefore it is difficult to interpret the HDO results of the actual bio-oil [12]. Although there are too many cross-interactions between bio-oil compounds, guaiacol is a suitable model compound representing the decomposition products of lignin pyrolysis, as it contains phenolic hydroxyl and methoxy groups like many degradation products of lignocellulose [2, 3, 42, 43]. It has been reported that incorporation of Mo and V in Ni/TiO_2 catalyst improved the catalyst performance for the HDO of guaiacol. In aqueous medium, $Ni\text{-}V/TiO_2$ was more effective resulting in better guaiacol conversion than Ni-Mo/TiO2 and showing more tolerance for water [44]. Ni metal was effective for ring opening activity while Co favored deoxygenation activity. The Ni catalyst favored the multiple hydrogenolysis of C-C bond, leading to carbon loss via methanization. Cobalt not only facilitated the

reduction and dispersion of nickel metal oxides but also enhanced the HDO activity of bimetallic Ni–Co catalyst [45]. Hydrodeoxygenation of guaiacol using silica alumina supported Ni-Pd and Ni-Pt overlayer catalysts under atmospheric pressure showed that Pd and Pt active sites of overlayer catalysts significantly enhanced deoxygenation activity and the BTX selectivity could be up to 80% on Ni-Pd overlayer catalyst [46]. HDO of guaiacol over NiB/SiO_2-Al_2O_3 and Ni/SiO_2-Al2O_3 catalysts showed that the conversion of guaiacol and the selectivity to cyclohexane were much higher on the former than the latter [47]. However, SiO_2-supported Ni-Mo bimetallic catalyst showed high selectivity towards AR-O bond cleavage in the HDO reactions of anisole, phenol and guaiacol, giving BTX selectivity more than 96% [48]. Lately, Mora-Vergara et al. [49] showed that the addition of potassium to alumina-supported NiMo and CoMo catalysts promoted selectivity to deoxygenated compounds in the HDO of guaiacol.

A potential method of reducing the cost of HDO process, is the development of new HDO catalysts from low cost materials. Red mud has interesting properties such as active components and relatively large surface area. The main objective of this research work is to evaluate the performance of RM-supported nickel catalyst for hydrodeoxygenation of bio-oils and guaiacol was used as a model compound for biomass pyrolysis oil. In view of the stability and poisoning resistance of RM, it can be a catalyst support for Ni in HDO process and it would be potentially much more cost-effective in comparison with other catalyst supports such as Al_2O_3, SiO_2, and TiO_2 that require complicated preparation procedures. In this paper the performance of the Ni/RM is compared with commercial Ni/SiO_2-Al_2O_3 obtained from Sigma Aldrich.

3. Material and methods

3.1. Material

Guaiacol, anisole, catechol, and nickel nitrate hexa hydrate ($Ni(NO_3).6H_2O$) were purchased from Alfa Aesar (Haverhill, MA, USA). Cyclohexane and toluene were bought from Pharmco-Aaper (Brookfield, CT, USA). Commercial nickel on silica/alumina (~65% wt. % Ni loading) catalyst powder, benzene, and phenol were purchased from Sigma Aldrich (St. Louis, MO, USA). Hexane and xylene were obtained from Fisher Scientific (Hampton, NH, USA). All chemicals were analytical grade and were used as received without any further purification. High purity (99%) hydrogen (Airgas, PA, USA) was used for HDO experiments.

3.2. Preparation and characterization of Ni/RM catalyst

Ni/RM catalysts were prepared at 40 wt. % nickel metal loading using wet impregnation method [50, 51]. The calculated amount of $Ni(NO_3).6H_2O$ equivalent to 40 wt. % nickel metal loading was dissolved in 100 ml deionized water and then mixed with red mud (particle size<90 μm). The mixture was heated to 70 °C and continuously stirred for 5 hours to prepare the catalyst precursor. The catalyst precursor was dried at 105 °C for 10 hours and then calcined in air at 620 °C in a muffle furnace (Thermo Scientific, Inc., Waltham, MA, USA) for 5 hours. The calcined material was reduced for 6 hours at 450 °C using a reducing gas mixture of 10% H_2 and 90% N_2 at flow rate of 20 ml/min to obtain the final catalyst.

The Brunauer-Emmet-Teller (BET) specific surface area of the catalysts were determined on a MS-16 BET analyzer (Quantachrome Instruments, Boynton Beach, FL,

USA). About 0.1 g catalyst sample was used in each measurement. Prior to the analysis, the catalyst samples were milled into fine powder using a SPEX Certiprep 6750 cryogenic miller (Metuchen, NJ, USA). All samples were degassed at 300 °C for 4 hours prior to duplicate measurements. A porous Al_2O_3 standard was measured along with each run to ensure consistency between the different samples.

Metal loading determination was carried out using inductively coupled plasma atomic emission spectrometry (ICP-AES) analysis. For this purpose, 0.5 g catalyst sample was digested in nitric acid at 95 °C for 1 h. Then 12 ml, 30 wt. % hydrogen peroxide was added to the digestion tube and cooled to room temperature [52]. The extracts were measured using a Thermo iCAP 6300 ICP-OES Inductively-Coupled Plasma Spectrophotometer (Thermo Fisher Scientific, Waltham, MA, USA) with Optical Emission.

Thermo gravimetric-temperature programmed reduction (TG-TPR) studies were carried out using a TGA Q500 (TA Instruments, Lindon, UT, USA). Twenty-five milligrams of catalyst (calcined form) was heated in a flow of 10% H_2 / 90% N_2 (20 ml/min) from room temperature to 700 °C at a heating rate of 10 °C/min. Hydrogen uptake was monitored by the change in sample weight according to the plot of derivative weight vs. temperature.

X-ray powder diffraction (XRD) analyses were carried out by Hazen Research Inc. (Golden, CO, USA). The samples were ground in a mortar and pestle with isopropyl alcohol and analyzed using a Bruker D8 Advance with Davinci design and a Lynxeye detector. The diffraction pattern was measured in the interval from 5 to 85 in 2Θ using a 0.02 step size and 40 s of counting time.

Scanning electron microscopy (SEM) analysis was conducted on a FEI Quanta FEG-650 (Thermo Fisher Scientific, MA, USA). For preparation of the specimens a small amount of catalyst was placed on a two-sided sticky tape resting on an aluminum holder and observed at different magnifications. Images were recorded using low vacuum secondary electron (LFD) detector.

3.3. Hydrodeoxygenation (HDO) experiments

All experiments were conducted in a Parr Series 4560 300 mL autoclave reactor (Parr Instruments, Moline, IL, USA). This reactor had a variable speed magnetic drive and turbine agitator. A temperature sensor, immersed in the reactor content, was used to measure the liquid temperature. The reaction temperature was maintained at its desired value with an accuracy of ±1 °C. The setup had an electrically heated jacket to ensure isothermal conditions. The temperature and speed of agitation were controlled by using a Parr 4848 controller. In each experiment, the reactor was charged with guaiacol (30 g) and catalyst (4.5 g). The reactor was then purged with N_2 to ensure an inert atmosphere. The reactor was then charged with high purity hydrogen supplied from a reservoir tank to desired pressures of 4.83, 5.52, or 6.21 MPa (700, 800, or 900 psi) via a pressure regulator. A gas sample was taken from a gas release valve from the gas sampling port for gas analysis when the reactor was at room temperature. The reactor was then heated to reaction temperature (300, 350, or 400 °C) at heating rate of 15 °C/min. The reaction time was recorded when the set temperature was reached. The reactor content was stirred at the desired speed of agitation (~1000 rpm) for all experiments. Seven liquid samples were collected at fixed time intervals for kinetic studies. Every time, a sample volume

equal to 0.3 cm^3 was collected. The change in volume of liquid inside the reactor was negligible. After the desired reaction time (30 minute), the reactor was cooled to room temperature using the internal cooling coil and an external air fan simultaneously. A gas sample was collected in a tedlar bag for gas analysis when the reactor was cooled to room temperature. The reproducibility of experiments was checked and the error in all experimental measurements was found to be less than 3%.

In a blank experiment (without catalyst) 30 g of guaiacol was charged into the reactor and the reactor was pressurized to 6.2 MPa (900 psi) with hydrogen and allowed to react for 30 minutes at 400 ° C. All experiments were conducted in triplicate.

3.4. Analysis of HDO products

Hydrogen consumption, gas analysis, and product yields were determined as described in previous work [12]. The liquid products of HDO experiments were analyzed by HPLC (Shimadzu Scientific, Columbia, MD) using a RID-10A detector and a Kromasil 100-5-C18 column obtained from AkzoNobel (Amsterdam, Netherlands). The HPLC was equipped with a LC-10AT pump, SCL-10Avp controller, and SIL-10A autosampler. CLASS-VP 7.3 SP1 software was used to analyze HPLC chromatograms. A CTO-10A column oven was used to maintain the column temperature at 55 °C during the analysis. The injection volume was 0.25 µl and acetonitrile at flow rate of 0.6 ml/min was used as the mobile phase. Data acquisition time was 60 minutes for all analyses.

The liquid samples were analyzed for guaiacol, anisole, catechol, phenol, cyclohexane, hexane, benzene, toluene, and xylene. To quantify the amount of each compound, five solutions of 20, 40, 60, 80, and 100 wt. % of each compound were

prepared and injected to HPLC system and peak area vs. concentration was plotted to obtain the calibration curve of the compounds.

The elemental composition of HDO products were determined using ThermoFischer Scientific Flash 2000 organic elemental analyzer (ThermoFisher Scientific,Waltham, MA, USA), and the oxygen content was calculated by difference according to ASTM D5291.

Conversion of guaiacol and product selectivity were calculated using equations (1) and (2) respectively [53]:

$$Conversion\ \% = \frac{Moles\ of\ guaiacol\ reacted}{Moles\ guaiacol\ fed} \times 100 \qquad (1)$$

$$C_p\ Selectivity\ \% = \frac{moles\ C_p}{\sum moles\ C_p} \times 100 \qquad (2)$$

Where C_p represents the content of products.

Kinetic studies using integral method was perform to estimate the reaction rate equations according to equation (3) [54].

$$-r_G = \frac{dC_G}{dt} = k.{C_G}^n \qquad (3)$$

Where r_G is the rate of disappearance of guaiacol, C_G is the concentration of guaiacol at time *t*, *k* is the reaction rate constant and *n* is the reaction order.

The water content of the aqueous products were determined by Karl-Fischer titration method using Hydranal® -composite 5 solution. A Metrohm 701KF Titrino and 703 titration stand setup (Brinkmann Instruments, Riverview, FL, USA) were used for the volumetric Karl Fischer titration.

4. Results and discussion

4.1. Characterization of Ni/RM catalyst

The BET specific surface area of RM support (calcined form) was relatively low (37.5 m^2/g), but the reduction of the calcined RM increased its specific surface area to 54.3 m^2/g. The increase in specific surface area was attributed to reduction of some metallic oxides.

The specific surface area of the Ni/RM catalyst precursor (calcined form) was 51.3 m^2/g while after activation by reduction, the BET specific surface area increased to 79.3 m^2/g. The increase in BET specific surface area after the reduction was attributed to the pores that were created in the catalyst precursor associated with reduction of NiO to Ni [55-58]. These results are in agreement with those reported in literature [59].

The ICP analysis of the RM and 40%Ni/RM catalyst showed that the major metals present in RM were Al, Ca, Fe, Na, Si and Ti and trace amounts of other metals such as As, Cd, Cu, Mo, Zn etc. (Table 4.1). The Ni content of the red mud was negligible but after the impregnation, the Ni content was 40.8%, which was close to the estimated amount incorporated. The Ni loading of the commercial Ni/SiO_2-Al_2O_3 catalyst was 63.3% (Table 4.1) which was close to the 65 wt. % stated on the sample bottle by the manufacturer (Sigma Aldrich).

TG-TPR was performed to investigate the reducibility of nickel oxide, RM support, and the interaction between nickel and the RM support. The TPR profile of RM showed three major reduction peaks at 279.9, 542.7, and 694.6 °C (Fig. B.1 in Appendix B). The peak at 279.89 °C could be due to the reduction of Fe_2O_3 to Fe_3O_4 and the

unresolved peaks centered at 542.68 °C and 694.6 °C could be due to reduction of Fe_3O_4 to FeO and then to elemental Fe [27].

Table 4. 1: ICP analysis of RM support, Ni/RM, and Ni/SiO_2-Al_2O_3catalysts.

Metal (wt. %)	RM	Ni/RM	Ni/SiO_2-Al_2O_3
Al	9.08	4.44	16.17
Ca	1.20	0.65	0.25
Fe	21.56	9.47	1.21
K	0.03	0.02	0.01
Mg	0.07	0.04	0.07
Na	7.17	3.51	0.05
Ni	<0.01	40.8	63.3
P	0.03	0.01	0.02
S	0.10	0.06	0.04
Si	4.35	2.53	12.71
Ti	4.10	1.53	0.35
Metal (mg/kg)	RM	Ni/RM	Ni/SiO_2-Al_2O_3
As	0.87	<DL*	<DL
B	9.41	0.85	<DL
Ba	10.4	4.55	7.27
Cd	5.79	3.37	<DL
Co	278	12.3	226
Cr	245	132	5.69
Cu	3.13	<DL	21.3
Mn	<DL	<DL	24.1
Mo	1.62	0.48	1.06
Pb	156	7.09	140
Se	<DL	<DL	<DL
Sr	23.1	2.28	9.57
Ti	<DL	<DL	<DL
Zn	2105	26.1	2994

* Less than detection limit (0.05 mg/kg)

The TPR profiles of Ni/RM catalyst showed two major reduction peaks at 442.22 and 583.11 °C (Fig. B.2 in Appendix B). The peak at 442.22 °C was attributed to reduction of nickel oxide, but this peak also indicated a possible interaction with RM

support since its intensity increased with increasing Ni content (data not reported) and its reduction temperature shifted towards that of nickel oxide (347.89 °C according to Fig. B.3 in Appendix B). This observation was in agreement with Jeangros et al. who observed interaction between SiO_2 and NiO during the reduction of NiO to Ni [57]. The peak at 583.11 °C was attributed to the reduction of RM components (mostly Fe_2O_3) since its intensity decreased as Ni loading increased (data not provided). Ni supported on Fe_2O_3 was prepared using wet impregnation method to investigate the effect of the presence of Fe_2O_3 (which was the major RM component) on the reducibility of Ni. The TPR profile of NiO/Fe_2O_3 (Fig. B.4 in Appendix B) showed interaction between NiO and Fe_2O_3 at 390.03 °C. The peak at 522.67 °C was ascribed to reduction of Fe_2O_3 to magnetite. These results suggested that, besides Fe_2O_3, Ni interacted with other components of the RM.

Fig. 4.1 shows the XRD pattern of fresh Ni/RM catalyst. Distinct sharp peaks observed at 2Θ 52.2°, 61° were attributed to elemental Ni from the reduction of NiO. The detection of NiO signal at 2Θ 43.7°, 50.9°, and 74.7° showed that nickel oxide was not completely reduced to elemental Ni after treatment with H_2 (Fig. 4.1) which is in agreement with Jeangros et al (2013) who reported that total NiO reduction did not occur until the reduction temperatures was above 600 C [57]. Detection of magnetite (Fe_3O_4) peaks at 2Θ 21.6°, 35.1°, 41.7°, and 74.3° were due to reduction of hematite (Fe_2O_3) that was present in the original RM [28].

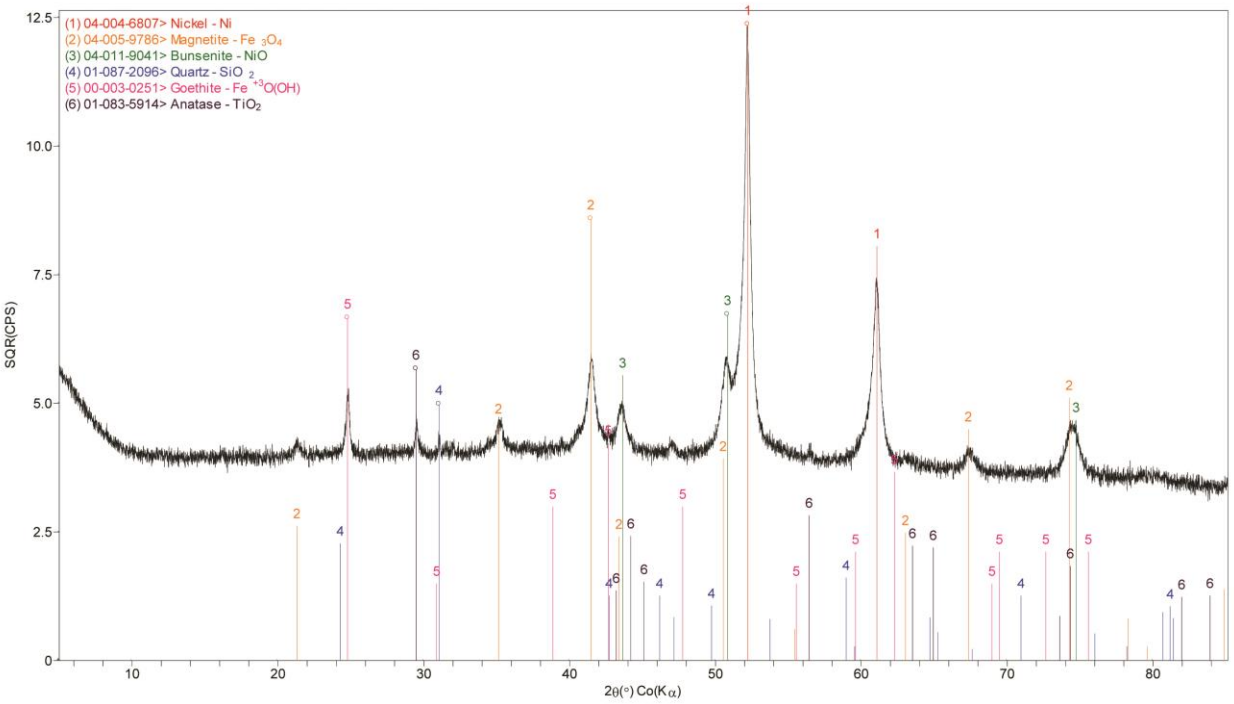

Fig. 4. 1: XRD pattern of fresh Ni/RM catalyst.

XRD pattern of used Ni/RM catalyst (Fig. 4.2) showed stronger NiO peaks compared to fresh catalyst suggesting that Ni was partially oxidized during HDO. This could be one reason for the partial deactivation of the catalyst. Additionally, iron nickel oxide (trevorite) (Fe_2NiO_4) peaks were also detected after HDO that could be another reason for partial deactivation of active Ni sites. The detection of weak elemental nickel peaks (2Θ 52.1° and 61°) in the used catalyst suggested that the catalyst was only partially deactivated.

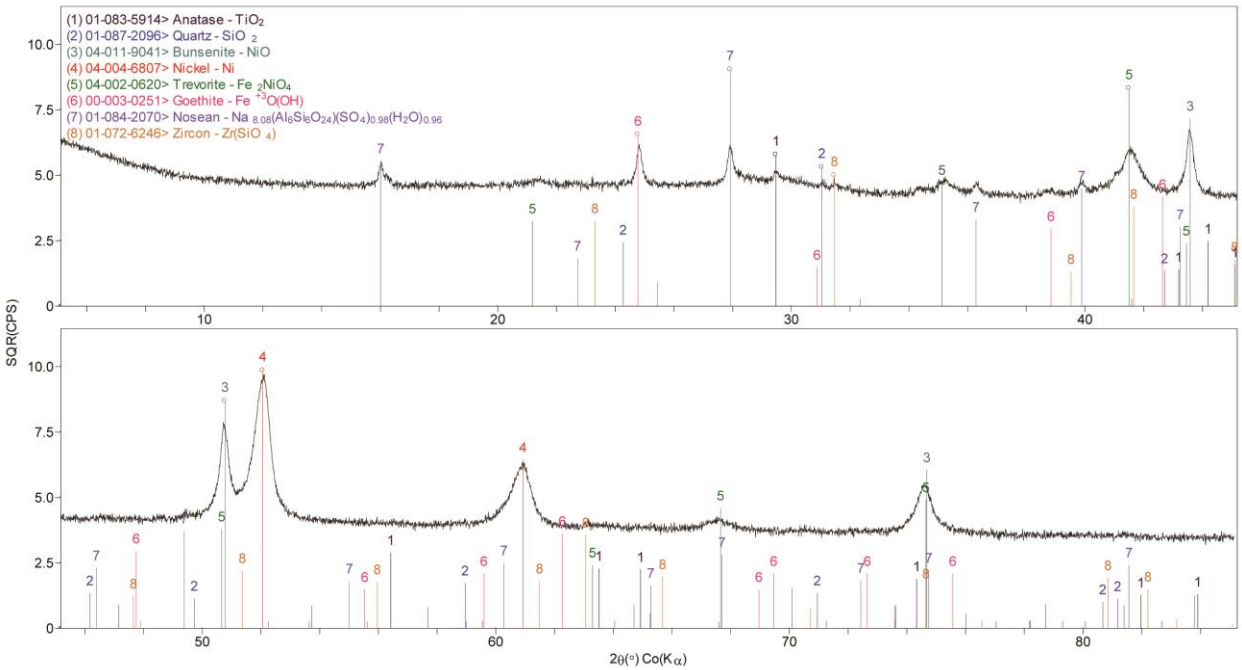

Fig. 4. 2: XRD pattern of used Ni/RM catalyst.

In order to recycle the catalyst, the used catalyst was regenerated in muffle furnace to burn off the deposited carbonaceous material (coke) at 400 °C for 4 h. The XRD pattern of the regenerated catalyst (Fig. 4.3) showed strong NiO diffraction peaks at 2Ɵ 43.9°, 50.8°, and 75°, which was due to the oxidation of nickel to NiO under heat treatment in air. Existence of hematite (Fe_2O_3) diffraction peaks in regenerated catalyst was ascribed to oxidation of magnetite. Furthermore, it was interesting to note that weak elemental Ni diffraction peaks were present in the XRD pattern of the regenerated catalyst (Fig. 4.3). This suggested that some Ni particles in the interior of the RM were not exposed to oxygen due to mass transfer limitations.

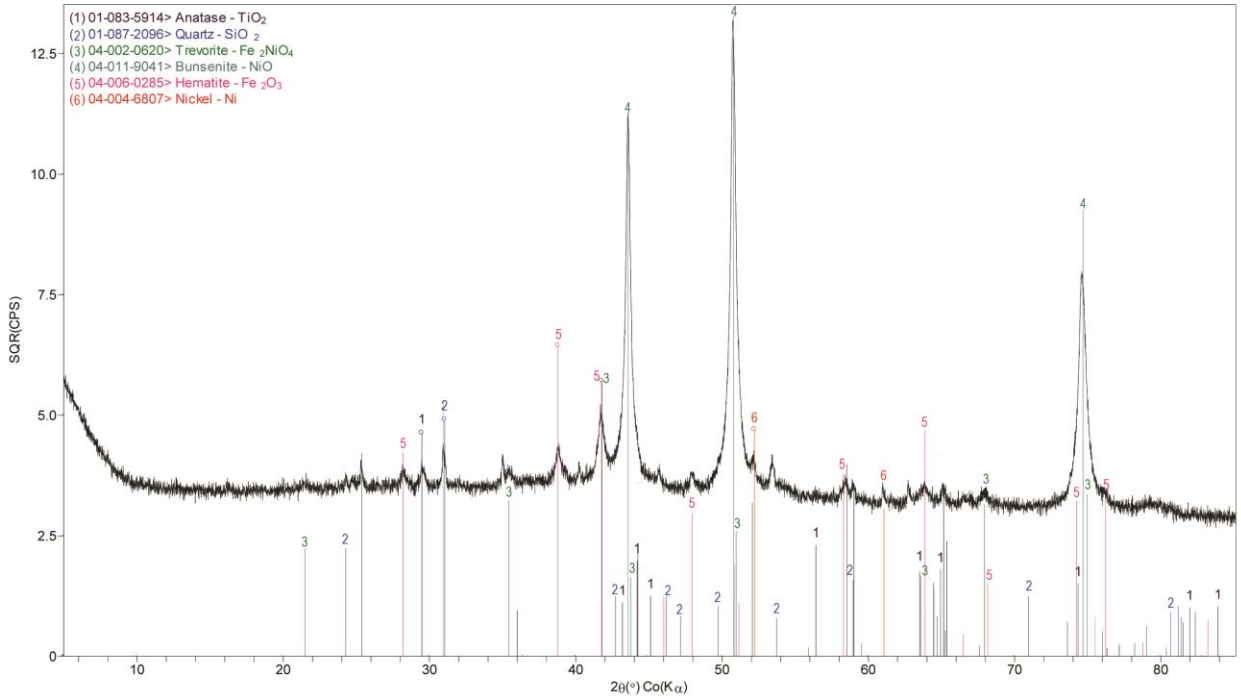

Fig. 4. 3: XRD pattern of regenerated Ni/RM catalyst.

The regenerated catalyst was then activated by reduction in H_2. The XRD pattern of the regenerated and activated catalyst (Fig. 4.4) showed similar diffraction peaks as the fresh catalyst (Fig. 4.1) suggesting complete regenerability of the catalyst, which was in contrast to the commercial catalyst that could not be regenerated using similar procedure. More detailed information on catalytic activity of the used catalyst and the recycled catalyst are discussed in section 3.6.

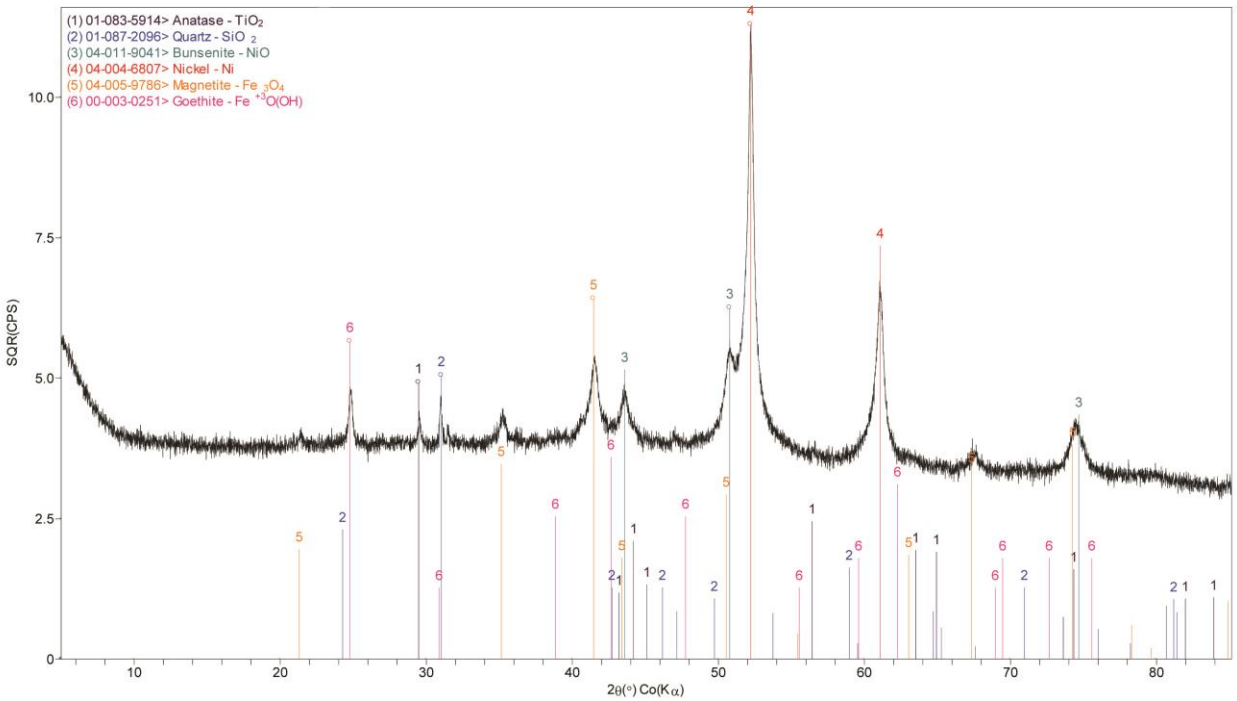

Fig. 4. 4: XRD pattern of regenerated and reduced Ni/RM catalyst.

The surface morphology of the catalyst was studied by using scanning electron microscopy (SEM). The SEM images of the Red Mud support, Ni/RM catalyst precursor (calcined form), fresh Ni/RM catalyst (reduced form), and used 40% Ni/RM catalyst are presented in Fig. 4.5. In the case of RM support (Fig. 4.5a), in addition to amorphous looking particles, crossed cocentric discs and spherical-shaped particles were observed. The SEM image of Ni/RM catalyst in calcined form is shown in Fig. 4.5b. Ni particles with relatively uniform morphology and approximate mean diameter of 90 nm were dispersed on the surface of RM components in the case of activated Ni/RM (Fig. 4.5c). The SEM picture for the used catalyst (Fig. 4.5d) showed that the catalyst was coated with coke after HDO process, which could inhibit the hydrogen transfer and partially deactivate the catalyst.

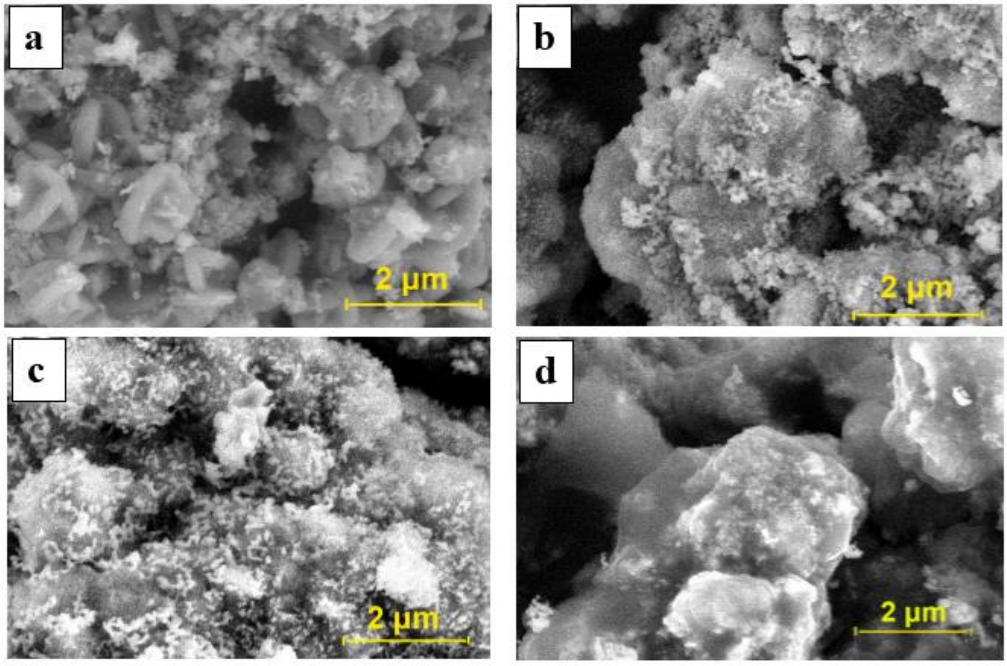

Fig. 4. 5: SEM images of a) Red Mud support, b) Ni/RM (calcined form), c) Ni/RM (reduced form), d) Used Ni/RM catalyst.

4.2. HDO products yield distribution and selectivity

In the blank experiment without catalyst, the guaiacol did not convert to any other compounds and neither did it produce any gas nor coke, hence the reactor was not catalytically active and did not influence the HDO experiments.

The major HDO liquid products using the nickel catalysts were catechol, anisole, phenol, cyclohexane, hexane, benzene, toluene, and xylene. CO, CO_2 and C_1—C_5 hydrocarbon gases as well as water and coke. When RM was treated using similar reaction conditions as Ni/RM catalyst and used in HDO experiment, the guaiacol conversion was only 2.7%. A relatively high amount of coke was formed (18.3 wt. %) and 96.3 wt. % of the final liquid products was unreacted guaiacol and small amounts of benzene, phenol, and anisole. The results of HDO experiments using RM support are

summarized in Table B.1 in Appendix B. Therefore the RM support contribution to HDO process was very low. The effects of reaction temperature and hydrogen pressure are discussed in subsections 3.2.1 and 3.2.2 respectively.

4.2.1. Reaction temperature effect

Fig. 4.6 shows the overall products yield distribution of guaiacol HDO as a function of reaction temperature. At all reaction temperatures, Ni/RM catalyst produced higher organic liquid yield compared to Ni/SiO_2-Al_2O_3. In contrast, higher amounts of gas and coke were formed in the case of Ni/SiO_2-Al_2O_3, which could be due to the higher specific surface area and higher Ni content of the catalyst. The aqueous liquid yield at reaction temperatures of 300, 350, and 400 °C were 9.8, 12.4 and 16.7 % respectively for Ni/RM catalyst while those for Ni/SiO_2-Al_2O_3 were 11.3, 15.6, and 21.1 % respectively. The higher aqueous liquid yield was due to increased methanation of carbon dioxide over the commercial Ni/SiO_2-Al_2O_3 (Table 4.2) [12, 60]. The aqueous phase was 99.9 wt. % H_2O.

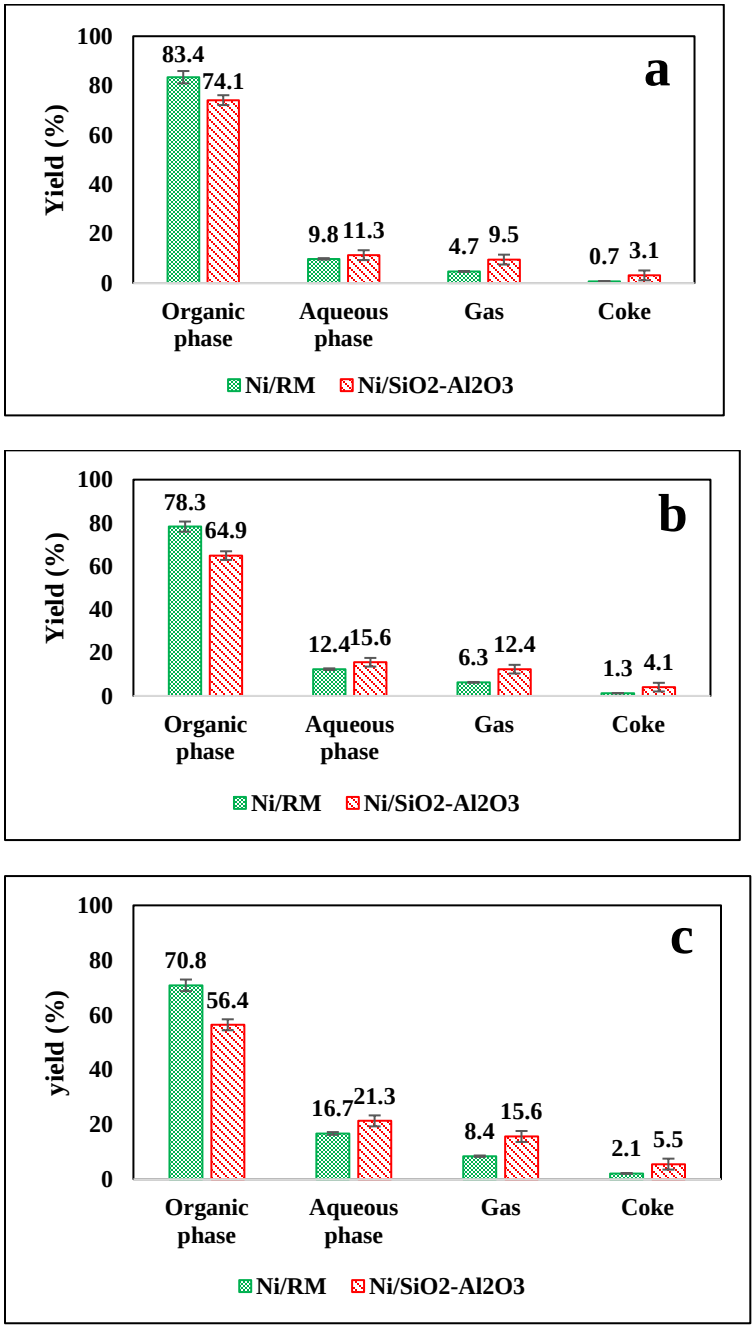

Fig. 4. 6: Products yield distribution using Ni/RM and Ni/SiO_2-Al_2O_3 at a) 300 °C, b) 350 °C, and c) 400 °C (error bars show the standard deviation of three measurements).

Table 4. 2: Hydrogen consumption and gas composition of guaiacol HDO at different temperatures (the initial hydrogen pressure was 6.21 MPa) (the standard deviation of all data were ± 0.05).

	Temperature (°C)					
	300		350		400	
Catalyst	Ni/RM	Ni/SiO_2-Al_2O_3	Ni/RM	Ni/SiO_2-Al_2O_3	Ni/RM	Ni/SiO_2-Al_2O_3
H_2 Consumption (mol H_2/kg guaiacol)	0.19	0.24	0.29	0.38	0.37	0.45
Gas composition (mol %)						
CO	6.8	0	5.4	0	4.4	0
CO_2	10.4	8.5	9.8	6.2	8.2	2.3
CH_4	42.2	57.3	49.6	66.9	55.8	71.5
C_2H_6	9.3	7.4	11.5	9.6	13.4	11.6
C_3H_8	17.3	15.4	11.6	9.8	9.6	8.4
C_4H_{10}	9.2	6.6	7.4	4.3	5.3	3.2
C_5H_{12}	4.1	3.7	3.7	2.1	2.1	1.7

Pressure changes during the HDO of guaiacol at different reaction temperatures are shown in Fig. B.5 (Appendix B). The total pressure profile using Ni/SiO_2-Al_2O_3 fell below the pressure profile of Ni/RM catalyst due to higher hydrogen consumption in the case of the commercial catalyst (Table 4.2).

Figs. 4.7 and 4.8 show the HDO product selectivity and guaiacol conversion as a function of reaction temperature for Ni/RM and Ni/SiO_2-Al_2O_3 catalysts respectively. Increasing the reaction temperature improved the conversion of guaiacol in all HDO experiments. At reaction temperatures of 300 and 350 °C; catechol, anisole, and phenol were produced due to demethylation, dehydroxylation, and demethoxylation of guaiacol respectively, however the selectivity to these compounds were lower for Ni/RM compared to Ni/SiO_2-Al_2O_3 (Figs. 4.7 and 4.8). In contrast, the selectivity to benzene, toluene, and xylene (BTX) was lower for Ni/SiO_2-Al_2O_3 suggesting that Ni/RM was more effective in hydrodeoxygenation than Ni/SiO_2-Al_2O_3.

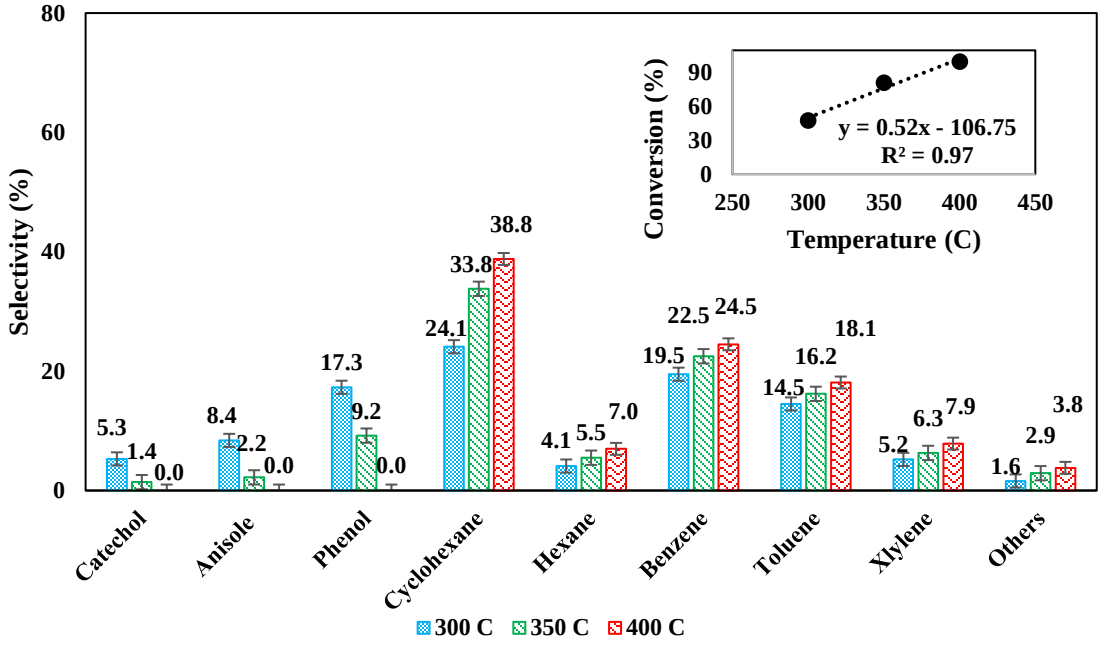

Fig. 4. 7: Guaiacol conversion and products selectivity at different temperatures using Ni/RM catalyst (error bars show the standard deviation of three measurements).

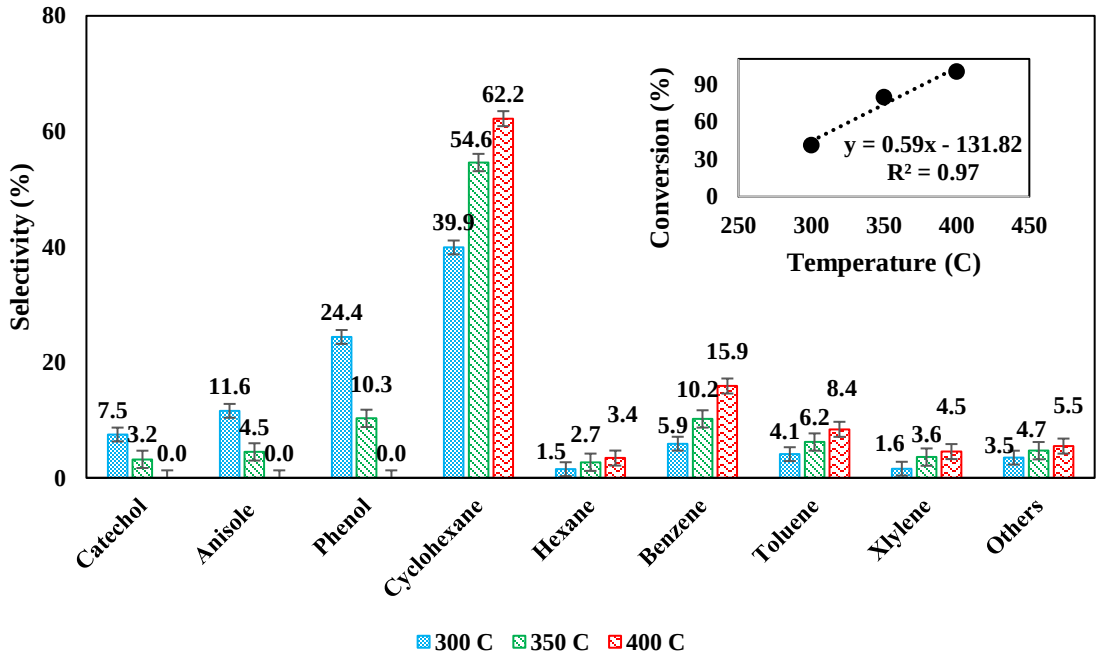

Fig. 4. 8: Guaiacol conversion and products selectivity at different temperatures using Ni/SiO_2-Al_2O_3 catalyst (error bars show the standard deviation of three measurements).

When the reaction temperature was increased from 300 °C to 400 °C the selectivity to oxygenated intermediates (catechol, anisole, and phenol) decreased significantly indicating that guaiacol was first converted to catechol, anisole, and phenol via demethylation, dehydroxylation, and demethoxylation, and subsequently to cyclohexane, benzene, toluene, and xylene. Hexane was also obtained in relatively lower selectivity as a result of ring opening. At reaction temperature of 400 °C complete hydrodeoxygenation of guaiacol was achieved with both catalysts. However, Ni/SiO_2-Al_2O_3 was more effective in hydrogenation of aromatic ring compared to Ni/RM resulting in benzene, toluene, and xylene selectivities of 24.5, 17.1, and 7.9 % respectively for Ni/RM while these values were 15.9, 8.4, and 4.5 % respectively for Ni/SiO_2-Al_2O_3. Higher rates of hydrogenation reaction over Ni/SiO_2-Al_2O_3 resulted in cyclohexane selectivity of 62.2 % versus 38.8 % for Ni/RM at 400 °C (Figs. 4.7 and 4.8). This result is also reflected in higher hydrogen consumption over Ni/SiO_2-Al_2O_3 compared to Ni/RM (Table 4.2). The major gas product was methane for both catalysts.

4.2.2. Hydrogen pressure effect

The influence of hydrogen pressure on the guaiacol HDO products yield distribution is shown in Fig. 4.9. Increasing the initial hydrogen pressure from 4.83 to 6.21 MPa increased the liquid product yield for both catalysts, however the organic liquid yield was much higher over Ni/RM. The increase in organic liquid yield could be due to an increase in concentration of adsorbed hydrogen on the catalyst surface and an increase in the amount of dissolved H_2 in the organic phase, as hydrogen pressure was increased

[12, 61, 62]. For Ni/RM, the gas yield decreased from 23.7% to 8.4% over this pressure range while the gas yield decreased from 41.4% to 16.6% for Ni/SiO_2-Al_2O_3. The coke yield decreased from 6.4% to 2.1% for Ni/RM and from 9.5% to 5.5% using Ni/SiO_2-Al_2O_3 (Fig. 4.9). This would suggest that higher levels of hydrogen pressure helped HDO reactions to predominate cracking and (re)polymerization reactions that produce gas and coke [63]. The increase in aqueous liquid yield by increasing hydrogen pressure could also confirm that higher H_2 pressures favored HDO reactions. Pressure profile during the HDO of guaiacol at different hydrogen pressures are shown in Fig. B.6 in Appendix B. The reaction pressure in the case of Ni/SiO_2-Al_2O_3 was lower than that of Ni/RM due to higher hydrogen consumption by the commercial catalyst (Table 4.3).

Table 4. 3: Hydrogen consumption and gas composition of guaiacol HDO at different pressures (the reaction temperature was 400 °C)(the standard deviation of all data were ± 0.05).

	Pressure (MPa)					
	4.83		5.52		6.21	
Catalyst	Ni/RM	Ni/SiO_2-Al_2O_3	Ni/RM	Ni/SiO_2-Al_2O_3	Ni/RM	Ni/SiO_2-Al_2O_3
H_2 Consumption (mol H_2/kg guaiacol)	0.22	0.29	0.31	0.36	0.39	0.45
Gas composition (mol %)						
CO	10.4	0	7.6	0	4.4	0
CO_2	18.7	14.4	10.1	7.7	8.2	2.3
CH_4	42.8	61.3	51.9	68.6	55.8	71.5
C_2H_6	10.2	8.7	11.5	9.3	13.4	11.6
C_3H_8	7.8	6.6	8.2	6.5	9.6	8.4
C_4H_{10}	5.7	4.2	5.5	3.7	5.3	3.2
C_5H_{12}	4.3	2.8	3.3	2.4	2.1	1.7

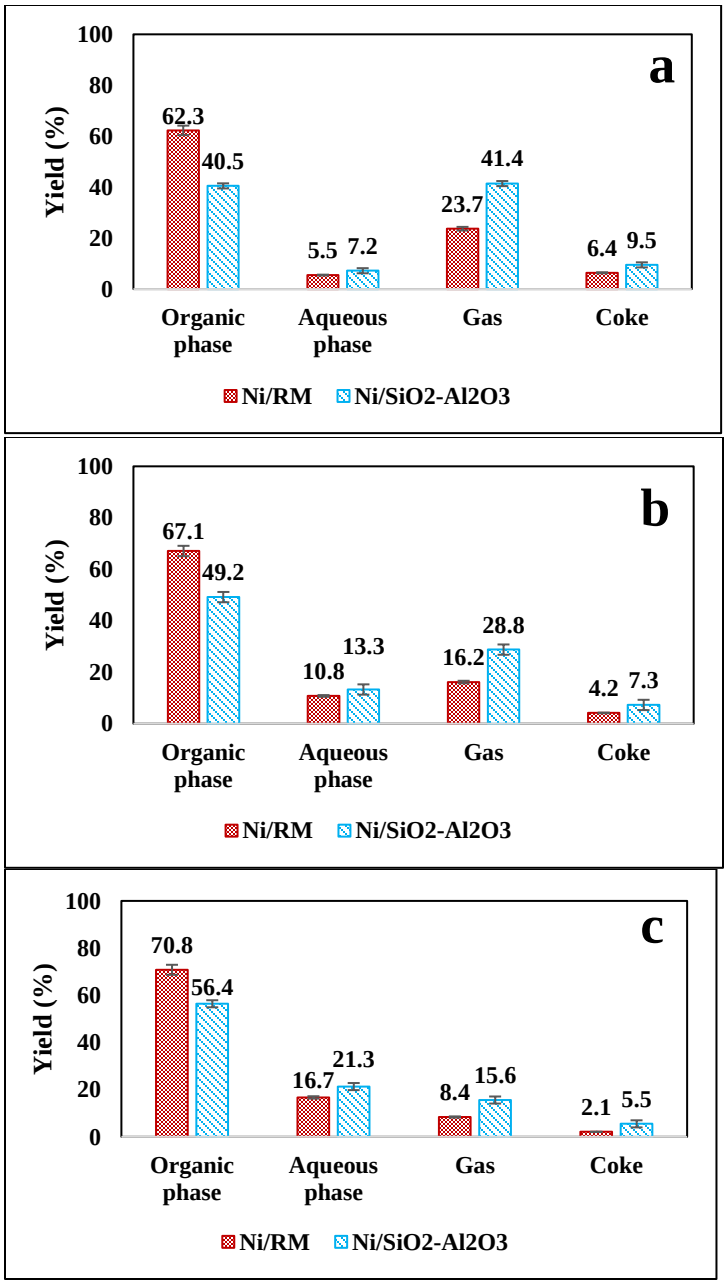

Fig. 4. 9: Products yield distribution using Ni/RM and Ni/SiO_2-Al_2O_3 at a) 4.83 MPa (700 psi), b) 5.52 MPa (800 psi), and c) 6.21 MPa (900 psi) (error bars show the standard deviation of three measurements).

During the catalytic hydrotreatment processes, multiple reactions may occur, including hydrogenation, hydrogenolysis, hydrodeoxygenation, hydrocracking, and

polymerization [5, 9]. Hydrogenation for ring saturation, hydrocracking for gasification, and methanation made hydrogen consumption exceed the deoxygenated stoichiometric ratio [9]. In order to reduce the hydrogen consumption, the direct deoxygenation without ring saturation is desirable in HDO. Figs. 4.10 and 4.11 show the guaiacol conversion and evolution of products as a function of hydrogen pressure over Ni/RM and Ni/SiO_2-Al_2O_3 respectively. At initial H_2 pressures of 4.83 MPa and 5.52 MPa, oxygenated intermediates (catechol, anisole, and phenol) were produced while these compounds were completely deoxygenated when the initial H_2 pressure was 6.21 MPa. However, higher selectivity to benzene, toluene, and xylene were observed (24.5, 18.1, and 7.9% respectively) for Ni/RM compared to Ni/SiO_2-Al_2O_3 (15.9, 8.4, and 4.5% respectively) resulting in less hydrogen consumption in the case of Ni/RM (Table 4.3). This result was attributed to higher ring hydrogenation activity of Ni/SiO_2-Al_2O_3 since this catalyst had higher Ni loading (63.3% according to Table 4.1) than Ni/RM (40%). Furthermore, higher catalytic activity of Ni/SiO_2-Al_2O_3 led to higher cyclohexane selectivity of 62.2 % (Fig 4.11) because of the hydrogenation of the aromatic ring and demethylation reaction resulting in lower BTX selectivity.

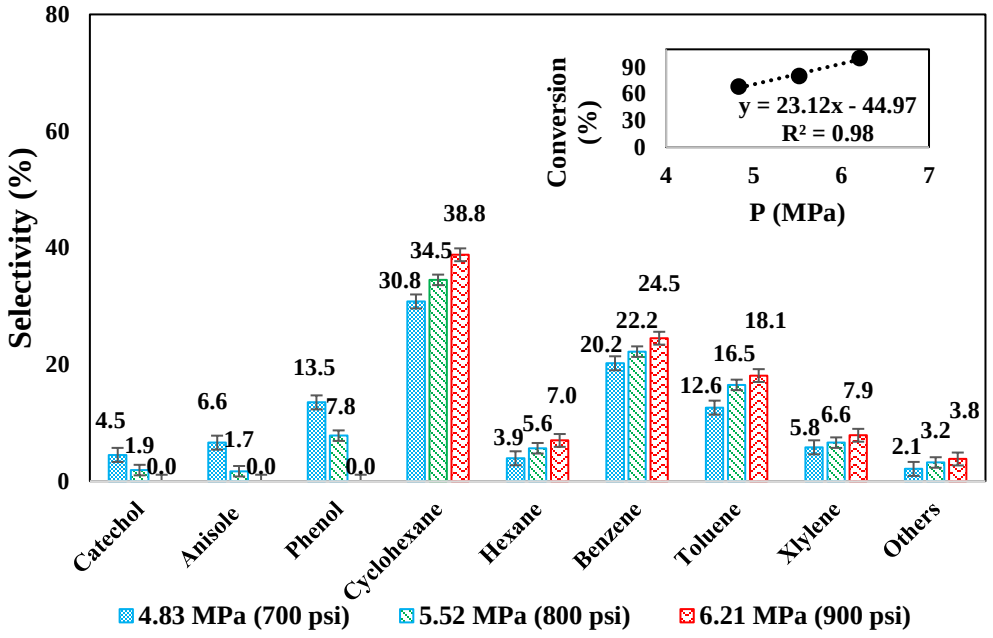

Fig. 4. 10: Guaiacol conversion and products selectivity at different hydrogen pressures using Ni/RM catalyst (error bars show the standard deviation of three measurements).

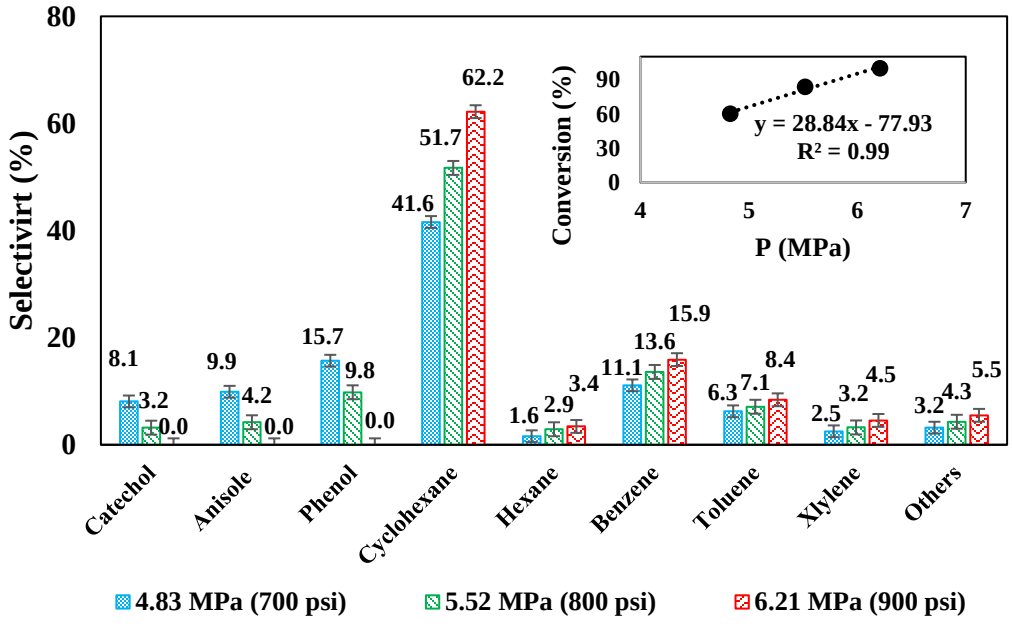

Fig. 4. 11: Guaiacol conversion and products selectivity at different hydrogen pressures using Ni/SiO_2-Al_2O_3 catalyst (error bars show the standard deviation of three measurements).

The major gas product for both catalysts was methane (Table 4.3) because of demethylation, methanation and cracking reactions. It is interesting to note that at all temperatures and pressures, the Ni/RM produced CO, whereas the Ni/SiO2-Al_2O_3 did not produce any CO probably because of the methanation reaction that was stronger in this catalyst than the Ni/RM.

Guaiacol HDO liquid products (organic and aqueous phases) were analyzed for Ni using ICP in order to investigate leaching effect. The Ni content of HDO products were below detection limit (0.05 mg/kg) suggesting that Ni did not leach into the HDO products (data not reported).

4.3. Evaluation of HDO process

To accurately visualize and extrapolate trends from elemental analysis, the elemental composition of the products were plotted in Van Krevelen-type diagrams. The molar O/C versus molar H/C ratios of the feed guaiacol and the HDO products are shown in Figs. 4.12 and 4.13 at different temperatures and initial hydrogen pressures respectively. The O/C ratio of HDO products decreased as a function of reaction temperature for both catalysts, however, higher hydrogenation occurred over Ni/SiO_2-Al_2O_3. At 300 °C the O/C ratio of HDO products of Ni/RM was 0.18 versus 0.22 for Ni/SiO_2-Al_2O_3. At 350 °C this value was relatively the same for Ni/RM and Ni/SiO_2-Al_2O_3 (0.09 and 0.10 respectively) however the H/C ratio at 300, 350, and 400 °C were 1.40, 1.46, and 1.59 respectively for Ni/RM versus 1.42, 1.63, and 1.93 respectively for Ni/SiO_2-Al_2O_3 HDO products. Thus, there was more hydrogenation with Ni/SiO_2-Al_2O_3

than Ni/RM. Moreover, the Van Krevelen plot of HDO products over Ni/RM catalyst at different H_2 pressures (Fig. 4.13) fell below the HDO products over Ni/SiO_2-Al_2O_3 showing that for HDO of guaiacol, less saturation of double bonds took place over Ni/RM catalyst resulting in lower hydrogen consumption, which is desirable in HDO process. These results were mainly attributed to higher catalytic activity of Ni/SiO_2-Al_2O_3 because of the higher Ni loading that favored hydrogenation and hydrocracking reactions. Also, to a lesser extent, silica and alumina can catalyze demethylation reaction [1, 20, 64] contributing to increased hydrogen consumption in the case of Ni/SiO_2-Al_2O_3.

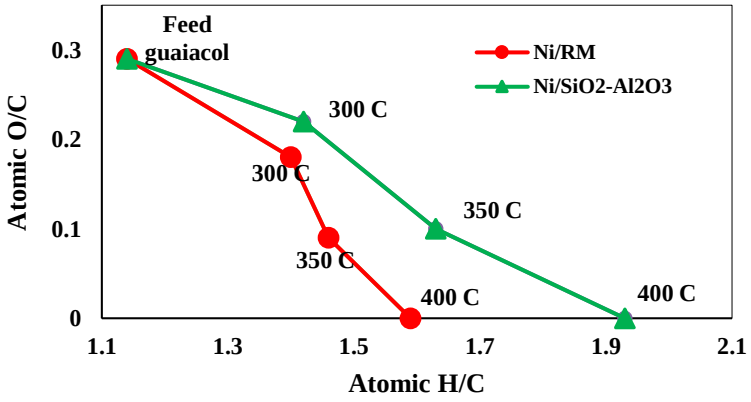

Fig. 4. 12: Van-Krevelen diagram of guaiacol HDO products at different reaction temperatures.

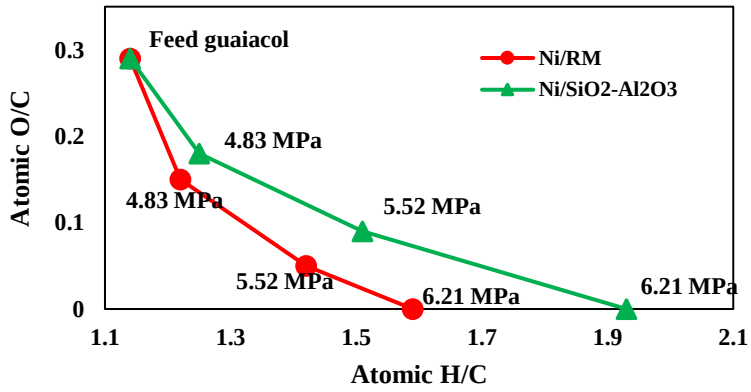

Fig. 4. 13: Van-Krevelen diagram of guaiacol HDO products at different initial hydrogen pressures.

4.4. Reaction pathways

For the study of HDO pathways of guaiacol over Ni/RM and Ni/SiO_2-Al_2O_3, HDO of catechol, anisole, phenol, cyclohexane, benzene, toluene, and xylene were carried out under the same conditions as the HDO of guaiacol. These reaction results are shown in Table 4.4. Guaiacol was first converted to catechol, anisole, and phenol via demethoxylation and dehydroxylation reactions. The selectivity to catechol, anisole, and phenol were 1.5, 2.3, 9.5 % respectively for Ni/RM and 3.4, 4.7, and 10.8 % respectively for the commercial catalyst after HDO of guaiacol. Anisole underwent demethylation, demethoxylation, and alkylation to produce phenol, benzene, and toluene respectively. Catechol was first converted to phenol via dehydroxylation and then converted to benzene. Benzene was initially formed via demethoxylation of anisole, dehydroxlylation of phenol, and demethylation of toluene, and then hydrogenated to cyclohexane. At relatively lower selectivity compared to other intermediates, xylene was formed via a transalkylation reaction [45, 46]. HDO of benzene produced cyclohexane through ring hydrogenation at selectivity of 88.2% and 67.6% over Ni/RM and Ni/SiO_2-Al_2O_3 respectively but ring opening was more pronounced over the commercial catalyst (32.4% selectivity) compared to Ni/RM (11.8% selectivity) (Table 4.4). A summary of the HDO pathways of guaiacol based on the observed product distribution is proposed in Fig. 4.14. Pathways 1, 2, and 3 are demethylation, demethoxylation, and dehydroxylation processes, respectively. Pathway 4 is hydrogenation which was more pronounced over Ni/SiO_2-Al_2O_3 than Ni/RM. Pathway 5 is a transalkylation reaction in which the methyl group is transferred to the aromatic ring [65]. In conclusion, similar reaction pathways

over both catalysts were observed while products selectivity were quite different as discussed in section 3.2. Overall, the conversion of oxygenated compounds (guaiacol, catechol, anisole, and phenol) were higher for Ni/RM compared to the commercial catalyst suggesting higher activity of Ni/RM catalyst for deoxygenation than hydrogenation (Table 4.4). The Ni/SiO_2-Al_2O_3 showed higher conversion for hydrogenation of BTX and ring opening compared to Ni/RM.

Table 4. 4: Conversion and selectivity of guaiacol and intermediates HDO (the standard deviation of all data were ± 0.5).

Sub.	Catalyst	Conv. (%)	Selectivity (%)							
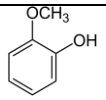	Ni/RM	83.2	1.5	2.3	9.5	34.8	5.7	23.1	16.6	6.5
	Ni/SiO_2-Al_2O_3	78.6	3.4	4.7	10.8	57.3	2.8	10.7	6.5	3.8
	Ni/RM	81.4	-	-	21.6	19.6	11.5	47.3	-	-
	Ni/SiO_2-Al_2O_3	76.4	-	-	36.9	31.4	7.6	24.1	-	-
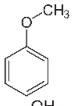	Ni/RM	71.3	-	-	14.5	17.4	4.9	38.1	15.7	9.4
	Ni/SiO_2-Al_2O_3	66.7	-	-	22.7	32.8	8.3	20.4	10.6	5.2
	Ni/RM	85.6	-	-	-	31.6	9.8	58.6	-	-
	Ni/SiO_2-Al_2O_3	74.9	-	-	-	58.3	5.4	36.3	-	-
	Ni/RM	68.2	-	-	-	-	100	-	-	-
	Ni/SiO_2-Al_2O_3	76.4	-	-	-	-	100	-	-	-
	Ni/RM	71.4	-	-	-	88.2	11.8	-	-	-
	Ni/SiO_2-Al_2O_3	89.3	-	-	-	67.6	32.4	-	-	-
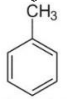	Ni/RM	78.6	-	-	-	34.4	15.6	44.4	-	5.6
	Ni/SiO_2-Al_2O_3	91.1	-	-	-	66.5	9.8	21.3	-	2.4
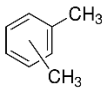	Ni/RM	74.3	-	-	-	26.7	13.6	37.3	22.4	-
	Ni/SiO_2-Al_2O_3	80.2	-	-	-	56.8	8.7	20.6	13.9	-

Reaction conditions: 350 °C, 6.21 MPa, 30 min

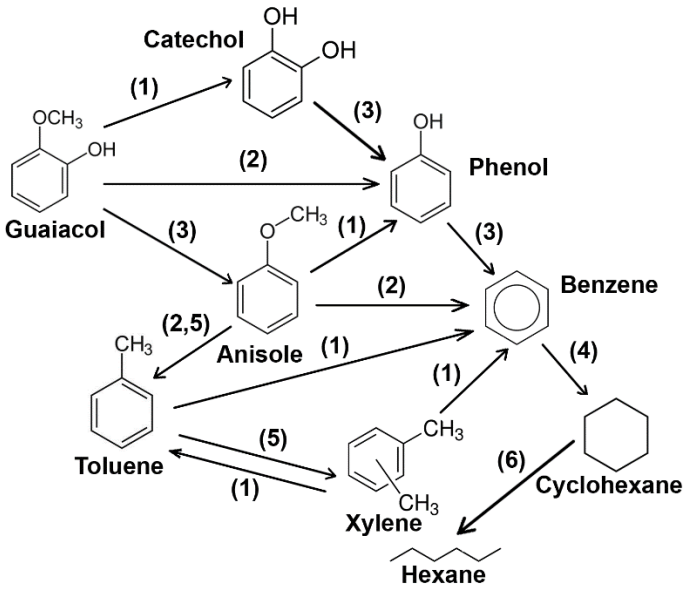

Fig. 4. 14: Reaction network of guaiacol HDO. 1: demethylation, 2: demethoxylation, 3: dehydroxylation, 4: hydrogenation, 5: transalkylation, 6: ring opening.

4.5. Kinetic studies

In order to determine the reaction order and rate constant of the reaction, the activity data (concentration and time) was fitted to power-law equation [54]. As shown in Fig. 4.15, the slope of a plot of $1/C_{guaiacol}$ as a function of reaction time is linear with slope of *k*, hence, HDO of guaiacol global kinetics followed the second order mechanism which was in agreement with other studies [44]. The rate constant of Ni/SiO_2-Al_2O_3 (55.8 ml/mol.s) was more than two times higher than the Ni/RM catalyst (24.4 ml/mol.s), which explains the higher activity of Ni/SiO_2-Al_2O_3 compared to Ni/RM. Ni/RM has shown better performance over Ni/SiO_2-Al_2O_3 since the latter favored ring hydrogenation reaction. Since the support was different for both catalysts, the activity difference could be due to both Ni loading and interaction with support. In the case of Ni/RM the elemental Ni loading was less than the nominal 40% because the XRD pattern showed the presence of NiO after the reduction with H_2. Apparent activation energy for each

catalyst was calculated based on the Arrhenius-type plots (equation 4) [54] (Fig. 4.16). The apparent activation energy for the Ni/RM and Ni/SiO_2-Al_2O_3 catalysts were 97.5 KJ/mol and 90.3 KJ/mol, respectively. These values were within the range of various values reported in literature [44, 46, 66]. Therefore the global kinetic model over Ni/RM and Ni/SiO_2-Al_2O_3 catalysts had the forms of equations (5) and (6) respectively:

$$\ln(k) = \ln(k_0) - \frac{E}{RT} \qquad (4)$$

$$-r_G = 56.26\, e^{\left(-\frac{97.5}{RT}\right)}.{C_G}^2 \qquad (5)$$

$$-r_G = 51.42\, e^{\left(-\frac{90.3}{RT}\right)}.{C_G}^2 \qquad (6)$$

The development of a more detailed kinetic model is out of the scope of this article.

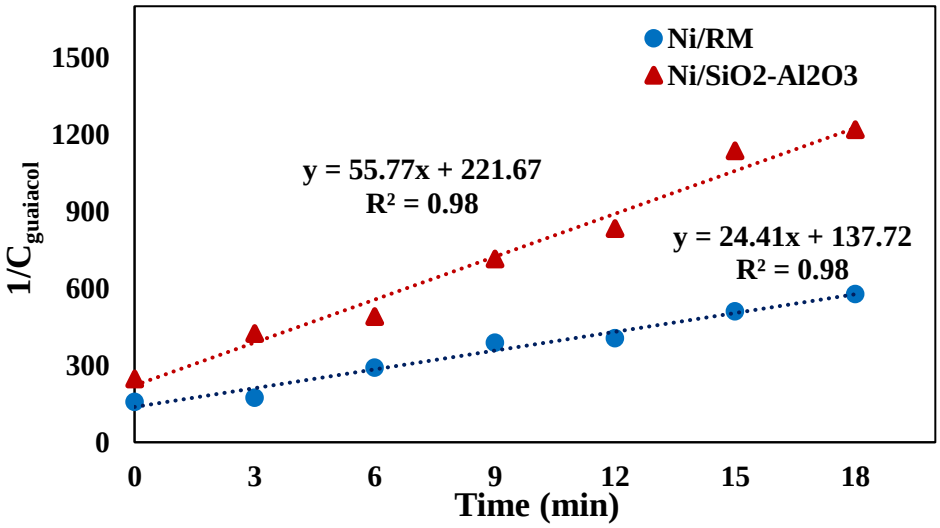

Fig. 4. 15: Determination of reaction order and rate constant by integral method: reaction temperature 400 °C, H_2 pressure 6.21 MPa (900 psi).

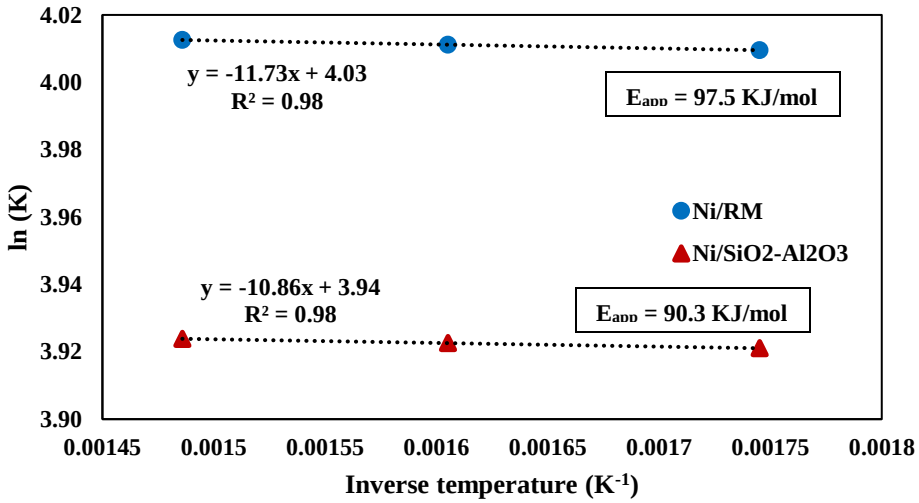

Fig. 4. 16: Arrhenius-type plot for guaiacol HDO on Ni/RM and Ni/SiO_2-Al_2O_3.

4.6. Catalyst deactivation and regeneration

As discussed in section 3.1, three mechanisms contributed to catalyst deactivation; coke formation, oxidation of Ni, and formation of iron nickel oxide. In order to evaluate the catalyst life, the recovered catalysts after HDO experiments were washed using a solution of 1:1 (wt. ratio) toluene/methanol and consecutively used in further HDO tests without any catalyst regeneration. The selectivity of HDO products changed as the catalyst deactivated. A summary of the results of these experiments is shown in Table 4.5. Metal loading, and pore structure of support have been proposed to affect coke deposition [9, 16]. After four consecutive runs using Ni/RM, the catalyst completely deactivated due to coking and possible oxidation of active Ni sites both of which can contribute to the reduction of BET specific surface area from 79.3 m^2/g to 59.2 m^2/g. After the fifth run the catalyst did not indicate any activity and the guaiacol did not undergo any HDO reactions. There was more coke built up on the catalyst surface that further reduced the BET specific surface area to 56.4 m^2/g. The Ni/SiO_2-Al_2O_3

completely deactivated after five consecutive runs and its BET specific surface area reduced from 118.4 m^2/g to 77.9 m^2/g. After the sixth run the catalyst did not show any activity for HDO reactions however its BET specific surface area further reduced to 72.2 m^2/g. The reduction in BET specific surface area suggested that coke was formed in the pores of the catalyst.

Table 4. 5: Catalyst recyclability results (reaction temperature 400 °C, H_2 initial pressure 6.21 MPa) (the standard deviation of conversion and selectivity data were ± 0.5, and the standard deviation of BET data were ±1.5).

Catalyst Reuse #	BET specific surface area (m^2/g)	Conv. (%)	Selectivity (%)							
			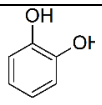	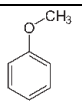	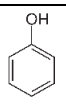				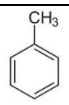	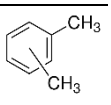
Ni/RM										
Fresh	79.3	100	0	0	0	40.2	7.3	25.5	18.8	8.2
Reuse 1	71.2	100	4.2	3.2	7.1	35.5	6.7	23.6	15.4	4.3
Reuse 2	67.5	81.4	7.9	8.9	5.6	32.8	4.9	21.9	14.8	3.2
Reuse 3	63.5	47.5	10.5	17.1	3.5	31.4	2.6	20.7	12.5	1.7
Reuse 4	59.2	23.7	15.8	19.9	1.2	30.1	1.5	19.4	11.3	0.8
Reuse 5	56.4	0	-	-	-	-	-	-	-	-
Ni/SiO_2-Al_2O_3										
Fresh	118.4	100	0	0	0	65.9	3.6	16.8	8.9	4.8
Reuse 1	107.4	100	2.5	3.2	5.5	59.8	3.3	12.6	8.8	4.3
Reuse 2	100.3	68.8	5.7	5.9	8.3	53.4	3.1	11.2	8.5	3.9
Reuse 3	91.6	54.3	6.6	9.4	9.5	51.5	2.8	8.7	7.9	3.6
Reuse 4	84.4	34.7	7.5	10.6	10.9	50.8	2.5	7.5	7.4	2.8
Reuse 5	77.9	17.2	10.9	11.7	11.7	48.6	2.1	6.6	6.3	2.1
Reuse 6	72.2	0	-	-	-	-	-	-	-	-

The spent catalysts were placed in muffle furnace to burn off the deposited coke at 400 °C for 4 h followed by reduction as explained in section 3.1. The regenerated/activated catalyst was used in HDO experiments. A summary of these HDO test results are shown in Table 4.6. Guaiacol conversion and HDO products selectivity over Ni/RM were similar to that of fresh catalyst (Table 4.5). These result indicated that the Ni/RM catalyst regained its activity after the regeneration/activation process.

However, the regeneration of the commercial Ni/SiO_2-Al_2O_3 was not possible following the same procedure and the catalyst did not show HDO activity after regeneration/reduction. The BET specific surface area of the regenerated Ni/SiO_2-Al_2O_3 catalyst was 88.8 m^2/g, which was much lower than the fresh catalyst (118.4 m^2/g) suggesting that some Ni particles probably formed stable compounds with the support phase during regeneration. Additionally, when exposed to air, the reduced Ni/SiO_2-Al_2O_3 catalyst underwent spontaneous oxidation that could be due to oxidation of free Ni particles that were not interacting with the support phase.

Table 4. 6: HDO results of regenerated catalysts (the standard deviation of conversion and selectivity data were within ± 0.5, and the standard deviation of BET data were ±1.5).

Catalyst	BET specific surface area (m^2/g)	Conv. (%)	Selectivity (%)							
			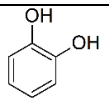	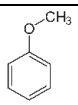	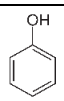					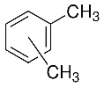
Ni/RM	79.9	100	0	0	0	39.7	7.5	26.2	19.1	7.5
Ni/SiO_2-Al_2O_3	88.8	0	-	-	-	-	-	-	-	-

5. Conclusion

Red mud, which is a waste material from the aluminum industry, was used as support material for preparation of nickel hydrogenation/hydrodeoxygenation catalyst. Hydrodeoxygenation of guaiacol as lignin model compound was investigated over red mud-supported nickel catalyst. For comparison, commercial Ni/SiO_2-Al_2O_3 was tested in HDO process under similar conditions. Unlike traditional HDO catalysts (CoMo/Al_2O_3 and NiMo/Al_2O_3), this catalyst did not require any pre-treatments such as sulfidation and it can be used as received. Also this catalyst is much cheaper than typical noble metal

catalysts that are widely used for HDO reactions. The Van-Krevelen diagrams of HDO products at different reaction temperatures and hydrogen pressures showed that increasing the reaction temperature and hydrogen pressure improved HDO reactions. Complete deoxygenation of guaiacol was achieved at a reaction temperature of 400 °C when the initial hydrogen pressure was 6.21 MPa (900 psi). Ni/RM showed higher activity for deoxygenation while hydrogenation of the aromatic ring was more pronounced for the commercial Ni/SiO_2-Al_2O_3. Consequently, the Ni/RM consumed less hydrogen than Ni/SiO_2-Al_2O_3. Hydrocracking and coke formation were significantly lower in the case of Ni/RM catalyst which is desirable in HDO process. The kinetics of guaiacol HDO followed second order model for both catalysts while higher rate constant and lower activation energy were determined for Ni/SiO_2-Al_2O_3 catalyst compared to Ni/RM. The increased catalytic activity of Ni/SiO_2-Al_2O_3 was ascribed to higher Ni loading and higher BET specific surface area of the catalyst.

Coke formation was the major mechanism of catalyst deactivation, although oxidation of active Ni sites and formation of iron nickel oxide could also contribute to catalyst deactivation. After regeneration by burning off the coke and reducing with hydrogen, the activity of the Ni/RM catalyst was completely restored in contrast to the commercial catalyst that was not regenerable. This study showed that Red Mud can serve as a nickel catalyst support for HDO process.

6. References

[1] K. Li, R. Wang, J. Chen, Energy Fuels 25 (2011) 854–863.

[2] H.Y. Zhao, D. Li, P. Bui, S.T. Oyama, Appl. Catal. A Gen. 391 (2011) 305–310.

[3] S. Ted Oyama, T. Onkawa, A. Takagaki, R. Kikuchi, S. Hosokai, Y. Suzuki, K.K. Bando, Top. Catal. 58 (2015) 201–210.

[4] Z. He, X. Wang, Catal. Sustain. Energy 1 (2012) 28–52.

[5] J. Wildschut, I. Melián-Cabrera, H.J. Heeres, Appl. Catal. B Environ. 99 (2010) 298–306.

[6] S. Raza, Y. Uemura, S. Bt, J. Anal. Appl. Pyrolysis 106 (2014) 57–62.

[7] S. Czernik, A. V. Bridgwater, Energy Fuels 18 (2004) 590–598.

[8] H. Wang, J. Male, Y. Wang, ACS Catal. 3 (2013) 1047-1070.

[9] P.M. Mortensen, J. Grunwaldt, P.A. Jensen, K.G. Knudsen, A.D. Jensen, Appl. Catal. A Gen. 407 (2011) 1–19.

[10] P. Weerachanchai, M. Horio, C. Tangsathitkulchai, Bioresour. Technol. 100 (2009) 1419–1427.

[11] C.S. Lira, F.M. Berruti, P. Palmisano, F. Berruti, C. Briens, A.A.B. Pécora, J. Anal. Appl. Pyrolysis 99 (2013) 23–31.

[12] H. Jahromi, F.A. Agblevor, Energy 141 (2017) 2186–2195.

[13] A. Gutierrez, R.K. Kaila, M.L. Honkela, R. Slioor, A.O.I. Krause, Catal. Today 147 (2009) 239–246.

[14] M.Á. González-Borja, D.E. Resasco, Energy Fuels 25 (2011) 4155–4162.

[15] C.A. Fisk, T. Morgan, Y. Ji, M. Crocker, C. Crofcheck, S.A. Lewis, Appl. Catal. A Gen. 358 (2009) 150–156.

[16] X. Zhu, L.L. Lobban, R.G. Mallinson, D.E. Resasco, J. Catal. 281 (2011) 21–29.

[17] V.N. Bui, D. Laurenti, P. Afanasiev, C. Geantet, Appl. Catal. B Environ. 101 (2011) 239–245.

[18] V.N. Bui, D. Laurenti, P. Delichère, C. Geantet, Applied Catal. B, Environ. 101 (2011) 246–255.

[19] Y. Romero, F. Richard, S. Brunet, Appl. Catal. B Environ. 98 (2010) 213–223.

[20] C. Sepulveda, R. Garcia, N. Escalona, D. Laurenti, L. Massin, M. Vrinat, Catal. Lett. 141 (2011) 987–995.

[21] D. Shen, C. Cheng, N. Liu, R. Xiao, Production of Biofuels and Chemicals from Lignin, Springer, 2016, pp. 289-320.

[22] A.L. Jongerius, Catalytic Conversion of Lignin for the Production of Aromatics, Gilderprint Drukkerijen, 2013 pp .8-15.

[23] E. Furimsky, Appl. Catal. A Gen. 199 (2000) 147–190.

[24] E. Furimsky, Ind. Eng. Chem. Prod. Res. Dev. 22 (1983) 34–38.

[25] Y. Yoshimura, T. Sato, H. Shimada, N. Matsubayashi, A. Nishijima, Appl. Catal. 73 (1991) 55–63.

[26] A. Agrawal, K.K. Sahu, B.D. Pandey, Res. Con. Rec. 42 (2004) 99–120.

[27] S. Sushil, V.S. Batra, Appl. Catal. B. Environ. 81 (2008) 64–77.

[28] B.K. Yathavan, F.A. Agblevor, Energy Fuels 27 (2013) 6858–6865.

[29] X. Lim, A. Sanna, J.M. Andresen, Fuel 119 (2014) 259–265.

[30] B. Klopries, W. Hodek, F. Bandermann, Fuel 69 (1990) 448-455.

[31] K.C. Pratt, V. Christoverson, Fuel 61 (1982) 460-462.

[32] A. Eamsiri, W.R. Jackson, K.C. Pratt, V. Christoverson, M. Marshall, Fuel 71 (1992) 449-453.

[33] J.J. Llano, R. Rosal, H. Sastre, F.V. Diez, Fuel 73 (1994) 688-694.

[34] S. Ordóñez, H. Sastre, F. V. Díez, Appl. Catal. B Environ. 29 (2001) 263–273.

[35] J. Alvarez, Appl. Catal. A. Gen. 128 (1995) 259–273.

[36] S. Ordóez, H. Sastre, F. V. Díez, J. Hazard. Mater. 81 (2001) 103–114.

[37] M. Martino, R. Rosal, H. Sastre, F. V Dõ, Appl. Catal. B. Environ. 20 (1999) 301-307.

[38] L.C.A. De Oliveira, A.P. Heitmann, L.D. Almeida, S. Herman, A.A. Mansur, C.S. De Castro, U.F. De Alfenas, J. Environ. Sci. 57 (2015) 3–5.

[39] O.D. Mante, F.A. Agblevor, Green Chem. 16 (2014) 3364-3377.

[40] J.R. Paredes, S. Ordóñez, A. Vega, Appl. Catal. B. Environ. 47 (2004) 37–45.

[41] S. Djerad, M. Crocoll, S. Kureti, L. Tifouti, W. Weisweiler, Catal. Today 113 (2006) 208–214.

[42] S.K. Wu, P.C. Lai, Y.C. Lin, Catal. Lett. 144 (2014) 878–889.

[43] J. Filley, C. Roth, J. Molecular Catal. A 139 (1999) 245–252.

[44] A. Aqsha, L. Katta, N. Mahinpey, Catal. Lett. 145 (2015) 1351–1363.

[45] N.T.T. Tran, Y. Uemura, S. Chowdhury, A. Ramli, Appl. Catal. A Gen. 512 (2016) 93–100.

[46] Q. Lai, C. Zhang, J.H. Holles, Appl. Catal. A Gen. 528 (2016) 1–13.

[47] L. Liu, Y. Liu, X. Gao, R. Zhang, Y. Zhai, J. Fuel Chem. Technol. 45 (2017) 932–938.

[48] T. He, X. Liu, Y. Ge, D. Han, J. Li, Z. Wang, J. Wu, Catal. Commun. 102 (2017) 127–130.

[49] I.D. Mora-Vergara, L. Hernández Moscoso, E.M. Gaigneaux, S.A. Giraldo, V.G. Baldovino-Medrano, Catal. Today 302 (2017) 125–135.

[50] Z. Xinghua, W. Tiejun, M. Longlong, W. Chuangzhi, Fuel 89 (2010) 2697–2702.

[51] X. Zhang, L. Chen, W. Kong, T. Wang, Q. Zhang, J. Long, Y. Xu, L. Ma, Energy 84 (2015) 83–90.

[52] R. Gavlak, R. Horneck, R.O. Miller, J. Kotuby-Amacher, Soil, plant and water reference methods for the western region. Western Coordinating Committee on Nutrient Management, 2000, pp. 129–134.

[53] X. Zhang, T. Wang, L. Ma, Q. Zhang, T. Jiang, Bioresour. Technol. 127 (2013) 306–311.

[54] J. Wiley, K. Hepburn, O. Levenspiel, Chemical Reaction Engineering, John Wiley and Sons, 1964, pp. 13-75.

[55] I. Coronado, M. Stekrova, L. García Moreno, M. Reinikainen, P. Simell, R. Karinen, J. Lehtonen, Biomass Bioenergy 106 (2017) 29–37.

[56] S. Chenna, R. Banerjee, P.A. Crozier, Chem. Cat. Chem., 3 (2011) 1051–1059.

[57] Q. Jeangros, T.W. Hansen, J.B. Wagner, C.D. Damsgaard, R.E. Dunin-Borkowski, C. Hébert, J. Van Herle, A. Hessler-Wyser, J. Mater. Sci. 48 (2013) 2893–2907.

[58] J. Pu, K. Nishikado, N. Wang, T.T. Nguyen, T. Maki, E.W. Qian, Appl. Catal. B Environ. 224 (2018) 69–79.

[59] C. Boscagli, C. Yang, A. Welle, W. Wang, S. Behrens, K. Raffelt, J.D. Grunwaldt, Appl. Catal. A Gen. 544 (2017) 161–172.

[60] S. Danaci, L. Protasova, J. Lefevere, L. Bedel, R. Guilet, P. Marty, Catal. Today 273 (2016) 234–243.

[61] N. Joshi, A. Lawal, Chem. Eng. Sci. 74 (2012) 1–8.

[62] H. Wan, R. V. Chaudhari, B. Subramaniam, Top. Catal. 55 (2012) 129–139.

[63] S. Asphaug. Catalytic hydrodeoxygenation of bio-oils with supported MoP-catalysts. Norwegian University of Science and Technology, 2013, pp. 50-56.

[64] T.-R. Viljava, R.S. Komulainen, A.O.I. Krause, Catal. Today 60 (2000) 83–92.

[65] Z. Cai, F. Wang, X. Zhang, R. Ahishakiye, Y. Xie, Y. Shen, Mol. Catal. 441 (2017) 28–34.

[66] M.D. Skoglund, C.L. Jackson, K.J. Mckim, H.J. Olson, S. Sabirzyanov, J.H. Holles, Applied Catal. A, Gen. 467 (2013) 355–362.

CHAPTER 5

5. HYDRODEOXYGENATION OF PINYON-JUNIPER CATALYTIC PYROLYSIS OIL USING RED MUD-SUPPORTED NICKEL CATALYSTS

1. Abstract

Red mud (RM) is an alkaline waste generated in the Bayer process of alumina production. In the present study red mud supported nickel catalysts (Ni/RM) were prepared at different concentrations of nickel (10, 20, 30, 40, 50, and 65 wt. %) and used to hydrodeoxygenate (HDO) pinyon-juniper (PJ) catalytic pyrolysis oil. Increasing the nickel content improved the activity of Ni/RM catalysts for HDO reactions. Maximum organic liquid yield (68.6%) was obtained when 40%Ni/RM was used. The upgraded oil had oxygen content of 1.35 wt. % and higher heating value of 45.77 MJ/kg compared to 24.88 wt. % and 28.41 MJ/kg, respectively, for the crude oil. For comparison, commercial Ni/SiO_2-Al_2O_3 was also evaluated in HDO experiments. The HDO oil properties obtained using 40%Ni/RM at reaction temperature of 400 °C was similar to that of commercial Ni/SiO_2-Al_2O_3 at reaction temperature of 450 °C. However, the organic liquid yield was much higher for 40%Ni/RM (68.6%) compared to the commercial Ni/SiO_2-Al_2O_3 (41.8%). The commercial Ni/SiO_2-Al_2O_3 produced more gas (27.6%) than the 40%Ni/RM (16.4%) and the coke yields for the commercial catalyst and Ni/RM catalyst were 7.3% and 4.2% respectively. Overall, application of Ni/RM improved HDO reactions and reduced cracking and coke formation compared to commercial Ni/SiO_2-Al_2O_3.

2. Introduction

The world's energy consumption is increasing due to population growth and economic developments. Fossil fuels consumption has increased significantly since the industrial revolution and constitutes more than 80% of the world primary energy consumption is derived from fossil fuels [1]. This excessive dependence on fossil fuels contributes to severe environmental degradation such as water, air and soil pollutions. Biomass provides a promising feedstock for producing renewable fuels and chemicals, especially liquid fuels [2-4]. A potentially efficient and cost-effective method for converting biomass to liquid fuel (bio-oil) is through fast pyrolysis. This method requires low capital investment and can be easily applied in commercial plants [5-7]. Fast pyrolysis is a thermochemical process that decomposes biomass components of cellulose, hemicellulose and lignin into bio-oil, bio-char, and gas [8, 9]. Pyrolysis oil has acidic and corrosive properties, high water content, and a relatively low energy density as compared to conventional petroleum-derived fuels, making it unusable as transportation fuels [10, 11]. Consequently, bio-oil upgrading is needed to reduce its water and oxygen contents [12].

Hydrodeoxygenation (HDO), which is considered an effective method for bio-oil upgrading, involves the stabilization and selective removal of oxygen from untreated bio-oil through its catalytic reaction with hydrogen [10, 13]. Catalysts play a critical role in bio-oil HDO, and many catalysts have been investigated [14]. Several categories of catalysts including noble metal and sulfided metal catalysts have been investigated [15, 16]. Noble metal catalysts such as Ru/C, Ru/TiO_2, Ru/Al_2O_3, Pt/C, and Pd/C were used for HDO of bio-oil [17, 18]. The results showed that Ru/C catalyst was superior to typical

HDO catalysts such as sulfided $NiMo/Al_2O_3$ and $CoMo/Al_2O_3$ for bio-oil upgrading [17]. However, the noble metal catalysts have limitations which include high cost and limited supply. The sulfided catalysts are less suitable for bio-oil HDO due to the economic factors of using sulfur, product contamination, and the poor stability of alumina support (deactivation by water) [19]. Non-noble metal catalysts such as metallic Ni, Cu, Fe or their bimetallic combination supported on Al_2O_3 were also investigated, and they were shown to be very active in bio-oil HDO [20]. However, the problem of alumina's poor tolerance of water still existed in these tests, which can easily cause catalyst deactivation [21]. Therefore, development of an effective, readily available catalyst support can play a crucial role in HDO process both technically and economically.

Developing catalysts from waste materials is an effective means of value addition to the waste. Red mud has received considerable attention in this regard. Red mud (RM) or red sludge is a caustic waste material generated during the Bayer process for alumina production [22]. There are many problems with managing RM slurry. Some of these problems are costly maintenance of RM pond areas, risk of caustic pollutants for all living organisms, leakage of alkaline contaminants into groundwater resources, and overflow of materials during rainy seasons that can cause harmful effects on surrounding environment [22, 23]. RM consists of compounds originally present in the parent mineral and those introduced during the Bayer process. The main chemical components of RM are Fe_2O_3, Al_2O_3, SiO_2, CaO, Na_2O, TiO, K_2O and MgO and a number of minor constituents such as Cr, V, S, Ni, Cu, Mn, Zn etc [23].

RM has been investigated as catalyst for various applications, including pyrolysis of biomass [24, 25], hydrogenation and liquefaction [26-31], hydrodechlorination and

desulfurization reactions [32-34], and exhaust gas clean-up [35, 36]. RM has also been used as catalyst in other reactions such as degradation of polyvinyl chloride containing polymer mixtures into fuel oil [37, 38], conversion of waste oil and waste plastic to fuel [39], heavy crude oil hydrotreating [40], ammonia decomposition in presence of sulfur compounds [41], and nitrile synthesis from aldehydes and hydroxylamine [42]. Furthermore, RM has recently been used as catalyst for removal of organics from water [43, 44], biodiesel production [45], and methanogenesis reaction [46]. The conversion of RM into a value added product such as heterogeneous catalyst can be considered a promising technology for the final destination of the residue.

The main objective of this work is to investigate the application of RM-supported nickel catalysts (Ni/RM) for upgrading of pyrolysis oil (bio-oil) via hydrodeoxygenation. Our previous study showed that Ni/RM can be used as an effective catalyst for the hydrodeoxygenation of guaiacol as a bio-oil model compound [47].

The pyrolysis oil in this research was obtained from catalytic pyrolysis of pinyon juniper (PJ) wood. PJ woodlands occupy about 30 million hectares in the western United States (including states of Arizona, California, Colorado, Idaho, Utah, Nevada, New Mexico, Oregon, and Wyoming). Domination of PJ woodlands decreases the herbaceous vegetation and increases bare lands, thus causing soil erosion and nutrition loss [24]. Studies have shown that expansion of PJ woodlands has reduced the amount of precipitation, increased soil erosion, and increase the potential of crown fires, hence, land management agencies are reducing the population of PJ woodlands [48-51]. In principle, PJ can become a potential biomass feedstock for production of bio-oil.

In view of its strong stability, sintering resistance, and poisoning resistance, it is expected that RM can serve as a promising catalyst support for HDO of bio-oil. Moreover, it is much cost-effective in comparison with other catalyst supports such as Al_2O_3, SiO_2, and TiO_2 which require complicated preparation procedures. Since silica and alumina are two major compounds of RM, commercial Ni/SiO_2-Al_2O_3 was tested in HDO process for comparison. Unlike traditional HDO catalysts (CoMo/Al_2O_3 and NiMo/Al_2O_3), this catalyst does not need any pre-treatments such as sulfidation and it can be used as received [12]. This catalyst is relatively cheaper than typical noble metal catalysts that are widely used for HDO reactions.

3. Material and methods

3.1. Material

PJ biomass chips were supplied by the U.S. Bureau of Land Management. RM was used as catalyst for fast pyrolysis of the PJ biomass. The wet red mud was dried at room temperature, reformulated and then ground and sieved to a particle size of 125−180 μm. The ground particles were calcined at 550 °C in a muffle furnace (Thermo Fisher Scientific, Waltham, MA) for 5 h before being used for the pyrolysis. The detailed characterization of the RM has been reported by Yathavan and Agblevor [24]. Analytical grade nickel nitrate hexahydrate ($Ni(NO_3).6H_2O$) was purchased from Alfa Aesar (Haverhill, MA, USA). High purity (99%) hydrogen (Airgas, PA, USA) was used for HDO experiments. Commercial Nickel on silica/alumina (~65 wt % loading Ni) catalyst powder, obtained from Sigma-Aldrich (St. Louis, MO, USA), was used (as received) in HDO experiments for comparison.

3.2. Pyrolysis of biomass

PJ biomass chips ground to pass a 2-mm mesh were used as feedstock for production of catalytic pyrolysis oil. The pyrolysis was carried out in a pilot plant bubbling fluidized bed reactor described in detail by Mante and Agblevor [52]. At feeding rate of 0.9 kg/h (2 lb/h), catalytic pyrolysis oil was produced at 400 ° C using RM catalyst. The pyrolytic products were condensed using a series of two ethylene glycol-cooled condensers and an electrostatic precipitator (ESP) operating at 30 kV. Details of the pyrolysis pilot plant can be found elsewhere [52].

3.3. Preparation of Ni/RM catalysts and characterization

Ni/RM catalysts were prepared at different concentrations of nickel using wet impregnation method [53, 54]. At room temperature the calculated amount of $Ni(NO_3).6H_2O$ was dissolved in 100 ml deionized water and then mixed with RM (particle size<90 μm). The mixture was heated to 70 °C and continuously stirred for 5 hours to prepare the catalyst precursor. The catalyst precursor was dried at 105 °C for 10 hours and then calcined at 620 °C for 5 hours. The catalyst precursor was reduced for 6 hours at 450 °C using a reducing gas mixture of 10% H_2 and 90% N_2 at flow rate of 20 ml/min to obtain the tested catalyst, which was designated as x wt.% Ni/RM (x= 10, 20, 30, 40, 50, 65).

The BET (Brunauer-Emmet-Teller) surface area of Ni/RM catalysts were determined on a MS-16 BET analyzer (Quantachrome Instruments, Boynton Beach, FL, USA). About 0.1 g catalyst sample was used in each measurement. All samples were degassed at 300 °C for 4 hours prior to duplicate simultaneous measurements. A

standard porous Al_2O_3 sample was analyzed along with each run to ensure consistency between the different samples.

TG-TPR (Thermogravimetric-temperature programmed reduction) studies were carried out using a TGA Q500 (TA Instruments, Lindon, UT, USA). Twenty-five milligrams of catalyst (calcined form) was heated in a flow of 10% H_2 / 90% N_2 (20 ml/min) from room temperature to 700 °C at a heating rate of 10 °C/min. Hydrogen uptake was monitored by the change of sample weight according to the plot of derivative weight vs. temperature.

X-ray powder diffraction (XRD) analyses were carried out by Hazen Research Inc. (Golden, CO, USA). The samples were pulverized by hand in a mortar and pestle with isopropyl alcohol and analyzed using a Bruker D8 Advance with Davinci design and a Lynxeye detector. The pattern was measured in the interval from 5 to 85 in 2Θ using a 0.02 step size and 40 s of counting time.

Scanning electron microscopy (SEM) analysis was conducted on a FEI Quanta FEG-650 (Thermo Fisher Scientific, MA, USA). For preparation of the specimens a small amount of catalyst was placed on a two-sided sticky tape resting on an aluminum holder and observed at different magnifications. Images were recorded using low vacuum secondary electron (LFD) detector.

For inductively-coupled plasma (ICP) analysis, 0.5 g catalyst sample was digested in nitric acid at 95 °C for 1 h. Then 12 ml 30 wt. % hydrogen peroxide was added to the digestion tube and cooled to room temperature [55]. The extracts were measured using a Thermo iCAP 6300 ICP-OES Inductively-Coupled Plasma Spectrophotometer (Thermo Fisher Scientific, MA, USA) with Optical Emission.

3.4. Hydrodeoxygenation of bio-oil

The bio-oil was subjected to HDO reactions in a Parr Series 4560 300 mL autoclave reactor (Parr Instruments, Moline, IL, USA). The reactor can withstand a maximum pressure of 14 MPa at 500 ° C. A Parr 4848 controller was used to control the internal temperature and impeller speed. In a typical test, bio-oil (20 g) and catalyst (3 g) were loaded into the reactor. The reactor was first flushed with nitrogen three times and then flushed with hydrogen three times to purge the reactor. High purity hydrogen was supplied from a reservoir tank via a pressure regulator. The reactor was then pressurized with hydrogen to 6.2 MPa and a gas sample was taken from a gas release valve from the gas sampling port for gas analysis when the reactor was at room temperature. The reactor was then heated to reaction temperature (400 or 450 °C) at heating rate of 15 °C/min using a heating mantle. The reaction time was recorded when the required temperature was reached. The stirrer speed was kept constant (~1000 rpm) in all experiments.

After the desired reaction time (30 minute), the reactor was cooled to room temperature using the internal cooling coil. A gas sample was collected in a tedlar bag for gas analysis when the reactor was cooled down to room temperature. Hydrogen consumption was measured using equation (1).

$$H_2\ consumption\ \left(\frac{mole H_2}{g\ biooil}\right) = \left(n_{i_{H2}} - x_{f_{H2}}.n_{f_{tot}}\right) \times \frac{1}{20\ g\ biooil} \qquad (1)$$

Where $n_{i_{H2}}$ is the initial number of mole of hydrogen, $x_{f_{H2}}$ is the final mole fraction of hydrogen, and $n_{f_{tot}}$ is the total number of mole of gas at the end of experiment.

After each experiment, the liquid products were collected in centrifuge tubes and centrifuged (using a 5702 R centrifuge, Eppendof, Germany) for 30 minutes at g-force of 2147 to separate the resulting aqueous and organic phases and residual solids and catalyst. Both liquid phases were separated and weighed for mass balance determination. The solids (catalyst and coke) were collected and dried at 95 °C for 6 hours. The vessel and reactor parts were rinsed with methanol-toluene mixture (1:1 vol. ratio) to collect any remaining catalyst and oil. The solvent washings were filtered through Watman 42 ashless filter paper (GE Healthcare, UK) and dried at 95 °C. The weight of filter paper was recorded before and after filtration.

The total mass of gaseous product was calculated using equation (2):

$$W_g = \sum_i x_i . MW_i . n_{tot} \qquad (2)$$

Where W_g is the total mass of gaseous product (g), x_i is the mole fraction of gas i, MW_i is the molecular weight of gas i (g/mole), and n_{tot} is the total number of moles of gas product. The yield of liquid, gas, and solid product were calculated using equations 3, 4, and 5 respectively.

$$Y_{liquid}(\%) = \frac{W_l}{W_f} \times 100 \qquad (3)$$

$$Y_{gas}(\%) = \frac{W_g}{W_f} \times 100 \qquad (4)$$

$$Y_{coke}(\%) = \frac{(W_s - W_C)}{W_f} \times 100 \qquad (5)$$

Where W_f is the mass of feed bio-oil and consumed hydrogen combined (g), W_l is the mass of liquid product (g), W_g is the mass of gas product (g), W_s is the weight of total solid residues (g), and W_c is the weight of catalyst (g).

An elemental carbon balance before and after each experiment was performed.

In a blank experiment, without catalyst, 20 g of PJ bio-oil was charged into the reactor and the reactor was pressurized to 6.2 MPa with hydrogen. The bio-oil was allowed to react for 30 minutes at 400 ° C. All experiments were conducted in triplicate.

3.5. Characterization of PJ wood, catalytic pyrolysis oil, and HDO products

3.5.1. Physical properties

The moisture content of the PJ wood was determined according to standard method ASTM E1756- 08 and the ash content was determined according to ASTM E1755-01 method. The water content of the crude bio-oil and hydrotreated oil were determined by Karl-Fisher titration method with Hydranal® -composite 5 solution. A Metrohm 701KF Titrino and 703 titration stand setup (Brinkmann Instruments, Riverview, FL, USA) were used for the volumetric Karl Fischer titration. The pH was measured using Mettler Toledo pH Meter and probe (Mettler−Toledo GmbH, Switzerland). The density and kinematic viscosity of the bio-oil and HDO oil were measured at 40 °C using Anton Parr Stabinger viscometer svm 3000 (Ashland, VA, USA).

3.5.2. Chemical properties

The higher heating value (HHV) of PJ wood, bio-oil, and hydrotreated oil were determined using IKA Model C2000 basic bomb calorimeter (IKA Inc., Wilmington, NC, USA). The elemental composition of biomass, bio-oil, and hydrogenated oil were determined using Thermo Fischer Scientific Flash 2000 organic elemental analyzer (Thermo Fisher Scientific, Waltham, MA, USA). Fourier transform infrared spectrum

(FTIR) over the range of 600 to 4000 nm was recorded using Avatar 360 FTIR instrument (Thermo Fisher Scientific, Waltham, MA, USA). The ^{13}C NMR spectra were recorded on a Bruker AvanceIII HD Ascend 500 MHz NMR spectrometer (Billerica, MA, USA). In a 5-mm sample probe about 0.5 g of oil was dissolved in 1.5 g deuterated solvent. Dimethyl sulfoxide-d_6 (DMSO-d_6) (Sigma-Aldrich, St. Louis, MO, USA) was used for catalytic pyrolysis oil and chloroform-d (Cambridge Isotope Laboratories, Inc., USA) was used for HDO oil. The observing frequency for the ^{13}C nucleus was 100.58 MHz, the pulse width was 10 μs, the acquisition time was 1.58 s, and the relaxation delay was 2 s. The spectra were obtained with 3000 scans and a sweep width of 20 kHz.

3.6. Gas analysis

Gas samples were collected in tedlar sampling bags from the sampling port installed on the reactor head and analyzed using a Varian 490-micro GC system (Agilent Technology, Santa Clara, CA, USA). The micro GC was equipped with two modules: a 10 m Molsieve 5A (MS) column, and a 10 m porous polymer (PPU) column. Each module had a thermal conductivity detector. MS was used to analyze hydrogen, methane, and carbon monoxide (CO), while carbon dioxide (CO_2) and C_1−C_5 hydrocarbons were analyzed on the PPU column. Gas concentrations were calculated relative to calibration curves of three standard gas mixtures supplied from Scotty Specialty Gases (Fremont, CA, USA). Gas samples were analyzed for H_2, CO, CO_2, CH_4, C_2H_4, C_2H_6, C_3H_8, C_4H_{10}, and C_5H_{12}.

4. Results and discussion

4.1. Characterization of PJ biomass and PJ pyrolysis oil

The biomass was characterized on the basis of moisture, ash content, elemental composition, and higher heating value (HHV) [56]. The physicochemical properties of the PJ wood are shown in Table 5.1. The ESP-condensed oil was used in HDO experiments because this was representative of all the oil fractions and had the least amount of water. The ESP oil was characterized for ash content, ultimate composition, HHV, pH, water content, density, and dynamic viscosity. The yield of organic liquid after catalytic fast pyrolysis of biomass was about 30 % mass of fed PJ wood (dry basis). The physicochemical properties of the raw bio-oil are shown in Table 5.1. The ultimate composition was similar to those reported by Yathavan and Agblevor [24].

Table 5. 1: Characterization of pinyon-juniper biomass and bio-oil*

Properties	PJ biomass	Catalytic PJ bio-oil
Elemental Composition (dry basis) (wt. %)		
Ash content	0.53 ± 0.06	0.00
Nitrogen	0.17 ±0.01	0.47 ± 0.04
Carbon	54.43 ± 0.11	67.42 ± 0.21
Hydrogen	6.27 ± 0.09	7.23 ± 0.07
Sulfur	<DL**	<DL**
Oxygen***	38.60 ± 0.12	24.88 ± 0.12
HHV (MJ/kg)	19.37 ± 0.11	28.41 ± 0.23
pH	NA	3.27 ± 0.05
Water content (wt. %)	6.65 ± 0.09	3.36 ± 0.08
Density (g/cm^3)	0.55 ± 0.03	1.16 ± 0.02
Dynamic viscosity (cP)	NA	95.5 ± 1.5

* Error are the standard deviation of two measurements
** Below detection limit
*** By difference

4.2. Characterization of Ni/RM catalysts

The BET specific surface area of RM was relatively low after calcination (37.51 m^2/g), but after reduction of the calcined RM it increased to 54.34 m^2/g. The increase in surface area was attributed to elimination of oxygen during the reduction.

The variation of BET specific surface area of Ni/RM catalysts vs. nickel loading is shown in Fig. 5.1. The specific surface area of the catalysts increased due to the reduction of NiO to Ni and formation of pores [57-60]. By increasing the nickel content from 10% to 65%, the BET surface area of the activated catalyst increased from 45.47 to 88.36 m^2/g. The increase in surface area with increase in nickel loading was in good agreement with other researchers [61]. Linear regressions of BET surface area vs. nickel loading showed R^2 of 0.99 and 0.96 respectively for the calcined form and reduced forms of the catalyst. The increase in surface area with increase in Ni content suggests that nickel was efficiently dispersed on RM support with minimum pore plugging during impregnation [62].

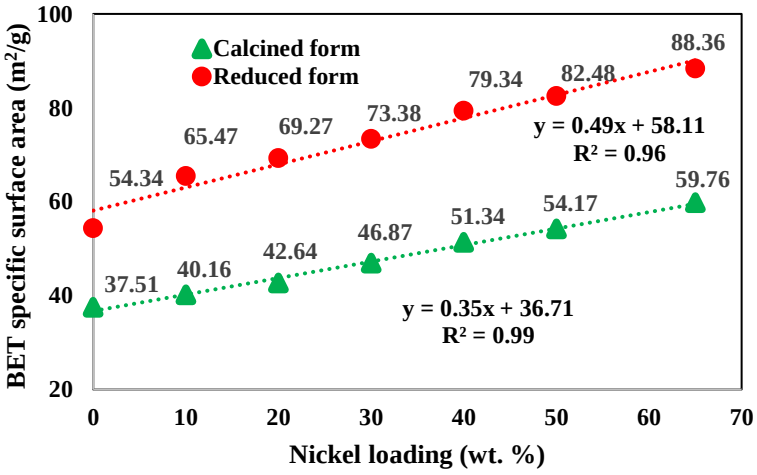

Fig. 5. 1: BET surface area of Ni/RM catalysts vs. nickel content in calcined and reduced forms.

TG-TPR was performed to investigate the reducibility of nickel oxide, RM support, and the interaction between nickel and the RM support (Figs. C.1 to C.8 in Appendix C show the TPR profile of individual samples). For comparison, TPR profiles of NiO, 40% Ni/RM catalyst, and RM support are shown in Fig. 5.2. TPR profile of RM indicated three major reduction peaks at 279, 542, and 694 °C (Fig. 5.2 and Fig. C.1 in Appendix C). The peak at 279 °C could be due to the reduction of Fe_2O_3 to Fe_3O_4 and the unresolved peaks centered at 542 °C and 694 °C could correspond to reduction of Fe_3O_4 to FeO and then to elemental Fe [23].

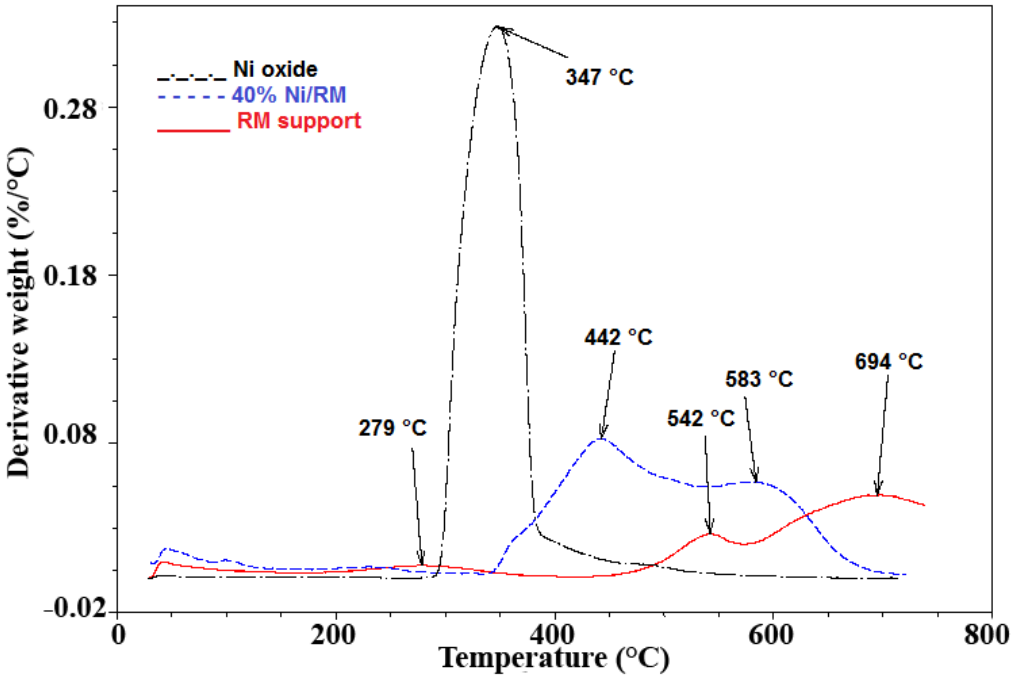

Fig. 5. 2: TG-TPR profile of RM support, 40% Ni/RM, and Ni oxide.

The TPR profiles of Ni/RM catalysts appeared to show strong interaction between the RM and NiO since the RM TPR peaks were reduced to two major reduction peaks

assigned as lower temperature peak and higher temperature peak as summarized in Table 5.2. There were no independent peaks of RM and NiO. The lower temperature peak appeared to have higher concentration of NiO than the higher temperature peak since its intensity increased with increased Ni content and its reduction temperature shifted towards that of nickel oxide (347 °C according to Fig. 5.2 and Fig. C.8 in Appendix C). This observation is in agreement with Jeangros et al. who observed interaction between SiO_2 and NiO during the reduction of NiO to Ni [58]. The intensity of the higher temperature peak decreased as Ni loading increased, but its reduction temperature also decreased with increased Ni content. The improvement in oxide catalyst reducibility (lower reduction temperature) with increase in metal content was attributed to interaction between the red mud support and NiO and has been reported for other oxide catalysts [60-68)]. In the case of 40 and 50 % Ni, small shoulders were detected between 350 and 400 °C, 400 and 450 °C and an unresolved peak at about 580 °C appeared in TPR profile of 65%Ni/RM. This seems to indicate that there are different NiO species that interacted differently with RM [69].

Table 5. 2: Reduction temperatures of Ni/RM catalysts according to TPR profiles.

Catalyst	Lower temperature peak (°C)	Higher temperature peak (°C)
10% Ni/RM	569	678
20% Ni/RM	540	668
30% Ni/RM	509	597
40% Ni/RM	442	583
50%Ni/RM	426	560
65% Ni/RM	412	486

Since the 40%Ni/RM catalyst performed best in terms of HDO reaction (described in details in section 3.3), this catalyst was further characterized by ICP, XRD,

and SEM. In order to investigate the effect of RM support and to verify the estimated amount of Ni added to the RM, ICP analyses were performed on RM and 40%Ni/RM catalyst. As shown in Table 5.3, the major metals present in RM were Al (9.08%), Ca (1.2%), Fe (21.56 %), Na (7.17%), and Si (4.35%) and trace amounts of other metals such as As, Cd, Cu, Mo, Zn and others. RM (in reduced form) was investigated in HDO experiment to determine the effect of support on the chemical reactions. The results of RM effect are presented in section 3.3. After impregnation of RM with nickel, the relative amounts of all metals decreased due to presence of 40% nickel. The ICP analysis of 40%Ni/RM showed a Ni content (40.8%), which was very close to the estimated amount added to the substrate.

Table 5. 3: ICP analysis of RM support and 40%Ni/RM catalyst.

Metal (wt. %)	RM	40%Ni/RM
Al	9.08	4.44
Ca	1.20	0.65
Fe	21.56	9.47
K	0.03	0.02
Mg	0.07	0.04
Na	7.17	3.51
Ni	<0.01	40.8
P	0.03	0.01
S	0.10	0.06
Si	4.35	2.53
Metal (mg/kg)	RM	40%Ni/RM
As	0.87	<DL
B	9.41	0.85
Ba	10.4	4.55
Cd	5.79	3.37
Co	278	12.3
Cr	245	132
Cu	3.13	<DL
Mn	<DL	<DL

Mo	1.62	0.48
Pb	156	7.09
Se	<DL	<DL
Sr	23.1	2.28
Zn	2105	26.1

Fig. 5.3 depicts the XRD patterns of fresh Ni/RM catalyst at different stages of processing and use. Distinct sharp peaks observed at 2Θ of 52.2°, 61° were attributed to metallic Ni produced from the reduction of NiO. The detection of NiO peaks in reduced 40%Ni/RM (2Θ of 43.7°, 50.9°, and 74.7°) showed that nickel oxide was not completely reduced to elemental Ni after the hydrogen treatment, perhaps because of mass transfer limitations (Fig. 5.3a) and temperature effect. It has been reported that complete reduction of NiO does not occur until the reduction temperature was above 600 ˚C [58], which appears to corroborate the current data, since the reduction temperature was 450 °C. The magnetite (Fe_3O_4) peaks detected in the spectrum were due to the reduction of hematite (Fe_2O_3) that was present in the RM [24].

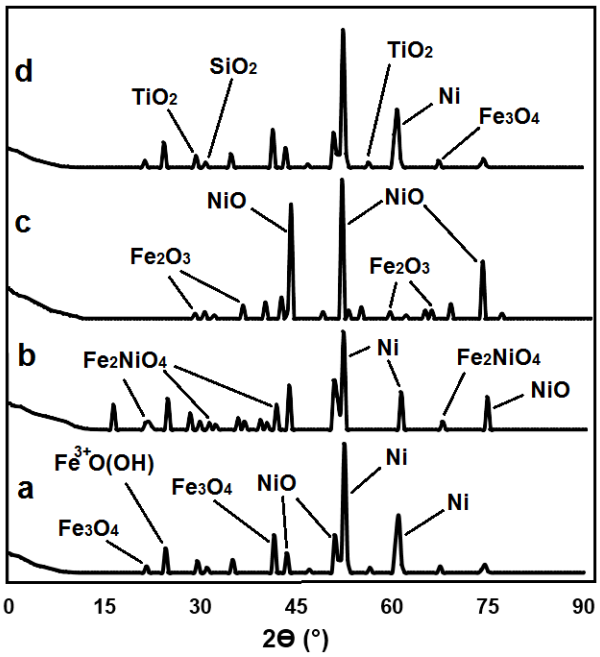

Fig. 5. 3: XRD patterns of a) fresh 40%Ni/RM HDO catalyst, b) used 40%Ni/RM catalyst (after HDO process), c) regenerated 40%Ni/RM catalyst after burning off the coke, and d) regenerated and reduced 40%Ni/RM HDO catalyst.

The XRD pattern of used 40%Ni/RM (Fig. 5.3b) catalyst showed stronger NiO peaks compared to the fresh catalyst, suggesting that some Ni was oxidized during HDO. This could be one reason for the partial deactivation of the catalyst. Additionally, trevorite (Fe_2NiO_4) peaks were also observed after HDO, which could also contribute to the deactivation of active Ni sites. Furthermore, the intensities of Ni peaks (2Θ of 52.1° and 61°) in the used catalyst were lower than those of the fresh catalyst, suggesting that there was overall deactivation of the catalyst.

In order to recycle the catalyst, the used catalyst was regenerated in a muffle furnace at 400 °C for 4 h to burn off the deposited carbonaceous compounds (coke), which was followed by reduction as described in material and methods section. The XRD

pattern of the regenerated catalyst (Fig. 5.3c) showed strong NiO diffraction peaks at 2Ɵ of 43.9°, 50.8°, and 75°, which were due to the oxidation of nickel into NiO under heat treatment in air. Furthermore, it was interesting to note the weak Ni diffraction peaks in the XRD pattern of the regenerated catalyst (Fig. 5.3c). It suggested mass transfer limitation of oxygen, which could not penetrate the bulk RM to oxidize the Ni buried in it. The detection of hematite (Fe_2O_3) diffraction peaks in the regenerated catalyst was ascribed to oxidation of magnetite.

When the regenerated catalyst was activated by reduction in H_2, its XRD pattern (Fig. 5.3d) showed similar diffraction peaks as the fresh catalyst (Fig. 5.3a) suggesting complete recyclability of the catalyst. More detailed information on catalytic activity of the used catalyst and the recycled catalyst are discussed in section 3.4.

The surface morphology of the catalyst was studied using scanning electron microscopy (SEM). The SEM images of the RM support, 40%Ni/RM catalyst precursor (calcined form), fresh 40%Ni/RM catalyst (reduced form), and used 40% Ni/RM catalyst are presented in Fig. 5.4. In the case of RM support (Fig. 5.4a), in addition to amorphous looking particles, crossed-cocentric discs and spherical-shaped particles were observed. Nickel oxide particles were dispersed in the RM support (Fig. 5.4b) in small clumps. Ni particles with relatively uniform morphology and approximate mean diameter of 90 nm were dispersed on the surface of the RM in the case of activated Ni/RM (Fig. 5.4c). The SEM picture for the used catalyst (Fig. 5.4d) showed that the catalyst was coated with coke after HDO process, which could affect the hydrogen transfer to active sites and also reduce catalyst activity.

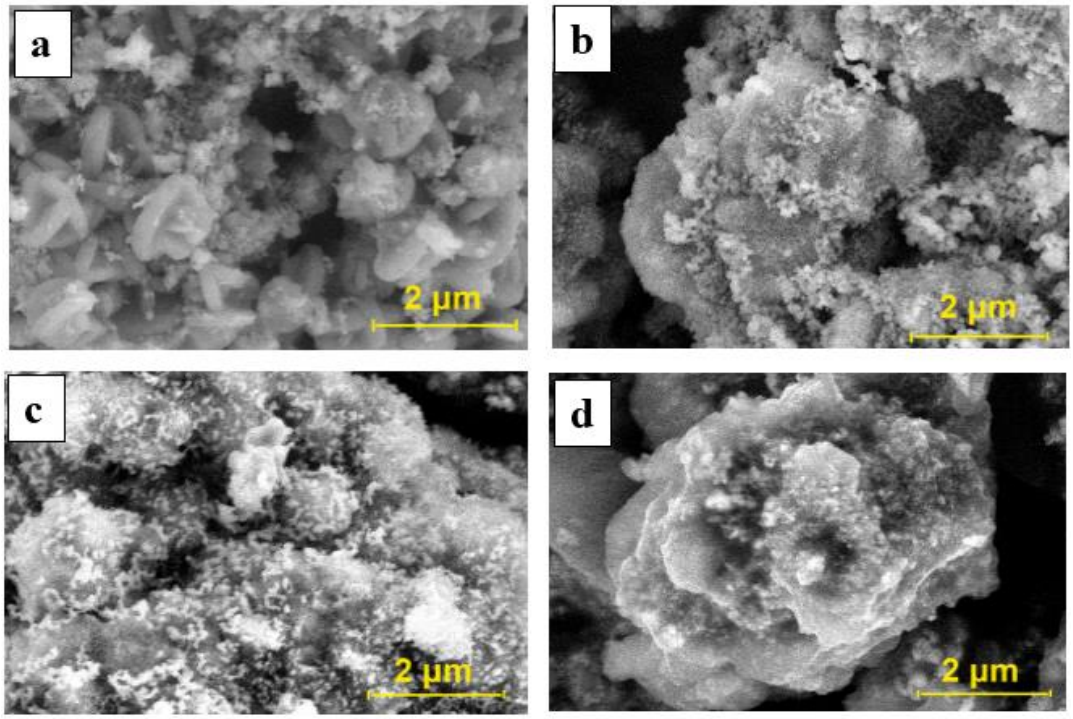

Fig. 5. 4: SEM images of Ni/RM catalyst at different stages: a) RM support, b) 40%Ni/RM (calcined form), c) 40%Ni/RM (reduced form) (fresh catalyst for HDO), d) used 40%Ni/RM catalyst after HDO process (coked catalyst).

4.3. Results of HDO experiments

4.3.1. Mass balance of HDO products

No catalytic activity was observed in the case of blank experiments and the bio-oil polymerized (solidified) due to the presence of highly reactive compounds in bio-oil such as sugar derivatives and phenolic compounds [70]. The reactor was not catalytically active and did not influence the experiment.

As expected, Ni loading had significant effect on HDO product yields distribution (Fig. 5.5). HDO experiment using RM (0% Ni loading) produced 48.2% solids (coke) and 43.4% gas and only 5.2% organic liquid. About 60.8% of the original carbon was recovered in the solid residues, 31.2% was converted to gaseous products and only 5.3%

was retained in the organic liquid product (Table 5.4). These results suggested that at 0%Ni loading, cracking and coke formation reactions were dominant compared to HDO reactions, hence, the RM support had very limited activity for HDO reactions but favored unwanted side reactions (coke and gas formation) in the absence of Ni.

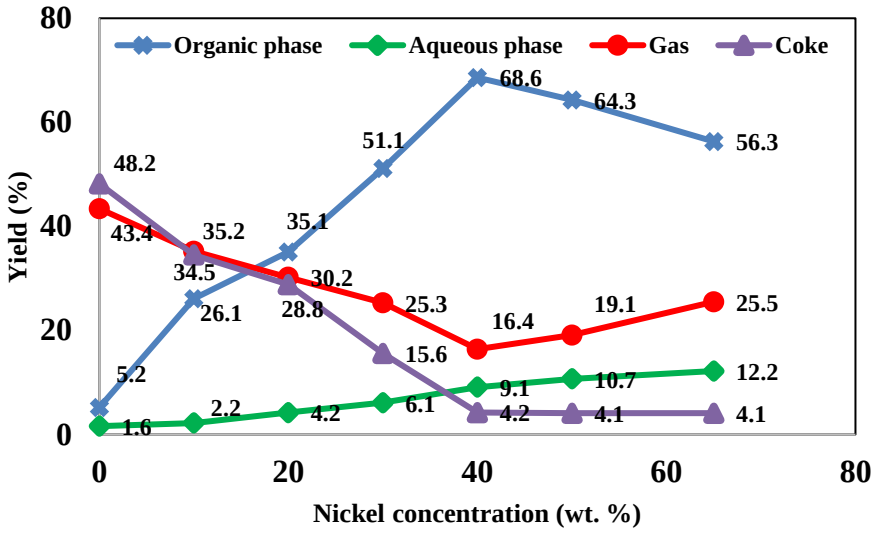

Fig. 5. 5: Effect of nickel concentration on HDO products (organic phase (HDO oil), aqueous phase (mostly water), gas, and coke) yield distribution (dry basis) using Ni/RM catalyst.

Table 5. 4: Total mass balance and carbon mass balance of HDO products at different nickel contents.

Ni loading (wt. %)	Total mass balance (wt. %)					Carbon balance (wt. %)				
	Organic	Aqueous	Gas	Coke	SUM	Organic	Aqueous	Gas	Coke	SUM
0	5.2	1.6	43.4	48.2	98.4	5.3	1.4	31.2	60.8	98.6
10	26.1	2.2	35.2	34.5	98.0	27.2	1.1	26.8	43.5	98.6
20	35.1	4.2	30.2	28.8	98.3	38.8	0.6	22.4	36.3	98.1
30	51.1	6.1	25.3	15.6	98.1	58.7	0.3	19.3	19.7	98.0
40	68.6	9.1	16.4	4.2	98.3	84.0	0.0	9.5	5.3	98.8

50	64.3	10.7	19.1	4.1	98.2	78.9	0.0	14.2	5.2	98.3
65	56.3	12.2	25.5	4.1	98.1	69.4	0.0	23.7	5.2	98.3

When the Ni loading was increased from 10% to 40%, the organic liquid yield increased from 26.1% to 68.6%, the gas yield decreased from 35.2% to 16.4%, and the coke yield decreased from 34.5% to 4.2% (Fig. 5.5). These results showed that increasing the Ni content improved HDO reactions and reduced coke formation and cracking reactions. Furthermore, the water yield increased from 2.2% to 9.1% indicating higher levels of HDO reactions that produced water. At Ni loading of 50% and 65% the organic liquid yields were 64.3% and 56.3% respectively and no significant changes were observed in coke yield. However, the gas yield increased to 19.1% and 25.5% respectively for Ni contents of 50% and 65%. Comparing the product yields distribution of the HDO experiments using 40, 50, and 65% Ni loading, it was concluded that HDO reactions for organic liquid were optimal at this reaction time (30 minutes) using 40%Ni/RM. The higher Ni loadings of 50% Ni and 65%Ni did not improve organic liquid production, but rather caused increased hydrocracking, which generated higher amounts of gas products. The physicochemical properties of the HDO oil such as elemental composition and HHV did not change significantly when Ni content increased from 40% to 50% and 65% (Table 5.5). In contrast, H_2 consumption increased due to higher levels of hydrocracking of HDO oil compounds and methanation of CO_2 and CO.

Table 5. 5: H_2 consumption, physicochemical properties of the liquid products, and gas product composition at different nickel concentrations using Ni/RM catalyst.

Properties	Temperature and reaction time were 400 °C, and 30 min respectively						
	RM	10% Ni/RM	20% Ni/RM	30% Ni/RM	40% Ni/RM	50% Ni/RM	65% Ni/RM
H_2 consumption (mol/g bio-oil)	0.002	0.021	0.035	0.046	0.053	0.061	0.072
Aqueous phase							
Water content (wt. %)	71.35	80.36	85.67	97.45	99.45	99.50	99.95
pH	4.11	4.35	5.47	6.36	6.91	6.93	6.93
HDO oil (organic phase)							
Elemental composition (dry basis) (wt. %)							
N	0.45	0.38	0.33	0.32	0.31	0.30	0.30
C	68.16	70.34	74.56	77.49	82.52	82.71	83.11
H	7.85	9.56	11.32	13.45	15.82	16.13	16.59
O	23.54	19.72	19.37	8.74	1.35	0.86	0
HHV (MJ/kg)	29.15	35.56	38.38	41.73	45.77	45.79	45.81
pH	3.65	4.23	5.04	5.78	NA	NA	NA
Water content (wt. %)	3.24	2.11	1.07	0.67	<DL*	<DL*	<DL*
Density (g/ml)	1.11	0.93	0.88	0.82	0.79	0.78	0.78
Dynamic viscosity (cP)	88.54	12.45	8.56	3.67	1.37	1.31	1.31
Gas composition (mole %)							
CO	12.11	6.02	5.28	4.37	3.32	2.84	2.23
CO_2	16.43	13.47	9.17	7.56	5.52	4.75	4.19
CH_4	43.77	54.15	59.75	61.36	67.34	68.26	69.76
C_2H_4	5.34	7.26	7.89	8.11	8.26	8.41	8.66
C_3H_8	10.21	9.34	8.55	7.78	7.56	7.61	7.67
C_4H_{10}	7.42	6.32	5.83	5.62	5.45	5.40	5.28
C_5H_{12}	4.35	3.41	3.34	3.16	2.47	2.32	2.19

* The detection limit was 0.05%.

The aqueous liquid (water) yield was 10.7% and 12.2% at Ni loadings of 50% and 65% respectively (Fig. 5.5), indicating slight increases compared to that of 40%Ni/RM (9.1%). This result is further explained in section 3.3.2. The highest fraction of original carbon (84%) retained in the organic liquid product was achieved when 40%Ni/RM was used for HDO experiment (Table 5.4). At this Ni loading, 9.5% of the initial carbon was converted to gas, and only 5.3% remained in the coke.

4.3.2. Characterization of HDO products

4.3.2.1. Physicochemical properties of HDO products

Changes in properties of HDO liquid and gas products composition at different Ni loadings are reported in Table 5.5. At 0%Ni (using only RM support), the carbon, hydrogen, and oxygen contents of the organic phase were 68.16, 7.58, and 23.54 wt. % respectively. The elemental composition changed slightly compared to 67.42, 7.23 and 24.88 wt. % of C, H, and O respectively of the original bio oil (Table 5.1), which, suggested there were minimal HDO reactions on the RM support. The RM support favored cracking and coke formation reactions and was considered as an inert support for the HDO reactions.

Increasing the Ni content from 10% to 40% significantly increased the hydrogen content of the organic HDO product from 9.56 wt. % to 15.83 wt. % while oxygen content was reduced from 19.72 wt. % to 1.35 wt. %. Hydrogen consumption increased from 0.021 mol/(g bio-oil) to 0.053 mol/(g bio-oil) when Ni loading increased from 10% to 40% (Table 5.1). As a critical scale-up parameter, the hydrogen consumption at Ni loading of 40% was slightly higher than the value reported by Agblevor et al. using sulfided cobalt/molybdenum oxide supported on zirconia [71]. The density of the oil was reduced by about 15% from 0.93 g/cm^3 to 0.79 g/cm^3 when the Ni loading increased from 10% to 40%. The dynamic viscosity decreased from 12.45 cP to 1.37 cP over this Ni loading range. The reduction in density and viscosity could be attributed to hydrocracking of high molecular weight compounds in the bio-oil during HDO [72, 73]. The reduction in acidity can be due to conversion of carboxylic acids in the bio-oil to other compounds during hydrodeoxygenation [74]. At Ni loadings of 50% and 65% the changes in elemental composition of HDO oils were not significantly different from that of 40% Ni loading (Table 5.5), however, the hydrogen consumptions were 0.061 mol/(g

bio-oil) and 0.072 mol/(g bio-oil) respectively. These results suggest that increased catalyst activity at 50% and 65% Ni loadings increased the rate of hydrocracking and methanation rather than HDO reactions as previously mentioned (Fig. 5.5). Furthermore, no significant changes were observed in the viscosity of HDO oil at Ni loadings of 50% and 65% compared to that of 40%Ni/RM.

In all HDO experiments, the major gas product was methane (Table 5.5). The concentration of methane increased from 54.15 mol% to 67.34 mol% when the Ni loading increased from 10% to 40%. Increasing the Ni loading decreased the concentration of CO and CO_2, because of methanation of these two gases due to increased catalyst activity [74-76]. The concentration of C_3-C_5 gases gradually decreased with increase in Ni content, which could be due to hydrocracking of these gases at higher Ni loadings. Increasing the Ni content from 40% to 50% and 65% increased the concentration of methane from 67.34 mol% to 68.26 mol% and 69.76 mol% respectively while CO and CO_2 decreased to 2.84 % and 4.75% respectively at 50% Ni loading and 2.23 mol% and 4.19 mol% respectively at 65% Ni loading.

4.3.2.2. FTIR analysis of HDO organic liquids

The FTIR spectra of the raw bio-oil and HDO oils at different Ni loadings are shown in Figs. C.9 to C.16 (Appendix C). For comparison, the FTIR spectra of the raw bio-oil and the HDO oil obtained from 40%Ni/RM are shown in Fig. 5.6. The absorbance peaks between 3050 and 3650 cm^{-1} were assigned to –OH stretching vibration, which indicated that phenolic compounds, carboxylic acids, water, and alcohols were produced during catalytic pyrolysis of PJ biomass. With the increase in Ni loading, the intensity of

these peaks gradually decreased or even disappeared in the HDO oil, which could be due to phenolic or alcoholic hydroxyl cleavage, elimination, intramolecular dehydration, or hydrodeoxygenation of –OH groups. Furthermore, during HDO, water could possibly migrate to the aqueous phase. The peaks between 2840 and 3010 cm^{-1} and the two other bands at 1376 and 1453 cm^{-1} were assigned to C–H stretching and deformation in methyl groups and methylene groups, respectively. The peaks intensified after HDO compared to the original bio-oil. The peaks at 1590-1610 cm^{-1} were attributed to benzene in-ring C–C stretching. These peaks decreased gradually with increasing Ni loading suggesting that the aromatics possibly underwent cracking, ring saturation, or polymerization to form coke. The peak at 1670 cm^{-1}, which was assigned to C=O stretching, gradually decreased with increase in Ni loading.

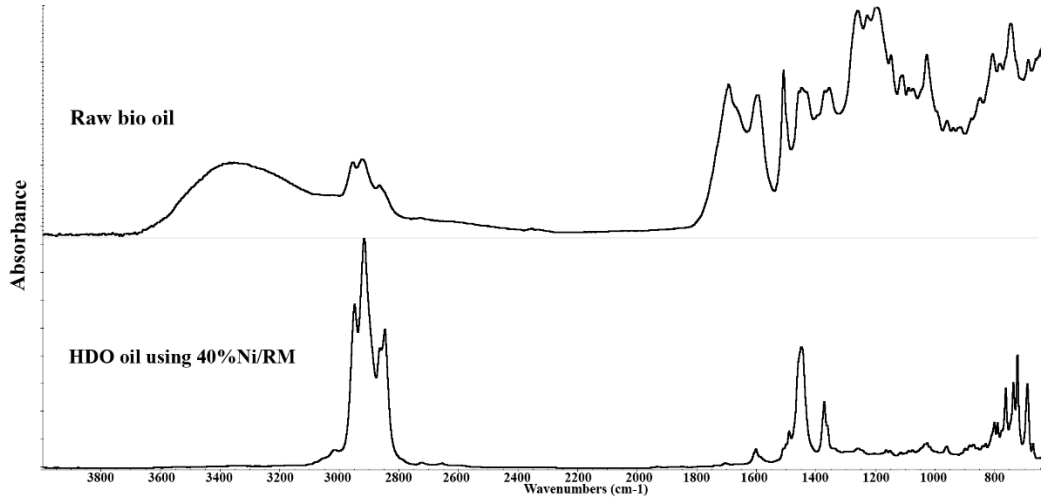

Fig. 5. 6: FTIR spectra of raw bio oil and HDO oil using 40%Ni/RM catalyst.

The appearance of typical carbonyl group C=O stretching vibrations at 1710 cm^{-1} showed that aldehydes or ketones were significant at 10% Ni loading, while at higher

loadings, these peaks disappeared. Similarly, at higher Ni loadings the C–O stretching absorption band at 1033 and 1100 cm^{-1} disappeared, which could be due to the deoxygenation of alcohols, phenols, or esters. The peaks between 740 and 830 cm^{-1} assigned to C–H out-of plane bending vibration from aromatics and their derivatives decreased gradually because of hydrogenation of the benzene ring. These results indicated that the oxygenated groups (–OH, C=O, and C–O) were significantly removed from the HDO oil. At 40% Ni loading, mostly hydrocarbon peaks were present as indicated by the peaks between 2840 and 3010 cm^{-1} and the two other bands at 1376 and 1453 cm^{-1} due to C–H stretching; the 1600 cm^{-1} due to aromatics; the 730-770 cm^{-1} due to monosubstituted C-H bend; and o, m, p- distributed C-H bend peaks between 735-840 cm^{-1} (Fig. 5.6). Compared to the FTIR spectrum of the raw bio-oil, the HDO oil of 40% Ni/RM indicated significant removal of oxygenated groups (Fig. 5.6) which corroborates the CHNOS analysis data in Table 5.5. At Ni loadings of 50% and 65% (Figs C.15 and C.16 in Appendix C), the aromatic peaks decreased significantly suggesting that there was increased hydrogenation of aromatics and/or hydrocracking of these compounds at higher catalyst activities compared to that of 40% Ni/RM. According to Fig. 5.6, it was clear that after HDO process, -OH peaks (at 3050 and 3650 cm^{-1}), C=O peaks (at 1670 cm^{-1} and1710 cm^{-1}), and C-O peaks (at 1033 and 1100 cm^{-1}) disappeared, whereas hydrocarbon peaks (C-C and C-H) increased significantly suggesting efficient removal of oxygen from the raw bio-oil.

4.3.2.3. ^{13}C NMR analysis of HDO organic liquids

The functional groups present in the crude bio-oil and HDO oils were characterized by semiquantitative integration of ^{13}C NMR spectra. The ^{13}C NMR spectra of the raw bio-oil, and HDO oils at different Ni loadings are shown in Fig. 5.7. The chemical shifts of various functional groups were assigned according to those reported in literature [54, 73]. The semi-quantitative analysis of the ^{13}C NMR functional groups are presented in Table 5.6. The crude bio-oil had high amounts of carbohydrate degradation products, alcohols, ethers, methoxylated phenols, carboxylic groups, aldehydes, and ketones.

Table 5. 6: Functional group distribution of crude bio-oil and HDO oils at different nickel concentrations from ^{13}C NMR spectral integration.

Chemical shift region (ppm)	Dominant type of carbon	Percentage of carbon based on ^{13}C NMR analysis							
		Feed bio-oil	RM	10% Ni/RM	20% Ni/RM	30% Ni/RM	40% Ni/RM	50% Ni/RM	65% Ni/RM
0-28	Saturated aliphatic groups	15.8	17.1	24.7	31.8	36.7	42.6	46.3	56.2
28-55	Unsaturated aliphatic groups	9.7	10.8	13.6	14.9	16.8	17.6	23.4	27.6
55-95	Alcohols, ethers, phenolic methoxys, anhydrosugars	15.4	14.8	11.3	8.4	4.2	0	0	0
95-165	Aromatics, Furans	45.7	44.6	41.5	40.9	40.1	39.8	30.3	16.2
165-180	Organic (carboxylic) acids, esters	8.6	8.2	5.3	2.1	1.4	0	0	0
180-215	Ketones, aldehydes	4.8	4.5	3.6	1.9	0.8	0	0	0

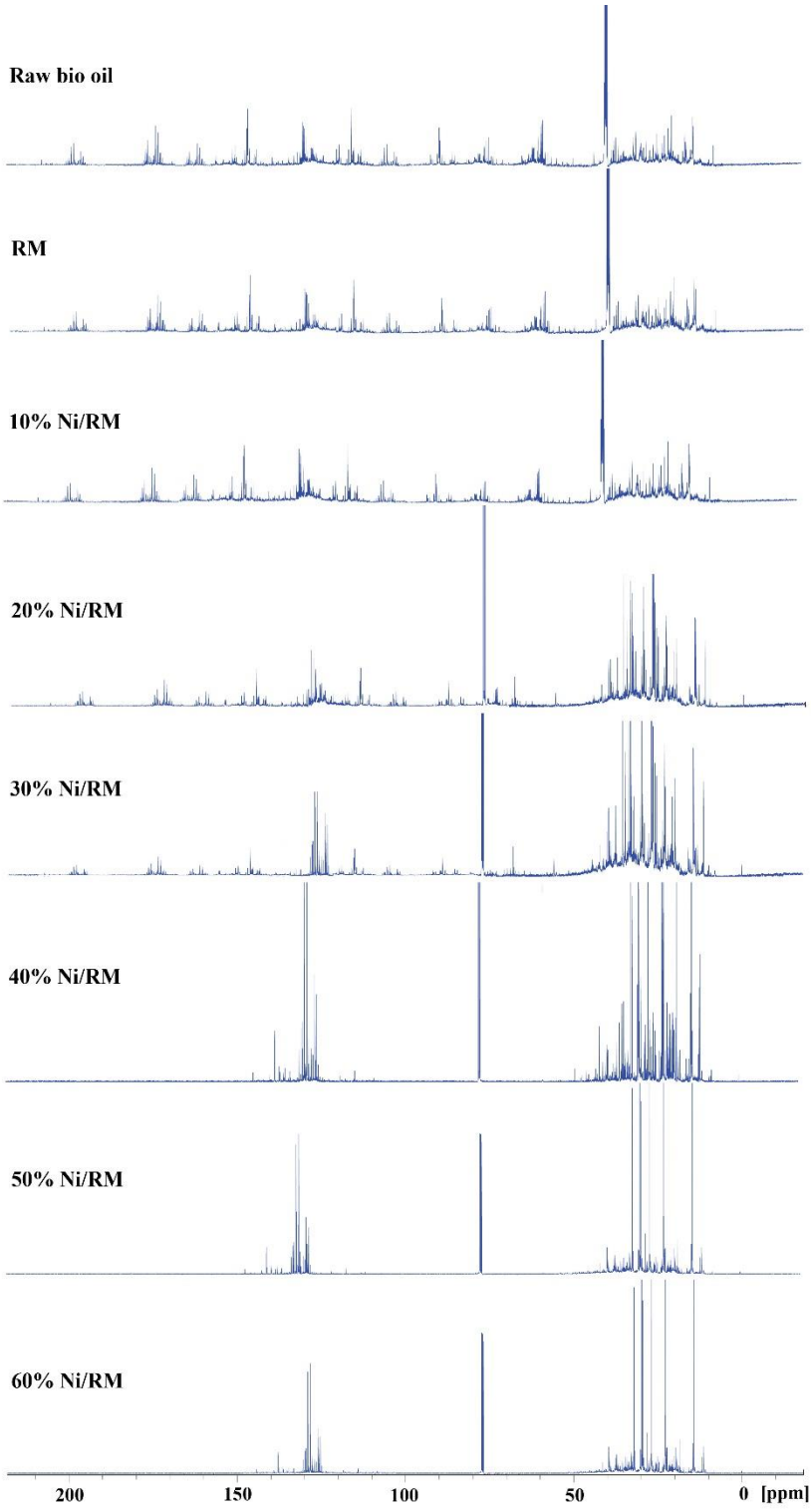

Fig. 5. 7: ^{13}C NMR spectra of raw bio oil and HDO oils at different Ni concentrations.

The characteristic peaks at 0-28 ppm assigned to saturated aliphatic carbon atoms increased during HDO due to hydrogenation of unsaturated aliphatics, HDO of alcohols, ethers, carboxylic acids, aldehydes, and ketones. Increasing the Ni loading from 10% to 40% increased the saturated aliphatic carbon atoms from 24.7% to 42.6% (Fig. 5.7 and Table 5.6) due to improved hydrogenation/hydrodeoxygenation of unsaturated compounds and oxygenated compounds.

The chemical shifts of 28-55 ppm assigned to the unsaturated carbon atoms that are separated from oxygen atoms by at least two bonds [77, 78], were present in the bio-oil and its content in the HDO oil increased as the Ni content of the catalyst increased. The chemical shifts of 55-95 ppm were assigned to aliphatic carbon atoms attached to oxygen atoms in alcohols, esters, and anhydrous carbohydrates. Increasing Ni loading, decreased the amount of alcohols, esters, and anhydrous carbohydrates due to increased catalyst activity. At Ni loadings of 40%, 50% and 65% no peaks were observed at chemical shifts between 55-95 ppm (Fig. 5.7 and Table 5.6) suggesting that there was complete deoxygenation of all the oxygenated compounds including the methoxy carbon that resonates at 55-57 ppm.

The characteristic peaks at chemical shift of 95-165 ppm were assigned to aromatic carbon atoms in phenolic compounds and furans. These carbon atoms decreased with increasing Ni loading due to hydrogenation/deoxygenation of these compounds. When Ni loading was increased from 40% to 65%, unsaturated aliphatics increased from 17.6% to 27.6% and aromatic compounds decreased from 39.8% to 16.2%. These results could be due to partial hydrogenation of aromatic compounds. The saturated aliphatics content increased from 42.6% to 56.2% due to increased hydrogenation of unsaturated

aliphatics (Fig. 5.7 and Table 5.6). However, hydrogenation of unsaturated aliphatics was not complete even at 65% Ni loading. Longer reaction times could result in complete hydrogenation of unsaturated aliphatic carbons, but longer reaction times are known to cause hydrocracking of organic compounds to gases, which will reduce the organic liquid yield [12, 73].

The chemical shifts at 165-180 ppm assigned to carboxylic acids and esters, decreased gradually and finally disappeared at high Ni loadings. Increasing the Ni loading from 10% to 30%, decreased these carboxylic carbon signals intensity from 5.3% to 1.4%. At higher Ni loadings, no characteristic peaks were observed between 165-180 ppm (Fig. 5.7 and Table 5.6), because of complete deoxygenation of these compounds.

Characteristic chemical shifts of 180-215 ppm assigned to carbon atoms of carbonyl groups (aldehydes and ketones) decreased from 4.8% in bio-oil to zero in HDO oil at 40% Ni loading indicating that aldehydes and ketones were completely deoxygenated.

4.4. Catalyst deactivation and regenerability

The 40%Ni/RM was used to investigate catalyst deactivation and recyclability by conducting several HDO runs without any regeneration or reduction of the catalyst between runs. As shown in Fig. C.17 in Appendix C, the organic liquid yield decreased from 68.6% to 6.8% after three consecutive batches while the gas yield increased from 16.4% to 41.5% and the coke yield increased from 4.2% to 47.4%. The properties of HDO oil obtained from this set of experiments are summarized in Table C.1 (Appendix C). The physicochemical properties of the HDO oil after the third run was about the same

as that of 0%Ni/RM HDO experiment (Table 5.5) which showed that the catalyst was completely deactivated after three suns. After the first HDO run, 4.2% coke formed on the catalyst (Fig. 5.5), but catalyst activity was drastically reduced during the second run and liquid yield was 51% and coke formation increased to 15%. Thus, coke formation may not be the main reason for catalyst deactivation [13]. As discussed in section 3.2., irreversible adsorption of oxygen at active Ni sites as well as formation of trevorite (Fe_2NiO_4) could be other reasons for catalyst deactivation.

The spent catalyst was placed in muffle furnace to burn off the deposited coke at 400 °C for 4 h followed by reduction as described in section 2.3. The regenerated/activated catalyst was then used in HDO experiments and the cycle was repeated five times. The product yields distribution using regenerated catalyst were almost identical as that of fresh 40%Ni/RM (Fig. 5.8). The physicochemical properties of the HDO oil obtained by using the regenerated catalysts were also consistent and about the same as that of fresh catalyst (Table 5.7). The yields of HDO oil obtained after five regenerations of Ni/RM catalyst were 68.1, 69.0, 67.5, 68.1, and 68.8 % respectively (Fig. 5.8). These values were within 1% error from their average suggesting efficient regeneration of the catalyst (also see Table 5.7). Moreover, the coke yield was 4.1 ± 0.2 % after catalyst regeneration experiments showing a good consistency between measurements, which showed reproducible catalyst regeneration/activation. These result indicated that the catalyst regained its activity after the regeneration/activation process. The regeneration of the commercial Ni/SiO_2-Al_2O_3 was not possible following the same procedure and the catalyst did not indicate HDO activity after reduction. Additionally,

when exposed to air, the reduced commercial catalyst caught fire due to spontaneous oxidation, while the reduced Ni/RM was stable on exposure to air.

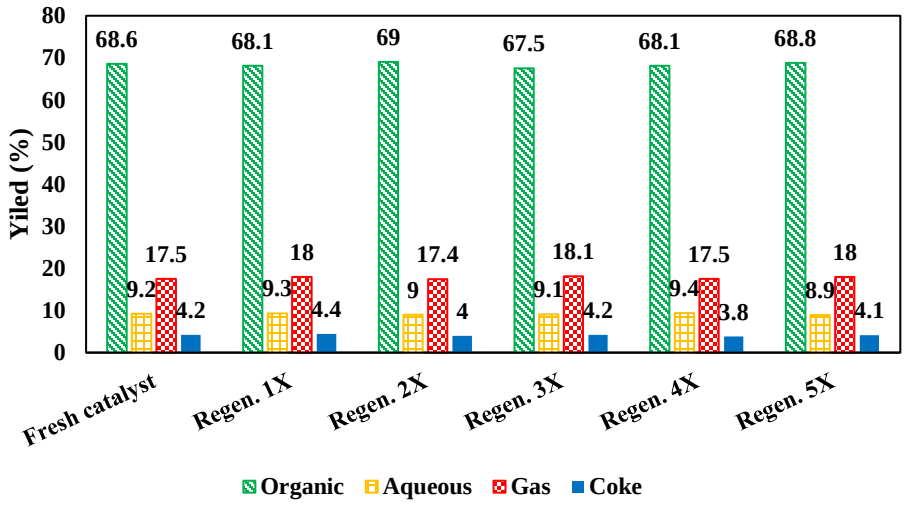

Fig. 5. 8: Products yield distribution using regenerated 40% Ni/RM catalyst.

Table 5. 7: Properties of HDO oil using regenerated 40% Ni/RM catalyst.

Properties	Catalyst regeneration #					
	Fresh	Regen. 1X	Regen. 2X	Regen. 3X	Regen. 4X	Regen. 5X
H_2 consumption (mol/g bio-oil)	0.053	0.050	0.055	0.051	0.056	0.051
Elemental composition (dry basis) (wt. %)						
N	0.31	0.32	0.30	0.29	0.33	0.32
C	82.52	82.36	82.54	82.67	82.41	82.55
H	15.82	15.56	15.78	15.46	15.72	15.35
O	1.35	1.76	1.38	1.58	1.54	1.78
HHV (MJ/kg)	45.77	45.01	45.01	45.12	45.05	45.02
Dynamic viscosity (cP)	1.37	1.37	1.41	1.35	1.36	1.39

4.5. Comparison of catalytic activity of Ni/RM with commercial Ni/SiO_2-Al_2O_3

For comparison, commercial (~65%)Ni/SiO_2-Al_2O_3 (as received) was used in HDO experiments at reaction temperatures of 400 °C and 450 °C. Product yields distribution of HDO experiments using 40%Ni/RM (400 °C and 450 °C), 65%Ni/RM

(400 °C and 450 °C), and commercial Ni/SiO_2-Al_2O_3 (400 °C and 450 °C) are shown in Fig. 5.9. The HDO oil properties obtained by using 40%Ni/RM at reaction temperature of 400 °C were similar to that of commercial Ni/SiO_2-Al_2O_3 at reaction temperature of 450 °C (Table 5.8). However, the organic liquid yield was much higher in the case of 40%Ni/RM (68.6%) than commercial Ni/SiO_2-Al_2O_3 (41.8%) (Fig. 5.9). The aqueous liquid yield in the case of 40%Ni/RM and commercial Ni/SiO_2-Al_2O_3 were 9.1% and 21.1% respectively (Fig. 5.9), which could be due to more methanation of CO and CO_2 over commercial Ni/SiO_2-Al_2O_3 (Table 5.8). The commercial Ni/SiO_2-Al_2O_3 produced more gas (27.6%) compared to 40%Ni/RM (16.4%) because of the higher activity of commercial Ni/SiO_2-Al_2O_3 for hydrocracking.

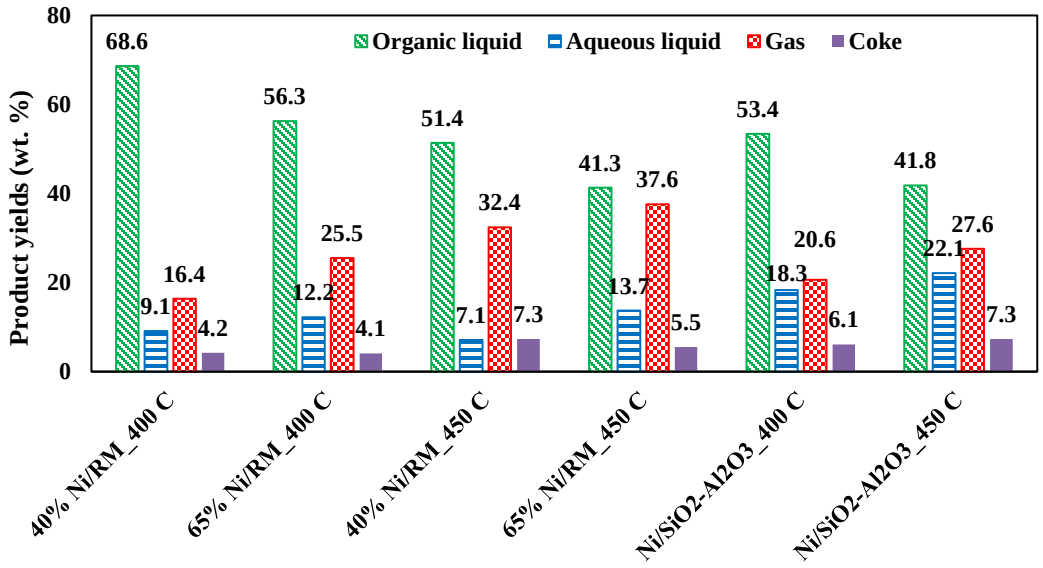

Fig. 5. 9: Products yield distribution using Ni/RM (40% and 65% Ni loading) and commercial Ni/SiO2-Al2O3 catalysts at reaction temperatures of 400 °C and 450 °C.

Table 5. 8: H_2 consumption, physicochemical properties of the liquid products, and gas product composition using commercial Ni/SiO2-Al2O3 catalyst.

Properties	Reaction time was 30 min					
	40%Ni/RM 400 °C	65%Ni/RM 400 °C	40%Ni/RM 450 °C	65%Ni/RM 450 °C	Ni/SiO_2-Al_2O_3 400°C	Ni/SiO_2-Al_2O_3 450°C
H_2 consumption (mol/g bio-oil)	0.053	0.072	0.056	0.083	0.061	0.095
Aqueous phase						
Water content (wt. %)	99.45	99.95	99.15	99.40	99.35	99.55
pH	6.91	6.93	6.94	6.96	6.87	6.89
HDO oil (organic phase)						
Elemental analysis (wt. %)						
N	0.31	0.30	0.26	0.17	0.21	0.13
C	82.52	83.11	83.13	83.18	79.81	82.94
H	15.82	16.59	16.61	16.65	11.65	15.66
O	1.35	0	0	0	8.33	1.27
HHV (MJ/kg)	45.77	45.81	45.83	45.85	42.58	45.16
pH	NA	NA	NA	NA	NA	NA
Water content (wt. %)	<DL	<DL	<DL	<DL	<DL	<DL
Density (g/ml)	0.79	0.78	0.78	0.78	0.91	0.81
Dynamic viscosity (cP)	1.37	1.31	1.30	1.30	3.43	1.38
Gas composition (mole %)						
CO	3.32	2.23	3.11	2.05	0	0
CO_2	5.52	4.19	4.25	3.17	4.12	0
CH_4	67.34	69.76	68.56	71.34	78.34	90.61
C_2H_4	8.26	8.66	8.47	9.14	7.34	4.23
C_3H_8	7.56	7.67	7.71	7.83	5.24	2.14
C_4H_{10}	5.45	5.28	5.33	4.15	3.14	1.87
C_5H_{12}	2.47	2.19	2.31	1.85	1.34	0.76

The 65%Ni/RM HDO oil yield was 41.3% at reaction temperature of 450 °C which was similar to the organic liquid yield obtained at the same temperature using the commercial catalyst (41.8% shown in Fig. 5.9). However, the yield of aqueous phase was higher, but the gas yield was lower because of increased methanation of CO_2 on the commercial catalyst (data not provided). The coke yield was also higher in the case of the commercial catalyst (7.3%) compared to 65%Ni/RM (5.5%) (Fig. 5.9). More details of HDO of PJ bio-oil using commercial Ni/SiO_2-Al_2O_3 has been reported elsewhere [12]. Overall, 40%Ni/RM catalyst produced higher organic liquid yield than the commercial catalyst, and HDO was performed at lower temperature (400 °C) than the commercial catalyst (450 °C) to obtain similar oil properties. The lower reaction temperature was

beneficial in preventing hydrocracking and coke formation (Fig. 5.9). Hence, the prepared 40%Ni/RM could be an alternative to commercial Ni/SiO_2-Al_2O_3 catalyst and could be potentially less expensive than the commercial catalyst as reported previously [47].

5. Conclusion

Red mud, which is a waste material from the alumina industry, was used as support material for preparation of nickel hydrogenation/hydrodeoxygenation catalysts at different nickel loadings. Increasing the nickel content improved the catalytic activity of Ni/RM for HDO reactions. The highest organic liquid yield (68.6%) was achieved when 40%Ni/RM was used. The catalyst partially deactivated due to deposition of carbonaceous compounds (coke), oxidation of active nickel sites, and formation of trevorite (Fe_2NiO_4) during HDO. The Ni/RM catalysts demonstrated catalytic activity comparable to commercial Ni/SiO_2-Al_2O_3 at a lower nickel loading and lower reaction temperature. Overall, Ni/RM catalyst improved HDO reactions versus hydrocracking and coke formation compared to commercial Ni/SiO_2-Al_2O_3. After regeneration by burning off the coke and reducing with hydrogen, the activity of the Ni/RM catalyst was completely restored; in contrast the commercial catalyst that was not regenerable. This study showed that RM can serve as a promising nickel catalyst support for HDO process.

As an effective HDO catalyst, it will be required to address the performance of Ni/RM in a continuous packed-bed reactor configuration to replace the batch reactor for upgrading of bio-oil and evaluate the catalyst life. Additionally, cross-interactions of HDO intermediates on Ni/RM catalyst needs to be studied in future to get better

understanding of the reaction mechanisms. Furthermore, detailed feasibility studies including technoeconomic analysis and energy balance for the entire pyrolysis-HDO process has to be carried out prior to scaling up of this process.

6. References

[1] S.H. Mohr, J. Wang, G. Ellem, J. Ward, D. Giurco, Projection of world fossil fuels by country, Fuel. 141 (2015) 120–135.

[2] N.R. Singh, W.N. Delgass, F.H. Ribeiro, R. Agrawal, Estimation of liquid fuel yields from biomass, Environ. Sci. Technol. 44 (2010) 5298–5305.

[3] M. Patel, A. Kumar, Production of renewable diesel through the hydroprocessing of lignocellulosic biomass-derived bio-oil: A review, Renew. Sustain. Energy Rev. 58 (2016) 1293–1307.

[4] B. Ma, F.A. Agblevor, Polarity-based separation and chemical characterization of fast pyrolysis bio-oil from poultry litter, Biomass Bioenergy. 64 (2014) 337–347.

[5] Y. Elkasabi, Q. Liu, Y.S. Choi, G. Strahan, A.A. Boateng, J.R. Regalbuto, Bio-oil hydrodeoxygenation catalysts produced using strong electrostatic adsorption q, Fuel. 207 (2017) 510–521.

[6] Y. Luo, V.K. Guda, E.B. Hassan, P.H. Steele, B. Mitchell, F. Yu, Hydrodeoxygenation of oxidized distilled bio-oil for the production of gasoline fuel type, Energy Convers. Manag. 112 (2016) 319–327.

[7] Q. Li, P.H. Steele, F. Yu, B. Mitchell, E.M. Hassan, Pyrolytic spray increases levoglucosan production during fast pyrolysis, J Anal. Appl. Pyrolysis. 100 (2013) 33–40.

[8] S. Cheng, L. Wei, X. Zhao, Y. Huang, D. Raynie, C. Qiu, J. Kiratu, Y. Yu, Directly catalytic upgrading bio-oil vapor produced by prairie cordgrass pyrolysis over Ni/HZSM-5 using a two stage reactor, AIMS Energy. 3 (2015) 227–240.

[9] Y. Luo, E.B. Hassan, V. Guda, R. Wijayapala, P.H. Steele, Upgrading of syngas hydrotreated fractionated oxidized bio-oil to transportation grade hydrocarbons, Energy Convers. Manag. 115 (2016) 159–166.

[10] M.B. Shemfe, S. Gu, P. Ranganathan, Techno-economic performance analysis of biofuel production and miniature electric power generation from biomass fast pyrolysis and bio-oil upgrading, Fuel. 143 (2015) 361–372.

[11] L. Liu, Y. Liu, X. Gao, R. Zhang, Y. Zhai, Hydrodeoxygenation of bio-oil model compounds over amorphous NiB/SiO2-Al2O3 catalyst in oil-water biphasic system, J. Fuel Chem. Technol. 45 (2017) 932–938.

[12] H. Jahromi, F.A. Agblevor, Upgrading of pinyon-juniper catalytic pyrolysis oil via hydrodeoxygenation, Energy. 141 (2017) 2186–2195.

[13] X. Zhang, T. Wang, L. Ma, Q. Zhang, T. Jiang, Hydrotreatment of bio-oil over Ni-based catalyst, Biores. Technol. 127 (2013) 306–311.

[14] Y. Li, C. Zhang, Y. Liu, S. Tang, G. Chen, R. Zhang, X. Tang, Coke formation on the surface of Ni/HZSM-5 and Ni-Cu/HZSM-5 catalysts during bio-oil hydrodeoxygenation, Fuel. 189 (2017) 23–31.

[15] X. Zhao, L. Wei, S. Cheng, J. Julson, Review of heterogeneous catalysts for catalytically upgrading vegetable oils into hydrocarbon biofuels, Catalysts. 7 (2017) 83.

[16] S. Cheng, L. Wei, X. Zhao, J. Julson, Application, Deactivation, and regeneration of heterogeneous catalysts in bio-oil upgrading, Catalysts. 6 (2016) 195.

[17] J. Wildschut, F.H. Mahfud, R.H. Venderbosch, H.J. Heeres, Hydrotreatment of fast pyrolysis oil using heterogeneous noble-metal catalysts, Ind. Eng. Chem. Res. 48 (2009) 10324–10334.

[18] Y. Huang, L. Wei, X. Zhao, S. Cheng, J. Julson, Y. Cao, Z. Gu, Upgrading pine sawdust pyrolysis oil to green biofuels by HDO over zinc-assisted Pd/C catalyst, Energy Convers. Manag. 115 (2016) 8–16.

[19] S. Cheng, L. Wei, X. Zhao, E. Kadis, Y. Cao, J. Julson, Z. Gu, Hydrodeoxygenation of prairie cordgrass bio-oil over Ni based activated carbon synergistic catalysts combined with different metals, N. Biotechnol. 33 (2016) 440–448.

[20] V.A. Yakovlev, S.A. Khromova, O. V Sherstyuk, V.O. Dundich, D.Y. Ermakov, V.M. Novopashina, M.Y. Lebedev, O. Bulavchenko, V.N. Parmon, Development of new catalytic systems for upgraded bio-fuels production from bio-crude-oil and biodiesel, Catal. Today. 144 (2009) 362–366.

[21] E. Furimsky, Catalytic hydrodeoxygenation, Appl. Catal. A Gen. 199 (2000) 147–190.

[22] A. Agrawal, K.K. Sahu, B.D. Pandey, Solid waste management in non-ferrous industries in India, Resour. Con. Rec. 42 (2004) 99–120.

[23] S. Sushil, V.S. Batra, Catalytic applications of red mud, an aluminium industry waste : A review, Appl. Catal. B. Environ. 81 (2008) 64–77.

[24] B.K. Yathavan, F.A. Agblevor, Catalytic pyrolysis of pinyon-juniper using red mud and HZSM-5, Energy Fuels. 27 (2013) 6858–6865.

[25] X. Lim, A. Sanna, J.M. Andresen, Influence of red mud impregnation on the pyrolysis of oil palm biomass-EFB, Fuel. 119 (2014) 259–265.

[26] B. Klopries, W. Hodek, F. Bandermann, Catalytic hydroliquefaction of biomass with red mud and CO-MO_3 catalysts, Fuel 69 (1990) 448-455.

[27] C.K. Pratt, V. Christoverson, Hydrogenation of a model hydrogen-donor system using activated red mud catalyst, Fuel. 61 (1982) 460-462.

[28] A. Eamsiri, W.R. Jackson, K.C. Pratt, V. Christoverson, M. Marshall, Activated red mud as a catalyst for the hydrogenation of coals and of aromatic compounds, Fuel. 71 (1992) 449-453.

[29] J.J. Llano, R. Rosal, H. Sastre, F.V. Diez, Catalytic hydrogenation of anthracene oil with red mud, Fuel. 73 (1994) 688-694.

[30] S. Ordóñez, H. Sastre, F. V. Díez, Characterisation and deactivation studies of sulfided red mud used as catalyst for the hydrodechlorination of tetrachloroethylene, Appl. Catal. B Environ. 29 (2001) 263–273.

[31] J. Alvarez, R. Rosal, H. Sastre, F.V. Diez, Characterization and deactivation of sulfided red mud used as hydrogenation catalyst, Appl. Catal. A. Gen. 128 (1995) 259–273.

[32] S. Ordóez, H. Sastre, F. V. Díez, Catalytic hydrodechlorination of tetrachloroethylene over red mud, J. Hazard. Mater. 81 (2001) 103–114.

[33] M. Martino, R. Rosal, H. Sastre, F. V Diez, Hydrodechlorination of dichloromethane , trichloroethane , trichloroethylene and tetrachloroethylene over a sulfided Ni / Mo-γ-alumina catalyst, Appl. Catal. B. Environ., 20 (1999) 301-307.

[34] L.C.A. De Oliveira, A.P. Heitmann, L.D. Almeida, S. Herman, A.A. Mansur, C.S. De Castro, U.F. De Alfenas, PET-modified Red mud as catalysts for oxidative desulfurization reactions, J. Environ. Sci. 57 (2015) 3–5.

[35] J.R. Paredes, S. Ordóñez, A. Vega, Catalytic combustion of methane over red mud-based catalysts, Appl. Catal. 47 (2004) 37–45.

[36] S. Djerad, M. Crocoll, S. Kureti, L. Tifouti, W. Weisweiler, Effect of oxygen concentration on the NO x reduction with ammonia over V2O5 –WO3 / TiO 2 catalyst, Catal. Today. 113 (2006) 208–214.

[37] J. Yanik, A. Uddin, K. Ikeuchi, Y. Sakata, The catalytic effect of red mud on the degradation of poly (vinyl chloride) containing polymer mixture into fuel oil, Polymer Degrad. Stab. 73 (2001) 335–346.

[38] A. Sınag, M. Sungur, M. Canel, Effect of experimental conditions on the yields during the copyrolysis of mustafa kemal pasa (MKP) lignite (Turkey) with low-density polyethylene, Energy Fuels. 20 (2006) 1609–1613.

[39] A.I. Cakici, J. Yanik, S. Uçar, T. Karayildirim, H. Anil, Utilization of red mud as catalyst in conversion of waste oil and waste plastics to fuel, J Mater. Cycles. Waste Manag. 6 (2004) 20–26.

[40] A. Iannibello, S. Marengo, A. Girelli, Bauxite-based catalysts in heavy crude oil hydrotreating, Appl. Catal. 3 (1982) 261-272.

[41] S. Uemiya, M. Uchida, H. Moritomi, R. Yoshiie, M. Nishimura, Ammonia Decomposition Catalyst with Resistance to Coexisting Sulfur Compounds, Mater. Trans. 46 (2005) 2709–2712.

[42] S.H. Khezri, N. Azimi, M. Mohammed-vali, B. Eftekhari-sis, Red mud catalyzed one-pot synthesis of nitriles from aldehydes and hydroxylamine hydrochloride under microwave irradiation, ARKIVOC 15 (2007) 162–170.

[43] N.I. Bento, P.S.C. Santos, T.E. de Souza, L.C.A. Oliveira, C.S. Castro, Composites based on PET and red mud residues as catalyst for organic removal from water, J. Hazard. Mater. 314 (2016) 304–311.

[44] J. Li, L. Xu, P. Sun, P. Zhai, X. Chen, H. Zhang, Z. Zhang, W. Zhu, Novel application of red mud: Facile hydrothermal-thermal conversion synthesis of hierarchical porous AlOOH and Al2O3 microspheres as adsorbents for dye removal, Chem. Eng. J. 321 (2017) 622–634.

[45] M. Senthil, K. Visagavel, C.G. Saravanan, K. Rajendran, Investigations of red mud as a catalyst in Mahua oil biodiesel production and its engine performance, Fuel Process. Technol. 149 (2016) 7–14.

[46] J. Ye, A. Hu, G. Ren, T. Zhou, G. Zhang, S. Zhou, Red mud enhances methanogenesis with the simultaneous improvement of hydrolysis-acidification and electrical conductivity, Biores. Technol. 247 (2018) 131–137.

[47] H. Jahromi, F. A. Agblevor, Hydrotreating of guaiacol: A comparative study of Red mud-supported nickel and commercial Ni/SiO_2-Al_2O_3catalysts, Appl. Catal. A. Gen. 558 (2018) 109–121.

[48] R. F. Miller, J. D. Bates, T. J. Svejcar, F. B. Pierson, L. E. Eddleman, Technical Bulletin 152; Corvallis Agricultural Experiment Station, Oregon State University, Corvallis, OR, 2005.

[49] P. E. Carrara, T. R. Carroll, The determination of erosion rates from exposed tree roots in the Piceance basin, Colorado. Earth Surf. Processes 4 (1979) 307−317.

[50] R. J. Ansley, H. T. Wiedemann, M. J. Castellano, J. E. Slosser, Herbaceous restoration of juniper dominated grasslands with chaining and fire, Rangel. Ecol. Manage. 59 (2006) 171−178.

[51] C. Baughman, T. A. Forbis, L. Provencher, Response of two sagebrush sites to low-disturbance, mechanical removal of pinyon and juniper, Invasive Plant Sci. Manage. 3 (2010) 122−129.

[52] O.D. Mante, F.A. Agblevor, Catalytic pyrolysis for the production of refinery-ready biocrude oils from six different biomass resources, Green Chem. 16 (2014) 3364-3377.

[53] Z. Xinghua, W. Tiejun, M. Longlong, W. Chuangzhi, Aqueous-phase catalytic process for production of pentane from furfural over nickel-based catalysts, Fuel. 89 (2010) 2697–2702.

[54] X. Zhang, L. Chen, W. Kong, T. Wang, Q. Zhang, J. Long, Y. Xu, L. Ma, Upgrading of bio-oil to boiler fuel by catalytic hydrotreatment and esterification in an efficient process, Energy. 84 (2015) 83–90.

[55] R. Gavlak, R. Horneck, R.O. Miller, J. Kotuby-Amacher, Soil, plant and water reference methods for the western region, 3rd Ed. (2005) 1679–169.

[56] S. V. Vassilev, D. Baxter, L.K. Andersen, C.G. Vassileva, An overview of the chemical composition of biomass, Fuel. 89 (2010) 913–933.

[57] S. Chenna, R. Banerjee, P.A. Crozier, Atomic-scale observation of the Ni activation process for partial oxidation of methane using in situ environmental TEM, Chem. Cat. Chem. 3 (2011) 1051–1059.

[58] Q. Jeangros, T.W. Hansen, J.B. Wagner, C.D. Damsgaard, R.E. Dunin-Borkowski, C. Hébert, J. Van Herle, A. Hessler-Wyser, Reduction of nickel oxide particles by hydrogen studied in an environmental TEM, J. Mater. Sci. 48 (2013) 2893–2907.

[59] I. Coronado, M. Stekrova, L. García Moreno, M. Reinikainen, P. Simell, R. Karinen, J. Lehtonen, Aqueous-phase reforming of methanol over nickel-based catalysts for hydrogen production, Biomass Bioenergy. 106 (2017) 29–37.

[60] J. Pu, K. Nishikado, N. Wang, T.T. Nguyen, T. Maki, E.W. Qian, Core-shell nickel catalysts for the steam reforming of acetic acid, Appl. Catal. B. Environ. 224 (2017) 69-79.

[61] C. Boscagli, C. Yang, A. Welle, W. Wang, S. Behrens, K. Raffelt, J.D. Grunwaldt, Effect of pyrolysis oil components on the activity and selectivity of nickel-based catalysts during hydrotreatment, Appl. Catal. A Gen. 544 (2017) 161–172.

[62] H.D. Demsash, K.V.K. Kondamudi, S. Upadhyayula, R. Mohan, Ruthenium doped nickel-alumina-ceria catalyst in glycerol steam reforming, Fuel Process. Technol. 169 (2018) 150–156.

[63] R. Molina, G. Poncelet, α-alumina-supported nickel catalysts prepared from nickel acetylacetonate: A TPR study, J. Catal. 173 (1998) 257–267.

[64] D. Wierzbicki, R. Baran, R. Debek, M. Motak, T. Grzybek, M.E. Galvez, P. Da Costa, The influence of nickel content on the performance of hydrotalcite-derived catalysts in CO2 methanation reaction, Int. J. Hydrogen Energy. 42 (2017) 23548–23555.

[65] H.-F. Wang, X.-Q. Gong, Y.-L. Guo, Y.-L. Guo, G.Z. Lu, P. Hu, A model to understand the oxygen vacancy formation in Zr-doped CeO_2: Electrostatic interaction and structural relaxation, J. Phys. Chem. C. 113 (2009) 10229–10232.

[66] V. Shapovalov, H. Metiu, Catalysis by doped oxides: CO oxidation by $Au_xCe_{1-x}O_2$, J. Catal. 245 (2007) 205–214.

[67] B. Li, H. Metiu, DFT Studies of Oxygen Vacancies on Undoped and Doped La_2O_3 Surfaces, J. Phys. Chem. C. 114 (2010) 12234–12244.

[68] H.Y. Kim, H.M. Lee, R.G.S. Pala, V. Shapovalov, H. Metiu, CO Oxidation by Rutile TiO_2 (110) Doped with V, W, Cr, Mo, and Mn, J. Phys. Chem. C. 112 (2008) 12398–12408.

[69] V.O.O. Gonçalves, P.M. de Souza, T. Cabioc'h, V.T. da Silva, F.B. Noronha, F. Richard, Hydrodeoxygenation of m-cresol over nickel and nickel phosphide based catalysts. Influence of the nature of the active phase and the support, Appl. Catal. B. Environ. 219 (2017) 619–628.

[70] S. Kadarwati, S. Oudenhoven, M. Schagen, X. Hu, M. Garcia-Perez, S. Kersten, C.Z. Li, R. Westerhof, Polymerization and cracking during the hydrotreatment of bio-oil and heavy fractions obtained by fractional condensation using Ru/C and NiMo/Al2O3 catalyst, J. Anal. Appl. Pyrolysis. 118 (2016) 136–143.

[71] F.A. Agblevor, D.C. Elliott, D.M. Santosa, M. V. Olarte, S.D. Burton, M. Swita, S.H. Beis, K. Christian, B. Sargent, Red mud catalytic pyrolysis of pinyon juniper and single-stage hydrotreatment of oils, Energy Fuels. 30 (2016) 7947–7958.

[72] S.K. Tanneru, P.H. Steele, Direct hydrocracking of oxidized bio-oil to hydrocarbons, Fuel. 154 (2015) 268–274.

[73] T.S. Kim, S. Oh, J.Y. Kim, I.G. Choi, J.W. Choi, Study on the hydrodeoxygenative upgrading of crude bio-oil produced from woody biomass by fast pyrolysis, Energy. 68 (2014) 437–443.

[74] H. Habazaki, M. Yamasaki, B.-P. Zhang, A. Kawashima, S. Kohno, T. Takai, K. Hashimoto, Co-methanation of carbon monoxide and carbon dioxide on supported nickel and cobalt catalysts prepared from amorphous alloys, Appl. Catal. A. Gen. 172 (1998) 131–140.

[75] W. Wang, W. Chu, N. Wang, W. Yang, C. Jiang, Mesoporous nickel catalyst supported on multi-walled carbon nanotubes for carbon dioxide methanation, Int. J. Hydrogen Energy. 41 (2016) 967–975.

[76] B. Nematollahi, M. Rezaei, E.N. Lay, Selective methanation of carbon monoxide in hydrogen rich stream over Ni/CeO2 nanocatalysts, J. Rare Earths. 33 (2015) 619–628.

[77] O.D. Mante, F.A. Agblevor, S.T. Oyama, R. McClung, The effect of hydrothermal treatment of FCC catalysts and ZSM-5 additives in catalytic conversion of biomass, Appl. Catal. A. Gen. 445–446 (2012) 312–320.

[78] G.D. Strahan, C.A. Mullen, A.A. Boateng, Characterizing biomass fast pyrolysis oils by 13C NMR and chemometric analysis, Energy Fuels. 25 (2011) 5452–5461.

CHAPTER 6

6. AQUEOUS PHASE SYNTHESIS OF HYDROCARBONS FROM LOW MOLECULAR WEIGHT OXYGENATES USING RED-MUD SUPPORTED NICKEL CATALYST

Part I: Aqueous phase synthesis of hydrocarbons from furfural reactions with low molecular weight biomass oxygenates

1. Abstract

Catalytic pyrolysis of lignocellulosic biomass generates water soluble low molecular weight oxygenates such as acetic acid, acetone, furfural, butanone, guaiacol, phenol etc. These compounds are usually not suitable for conventional hydrocarbon fuel application. A new heterogeneous catalyst has been developed that simultaneously catalyzes addition, hydrodeoxygenation, and hydrogenation of these small oxygenate molecules in aqueous medium to produce C_6 to C_{14} hydrocarbons in a one-pot synthesis. In these syntheses, acetic acid, propionic acid, furfural, butanone, pentanone, heptanone, and 2,6-dimethyl 4-heptanone reacted to produce straight and branched chain alkanes. The aldehydes reacted with furan to form straight chain liquid hydrocarbons while the ketones reacted with 2-methylfuran to produce branched chain liquid hydrocarbons. All the reactions occurred in the aqueous media at 350 $^{\circ}$C. The gaseous products included low molecular weight hydrocarbons such as methane, propane, butane, and pentane. Thus, it has been demonstrated for the first time that it is possible to produce a wide range of hydrocarbons from low molecular weight biomass derived oxygenates for fuels and chemical applications.

2. Introduction

The production of hydrocarbon fuels from renewable biomass sources remains a major challenge to the research community.[1-4] Although progress has been made in the pyrolysis of biomass to liquid fuels,[5, 6] there are still major challenges in the quality of the fuel especially in its application as a transportation fuel.[7, 8] The pyrolysis oils are unstable, acidic, viscous, reactive, low energy density, and high oxygen content; therefore, cannot be directly used as transportation fuels.[9] Furthermore, there are only a few companies that are producing the raw pyrolysis oils as heating fuels on commercial basis.[10, 11] Current research efforts are focused on stabilizing the pyrolysis oils to enable them to be co-processed with petroleum feeds, processed on standard unit operations, and potential processing in standalone biorefinery plants.[12] The stability improvement studies include esterification, low severity hydrotreatment, catalytic pyrolysis.[13] The focus of this paper is on the catalytic pyrolysis oils of lignocellulosic biomass. Although catalytic pyrolysis (*in situ* and *ex situ*) produces a much more stable pyrolysis oil with lower oxygen content and higher energy density, it suffers from major deficiencies: it produces large quantities of non-condensable gases and large quantities of low molecular weight water-soluble oxygenates.[12, 14-17] The water-soluble oxygenates pose several challenges including wastewater treatment, loss of carbon, and overall decrease in product yield.[18, 19] The aqueous phase pyrolysis products which constitute 10 to 30 wt. % of the products are dissolved in water in concentration of 10-20 wt. %.[12, 17, 18] The recovery of these water-soluble products from the aqueous phase to improve the overall efficiency of the biofuel production has also been a challenge.[20, 21] Several methods have been investigated using

both model compounds, fractionated pyrolysis oils, and raw aqueous phase oils.[17, 22-25] These upgrading results show promise, but none has been commercialized.

In this paper we report aqueous phase hydrotreatment of low molecular weight water-soluble products into a wide range of hydrocarbons using a novel catalyst in a one-pot synthesis process. The results show interaction between various aqueous phase compounds. Although model compounds are reported in this paper, when applied to real biomass aqueous phase pyrolysis oil, the results were very similar. The ultimate goal of this research is to produce hydrocarbon fuels and chemicals from biomass.

3. Material and methods

3.1. Materials

The selection of model compounds for this research was based on the analysis of the aqueous phase red mud catalytic pyrolysis liquids. The major compounds detected in this liquid were used for the model compounds studies to elucidate the reactions that occur during the hydrotreating of the aqueous phase liquids reported elsewhere.[22-27] The liquid was obtained from the red mud catalytic pyrolysis of pinyon juniper wood. The model compounds used for these studies were obtained from various chemical vendors and were used as received without any further purification. The compounds included acetic acid (EMD Millipore Billareca, MD, USA), guaiacol, anisole, 2,3-butanedione, 3-hydroxy-2-butanone (Alfa Aesar, Haverhill, MA, USA), acetaldehyde, phenol, benzene, furfural, furan, 2-methylfuran (Sigma Aldrich, St Louis, MO, USA), acetone, ethanol, toluene, methanol (Pharmaco-AAPER, Orange County, CA, USA). Various standards were also obtained from these companies for product identification and quantification.

3.2. Catalyst preparation and characterization

Nickel/red mud (Ni/RM) catalyst was prepared in-house using the procedure described by Jahromi and Agblevor.[28, 29]

Ni/RM catalysts were prepared at 40 wt. % nickel metal loading using wet impregnation method.[28-32] At room temperature the calculated amount of $Ni(NO_3).6H_2O$ was dissolved in 100 ml deionized water and then mixed with red mud (particle size <90 μm). The mixture was heated to 70 °C and continuously stirred for 5 hours to prepare the catalyst precursor. The catalyst precursor was dried at 105 °C for 10 hours and then calcined in a muffle furnace (Thermo Scientific, Inc., Waltham, MA, USA) at 620 °C for 5 hours. The calcined material was reduced for 6 hours at 450 °C with a reducing gas mixture of 10% H_2 and 90% N_2 at flow rate of 20 ml/min to obtain the final catalyst, which was labelled Ni/RM.

The preparation of the reduced red mud catalyst (RRM) was similar to that of the Ni/RM except that the Ni addition step was eliminated. The red mud catalyst precursor was dried at 105 °C, for 10 h and calcined in a muffle furnace at 620 °C for 5 hours. The precursor was then reduced with 10% H_2 and 90% N_2 at a flow rate of 20 ml/min to obtain the final catalyst which was labelled RRM.

The catalysts were characterized by thermogravimetric-temperature programmed reduction (TG-TPR), Brunauer–Emmett–Teller (BET) surface area analyzer, X-ray diffraction (XRD), inductively coupling plasma (ICP), and scanning electron microscopy (SEM) as reported previously.[28, 29]

3.3. Aqueous phase hydrodeoxygenation experiments

All aqueous phase hydrodeoxygenation (AQHDO) experiments were conducted in a Parr Series 4560 300 mL autoclave reactor (Parr Instruments, Moline, IL, USA). This reactor had a variable speed magnetic drive and turbine agitator. A pressure gauge was used to measure the total pressure inside the reactor. A K-thermocouple immersed in the reactor was used to measure the reactant temperature. The reaction temperature was maintained at its desired value with an accuracy of ±1 °C. The setup had an electrically heated jacket to ensure isothermal conditions. The temperature and speed of agitation were controlled by a Parr 4848 controller.

In each experiment, the reactor was charged with reactant (100 g) and Ni/RM catalyst (3 g). The reactant consisted of 15 wt. % organic compound. Thus, for a single compound 15 g of material was added to 85 g water and 3 g catalyst was added. It was assumed that the water was only a reaction medium. If two compounds were under investigation, then 7.5 g of each compound was dissolved in the water. The combination of various compounds investigated are shown in section 3.5. The reactor was purged with N_2 to ensure an inert atmosphere. The reactor was then charged with high purity hydrogen supplied from a reservoir tank to the desired pressures of 6.21 MPa (900 psi). A gas sample was taken from a gas release valve from the gas sampling port for gas analysis when the reactor was at room temperature. The reactor was then heated to reaction temperature (350 °C) at heating rate of 15 °C/min. The reaction time was recorded when the set temperature was reached. After the desired reaction time (30 minute), the reactor was cooled to room temperature using the internal cooling coil. A gas sample was collected in a tedlar bag for gas analysis when the reactor was cooled to room

temperature. The reproducibility of experiments was checked and the error in all experimental measurements was found to be less than 3%.

Another set of experiments was carried out on the RRM (catalyst support), which did not contain any nickel to determine the effect of the support on the reactions. The reaction conditions were identical to those for the Ni/RM.

In blank experiments (without catalyst) 100 g of reaction mixture was charged into the reactor and the reactor was pressurized to 6.2 MPa (900 psi) with hydrogen and allowed to react for 30 minutes at 350 °C to determine if the reactor walls played any role in the observed reactions. All experiments were conducted in triplicate. The blank experiments showed no reactivity of the reactor walls. All results reported are therefore assumed to have no reactor wall influence.

3.4. Analysis of AQHDO products

Hydrogen consumption was measured according to the procedure reported previously.[33] Gas analysis was performed using Agilent 490 micro-GC. The micro-GC was equipped with molsieve 5A and porous polymer (PP) columns and two TCD detectors for each column.[33] The liquid products of AQHDO experiments were analyzed by HPLC (Shimadzu Scientific, Columbia, MD, USA) using a RID-10A detector and a Kromasil 100-5-C18 column (AkzoNobel Amsterdam, Netherlands). The HPLC was equipped with a LC-10AT pump, SCL-10Avp controller, and SIL-10A autosampler. CLASS-VP 7.3 SP1 software was used to analyze HPLC chromatograms. A CTO-10A column oven was used to maintain the column temperature at 55 °C during the analysis.

The injection volume was 0.25 µl and acetonitrile at flow rate of 0.6 ml/min was used as the mobile phase. Data acquisition time was 80 minutes for all analyses.

The liquid samples were analyzed for furfural, furfuryl alcohol (FOL), tetrahydrofurfuryl alcohol (THFA), furan, 2-methylfuran (2-MF), tetrahydrofuran (THF), 2-methyltetrahydro furan (2-MTHF), butanone, 2-butanol, 2-butanone, 2-pentanone, 3-petanone, 3-pentanol, 2-heptanone, ethanol, ethyl acetate, acetaldehyde, propionaldehyde, propanol, acetone, hexane, heptane, 3-methyloctane, 3-ethyloctane, 2-methylheptane, 4-methylnonane. The identity of the synthesized compounds were confirmed by GC/MS (Shimadzu GC/MS-QP5000, Shimadzu Scientific, Columbia, MD, USA) and NMR (^{1}H and ^{13}C) using a BRUKER 500 MHz (BRUKER Corporation, Japan).

The elemental composition of AQHDO products were determined using ThermoFischer Scientific Flash 2000 organic elemental analyzer (ThermoFisher Scientific, Waltham, MA, USA) (CHNS configuration), and the oxygen content was calculated by difference according to ASTM D5291.

4. Results

The characterization of the Ni/RM catalyst has been reported elsewhere and will not be repeated here.[28, 29] The AQHDO results were grouped according to the main substrates investigated. AQHDO of individual compounds on red mud supported nickel (Ni/RM) and reduced red mud (RRM) are reported below.

4.1. Aqueous phase acetic acid HDO on Ni/RM and RRM

The 15 wt. % acetic acid water solution was hydrotreated on Ni/RM without any other compound as a baseline for comparison. The liquid products were ethanol, propanol, acetaldehyde, ethyl acetate, and acetone, which are reduction products of acetic acid and cross reactions of the reaction products (Table 6.I.1).[34] The ethyl acetate derived from the reaction of acetic acid with ethanol and the propanol from the hydrogenation of acetone.[34, 35] The most interesting aspect of the aqueous phase hydrodeoxygenation (AQHDO) of acetic acid was the formation of acetone which was not reported by other researchers using nickel catalyst.[34, 36] The acetone was formed by the reaction of two acetic acid molecules in ketonization reaction shown in equation (1) below.[34, 36]

Table 6.I. 1: AQHDO of individual compounds using Ni/RM catalyst

Parameter	Reactant			
	Acetic acid	Propionic acid	Furfural	2,3-butanedione
Conversion (%)	78.5	85.3	100	100
H_2 consumption (mol H_2)	1.17	1.04	0.89	0.67
Product distribution (wt. %) (H_2O- free basis)				
	Acetaldehyde (6.7)	Propionaldehyde (56.2)	Furan (36.1)	2-butanone (63.7)
	Ethanol (17.3)	Propanol (31.5)	2-MF (31.9)	2-butanol (36.3)
	Acetone (30.7)	3-pentanone (6.6)	THF (14.8)	
	Ethyl acetate (29.5)	3-pentanol (5.7)	2-MTHF (17.2)	
	Isopropyl alcohol (15.8)			
Gas analysis (mol %) (H_2- free basis)				
CO	5.9	6.9	3.6	-
CO_2	9.0	13.4	6.2	-
CH_4	46.6	24.1	18.5	-
C_2H_6	25.2	6.5	-	-
C_3H_8	13.4	34.7	-	-
C_4H_{10}	-	-	34.4	100
C_5H_{12}	-	14.4	37.4	-

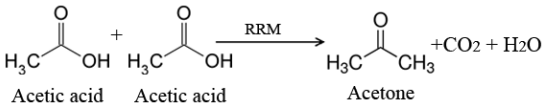

(1)

The gaseous products analyzed using micro GC were dominated by methane, ethane, and propane (Table 6.I.1), which were due to methanation of CO_2 and CO as well as cracking of other low molecular weight hydrocarbon components (Table 6.I.1).

When aqueous acetic acid was treated under similar conditions using RRM, only acetone was detected in the liquid products (Table 6.I.2), clearly showing that RRM catalyzed the ketonization reaction, which is in agreement with Yathavan and Agblevor who observed production of high levels of ketones in the biomass pyrolysis products.[16] The acetic acid reduction products were catalyzed by the elemental Ni as is known from literature.[27, 34, 36]

Table 6.I. 2: Catalytic processing of carboxylic acids using RRM catalyst support.

Parameter	Reactant (under N_2)		Reactant (under H_2)	
	Acetic acid	Propionic acid	Acetic acid	Propionic acid
Conversion (%)	67.6	73.4	69.3	74.7
Product distribution (wt. %) (H_2O- free basis)				
	Acetone (100)	3-pentanone (100)	Acetone (100)	3-pentanone (100)
Elemental composition (wt. %)				
C	62.06 ± 0.03	69.74 ± 0.05	62.04 ± 0.02	69.77 ± 0.03
H	10.35 ±0.04	11.64 ± 0.02	10.36 ±0.05	11.61 ± 0.04
O	27.59 ±0.02	18.62 ± 0.04	27.60 ±0.01	18.62 ± 0.01
Gas analysis (mol %) (N_2 and H_2- free basis)				
CO_2	100	100	100	100
^{13}C NMR chemical shifts (ppm)	30.06, 205.69	7.37, 34.95, 211.23	30.09, 205.63	7.39, 34.91, 211.26

4.2. Aqueous phase HDO of propionic acid on Ni/RM and RRM

The AQHDO reaction of the propionic acid on Ni/RM followed a similar pathway as the acetic acid. In this case, there were two major pathways, reduction of propionic acid to propanal (propionaldehyde) and propanol[37, 38] and ketonization of propionic acid to pentanone.[26] In addition to these two major compounds, other compounds such as 3-pentanol (as a result of partial hydrogenation of 3-pentanone), and gases were produced (Table 6.I.1).[39] When RRM was used as the catalyst, only pentanone was produced, which corroborated the acetic acid ketonization reaction. The reaction for this process is shown below (reaction 2):

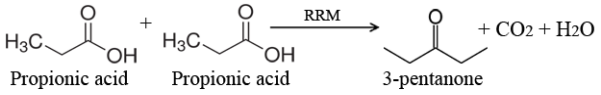

(2)

4.3. Aqueous phase furfural HDO on Ni/RM and RRM

The AQHDO of furfural was conducted in a similar manner as the acetic acid using Ni/RM. The compounds detected in the liquid products were THF, 2-MTHF, furan, and 2-MF. These products were clearly partial hydrogenation and hydrodeoxygenation of furfural (Table 6.I.1).[40-43] In addition to these products, there were gaseous products dominated by methane, butane, and pentane (Table 6.I.1). When aqueous furfural was run on the RRM, there was no reaction; clearly confirming that the products detected were due to the nickel hydrodeoxygenation and not much contribution from the RRM support, which was in contrast to the acetic and propionic acids reactions.

4.4. Aqueous phase HDO of 2,3-butanedione on Ni/RM and RRM

The AQHDO of the 2,3-butanedione was similar to those for the other compounds. In this case, the main products were butanol, butanone, and butane (Table

6.I.1). Butanol and butanone formation were all attributed to the AQHDO on the Ni catalyst because when the 2,3-butanedione was run on RRM, no products were formed, which again confirmed that RRM did not participate in the hydrodeoxygenation of the ketone.

4.5. Aqueous phase HDO of dual compounds on Ni/RM and RRM

In these series of studies, dual reactants were investigated to assess the interactions between them. The reactions of these dual mixtures are discussed below.

4.5.1. Aqueous phase HDO of acetone/furfural on Ni/RM and RRM

Acetone is one of the soluble oxygenates found in the biomass pyrolysis aqueous phase products, and it is also an intermediate in the AQHDO of acetic acid. The reactions of acetone with furfural were investigated under similar AQHDO conditions as those described above to support the proposed pathways for the acetic acid reactions with furfural.

In the case of acetone/furfural AQHDO on Ni/RM the only liquid hydrocarbon produced was 2-methylheptane (octane) which was immiscible with water. The other liquid products were THF, 2-MTHF, and furan (Table 6.I.3). When the reaction was conducted on RRM, there were no products either in the liquid or gas phases. Since no 2-MF was detected in the acetone/furfural AQHDO, it was hypothesized that the octane was produced from the reaction of 2-MF with acetone. This hypothesis was proven by conducting AQHDO on RRM using 2-MF and acetone. The only organic product of this reaction was octane, which was identified with HPLC, ^{13}C NMR, and CHNOS analyses

(Table 6.I.4). The reaction was stoichiometric with 100% conversion and stoichiometric yield of octane (reaction 3).

Table 6.I. 3: AQHDO of dual compounds using Ni/RM catalyst.

Parameter	Reactant						
	Acetone/ furfural	Acetic acid / furfural	Propionic acid/ furfural	2,3-butanedione / furfural	2-pentanone / furfural	2-heptanone / furfural	2,6-dimethyl-4-heptanone / furfural
Conversion (%)	93.2	100	100	100	95.6	91.5	88.4
H_2 consumption (mol H_2)	1.24	1.48	1.32	1.39	1.34	1.27	1.21
Product distribution (wt. %) (H_2O- free basis)							
	2-methylheptane (54.7)	Acetone (11.5)	3-pentanone (9.4)	3-methyloctane (54.2)	4-methylnonane (56.2)	6-methylundecane (55.7)	2-methyl-4 (2-methylpropane) - nonane (50.8)
	Furan (20.6)	Hexane (36.9)	Heptane (38.1)	Furan (11.9)	Furan (17.3)	Furan (21.8)	Furan (32.2)
	THF (18.4)	2-methylheptane (28.7)	3-ethyloctane (34.7)	2-butanone (6.0)	THF (18.6)	THF (15.7)	THF (11.4)
	2-MTHF (6.3)	THF (13.3)	THF (8.5)	THF (17.5)	2-MTHF (7.9)	2-MTHF (6.8)	2-MTHF (5.6)
		2-MTHF (9.6)	2-MTHF (9.3)	2-MTHF (10.4)			
Gas analysis (mol %) (H_2- free basis)							
CO	4.1	6.7	6.2	6.2	5.9	4.7	5.6
CO_2	10.9	13.3	13.5	14.4	15.1	14.4	15.3
CH_4	24.4	30.3	22.9	16.6	15.3	21.3	22.1
C_2H_6	-	21.9	12.7	-	-	-	-
C_3H_8	22.7	10.8	21.3	-	-	-	-
C_4H_{10}	32.3	9.7	13.1	43.9	22.1	26.6	30.5
C_5H_{12}	5.6	7.3	10.3	18.8	41.6	33.3	26.5

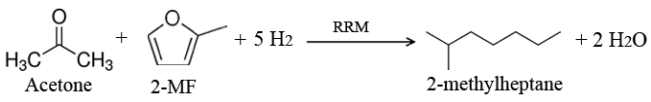

(3)

The 2-methylheptane (octane) formation was attributed to the addition of acetone to a cyclic ether (2-MF) and elimination of water through hydrodeoxygenation reaction, which occurred on the RRM. It is interesting to note that the addition of the ketone to the 2-MF ring resulted in ring opening and saturation catalyzed by the RRM to produce 2-methylheptane.

The production of THF, 2-MTHF, and furan were attributed to HDO of the furfural on elemental nickel.[40, 41] The furan was converted to THF through ring saturation and the 2-MTHF was produced from the saturation of the 2-MF ring. It appears that the reaction of 2-MF with acetone was slower than the ring saturation reaction and thus some of the 2-MF formed initially was converted to 2-MTHF. Significant amounts of butane was detected in the gaseous products because of the ring opening and further hydrogenation of THF on the nickel (Table 6.I.3). Further investigation of the reaction with furan showed that acetone and other ketones did not react with this compound despite the fact that it is also a cyclic ether.

Table 6.I. 4: AQHDO of dual compounds using RRM catalyst support.

Parameter	Reactant					
	Acetaldehyde/ furan	Acetone/ 2-MF	Butanone/ 2-MF	2-pentanone/ 2-MF	2-heptanone/ 2-MF	2,6-dimethyl-4-heptanone/ 2-MF
Conversion (%)	100	100	100	100	100	100
H_2 consumption (mol H_2)	0.55	0.44	0.46	0.44	0.33	0.26
Product distribution (wt. %) (H_2O- free basis)						
	n-hexane (100)	2-methylheptane (100)	3-methyloctane (100)	4-methylnonane (100)	6-methylundecane (100)	2-methyl-4 (2-methylpropane) nonane (100)
Elemental composition (wt. %)						
C	83.70 ± 0.03	84.19 ± 0.02	84.37 ± 0.03	84.51 ± 0.04	84.72 ± 0.02	84.85 ± 0.04
H	16.30 ± 0.04	15.81 ± 0.04	15.63 ± 0.02	15.49 ± 0.01	15.28 ± 0.02	15.15 ± 0.03

^{13}C NMR chemical shifts (ppm)	14.16, 22.89, 31.87	14.15, 22.04, 22.71, 27.23, 28.09, 32.30, 39.17	14.17, 22.05, 22.87, 23.56, 24.67, 27.45, 28.31, 32.89, 39.43	14.22, 14.84, 19.78, 20.34, 23.24, 24.12, 29.57, 32.69, 37.01, 39.67,	14.21, 14.78, 22.25, 22.84, 23.19, 24.56, 27.39, 28.36, 29.36, 32.14, 37.55, 39.37	11.27, 14.28, 14.82, 22.52, 22.47, 23.91, 24.62, 25.28, 27.54, 28.52, 29.38, 32.28, 37.83, 39.71

4.5.2. Neat and aqueous phase HDO of acetic acid/furfural on Ni/RM and RRM

The AQHDO of the acetic acid/furfural mixture on the Ni/RM catalyst showed very interesting results. The products consisted of n-hexane, 2-methylheptane, THF, 2-MTHF, and acetone (Table 6.I.3). The THF and 2-MTHF were typical furfural hydrodeoxygenation products as shown in the AQHDO of furfural on Ni/RM. However, what was significant was the near absence of the acetic acid AQHDO products observed when it was run alone and the absence of some of the furfural AQHDO products (furan and 2-MF). In place of the acetic acid AQHDO products, hexane and octane were the major compounds detected in the liquid products, which were immiscible with the water. The formation of these two products was explained in terms of the reaction network shown below.

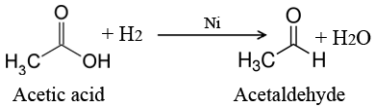

(4)

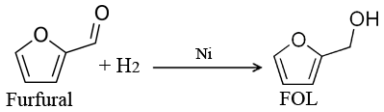

(5)

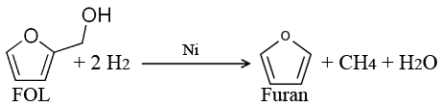

(6)

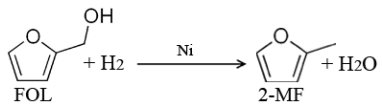

(7)

(8)

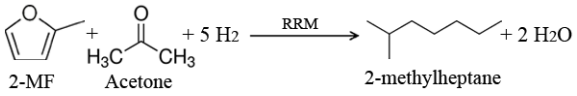

(9)

Products of reactions (4), (5), (6) and (7) were intermediate products formed on the nickel surface, but reactions (8) and (9) were formed on the RRM surface. To verify this hypothesis, pure reactants for reaction (8) (furan and acetaldehyde) were obtained from vendors and reacted on the RRM. The only organic product detected was n-hexane (C_6H_{14}) (Table 6.I.4), which was immiscible with water and was easily separated as a very pure product. The structure of C_6H_{14} was verified by GC/MS and ^{13}C NMR of the sample (Table 6.I.4) and comparing it to those of authentic standards.

Similarly, pure reactants of reaction (9) (2-MF and acetone) were obtained from vendors and reacted on the RRM and this produced only 2-methylheptane with stoichiometric amount of hydrogen consumption (Table 6.I.4). The ^{13}C NMR of the synthesized 2-methylheptane was in agreement with the published ^{13}C NMR of 2-methylheptane.[44] Thus, it is clear that the RRM was responsible for the addition and hydrodeoxygenation reactions of the intermediate products. The role of nickel then was to produce the intermediate reactants, which then reacted on the RRM. The THF and 2-MTHF did not participate in these reactions and were still present in the products (Table 6.I.3). The reaction rate of the AQHDO was probably slower than the formation of THF and 2-MTHF reactions and therefore some of the furan and 2-MF were saturated to form

these compounds. The acetone for reaction (9) was attributed to the ketonization reaction shown in reaction (1) and discussed in section 3.5.1. The overall reaction network of acetic acid AQHDO is shown in Fig. 6.I.1.

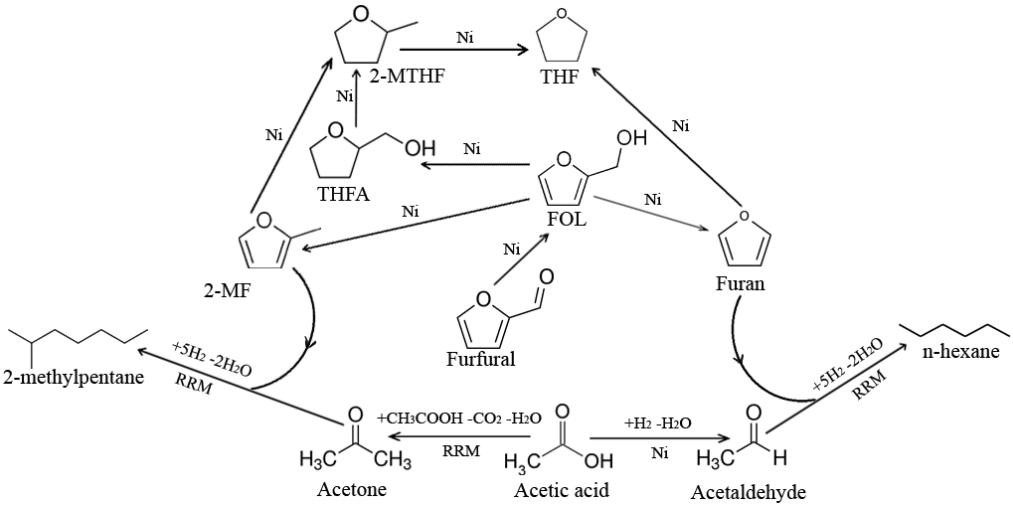

Fig. 6.I. 1: Overall reaction network of acetic acid/furfural AQHDO using Ni/RM catalyst.

When the acetic acid/furfural HDO was run in the neat form, there was rapid deactivation of the catalyst and large amounts of coke and gases were produced. The liquid products yield was very low but the composition of the liquid products was similar to that of the aqueous acetic acid/furfural HDO.

The cokes formed on the catalyst surface from both aqueous acetic acid/furfural and neat acetic acid/furfural HDO were examined with thermogravimetric analyzer (TGA) in nitrogen and air atmospheres. When nitrogen was used for the TGA, no weight loss was detected, showing that no volatile compounds were left on the catalyst and only coke was present. However, when air was used on the recovered catalyst, the aqueous

acetic acid/furfural HDO coke produced only one weight loss peak at 289 °C. The neat acetic acid/furfural HDO coke had four weight loss peaks (Fig. 6.I.2). The first peak corresponded with the peak produced in aqueous acetic acid, but the three other weight loss peaks occurred at higher temperatures of 350, 390, and 486 °C. The occurrence of the three extra peaks at higher temperature suggested that there was further deoxygenation of the initial coke formed resulting in a coke with less H_2 and O_2 contents.

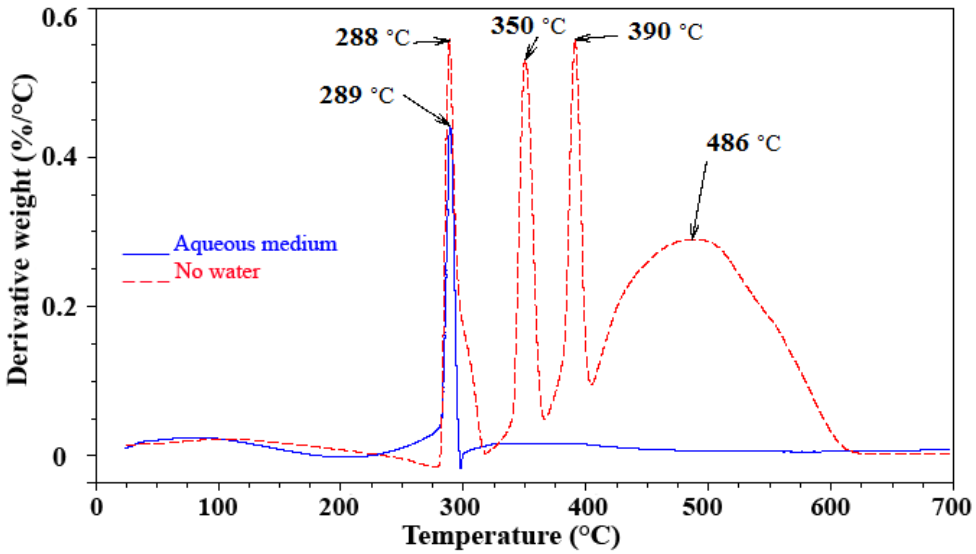

Fig. 6.I. 2: TGA of the used catalyst in aqueous medium (blue solid line) and in absence of water (red dashed line).

4.5.3. AQHDO of propionic acid/furfural on Ni/RM and RRM

The AQHDO of the propionic acid/furfural mixture on the Ni/RM catalyst showed interesting results with similar pathway to that of acetic acid/furfural. The products consisted of 3-pentanone, heptane, 3-ethyloctane, THF and 2-MTHF (Table 6.I.3). The THF and 2-MTHF were typical furfural hydrodeoxygenation products as shown in the AQHDO of furfural on Ni/RM. However, what was significant was the

absence of the propionic acid AQHDO products observed when it was run alone and the absence of some of the furan and 2-MF. Instead of the propionic acid AQHDO products, heptane and 3-ethyloctane were the major compounds detected in the liquid products, which was immiscible with the water. The formation of these two products was explained in terms of the reactions (10) and (11).

(10)

(11)

The addition hydrodeoxygenation reactions (10) and (11) occurred on the RRM. The 3-pentanone for reaction (11) was due to ketonization of propionic acid on RRM (reaction 2), which was then converted to $C_{10}H_{12}$ (3-ethyloctane) through addition hydrodeoxygenation on the RRM.

4.5.4. Aqueous phase HDO of 2,3-butanedione/furfural on Ni/RM and RRM

2,3-butanedione is one of the compounds found in the catalytic pyrolysis products of lignocellulosic biomass and so it was also investigated to ascertain if it produced any hydrocarbons. The 2,3-butanedione/furfural AQHDO on Ni/RM produced 3-methyloctane (C_9H_{20}), furan, butanone, THF, and MTHF liquid products as well as gases (Table 6.I.3). The AQHDO converted the furfural to furan and 2-MF on the nickel (reactions 5, 6, 7) while the 2,3-butanedione was converted to butanone (reaction 12). The butanone which behaves like other ketones such as acetone reacted only with 2-MF

and not with furan (reaction 13). Thus, in this process, the butanone reacted with the 2-MF to produce 3-methyloctane (C_9H_{20}) while the furan, THF, and 2-MTHF did not react and were part of the final liquid product (Table 6.I.3). Also a small quantity of butanone (~ 6 wt. %) remained unreacted in the final product probably because there was insufficient amount of 2-MF.

When the 2,3-butanedione/furfural was taken through AQHDO on RRM, there was no reaction, but when butanone/2-MF was reacted on the RRM, 3-methyloctane (C_9H_{20}) was the only organic product at 100% conversion, high selectivity, and no gases were produced (Table 6.I.4). Because the C_9H_{20} was immiscible with water, this product was easily separated and its identity confirmed by ^{13}C NMR, GC/MS, and CHNOS analyses (Table 6.I.4). It is therefore clear that the active reactant was the 2-MF and not the furfural itself. Thus, if the furfural cannot be reduced to 2-MF, the production of the hydrocarbon will not occur because the addition reaction occurred on the RRM surface and RRM could not reduce the furfural to 2-MF. The presence of nickel in the catalyst was therefore very crucial for the effectiveness of this process.

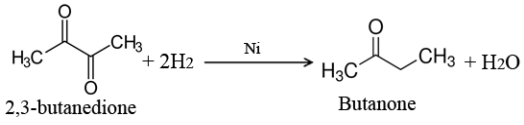

2,3-butanedione Butanone (12)

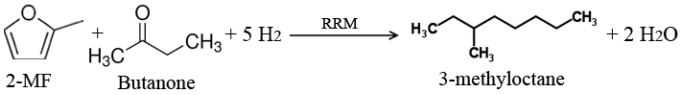

2-MF Butanone 3-methyloctane (13)

4.5.5. Aqueous phase HDO of 2-pentanone/furfural on Ni/RM and RRM

The AQHDO of furfural and 2-pentanone was similar to those of acetone and butanone, in that the reaction occurred between the 2-MF and 2-pentanone to produce 4-methylnonane ($C_{10}H_{22}$), a branched hydrocarbon as shown in the equations below (reaction 14):

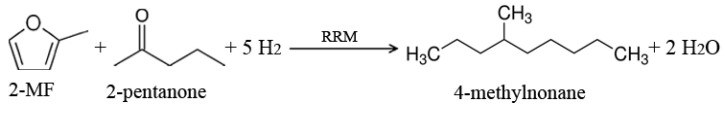

(14)

In addition to the $C_{10}H_{22}$ hydrocarbon, other compounds produced were furan, and THF, which were the reduction products of furfural (Table 6.I.3). The AQHDO of 2-MF and 2-pentanone on RRM produced only $C_{10}H_{22}$, which was confirmed by ^{13}C NMR, GC/MS, and CHNOS analyses (Table 6.I.4).

4.5.6. Aqueous phase HDO of 3-heptanone/furfural and 2,6-dimethyl-4-heptanone/furfural on Ni/RM and RRM

The reactions of these ketones were similar to the other ketones described above. It was a two-step reaction where the furfural was first reduced to furan and 2-MF on the nickel and subsequently the addition reaction occurred on the RRM support. The only major difference was longer chain hydrocarbons were produced in addition to the furan, THF, and gases (Table 6.I.3). For the 2-heptanone/furfural AQHDO reaction, 6-methylundecane ($C_{12}H_{26}$) was produced while for the 2,6-dimethyl-4-heptanone, 2-methyl-4(2-methylpropane)-nonane ($C_{14}H_{30}$) was produced. When 2-MF was reacted with these two ketones on RRM only one organic compound was produce for each of them (Table 6.I.4). For 3-heptanone/2-MF the only product was $C_{12}H_{26}$ (reaction 15)

while for 2,6-dimethyl-4-heptanone/2-MF the only product was $C_{14}H_{30}$ (reaction 16). The identities of these compounds were confirmed by ^{13}C NMR, and GC/MS analyses because they were immiscible with water and were therefore separated in very pure forms (Table 6.I.4).

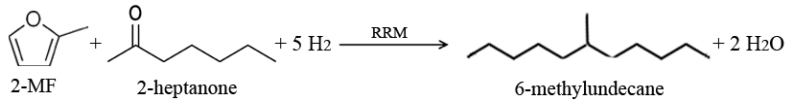

(15)

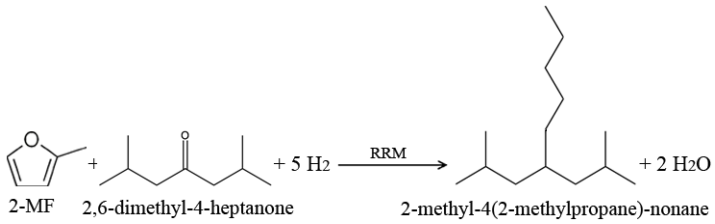

(16)

5. Discussions

The results of the AQHDO of the various compounds clearly showed that low molecular weight oxygenates from biomass could be hydrotreated in aqueous phase to produce a wide range of long chain hydrocarbon compounds. These products were readily separated because of immiscibility with water. In principle, these were catalytic reactions between unsaturated cyclic ethers (e.g. furan and 2-MF) with linear and branched ketones, and linear aldehydes in water reaction medium. The driving factor appeared to be the partial reduction products of a few small molecules such as acetic and propionic acids, furfural, and 2,3-butanedione to active reactants, that underwent several addition and hydrodeoxygenation reactions to produce hydrocarbons of various carbon chain lengths. In contrast, ketones such as acetone, pentanone, heptanone, and 2,6-dimethyl-4-heptanone did not require activation to be converted into long chain hydrocarbons.

The reduction of furfural to furan and 2-MF (ether) was crucial for these reactions. The double bonds in furan and 2-MF appeared to be also very important for these reactions because when the furan ring was saturated to THF or the 2-MF saturated to 2-MTHF, they did not react with any of the ketones and aldehydes. A very important role of nickel in this process was to produce partially reduced intermediate compounds that underwent further reactions with other reduced components. If the nickel was too active and produced unsaturated furans, there were no addition reactions and no subsequent increase in carbon chain lengths.

Similarly, acetic and propionic acids did not react with any of the components unless they were either reduced to acetaldehyde and propionaldehyde or ketonized to acetone and pentanone respectively before they underwent any of the addition reactions. When acetone was reduced to propanol, it did not partake in any of the reactions. The 2,3-butanedione and hydroxyl-butanone also did not react until they were converted to butanone.

The RRM appeared to play a very important role in these reactions. When the RRM support was replaced with silica-alumina, none of these reactions was observed and the major products were gases (data not reported). The RRM therefore served as the site for addition and hydrodeoxygenation of the reactants. In the case of acetic and propionic acids, the RRM also catalyzed the ketonization reactions with the loss of H_2O and CO_2, but more importantly, it did not reduce the acetone and pentanone to propanol and pentanol respectively which were inactive. The RRM also catalyzed ketonization of acid mixtures to produce a mixture of ketones. For example a mixture of propionic and acetic

acid produced acetone, butanone, and pentanone which can then react with the 2-methyfuran.

It is also interesting to note that RRM produced only one addition compound for each pair of pure ketones, aldehydes, and cyclic ethers investigated. When several pairs of compounds were investigated, they appeared to react independently and produced the sum of compounds produced from the individual pairs.

In the reactions of the aldehydes (acetaldehyde, propionaldehyde) with the cyclic ether (furan), the presence of H_2 and H_2O was important. These reactions involved the nucleophilic addition to the carbon-oxygen double (carbonyl carbon) bond catalyzed by the RRM. The addition compound was then hydrodeoxygenated to the subsequent longer chain alkanes. The exact sequence of the reactions is not well understood at this time. However, in all cases investigated, no alkene compounds were detected in any of the products. Furthermore, aromatic aldehydes did not undergo the addition reactions under our current conditions.

The ketones such as acetone, butanone, pentanone, heptanone, and 2,6-dimethyl-4-heptanone reacted with 2-MF but not with the furan or any of the saturated furans. Similarly, substituted butanones such as 2,3-butanedione and 2-hydroxy butanone did not react with 2-methylfuran unless they were converted to butanone before they underwent the reaction. Alcohols did not undergo any of these reactions and neither did aromatic ketones. In the case of ketones, the nucleophilic addition was also on the carbon-oxygen double bond (carbonyl carbon) and therefore branched hydrocarbons were produced in all cases studied.

The aqueous medium was very critical for the reactions; in the absence of water, there was rapid coking and deactivation of the catalyst especially when the medium was acidic. The coke properties for neat acids were different from those produced under aqueous conditions. This observation is similar to the effect of steam on FCC reactions in the hydrocracking processes in the petroleum industry. Clearly, these are unique reactions that we called “alkyl addition hydrodeoxygenation” because in all cases, it appeared the linear or branched chain ketone or aldehyde was added to the unsaturated cyclic ether ring then followed by ring opening and saturation to form the aliphatic hydrocarbons. The use of aqueous medium for the synthesis of the hydrocarbons also made the separation of the products very easy because of immiscibility of products with the synthesis medium.

In the reactions of the furans (furan or 2-MF), the number of carbons was conserved and therefore the length of the aliphatic carbon chain produced was always the sum of the carbons in the two reactants. Thus, 2-MF which has five carbons when reacted with butanone will produce alkane with nine carbons and similarly 2,6-dimethyl-4-heptanone (9 carbons) reacted with 2-MF to produce 14-carbon aliphatic hydrocarbon ($C_{14}H_{30}$). It is important to emphasize that all the compounds investigated in this work were identified in the aqueous phase catalytic pyrolysis products of pinyon juniper wood.

6. Conclusion

It has been demonstrated that through unique catalyst activity, low molecular weight water-soluble oxygenates found in biomass pyrolysis products can be hydrotreated in aqueous phase to form long chain aliphatic hydrocarbons. Aliphatic hydrocarbons containing 14 or more carbon chains can be produced from these addition

hydrodeoxygenation reactions in a one-pot synthesis. This method can also be used to synthesize pure compounds with almost 100% conversion, high selectivity, and excellent yields on RRM. The reactions occurred in water, which reduced coke formation on the catalyst and made separation of products very easy. These syntheses provide elegant and efficient method of producing hydrocarbon fuels and chemicals from renewable biomass resources.

7. References

(1) Zhang, Y.; Bi, P.; Wang, J.; Jiang, P.; Wu, X.; Xue, H.; Liu, J.; Zhou, X.; Li, Q. Production of Jet and Diesel Biofuels from Renewable Lignocellulosic Biomass. *Appl. Energy* **2015**, *150*, 128–137.

(2) Patel, M.; Kumar, A. Production of Renewable Diesel through the Hydroprocessing of Lignocellulosic Biomass-Derived Bio-Oil: A Review. *Renew. Sustain. Energy Rev.* **2016**, *58*, 1293–1307.

(3) Nabgan, W.; Tuan Abdullah, T. A.; Mat, R.; Nabgan, B.; Gambo, Y.; Ibrahim, M.; Ahmad, A.; Jalil, A. A.; Triwahyono, S.; Saeh, I. Renewable Hydrogen Production from Bio-Oil Derivative via Catalytic Steam Reforming: An Overview. *Renew. Sustain. Energy Rev.* **2017**, *79*, 347–357.

(4) Kang, S.; Fu, J.; Ye, Y.; Liao, W.; Xiao, Y.; Yang, P.; Liu, G. One-Pot Production of Hydrocarbon Oils from Biomass Derived Γ-Valerolactone. *Fuel* **2018**, *216*, 747–751.

(5) Shamsul, N. S.; Kamarudin, S. K.; Rahman, N. A. Conversion of Bio-Oil to Bio Gasoline via Pyrolysis and Hydrothermal: A Review. *Renew. Sustain. Energy Rev.* **2017**, *80*, 538–549.

(6) Makarfi Isa, Y.; Ganda, E. T. Bio-Oil as a Potential Source of Petroleum Range Fuels. *Renew. Sustain. Energy Rev.* **2018**, *81*, 69–75.

(7) Yang, T.; Jie, Y.; Li, B.; Kai, X.; Yan, Z.; Li, R. Catalytic Hydrodeoxygenation of Crude Bio-Oil over an Unsupported Bimetallic Dispersed Catalyst in Supercritical Ethanol. *Fuel Process. Technol.* **2016**, *148*, 19–27.

(8) Zhang, L.; Liu, R.; Yin, R.; Mei, Y. Upgrading of Bio-Oil from Biomass Fast Pyrolysis in China: A Review. *Renew. Sustain. Energy Rev.* **2013**, *24*, 66–72.

(9) Zhang, X.; Chen, L.; Kong, W.; Wang, T.; Zhang, Q.; Long, J.; Xu, Y.; Ma, L. Upgrading of Bio-Oil to Boiler Fuel by Catalytic Hydrotreatment and Esterification in an Efficient Process. **2015**, *84*, 83–90.

(10) Cai, W.; Liu, R.; He, Y.; Chai, M.; Cai, J. Bio-Oil Production from Fast Pyrolysis of Rice Husk in a Commercial-Scale Plant with a Downdraft Circulating Fluidized Bed Reactor. *Fuel Process. Technol.* **2018**, *171*, 308–317.

(11) Cai, W.; Liu, R. Performance of a Commercial-Scale Biomass Fast Pyrolysis Plant for Bio-Oil Production. *Fuel* **2016**, *182*, 677–686.

(12) Sanna, A.; Vispute, T. P.; Huber, G. W. Hydrodeoxygenation of the Aqueous Fraction of Bio-Oil with Ru/C and Pt/C Catalysts. *Appl. Catal. B Environ.* **2015**, *165*, 446–456.

(13) Furimsky, E. Catalytic Hydrodeoxygenation. *Appl. Catal. A Gen.* **2000**, *199*, 147–190.

(14) Mante, O. D.; Agblevor F. A. Catalytic Pyrolysis for the Production of Refinery-Ready Biocrude oils from Six Different Biomass Sources. *Green Chem.* **2014**, 16, 3364-3377.

(15) Ma, B.; Agblevor, F. A. Polarity-Based Separation and Chemical Characterization of Fast Pyrolysis Bio-Oil from Poultry Litter. *Biomass and Bioenergy* **2014**, *64*, 337–347.

(16) Yathavan, B. K.; Agblevor, F. A. Catalytic Pyrolysis of Pinyon-Juniper Using Red Mud and HZSM-5. *Energy and Fuels* **2013**, *27*, 6858–6865.

(17) Abnisa, F.; Wan Daud, W. M. A.; Arami-Niya, A.; Ali, B. S.; Sahu, J. N. Recovery of Liquid Fuel from the Aqueous Phase of Pyrolysis Oil Using Catalytic Conversion. *Energy and Fuels* **2014**, *28*, 3074–3085.

(18) Jain, A. B.; Vaidya, P. D. Kinetics of Aqueous-Phase Hydrogenation of Model Bio-Oil Compounds over a Ru/C Catalyst. *Energy and Fuels* **2015**, *29*, 361–368.

(19) Vispute, T. P.; Huber, G. W. Production of Hydrogen, Alkanes and Polyols by Aqueous Phase Processing of Wood-Derived Pyrolysis Oils. *Green Chem.* **2009**, *11*, 1433-1445.

(20) Xinghua, Z.; Tiejun, W.; Longlong, M.; Chuangzhi, W. Aqueous-Phase Catalytic Process for Production of Pentane from Furfural over Nickel-Based Catalysts. *Fuel* **2010**, *89* , 2697–2702.

(21) Ben, H.; Mu, W.; Deng, Y.; Ragauskas, A. J. Production of Renewable Gasoline from Aqueous Phase Hydrogenation of Lignin Pyrolysis Oil. *Fuel* **2013**, *103*, 1148–1153.

(22) Faba, L.; Díaz, E.; Ordóñez, S. Aqueous-Phase Furfural-Acetone Aldol Condensation over Basic Mixed Oxides. *Appl. Catal. B Environ.* **2012**, *113–114*, 201–211.

(23) Nakagawa, Y.; Nakazawa, H.; Watanabe, H.; Tomishige, K. Total Hydrogenation of Furfural over a Silica-Supported Nickel Catalyst Prepared by the Reduction of a Nickel Nitrate Precursor. *Chem. Cat. Chem.* **2012**, *4*, 1791–1797.

(24) Li, G.; Li, N.; Yang, J.; Wang, A.; Wang, X.; Cong, Y.; Zhang, T. Synthesis of Renewable Diesel with the 2-Methylfuran, Butanal and Acetone Derived from Lignocellulose. *Bioresour. Technol.* **2013**, *134*, 66–72.

(25) Ulfa, S. M.; Mahfud, A.; Rahman, M. F. Influence of Solvent on Liquid Phase Hydrodeoxygenation of Furfural-Acetone Condensation Adduct Using Ni/Al_2-O_3-ZrO_2. *IOP Conf. Ser. Mater. Sci. Eng.* **2017**, *172*.

(26) Baylon, R. A. L.; Sun, J.; Martin, K. J.; Venkitasubramanian, P.; Wang, Y. Beyond Ketonization: Selective Conversion of Carboxylic Acids to Olefins over Balanced Lewis Acid–base Pairs. *Chem. Commun.* **2016**, *52*, 4975–4978.

(27) Elliott, D. C.; Hart, T. R. 73 Catalytic Hydroprocessing of Chemical Models for Bio-Oil. **2009**, 23, 631–637.

(28) Jahromi, H.; Agblevor, F. A. Hydrotreating of Guaiacol: A Comparative Study of Red Mud-Supported Nickel and Commercial Ni/SiO2-Al2O3catalysts. *Appl. Catal. A Gen.* **2018**, *558*, 109–121.

(29) Jahromi, H.; Agblevor, F. A. Hydrodeoxygenation of Pinyon-Juniper Catalytic Pyrolysis Oil Using Red Mud-Supported Nickel Catalysts. *"Applied Catal. B, Environ.* **2018**, *236* (2010), 1–12.

(30) Guil-Lopez, R.; Navarro, R. M.; Fierro, J. L. G. Controlling the Impregnation of Nickel on Nanoporous Aluminum Oxide Nanoliths as Catalysts for Partial Oxidation of Methane. *Chem. Eng. J.* **2014**, *256*, 458–467.

(31) Kalai, D. Y.; Stangeland, K.; Jin, Y.; Yu, Z. Active and Stable Hydrotalcite Derived Ni Catalysts for CO2reforming of Methane: Comparison with Catalysts by Incipient Wetness. *J. CO_2 Util.* **2018**, *25*, 346–355.

(32) Wang, H.; Yang, L.; Sui, X.; Karahan, H. E.; Wang, X.; Chen, Y. Selective Synthesis of Single Walled Carbon Nanotubes on Metal (Iron, Nickel or Cobalt) Sulfate-Based Catalysts. *Carbon N. Y.* **2018**, *129*, 128–136.

(33) Jahromi, H.; Agblevor, F. A. Upgrading of Pinyon-Juniper Catalytic Pyrolysis Oil via Hydrodeoxygenation. *Energy* **2017**, *141*, 2186–2195.

(34) Joshi, N.; Lawal, A. Hydrodeoxygenation of Acetic Acid in a Microreactor. *Chem. Eng. Sci.* **2012**, *84*, 761–771.

(35) Chen, H.; Zhao, J.; Li, S.; Xu, J.; Shen, J. Effects of Water on the Hydrogenation of Acetone over Ni/MgAlO Catalysts. *Cuihua Xuebao/Chinese J. Catal.* **2015**, *36*, 380–388.

(36) Hu, X.; Dong, D.; Shao, X.; Zhang, L.; Lu, G. Steam Reforming of Acetic Acid over Cobalt Catalysts: Effects of Zr, Mg and K Addition. *Int. J. Hydrogen Energy* **2017**, *42*, 4793–4803.

(37) Alotaibi, M. A.; Kozhevnikova, E. F.; Kozhevnikov, I. V. Deoxygenation of Propionic Acid on Heteropoly Acid and Bifunctional Metal-Loaded Heteropoly Acid Catalysts: Reaction Pathways and Turnover Rates. *Appl. Catal. A Gen.* **2012**, *447–448*, 32–40.

(38) Otyuskaya, D.; Thybaut, J. W.; Alexiadis, V.; Alekseeva, M.; Venderbosch, R.; Yakovlev, V.; Marin, G. B. Fast Pyrolysis Oil Stabilization Kinetics over a Ni-Cu Catalyst Using Propionic Acid as a Model Compound. *Appl. Catal. B Environ.* **2018**, *233*, 46–57.

(39) Lugo-José, Y. K.; Monnier, J. R.; Williams, C. T. Gas-Phase, Catalytic Hydrodeoxygenation of Propanoic Acid, over Supported Group VIII Noble Metals: Metal and Support Effects. *Appl. Catal. A Gen.* **2014**, *469*, 410–418.

(40) Wang, C.; Luo, J.; Liao, V.; Lee, J. D.; Onn, T. M.; Murray, C. B.; Gorte, R. J. A Comparison of Furfural Hydrodeoxygenation over Pt-Co and Ni-Fe Catalysts at High and Low H2pressures. *Catal. Today* **2018**, *302* (December 2016), 73–79.

(41) Fu, Z.; Wang, Z.; Lin, W.; Song, W.; Li, S. High Efficient Conversion of Furfural to 2-Methylfuran over Ni-Cu/Al2O3catalyst with Formic Acid as a Hydrogen Donor. *Appl. Catal. A Gen.* **2017**, *547*, 248–255.

(42) Yin, D.; Ren, H.; Li, C.; Liu, J.; Liang, C. Highly Selective Hydrogenation of Furfural to Tetrahydrofurfuryl Alcohol over MIL-101(Cr)-NH 2 Supported Pd Catalyst at Low Temperature. *Chinese J. Catal.* **2018**, *39*, 319–326.

(43) Xiong, K.; Wan, W.; Chen, J. G. Reaction Pathways of Furfural, Furfuryl Alcohol and 2-Methylfuran on Cu(111) and NiCu Bimetallic Surfaces. *Surf. Sci.* **2016**, *652*, 91–97.

(44) https://www.sigmaaldrich.com/spectra/fnmr/FNMR010916.PDF.

Part II: Aqueous phase synthesis of hydrocarbons from reactions of guaiacol and low molecular weight oxygenates

1. Abstract

Catalytic pyrolysis of lignocellulosic biomass generates water-soluble low molecular weight oxygenates such as acetic acid, acetone, furfural, butanone, guaiacol, phenol and others in significant quantities that will affect the profitability of the biorefinery process. A new heterogeneous catalyst has been developed that catalyzes the reaction of ketones with unsaturated ethers in aqueous medium to produce C_6 to C_{15} hydrocarbons in a one-pot synthesis. These reactions are called "***carbonyl alkylations***" because the carbonyl carbon chain was added to the aromatic ring and the oxygen was eliminated without loss of carbon. The C_1 to C_4 ketones and aldehydes produce alkylated benzenes while the C_5 and higher carbonyl compounds alkylated the benzene ring but also caused ring opening to produce long chain internal alkene compounds. All the reactions occurred in the aqueous media at 300-350 ˚C on a supported nickel catalyst. The gaseous products included low molecular weight hydrocarbons such as methane, propane, butane, and pentane. Thus, it has been demonstrated for the first time that it is possible to produce a wide range of hydrocarbons from low molecular weight biomass derived oxygenates.

2. Introduction

Although the high oxygen content of biomass feedstocks makes them biodegradable and therefore environmentally friendly, they are also responsible for their low energy densities and their removal using various technologies have been a major

challenge for the research community.[1-4] Pyrolysis which is one of the thermochemical routes for biomass conversion produces pyrolysis oils that are unstable, acidic, viscous, reactive, low energy density, and high oxygen content and therefore not compatible with current petroleum based transportation fuels nor can they be used for standalone applications without considerable upgrading.[5] Current research efforts are focused on stabilizing the pyrolysis oils to enable them to be co-processed with petroleum feeds,[6] processed on standard unit operations, and potential processing in standalone biorefinery plants.[7] The stability improvement studies include esterification,[8, 9] low severity hydrotreatment,[10-12] catalytic pyrolysis.[13-16] The focus of this paper is the catalytic pyrolysis oils of lignocellulosic biomass. Although catalytic pyrolysis (*in situ* and *ex situ*) produces more stable pyrolysis oil with lower oxygen content and higher energy density, it suffers from major deficiencies: it produces large quantities of non-condensable gases and large quantities of low molecular weight water-soluble oxygenates.[7, 17-20] The water-soluble oxygenates pose several challenges including wastewater treatment, loss of carbon, and overall decrease in product yield. The water-soluble oxygenates with are found in concentrations of 10-20 wt. % of the aqueous phase constitute 10 to 30 wt. % of the total product yield.[5, 7, 19] The recovery of these water-soluble products from the aqueous phase to improve the overall efficiency of the biofuel production has been a subject of several investigations.[21-28] Li et al[21] investigated the synthesis of renewable diesel fuel from model compounds such as 2-methylfuran, acetone, and butanal using Nafion-212 and Ni-WxC/C in a two-step process. In this process, 2-methylfuran were reacted with either butanal or acetone on the Nafion-212 catalyst at 50 C to form a longer chain oxygenated compound, which was then

deoxygenated in the second step using Ni-WxC/C at 350 ^{o}C to produce hydrocarbons. Huber et al[22] also investigated the production of liquid alkanes through aqueous phase processing of biomass-derived carbohydrates using acid catalyzed dehydration of the carbohydrates which was followed by aldol condensation over basic solid catalysts to form larger molecules. The larger oxygenated molecules were then hydrotreated using Pd/Al_2O_3 catalyst to produce a large number of complex alkane compounds. These alkanes derived mostly from the condensation of reaction of furan compounds and there were no lignin derived compounds. Bergem et al[23] investigated the aqueous phase hydrogenation of model compounds and light oxygenate fraction of bio-oil over supported ruthenium catalysts (Ru/TiO2, Ru/C) at reaction temperatures 100-150 ^{o}C. These studies included the model compounds such as acetic acid, formic acid and hydroxyacetone as well as fractions of aqueous phase pyrolysis oils. The liquid products were mostly mono alcohols from the hydrogenation of ketones and aldehydes while hydroxyketones were converted into diols. No liquid hydrocarbons were reported for both Ru/TiO2 and Ru/C. The catalyst was very effective for the model compounds, but the reaction rate slowed down when the aqueous bio-oil fraction was hydrotreated. The gaseous products were methane, ethane, CO, CO_2 and other low molecular weight hydrocarbons. Xu et al[24] investigated *in situ* hydrogenation of furfural mixed with additives over Raney nickel catalysts in N_2-atmosphere in water and methanol. They reported that the addition of secondary compounds such as acetic acid, acetone, or phenol reduced the conversion of furfural and changed the product distribution. The products of these reactions were mostly oxygenated compounds and no liquid hydrocarbons were reported for reaction conditions of 160-220 $^{\circ}$C for 4 hours in batch autoclave reactors.

Ulfa et al[25] investigated the effect of solvent on the liquid phase hydrodeoxygenation of furfural-acetone condensation adduct using Ni/Al_2O_3-ZrO_2 and reported the formation n-tridecane and other oxygenated compounds, but the yields and selectivities were low and the reaction times were very long (8 h HDO) at 150-200 ˚C. The process was also two-steps with the first step using MgO and CaO to produce the furfural-acetone adduct in low yields after 6 hours reaction. The product distribution varied according to whether the reaction medium was water or water/acetone. Hronec et al[26] conducted nickel catalyzed hydrogenation of aldol condensation product of furfural with cyclopentanone to produce C_{15} cyclic ethers. This was a three-step process in which furfural was first converted into cyclopentanone, then the cyclopentanone was condensed with furfural using base catalyzed aldol condensation, and finally, the condensation product was hydrogenated with 5%Pd/C catalyst in hydrocarbon solvents. The cyclic ethers were produced without furan ring opening. Li et al[27] investigated the production of aqueous phase renewable gasoline from the hydrodeoxygenation of aqueous solutions prepared by hydrolysis of sugar maple using Ruthenium/Carbon (Ru/C) and Pt/Zirconium phosphate (Pt/ZrP) catalysts in three-step process. The process involved hot water treatment or acid hydrolysis of the wood followed by a two-step hydrodeoxygenation of the hydrolyzates using Ru/C at 393 K followed by Pt/ZrP treatment at 518 K. The reaction products were a mixture oxygenated products including monoalcohols such as ethanol, butanol, pentanol; ketones such as butanone, hexanone and acids such as pentanoic acid, butanoic acid; diols such as propanediol, pentanediol; and sugar alcohols such as xylitol and sorbitol. The only liquid hydrocarbon product reported was hexane with low selectivity. The mixture of alcohols, ketones, acids had estimated octane number of 96.5 and was

considered as suitable fuel for gasoline application. However, since the oxygen content of the mixture was very high, the energy density of such a fuel will be low and can only be used as a gasoline fuel additive. Faba et al[28] investigated furfural-acetone condensation on mixed oxides such as Mg-Zr, Mg-Al and Ca-Zr. The results showed the formation of several long chain (C8 and C13) oxygenated compounds. However, this process will require hydrodeoxygenation to convert the oxygenated compounds to hydrocarbons. Baylon et al[29] showed that mixed carboxylic acids can be converted to C3 –C6 olefins with up to 60 mol% carbon yield through a cascade of ketonization, aldolization and self-deoxygenation using a $Zn_xZr_yO_z$ catalysts. They also reported improved yield of olefins by co-feeding with hydrogen.

Cross-reactivity of guaiacol and propionic acid blends during hydrodeoxygenation over Ni-supported catalyst has also been reported by Sankaranarayanan et al[30] in which Ni/h-ZSM-5, Ni/SBA-15, Ni/Al-SBA-15 acidic catalysts were investigated in decalin medium. The major product of guaiacol reactions with high selectivity was cyclohexane, the mixture showed reaction of methanol with propionic acid to form an ester. Other compounds formed with low selectivities were hydrogenated benzene compounds.

Several of the methods discussed above using model compounds, fractionated pyrolysis oils, and raw aqueous phase oils have focused on furfural based reactions and show promise, but none has been commercialized. Furthermore, these hydrotreating and ketonization methods require multiple steps to produce liquid hydrocarbons suitable for fuel applications. To our knowledge there is no published equivalent studies using lignin-derived monomers in synthesizing hydrocarbon molecules other than the numerous hydrotreatment studies on guaiacol, anisole, and phenols. In this paper we report aqueous

phase hydrotreatment of low molecular weight water-soluble products and guaiacol into a wide range of hydrocarbons using a novel catalyst in a one-pot synthesis process. Although model compounds are reported in this paper, the process has also been applied to real biomass aqueous phase pyrolysis products, which produced very similar results without catalyst deactivation. The ultimate goal of this research is to produce hydrocarbon fuels and chemicals from biomass catalytic pyrolysis oils.

3. Material and methods

3.1. Materials

The selection of model compounds for this research was based on the analysis of the aqueous phase red mud catalytic pyrolysis liquids. The major compounds detected in this liquid were used for the model studies to elucidate the reactions that occur during the hydrotreating of the aqueous phase organics. The aqueous phase organic liquid was obtained from the red mud catalytic pyrolysis of pinyon juniper wood. The model compounds were obtained from various chemical vendors and were used as received without any further purification. The compounds included acetic acid (EMD Millipore Billareca, MD, USA), guaiacol, anisole, 2,3 butanedione, 3-hydroxy-2-butanone (Alfa Aesar, Haverhill, MA, USA), acetaldehyde, phenol, benzene, furfural, furan, 2-methylfuran (Sigma Aldrich, St Louis, MO, USA), acetone, ethanol, toluene, methanol (Pharmaco-AAPER, Orange County, CA, USA). Various standards were also obtained from these companies for product identification and quantification.

3.2. Catalyst preparation and characterization

Nickel/red mud (Ni/RM) catalyst was prepared in-house using the procedure described by Jahromi and Agblevor.[31, 32] Ni/RM catalysts were prepared at 40 wt. % nickel metal loading using wet impregnation method.[31-35] The calculated amount of $Ni(NO_3).6H_2O$ was dissolved in 100 ml deionized water at room temperature and then mixed with red mud (particle size <90 μm). The mixture was heated to 70 °C and continuously stirred for 5 hours to prepare the catalyst precursor. The catalyst precursor was dried at 105 °C for 10 hours and then calcined in a muffle furnace (Thermo Scientific, Inc., Waltham, MA, USA) at 620 °C for 5 hours. The calcined material was reduced for 6 hours at 450 °C with a reducing gas mixture of 10% H_2 and 90% N_2 at flow rate of 20 ml/min to obtain the final catalyst, which was labelled Ni/RM.

The preparation of the reduced red mud catalyst (RRM) was similar to that of the Ni/RM except that the Ni addition step was omitted. The red mud catalyst precursor was dried at 105 °C, for 10 h and calcined in a muffle furnace at 620 °C for 5 hours. The precursor was then reduced with 10% H_2 and 90% N_2 at a flow rate of 20 ml/min to obtain the final catalyst which was labelled RRM.

The catalysts were characterized by thermogravimetric-temperature programmed reduction (TG-TPR), Brunauer–Emmett–Teller (BET) surface area analyzer, X-ray diffraction (XRD), inductively coupling plasma (ICP), and scanning electron microscopy (SEM) as reported previously.[31, 32]

3.3. Aqueous phase hydrodeoxygenation experiments

All aqueous phase hydrodeoxygenation (AQHDO) experiments were conducted in a Parr Series 4560 300 mL autoclave reactor (Parr Instruments, Moline, IL, USA). This

reactor had a variable speed magnetic drive and turbine agitator. A K-thermocouple immersed in the reactor was used to measure the reactant temperature. The setup had an electrically heated jacket to ensure isothermal conditions. The temperature and speed of agitation were controlled by a Parr 4848 controller.

In each experiment, the reactor was charged with reactant (100 g) and Ni/RM catalyst (3 g). The reactant consisted of 15 wt. % organic compound and 85% water. Thus, for a single compound HDO, 15 g of material was added to 85 g water and 3 g catalyst was added. It was assumed that the water was only a reaction medium. If two compounds were under investigation, then 7.5 g of each compound was dissolved in the water. The reactor was purged with N_2 to ensure an inert atmosphere. The reactor was then charged with high purity hydrogen supplied from a reservoir tank to the desired pressure of 6.21 MPa (900 psi). The reactor was heated to reaction temperature (350 °C) at heating rate of 15 °C/min. The reaction time was recorded when the set temperature was reached. After the desired reaction time (30 minute), the reactor was cooled to room temperature using the internal cooling coil and gas samples were collected in a tedlar bag for gas analyses. The reproducibility of experiments was checked and the error in all experimental measurements was found to be less than 3%.

Another set of experiments was carried out on the RRM using reaction conditions that were identical to those for the Ni/RM. The RRM is similar to the support for the Ni/RM and it was used to assess the influence of the support on the overall Ni/RM catalyst activity.

In blank experiments (without catalyst) 100 g of reaction mixture was charged into the reactor and the reactor was pressurized to 6.2 MPa (900 psi) with hydrogen and

allowed to react for 30 minutes at 350 °C to determine if the reactor walls played any role in the observed reactions. All experiments were conducted in triplicate. The blank experiments showed no reactivity of the reactor walls. All results reported are therefore assumed to have no reactor wall influence.

3.4. Analysis of AQHDO products

Hydrogen consumption was measured according to the procedure reported previously.[36] Gas analysis was performed using Agilent 490 micro-GC which was equipped with molsieve 5A and porous polymer (PP) columns and two TCD detectors for each column.[36] The liquid products of AQHDO experiments were analyzed by HPLC (Shimadzu Scientific, Columbia, MD, USA) using a RID-10A detector and a Kromasil 100-5-C18 column (AkzoNobel Amsterdam, Netherlands). The HPLC was equipped with a LC-10AT pump, SCL-10Avp controller, and SIL-10A autosampler. CLASS-VP 7.3 SP1 software was used to analyze HPLC chromatograms. A CTO-10A column oven was used to maintain the column temperature at 55 °C during the analysis. The injection volume was 0.25 μl and acetonitrile at flow rate of 0.6 ml/min was used as the mobile phase. Data acquisition time was 80 minutes for all analyses.

The liquid samples were analyzed for guaiacol, anisole, catechol, phenol, cyclohexane, hexane, benzene, toluene, xylene, ethylbenzene, isopropylbenzene, 3-methyloctane, 2-methylheptane, butylbenzene, and other reaction products. The identity of the synthesized liquid compounds were confirmed by NMR (^{1}H and ^{13}C) (Bruker 500 MHz, Bruker Corporation, Japan), GC/MS (Shimadzu GC/MS-QP5000, Shimadzu Scientific, Columbia, MD, USA), and CHNOS analyses.

The elemental composition of AQHDO products were determined using ThermoFischer Scientific Flash 2000 organic elemental analyzer (ThermoFisher Scientific,Waltham, MA, USA), and the oxygen content was calculated by difference according to ASTM D5291.

4. Results

The characterization of the Ni/RM catalyst has been reported elsewhere[31, 32] and will not be repeated here. The AQHDO results were grouped into single compounds and dual compounds to determine the effect of mixing these reactants in cross-reactions. AQHDO of individual compounds on red mud supported nickel (Ni/RM) catalyst and reduced red mud (RRM) (catalyst support) are reported below.

4.1. Aqueous phase guaiacol HDO on Ni/RM and RRM

The AQHDO of guaiacol on Ni/RM produced two immiscible liquids, a small amount of coke, and gases. The organic liquid contained benzene, toluene, xylene, hexane, cyclohexane, methanol, phenol, catechol, and anisole (Table 6.II.1), which was similar to the composition of HDO of guaiacol without aqueous phase reported by Jahromi and Agblevor.[31] The production of these large numbers of compounds from guaiacol was attributed to three competing hydrodeoxygenation pathways. One pathway was through the production of anisole and the others were through the catechol and phenol. The anisole pathway led to the production of anisole, phenol, benzene, toluene, cyclohexane, and hexane while the catechol pathway led to the production of catechol, phenol, benzene, toluene, xylene, cyclohexane, and hexane. The phenol pathway products were similar to the catechol pathway with the exception of catechol. The

detailed explanation of mechanism of these competing pathways were reported in Jahromi and Agblevor.[31] The anisole pathway will be shown to be the key for the hydrocarbon production from low molecular weight oxygenates.

The gaseous product consisted of methane, propane, and carbon dioxide, which was similar to those produced from HDO of neat guaiacol.[31] One major difference between the AQHDO and the HDO was the influence of water on the coke formation. The presence of steam at the reaction conditions (350 ºC, 6.9 MPa) appeared to moderate the production of coke and its characteristics as discussed in section 3.3.1.

There was no reaction during the AQHDO of guaiacol on RRM. This clearly showed that the nickel catalyzed the production of the above compounds through hydrodeoxygenation, hydrogenation, ring saturation, and ring opening reactions.[37-40]

4.2. Aqueous phase HDO of 2,3-butanedione and 3-hydroxy-2-butanone on Ni/RM and RRM

The AQHDO of the 2,3-butanedione and 3-hydroxy-2-butanone showed similar reaction products. Both reactants produced one liquid phase containing butanol and butanone, which were attributed to the hydrodeoxygenation on elemental Ni (Table 6.II.1). When AQHDO of 2,3-butanedione and 3-hydroxy-2-butanol were carried out on RRM, there were no reactions for any of these reactants, which again confirmed that RRM did not catalyze the hydrodeoxygenation of the primary reactants. The gaseous products of the Ni/RM AQHDO were butane, methane, and carbon dioxide (Table 6.II.1).

Table 6.II. 1: AQHDO of individual compounds using Ni/RM catalyst.

Parameter	Reactant		
	Guaiacol	2,3-butanedione	3-hydroxy-2-butanone
Conversion (%)	91.4	100	100
H_2 consumption (mol H_2)	0.97	0.66	0.57
Product distribution (wt. %) (H_2O- free basis)			
	Catechol (1.2)	Butanol (57.7)	Butanol (72.4)
	Anisole (2.6)	Butanone (42.3)	Butanone (27.6)
	Phenol (7.5)		
	Benzene (23.1)		
	Toluene (15.6)		
	Xylene (5.5)		
	Hexane (5.7)		
	Cyclohexane (33.5)		
	Methanol (5.3)		
Gas analysis (mol %) (H_2- free basis)			
CO	5.8	1.1	0.8
CO_2	12.5	6.8	9.4
CH_4	64.7	58.2	58.1
C_2H_6	3.3	-	-
C_3H_8	9.8	3.3	2.4
C_4H_{10}	2.3	30.3	28.7
C_5H_{12}	1.1	-	-

4.3. Aqueous phase HDO of dual compounds on Ni/RM and RRM

In these series of studies, dual reactants were investigated to assess the interactions between them. Thus, a combination of acetic acid/guaiacol, acetone/guaiacol, 2,3-butanedione/guaiacol, 2-butanone/guaiacol, acetic acid/propionic acid, 3-heptanone/guaiacol, and 2,6-dimethyl-4-heptanone/guaiacol were investigated using AQHDO. The combination of reactants is shown in Tables 6.II.2-6.II.4. In addition, independent reactions with anisole were also investigated.

Table 6.II. 2: AQHDO of guaiacol dual compounds using Ni/RM catalyst.

Parameter	Reactant	
	Acetic acid/ Guaiacol	Acetone/ Guaiacol
Conversion (%)	100	100
H_2 consumption (mol H_2)	1.34	1.17
Product distribution (wt. %) (H_2O- free basis)		
	Methanol (4.2)	Methanol (3.9)
	Catechol (1.3)	Catechol (1.2)
	Phenol (2.5)	Phenol (1.9)
	Benzene (11.6)	Benzene (8.3)
	Cyclohexane (9.8)	Cyclohexane (6.7)
	n-hexane (7.9)	n-hexane (6.5)
	Ethylbenzene (11.3)	Isopropylbenzene (22.4)
	Ethylcyclohexane (16.4)	Isopropylcyclohexane (35.8)
	Isopropylbenzene (9.5)	2-methyloctane (13.3)
	Isopropylcyclohexane (13.2)	
	n-octane (5.4)	
	2-methyloctane (6.9)	
Gas analysis (mol %) (H_2- free basis)		
CO	3.4	-
CO_2	7.1	6.3
CH_4	47.5	49.6
C_2H_6	20.7	-
C_3H_8	16.8	37.9
C_4H_{10}	2.2	3.4
C_5H_{12}	1.5	2.6

4.3.1 Aqueous phase HDO of acetic acid/guaiacol on Ni/RM and RRM

Both acetic acid and guaiacol are pyrolysis products derived from lignocellulosic biomass, which are usually found in larger fractions in the aqueous phase of the catalytic pyrolysis products.[7, 17, 41, 42] The guaiacol was reacted with acetic acid with and without aqueous phase to produce long chain hydrocarbons. As expected, most of the acetic acid AQHDO products[43, 44] were not detected and some of the guaiacol AQHDO products[29, 31, 45-47] were also absent. The AQHDO products of this mixture were more complex than

those for the individual compounds. HPLC analysis was used to identify twelve major compounds in the organic liquid product: methanol (CH_3OH), n-hexane (C_6H_{14}), n-octane (C_8H_{18}), ethylbenzene (C_8H_{10}), benzene (C_6H_6), cyclohexane (C_6H_{12}), ethylcyclohexane (C_8H_{16}), isopropylbenzene (C_9H_{12}), 2-methyloctane (C_9H_{20}), isopropylcyclohexane (C_9H_{18}), phenol (C_6H_5O) and catechol ($C_6H_6O_2$) (Table 6.II.2). Some of these products were the same as those detected in the AQHDO reactions of guaiacol, however new compounds such as n-octane, 2-methyloctane, ethylbenzene, isopropylbenzene, isopropylcyclohexane, and ethylcyclohexane were not detected in the AQHDO of either reactant. We hypothesized that these six compounds were produced from the reaction of acetic acid reduction intermediates (acetaldehyde and acetone) with guaiacol reduction intermediate (anisole). Further, we hypothesized that some of the reactions occurred on the RRM support. The proposed reactions are shown below:

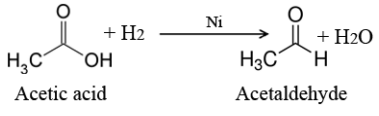

(1)

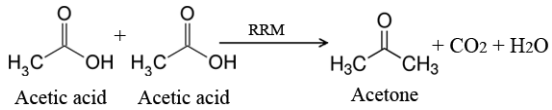

(2)

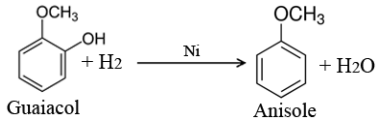

(3)

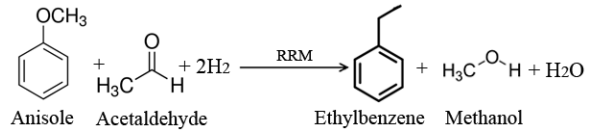

(4)

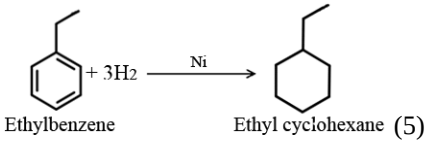

(5)

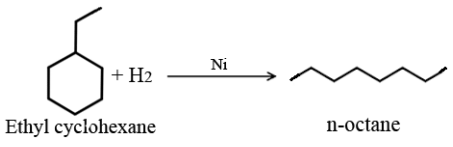

(6)

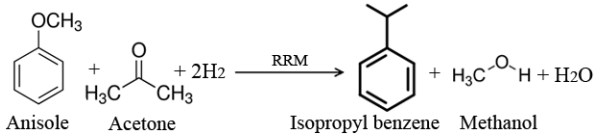

(7)

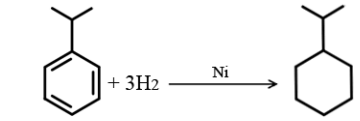

(8)

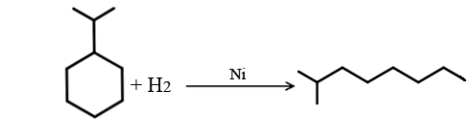

(9)

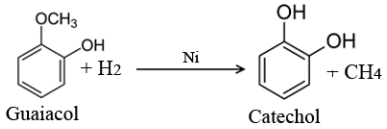

(10)

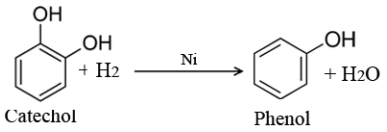

(11)

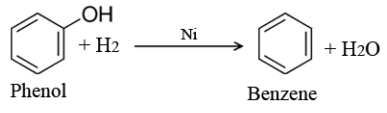

(12)

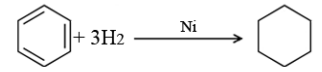

(13)

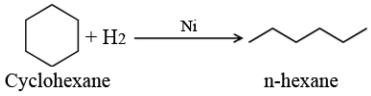

(14)

Reactions (1) and (2) were the intermediate products from the reduction and ketonization respectively of acetic acid[29, 43] and (3) was the reduction of guaiacol to anisole on elemental Ni.[31] These reaction intermediates were responsible for the plethora

of reactions and products observed for this process. The two most important reactions of the intermediates were (4) and (7). These reactions occurred on the RRM and then the subsequent reactions occurred on the nickel surface. As a proof of this hypothesis, these two reactions were carried out using pure reactants (anisole/acetaldehyde and anisole/acetone) on RRM under similar conditions as the Ni/RM (Table 6.II.3). As expected, water, methanol, and ethylbenzene were produced from the anisole/acetaldehyde; isopropyl benzene, methanol, and water were produced from anisole/acetone mixtures. There were no gas products in any of the reactions. In both (4) and (7) there was "***carbonyl alkylation***" of the benzene ring producing ethylbenzene and isopropylbenzene (cumene) with loss of water and methanol. These hydrocarbons formed two phases with water and therefore were easily separated as pure products with little contamination from methanol. The conversion was 100% and the reaction was stoichiometric with respect to yields of methanol, ethylbenzene, and isopropylbenzene. None of the other hydrocarbon products in reactions (5), (6), (8)-(14), that were detected in Ni/RM were found in the RRM AQHDO products. Because of the high purity of the ethylbenzene and isopropylbenzene with only minor contamination from methanol, they were authenticated by running ^{13}C NMR of the products and comparing them with authentic standards (Table 6.II.3). As shown in Table 6.II.3, there was no doubt that these two compounds were produced on the RRM. In case of the Ni/RM products, these were very complex mixtures, but FTIR and CHNOS analysis revealed that they were mostly hydrocarbon products with low oxygen content from phenol and catechol.

The formation of 2-methyloctane (C_9H_{20}), n-octane (C_8H_{18}) and all the other hydrocarbons required benzene ring saturation and opening, which did not occur on the

RRM. The 2-methyloctane and n-octane were identified by comparing their HPLC retention times to that of pure compounds. Reactions (5), (6), (8) and (9) occurred because of benzene ring saturation and opening of the initial products from (4) and (7) while reactions (10)-(14) originated from the parallel catechol and phenol reduction pathways of guaiacol, which resulted in benzene ring opening and saturation due to elemental Ni.

Gaseous products were also formed in the case of the Ni/RM. These products were dominated by methane, ethane, and propane, which derived from cracking of some of the hydrocarbon products (Table 6.II.2). The overall reaction network of acetic acid/guaiacol on Ni/RM catalyst is illustrated in Fig. 6.II.1.

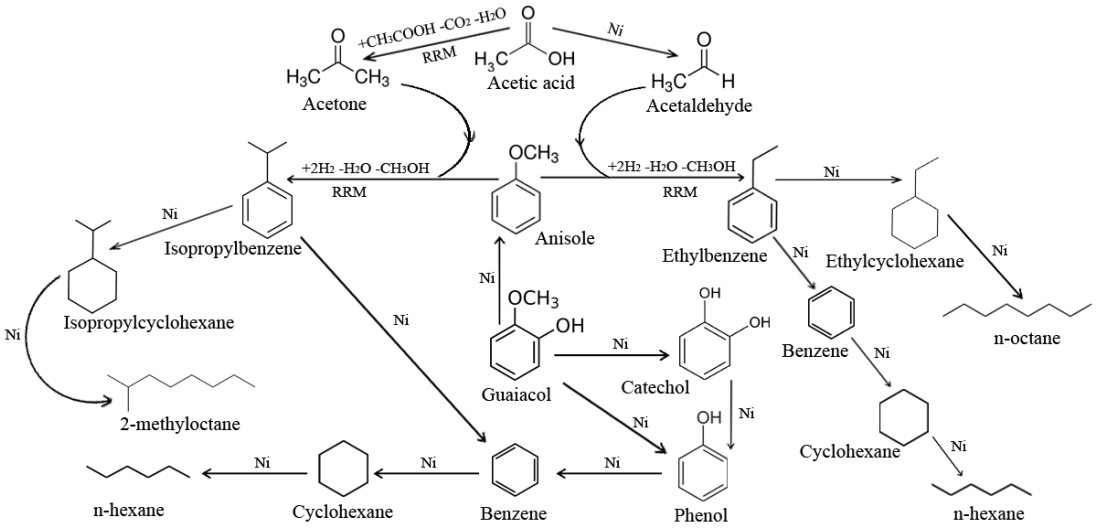

Fig. 6.II. 1: Reaction network of acetic acid/guaiacol on Ni/RM catalyst.

The AQHDO of acetic acid/guaiacol also produced a small amount of coke, but when the HDO was conducted on Ni/RM without water, about 46% of the product was coke, 15% liquid and 38% gas. The composition of the liquid and gaseous products were similar to the AQHDO products. The thermogravimetric analysis (TGA) of the coke

from the two reactions, in air showed very complex weight loss patterns (Fig. 6.II.2). The TGA data showed a major weight loss peak at 331 ˚C and minor peaks at 462 and 614 ˚C for the AQHDO coke. In contrast, the HDO coke showed several major weight loss peaks at 329, 351, 419, 440, 568, 580 ˚C and minor weight loss at 628 ˚C (Fig. 6.II.2). The TGA clearly showed that not only did the water influence the yield of coke, but it also influenced its composition. Under neat HDO conditions, the initial coke degradation temperature at 329 ˚C was similar to that of the AQHDO coke. However, after the initial HDO coke formation at 329 ˚C, there were more complex coke formation reactions that produced cokes that decomposed at much higher temperatures, probably because these had lower oxygen contents.

The presence of steam in the AQHDO prevented the formation of these complex coke species and reduced coke yield.

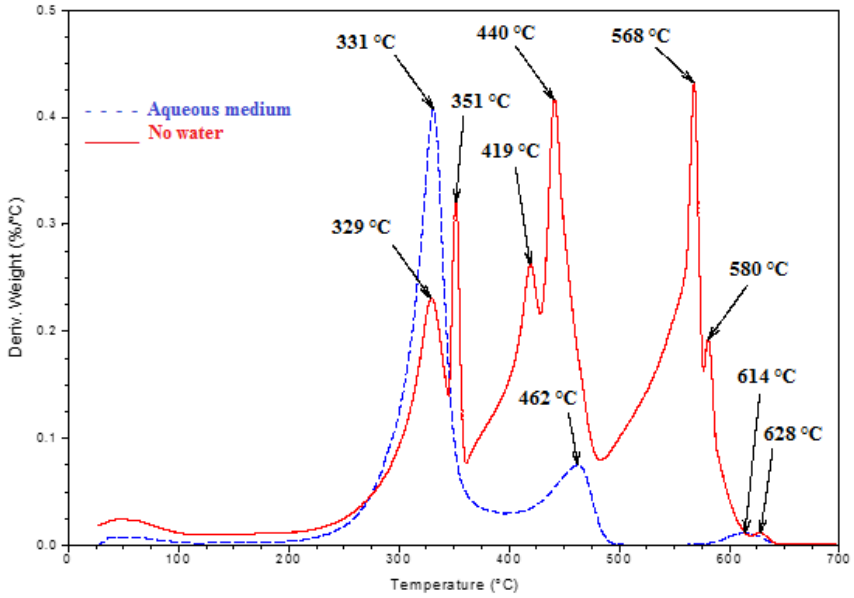

Fig. 6.II. 2: TGA of used catalyst in aqueous medium (blue dashed-line) and in absence

of water (red solid-line).

Table 6.II. 3: AQHDO of dual compounds using RRM catalyst.

	Reactant						
Parameter	Anisole/ acetaldehyde	Anisole/ Acetone	Anisole/ 2-butanone	Anisole/ 3-pentanone	Acetic acid/ Propionic acid	Anisole/ 3-heptanone	Anisole/ 2,6-dimethyl-4-heptanone
Conversion (%)	100	100	100	100	100	100	100
H_2 consumption (mol H_2)	0.16	0.16	0.15	0.36	0.00	0.34	0.27
Product distribution (wt. %) (H_2O- free basis)							
	Ethylbenzene (76.8) Methanol (23.2)	Isopropylbenzene (78.9) Methanol (21.1)	Sec-butylbenzene (80.7) Methanol (19.3)	3-ethyl-non-6-ene (82.3) Methanol (17.7)	Acetone (37.7) 3-pentanone (21.9) 2-butanone (40.4)	7-ethyl-undec-3-ene (85.2) Methanol (14.8)	2-methyl-4(2-methylpropane)-dec-7-ene (86.8) Methanol (13.2)
Elemental composition (wt. %)							
C	90.49 ± 0.03	90.02 ± 0.04	89.53 ± 0.04	85.73 ± 0.02	-	85.72 ± 0.05	85.71 ± 0.03
H	9.51 ± 0.02	9.98 ± 0.03	10.47 ± 0.06	14.27 ± 0.05	-	14.28 ± 0.02	14.29 ± 0.03
^{13}C NMR chemical shifts (ppm)							
	15.78, 29.12, 126.68, 127.45, 128.06, 144.21	24.02, 34.18, 125.79, 126.42, 128.34, 148.83	12.31, 21.91, 31.33, 41.81, 125.85, 127.11, 128.25, 147.69	11.37, 14.73, 20.45, 22.72, 29.28, 32.57, 39.41, 134.45, 144.11	7.29, 7.34, 28.84, 30.12, 34.89, 36.25, 205.75, 208.51, 211.19	14.61, 20.48, 22.12, 22.79, 23.51, 24.63, 28.69, 29.27, 31.81, 37.36, 39.14, 135.46, 146.21	14.17, 21.38, 22.17, 22.98, 23.74, 24.19, 24.98, 26.83, 30.13, 38.45, 46.35, 51.94, 53.17, 137.28, 150.84

Table 6.II. 4: AQHDO of anisole dual compounds using Ni/RM catalyst.

Parameter	Reactant				
	Anisole/ Acetone	Anisole/ 2,3-butanedione	Anisole/ 3-pentanone	Anisole/ 3-heptanone	Anisole/ 2,6-dimethyl-4-heptanone
Conversion (%)	100	100	100	100	100
H_2 consumption (mol H_2)	1.12	1.29	1.84	1.88	1.59
Product distribution (wt. %) (H_2O- free basis)					
	Methanol (7.5)	Methanol (10.1)	Methanol (8.8)	Methanol (5.7)	Methanol (4.3)
	Benzene (9.4)	Benzene (8.2)	Benzene (7.5)	Benzene (7.1)	Benzene (6.6)
	Cyclohexane (8.3)	Cyclohexane (11.7)	Cyclohexane (10.2)	Cyclohexane (9.8)	Cyclohexane (9.4)
	Isopropylbenzene (22.7)	Sec-butylbenzene (31.5)	3-ethyl-non-6-ene (23.6)	7-ethyl-undec-3-ene (25.0)	2-methyl-4(2-methylpropane)-dec-7-ene (20.8)
	Isopropylcyclohexane (34.3)	3-methylnonane (38.5)	3-ethylnonane (49.9)	5-ethylundecane (52.4)	2-methyl-4(2-methylpropane)-decane (58.9)
	2-methyloctane (17.8)				
Gas analysis (mol %) (H_2- free basis)					
CO_2	12.8	10.8	9.9	9.5	8.4
CH_4	48.7	42.5	41.3	46.0	56.7
C_2H_6	-	-	-	2.1	3.4
C_3H_8	35.6	12.4	11.8	27.3	22.5
C_4H_{10}	1.7	33.1	3.7	8.1	4.5
C_5H_{12}	0.6	1.4	32.6	6.7	3.9

4.3.2 Aqueous phase HDO acetone/guaiacol on Ni/RM and RRM

Acetone is one of the soluble oxygenates found in the biomass pyrolysis aqueous phase products, and it is an intermediate product in the AQHDO of acetic acid. The reactions of acetone with guaiacol were investigated under similar AQHDO conditions as those described above to corroborate the proposed pathways for the acetic acid reactions with guaiacol. This reaction produced less complex product mixture than the acetic acid/guaiacol AQDHO and comprised of aliphatic, aromatic, and alkylated aromatics. The major products detected were: 2-methyloctane, isopropylbenzene, isopropylcyclohexane, benzene, cyclohexane, hexane, methanol, phenol, and catechol (Table 6.II.2). When the same AQHDO was conducted on the RRM using

guaiacol/acetone there was no reaction. However, when anisole, a reduction intermediate of guaiacol was investigated with acetone, it produced water, methanol, and isopropylbenzene and no other products (Table 6.II.3). The conversion was 100% and the yields of products were stoichiometric. It was hypothesized that the most important reaction was the "***carbonyl alkylation***" of anisole to form isopropylbenzene on the RRM, which then underwent further reactions on the nickel to form other hydrocarbons. The concept of ***carbonyl alkylation*** is new and involves alkylation of aromatic ring using carbonyl compound instead alkylhalides as obtains in Friedel-Crafts alkylation. The isopropylbenzene was identified using methods described above. The reaction pathways for this process were similar to those described for acetic acid/guaiacol in equations (7)-(14), since in that process acetone was produced, which underwent similar reactions producing the same compounds.

It is noteworthy that the benzene ring was alkylated but neither saturated nor opened on the RRM. The proposed pathways for the observed reactions was probably the initial HDO of the guaiacol to anisole on the nickel surface which then reacted with acetone on the RRM to form isopropylbenzene. Once the isopropylbenzene was produced, it underwent ring saturation and ring opening reactions on the nickel sites producing isopropylcyclohexane and 2-methyloctane respectively (Table 6.II.2), which reduced the yield of the isopropylbenzene in the mixture compared to when it was run on the RRM without any nickel present. The parallel guaiacol reduction reactions also produced benzene, cyclohexane, and hexane.

When anisole/acetone AQHDO was conducted on Ni/RM, there was less number of compounds produced compared to the acetone/guaiacol reaction (Table 6.II.4).

Compounds such as phenol, catechol, and hexane were not detected in the products, which showed that these compounds derived from the parallel reaction of guaiacol that produces catechol, phenol, benzene and hexane.

4.3.3. Aqueous phase HDO of 2,3-butanedione/guaiacol and 2-butanone/ guaiacol on Ni/RM and RRM

Butanone and 2,3-butanedione are compounds found in the catalytic pyrolysis products of lignocellulosic biomass and so they were investigated to ascertain if they produced any hydrocarbons with guaiacol. The AQHDO was performed as described for acetic acid/guaiacol combination. Since the acetic acid/guaiacol and acetone/guaiacol tests showed that the carbonyl alkylation (CA) reaction occurred on the RRM and the active reactants were anisole and not guaiacol, an initial test was conducted to show if this observation was also applicable to 2-butanone and 2,3-butanedione. In both cases, 2-butanone/guaiacol and 2,3-butanedione/guaiacol did not react on RRM. However, 2-butanone/anisole reacted and 2,3-butanedione/anisole did not react. The 2-butanone/anisole produced sec-butylbenzene ($C_{10}H_{14}$), methanol, and water but no other organic compounds (Table 6.II.3); which also confirmed that the carbonyl alkylation reaction always occurred on the RRM. The sec-butylbenzene identity was confirmed by comparing its ^{13}C NMR with published ^{13}C NMR of sec-butylbenzene.[48] The ^{13}C NMR chemical shifts of the synthesized sec-butylbenzene are shown in Table 6.II.3. The AQHDO of 2,3-butanedione/anisole on Ni/RM produced four organic liquid products: sec-butylbenzene ($C_{10}H_{14}$), 3-methylnonane ($C_{10}H_{14}$), benzene, cyclohexane, and methanol (Table 6.II.4). The methanol was obviously produced from the demethoxylation

of anisole while sec-butylbenzene was the carbonyl alkylation product of butanone and anisole on RRM. It is therefore clear that 2,3-butanedione was first reduced to butanone before it reacted with the anisole and the reduction was obviously on the elemental Ni as discussed in section 3.2. The 3-methylnonane ($C_{10}H_{22}$) was produced from the saturation and ring opening of sec-butylbenzene. Cyclohexane was produced from the saturation of the benzene ring and the benzene was produced from the hydrodeoxygenation of anisole. The ring saturation and ring opening reactions were catalyzed by the elemental Ni and not RRM, because the RRM produced sec-butylbenzene and no 3-methylnonane. The proposed reaction pathways are shown below (reactions 15-17).

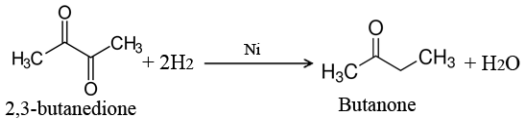

2,3-butanedione Butanone (15)

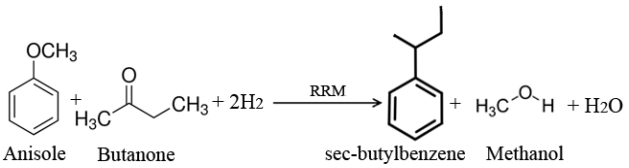

Anisole Butanone sec-butylbenzene Methanol (16)

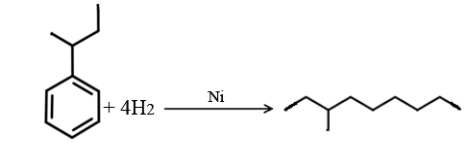

sec-butylbenzene 3-methylnonane (17)

4.3.4. Aqueous phase HDO of 3-pentanone/anisole on RRM and Ni/RM

3-pentanone is also one of the compounds found in aqueous phase catalytic pyrolysis products and because the active reactant is anisole and not guaiacol, the reactions were carried out using anisole instead of guaiacol. In the AQHDO of 3-pentanone/anisole on RRM, the products were 3-ethyl-non-6-ene ($C_{11}H_{22}$), methanol, and

water (Table 6.II.3). Neither benzene nor alkane compounds were detected in this reaction. Because of the high purity of this compound, its composition was verified with UV, GC/MS and ^{13}C NMR analyses. The ^{13}C NMR analysis data showed that there was only one double bond in the structure of the compound and this was further confirmed by GC/MS data. The formation of 3-ethyl-non-6-ene clearly suggested that there was benzene ring opening in this case, but the saturation of the double bonds were incomplete. This is unlike the acetaldehyde, acetone, and butanone reactions, which produced ethylbenzene, isopropylbenzene, and sec-butylbenzene respectively without ring opening or saturation. Ring opening is therefore not completely confined to the elemental Ni catalysis, but it is not clear what controls ring opening reaction on the RRM. It appears ring opening and double bond saturation were much weaker on the RRM than on the Ni/RM.

When AQHDO of 3-pentanone/anisole was conducted on the Ni/RM, more compounds were produced compared to RRM because of the ring opening and saturation reactions. The products consisted of 3-ethyl-non-6-ene, 3-ethylnonane, benzene, cyclohexane, and methanol (Table 6.II.4). The proposed pathways are shown below (reactions 18-21):

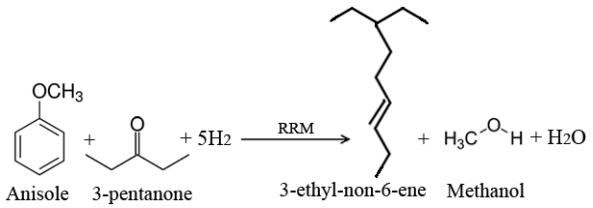

(18)

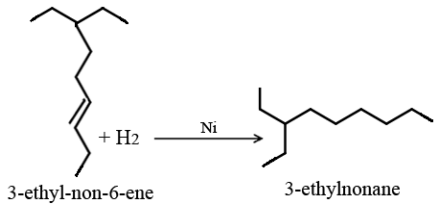

(19)

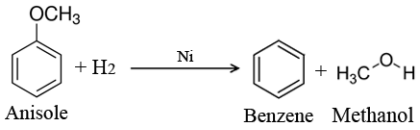

(20)

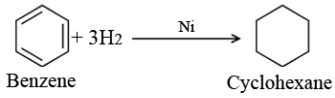

(21)

Because anisole was used instead of guaiacol, the product slate was less complicated and did not include parallel reaction products from the catechol and phenol pathways as was observed for acetic acid/guaiacol and acetone/guaiacol reactions. In addition to the above hydrocarbons, gaseous products were also produced which were mainly methane and pentane (Table 6.II.4).

4.3.5. Aqueous phase HDO of propionic acid/acetic acid on RRM

Propionic acid is also one of the small molecules found in the aqueous phase of biomass catalytic pyrolysis oils. This molecule appears to be very important because it could undergo ketonization reaction to produce pentanone and therefore produce longer chain hydrocarbons. Propionic acid/acetic acid mixture was investigated for the potential ketones production. The AQHDO of propionic acid/acetic acid on RRM produced acetone, 2-butanone, and 3-pentanone as well as CO_2 and H_2O (Table 6.II.3). The 3-pentanone was produced from the ketonization of propionic acid,[29] acetone was produced from acetic acid, [29] while the butanone was produced from cross-ketonization

of propionic acid and acetic acid. Since there were no liquid product side reactions, the identity of the products were established by comparing the ^{13}C NMR of these products (Table 6.II.3) with those of authentic standards.

The reaction pathways for the ketonization reactions are shown in the equations below (reactions 22-24):

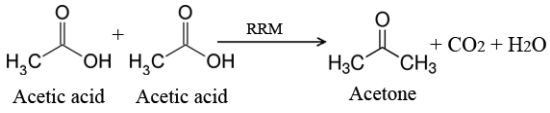

(22)

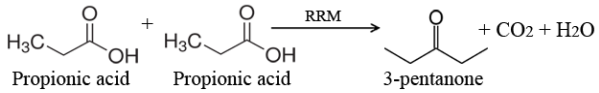

(23)

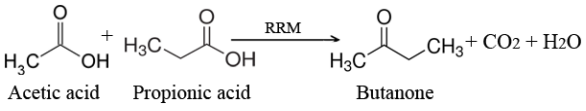

(24)

4.3.6. Aqueous phase HDO of 3-heptanone/anisole on Ni/RM and RRM

Heptanone is also one of the ketones found in the aqueous phase catalytic pyrolysis products and it was also investigated in the AQHDO process. The AQHDO of 3-heptanone/anisole on RRM produced only three compounds $C_{13}H_{26}$ (7-ethyl-undec-3-ene), methanol, and water (Table 6.II.3). Similar to the 2-penatnone reaction, no aromatic compound was produced. The alkene compound, which was immiscible with water was isolated in very high purity and high yield and characterized using ^{13}C NMR and GC/MS. The ^{13}C NMR analysis of this compound showed the presence of one double bond in this branched alkene, suggesting that there was benzene ring opening and partial hydrogenation of the double bonds. The structure was confirmed by GC/MS as shown in Table 6.II.5.

The AQHDO of 3-heptanone/anisole on Ni/RM produced more compounds comprising $C_{13}H_{26}$ (alkene), $C_{13}H_{28}$ (5-ethylundecane), benzene, cyclohexane and methanol (Table 6.II.4). The $C_{13}H_{26}$ underwent saturation reaction on the elemental Ni to produce $C_{13}H_{28}$. The methanol was produced from the hydrodeoxygenation of the methoxy group while cyclohexane derived from the saturation of the benzene ring. The proposed reaction pathways are shown below (reactions 25, 26):

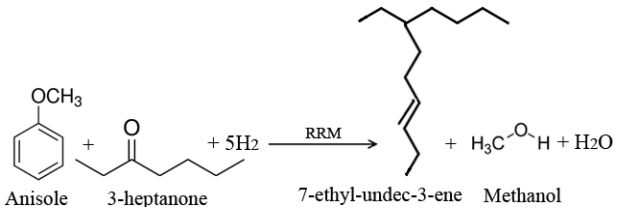

(25)

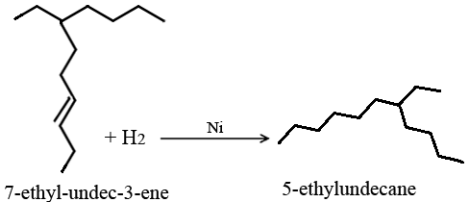

(26)

4.3.7. Aqueous phase HDO of 2,6-dimethyl-4-heptanone/anisole on Ni/RM and RRM

The 2,6-dimethy-4-heptanone (2,6D4H) was used as a model in place of 2,2-dimethyl-3-heptanone which was identified in the aqueous phase biomass catalytic pyrolysis products, because the biomass compound was not found from commercial vendors. This was the most structurally complicated ketone identified from the mixture. The AQHDO of 2,6DM4H/anisole on RRM produced $C_{15}H_{30}$ (2-methyl-4(2-methylpropane)-dec-7-ene), methanol, and water (Table 6.II.3). This compound was immiscible with water and therefore it was easily separated and characterized using ^{13}C NMR and GC/MS. The UV spectra showed the presence of a double bond in the structure

and the ^{13}C NMR and GC/MS analyses confirmed that there was one double bond in this compound (Table 6.II.5). This compound had a more complicated branching than either the C_{11} or C_{13} compounds.

The AQHDO of 2,6DM4H/anisole on Ni/RM produced saturated alkane component of the alkene (2-methyl-4(2-methylpropane)-decane) as well as benzene, cyclohexane, and methanol (Table 6.II.4). The reaction pathways are shown below:

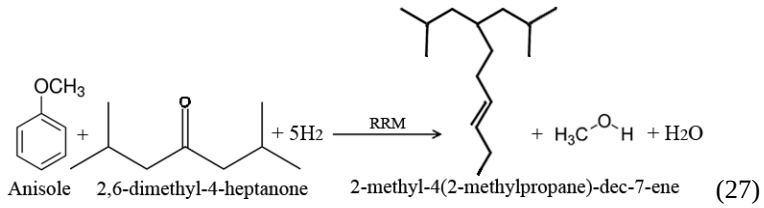

(27)

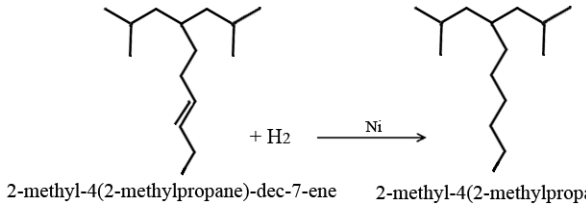

(28)

In addition to the above compounds, some gases were also produced and were mostly methane.

Table 6.II. 5: Classification of synthesized hydrocarbons.

Class	Name	Formula	MW (g/mol)	Structure
Alkylated aromatics				
	Ethylbenzene	C_8H_{10}	106.17	
	Isopropylbenzene (cumene)	C_9H_{12}	120.19	
	Sec-butylbenzene	$C_{10}H_{14}$	134.22	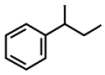
Cyclic paraffins				
	Ethylcyclohexane	C_8H_{16}	112.21	

Isopropyl cyclohexane	C_9H_{18}	126.24	
Internal olefins			
3-ethyl-non-6-ene	$C_{11}H_{22}$	154.33	
7-ethyl-undec-3-ene	$C_{13}H_{26}$	182.39	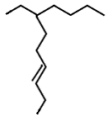
2-methyl-4(2-methylpropane)-dec-7-ene	$C_{15}H_{30}$	210.45	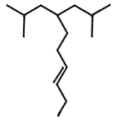
Linear paraffins			
n-octane	C_8H_{18}	114.26	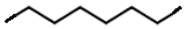
2-methyloctane	C_9H_{20}	128.29	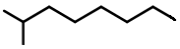
3-methylnonane	$C_{10}H_{22}$	142.32	
3-ethylnonane	$C_{11}H_{24}$	156.35	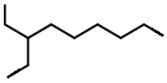
5-ethylundecane	$C_{13}H_{28}$	184.41	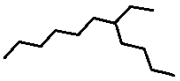
2-methyl-4(2-methylpropane)-decane	$C_{15}H_{32}$	212.47	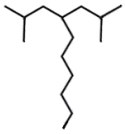

5. Discussions

The results of the AQHDO of the various compounds clearly showed that low molecular weight oxygenates can undergo "***carbonyl alkylation***" reaction in the aqueous phase to produce a wide range of long chain hydrocarbon compounds. In principle, these were catalytic reactions between unsaturated aryl alkyl ether (anisole) with aldehydes and ketones in water medium. The driving factor appeared to be a few small molecules such as acetic acid, propionic acid, 2,3-butanedione, and guaiacol whose reduction products underwent several reactions to produce hydrocarbons of various chain lengths. Because the carbonyl carbon chain alkylated the benzene ring with the elimination of water and

methanol, the carbon chain lengths were always the sum of carbons in the ketone or aldehyde and the carbons in the benzene ring, which can be represented by the formula C_{n+6}, where n is the number of carbon atoms in the carbonyl compound and 6 is the number of carbon atoms in the benzene. The methoxy carbon was eliminated as methanol during the reaction. The entire reaction was termed "***carbonyl alkylation***".

Carboxylic acids did not react directly with guaiacol to produce hydrocarbons, instead, it was their reduction and ketonization products that were the effective reactants. The acids were converted into aldehydes and ketones, which then participated in the reaction to produce the hydrocarbons. The aldehydes were produced from the Ni catalyzed reduction of the acids while the ketones were produced from the RRM catalyzed ketonization of the acids. The Ni/RM therefore generated the two intermediate reactants from each acid for the hydrocarbon production.

Other substituted compounds such as 2-hydroxyacetone, 2,3-butanedione, 2-hydroxybutanone were all inactive until they were activated by converting them into unsubstituted ketones by Ni/RM catalysis before they reacted with anisole.

The guaiacol itself did not react directly with the acids, ketones, or aldehydes, but instead it was the reduction product of guaiacol, anisole, that reacted to produce the hydrocarbons. The hydrodeoxygenation of guaiacol on Ni/RM proceeded through three parallel pathways: anisole, catechol, and phenol pathways.[31] The catechol and phenol as well as their pathway intermediates such as, benzene, cyclohexane, and hexane were not reactants in the carbonyl alkylation reactions. Anisole could also be hydrodeoxygenated to produce phenol, benzene and toluene, but it appeared these reactions were slower than

the carbonyl alkylation reactions on the RRM and therefore hydrocarbon production was predominant.

The reactions of anisole with ketones and aldehydes catalyzed by RRM can be classified into two groups: short chain C_1 to C_4 reactions and long chain C_5 to C_9 reactions. The C_1 to C_4 ketones and aldehydes produced alkylated benzenes when they reacted with anisole on RRM. It was hypothesized that this was a carbonyl alkylation reaction catalyzed by RRM. The carbonyl oxygen double bond was the point of attack and the carbonyl carbon was attached to the benzene ring to form alkylated benzene. This was evidenced by the fact that the aldehydes always formed linear alkylbenzenes while the ketones always formed branched alkylbenzenes. There were no benzene ring opening and ring saturation byproducts in these reactions on RRM. Thus, formaldehyde formed methylbenzene (toluene), acetaldehyde formed ethylbenzene, while acetone and butanone formed isopropylbenzene and sec-butylbenzene respectively. The byproducts of these reactions were water and methanol, which made the separation easy because of the immiscibility between the hydrocarbons and the aqueous phase.

Although the reactions of the C_5 to C_9 ketones with anisole were also carbonyl alkylation, they were quite different from the C_1 to C_4 reactions because there were ring openings on RRM to form branched alkenes. The products of these reactions were long chain branched alkene compounds with one internal double bond in the structure. Although benzene has three double bonds, two of them appeared to be hydrogenated and only the third double bond remained intact. Thus, 2-pentanone reacted with anisole to produce 7-methyldecene, 3-pentanone reacted to form 7-ethylnonene, while 2,6-

dimethyl-4-heptanone reacted to form 2-methyl-4(2-methylpropane)-dec-7-ene (see structures in Table 6.II.5). The byproducts were water and methanol.

The RRM appeared to play a very important role in these reactions of the Ni/RM. When the RRM support was replaced with silica-alumina, none of these liquid hydrocarbon reactions were observed and the major products were gases (data not reported). Furthermore, Sankaranarayanan et al[30, 49] reported HDO of guaiacol and anisole on supported nickel catalysts, but did not detect any of the long chain hydrocarbons that was detected in these studies. Bayon et al[29] studied ketonization of carboxylic acid and selectively produced C_3 to C_6 olefins on $Zn_xZr_yO_z$ catalysts, but did not report production of long chain internal olefins. The RRM therefore served as the site for carbonyl alkylation of the reaction intermediates from the nickel reduction. In the case of acetic and propionic acids, the RRM also catalyzed the ketonization reaction with the loss of H_2O and CO_2 and therefore two different hydrocarbon molecules were produced from the aldehyde and ketone intermediates.

The reactions of C_1-C_4 aldehydes or ketones with anisole, which resulted in the alkylation of the benzene ring is a unique class of reactions unlike the traditional Friedel-Crafts aromatic alkylation reactions.[50-53] Furthermore, the opening of the benzene ring when it was alkylated with C_5-C_9 carbonyls suggested that these were new classes of chemical reactions that need further studies. The exact mechanism of these reactions are still under investigation.

The aqueous medium was also very important for these reactions. In the absence of water, there was rapid coking and deactivation of the catalyst especially when the medium was acidic. The neat HDO coke properties were different from those produced

under the aqueous conditions. This observation is similar to the effect of steam on FCC reactions in the hydrocracking processes in the petroleum industry.[54-56]

In addition to the Ni initiating the hydrocarbon formation reactions by catalyzing the production of the reaction intermediates, it also hydrogenated double bonds in the benzene ring for both benzene and alkylated benzene compounds. The Ni also catalyzed the saturation of the double bonds in the alkene compounds. Furthermore, the Ni catalyzed the benzene ring opening to produce hexane and other straight chain hydrocarbons. Thus, a large number of hydrocarbons compounds were produced, which were mixtures of linear and branched chain alkanes, branched alkenes, aromatics, alkylated aromatics, and cycloalkanes.

6. Conclusion

It has been demonstrated that through unique catalyst activity, low molecular weight water-soluble oxygenates found in biomass pyrolysis products can be hydrotreated to form long chain aliphatic and alkylated aromatic hydrocarbons. Aliphatic hydrocarbon groups as long as 15 carbon chains can be produced from these carbonyl alkylation reactions in a one-pot synthesis. This method can also be used to synthesize very pure hydrocarbon compounds with almost 100% conversion, high selectivity, and excellent yields. For example, ethylbenzene and isopropylbenzene, which are feedstocks for polystyrene and phenol respectively, can be synthesized from anisole, acetaldehyde, and acetone and the only co-products are methanol and water, which dissolve in the aqueous phase. These reactions occur in water, which reduces coke formation on the catalyst. These syntheses provide elegant and efficient methods of producing hydrocarbon fuels and chemical feedstocks from renewable biomass resources. This

method appears to be the method used in nature to produce hydrocarbons from biomass resources over geologic times.

7. References

[1] Y. Zhang, P. Bi, J. Wang, P. Jiang, X. Wu, H. Xue, J. Liu, X. Zhou, Q. Li, *Appl. Energy* **2015**, *150*, 128–137.

[2] M. Patel, A. Kumar, *Renew. Sustain. Energy Rev.* **2016**, *58*, 1293–1307.

[3] W. Nabgan, T. A. Tuan Abdullah, R. Mat, B. Nabgan, Y. Gambo, M. Ibrahim, A. Ahmad, A. A. Jalil, S. Triwahyono, I. Saeh, *Renew. Sustain. Energy Rev.* **2017**, *79*, 347–357.

[4] S. Kang, J. Fu, Y. Ye, W. Liao, Y. Xiao, P. Yang, G. Liu, *Fuel* **2018**, *216*, 747–751.

[5] F. A. Agblevor, D. C. Elliott, D. M. Santosa, M. V Olarte, S. D. Burton, M. Swita, S. H. Beis, K. Christian, B. Sargent, **2016**, 30, 7947-7058.

[6] F. A. Agblevor, O. Mante, R. Mcclung, S. T. Oyama, *Biomass and Bioenergy* **2012**, *45*, 130–137.

[7] A. Sanna, T. P. Vispute, G. W. Huber, *Appl. Catal. B Environ.* **2015**, *165*, 446–456.

[8] L. Ciddor, J. A. Bennett, J. A. Hunns, K. Wilson, A. F. Lee, *J. Chem. Technol. Biotechnol.* **2015**, *90*, 780–795.

[9] Y. Liu, Z. Li, J. J. Leahy, W. Kwapinski, *Energy and Fuels* **2015**, *29*, 3691–3698.

[10] D. C. Elliott, T. R. Hart, G. G. Neuenschwander, L. J. Rotness, M. V. Olarte, A. H. Zacher, Y. Solantausta, *Energy and Fuels* **2012**, *26*, 3891–3896.

[11] H. Wang, S. J. Lee, M. V. Olarte, A. H. Zacher, *ACS Sustain. Chem. Eng.* **2016**, *4*, 5533–5545.

[12] M. V. Olarte, A. H. Zacher, A. B. Padmaperuma, S. D. Burton, H. M. Job, T. L. Lemmon, M. S. Swita, L. J. Rotness, G. N. Neuenschwander, J. G. Frye, et al., *Top. Catal.* **2016**, *59*, 55–64.

[13] F. A. Agblevor, S. Beis, O. Mante, N. Abdoulmoumine, *Ind. Eng. Chem. Res.* **2010**, *49*, 3533–3538.

[14] D. A. Ruddy, J. A. Schaidle, J. R. Ferrell, J. wang, L. Moens, J. E. Hensley, *Green Chem.* 2014, *16*, 454-490.

[15] S. Wan, Y. Wang, *Front. Chem. Sci. Eng.* **2014**, *8*, 280–294.

[16] K. Iisa, R. J. French, K. A. Orton, M. M. Yung, D. K. Johnson, J. ten Dam, M. J. Watson, M. R. Nimlos, *Energy & Fuels* **2016**, *30*, 2144–2157.

[17] O. D. Mante, F. A. Agblevor, *Green Chem.* **2014**, *16*, 3364-3377.

[18] B. Ma, F. A. Agblevor, *Biomass and Bioenergy* **2014**, *64*, 337–347.

[19] B. K. Yathavan, F. A. Agblevor, *Energy and Fuels* **2013**, *27*, 6858–6865.

[20] F. Abnisa, W. M. A. Wan Daud, A. Arami-Niya, B. S. Ali, J. N. Sahu, *Energy & Fuels* **2014**, *28*, 3074–3085.

[21] G. Li, N. Li, J. Yang, A. Wang, X. Wang, Y. Cong, T. Zhang, *Bioresour. Technol.* **2013**, *134*, 66–72.

[22] G. W. Huber, J. N. Chheda, C. J. Barrett, J. A. Dumesic, *Sci.* **2005**, *308*, 1446-1450.

[23] H. Bergrem, R. Xu, R. C. Brown, G. W. Huber, *Green Chem.* **2017**, *19*, 3252-3262.

[24] Y. Xu, S. Qiu, J. Long, C. Wang, J. Chang, J. Tan, Q. Liu, L. Ma, T. Wang, Q. Zhang, *RSC Adv.* **2015**, *5*, 91190–91195.

[25] S. M. Ulfa, A. Mahfud, S. Nabilah, M. F. Rahman, *Mater. Sci. Eng.* **2017**, *172*, 012053.

[26] M. Hronec, K. Fulajtárová, T. Liptaj, T. Soták, N. Prónayová, *ChemistrySelect* **2016**, *1*, 331–336.

[27] N. Li, G. A. Tompsett, T. Zhang, J. Shi, C. E. Wyman, G. W. Huber, *Green Chem.* **2011**, *13*, 91–101.

[28] L. Faba, E. Díaz, S. Ordóñez, *Appl. Catal. B Environ.* **2012**, *113–114*, 201–211.

[29] R. A. L. Baylon, J. Sun, K. J. Martin, P. Venkitasubramanian, Y. Wang, *Chem. Commun.* **2016**, *52*, 4975–4978.

[30] T. M. Sankaranarayanan, M. Kreider, A. Berenguer, S. Gutiérrez-Rubio, I. Moreno, P. Pizarro, J. M. Coronado, D. P. Serrano, *Fuel* **2018**, *214*, 187–195.

[31] H. Jahromi, F. A. Agblevor, *Appl. Catal. A Gen.* **2018**, *558*, 109–121.

[32] H. Jahromi, F. A. Agblevor, *Applied Catal. B, Environ.* **2018**, *236*, 1–12.

[33] R. Guil-Lopez, R. M. Navarro, J. L. G. Fierro, *Chem. Eng. J.* **2014**, *256*, 458–467.

[34] H. Wang, L. Yang, X. Sui, H. E. Karahan, X. Wang, Y. Chen, *Carbon N. Y.* **2018**, *129*, 128–136.

[35] D. Y. Kalai, K. Stangeland, Y. Jin, Z. Yu, *J. CO2 Util.* **2018**, *25*, 346–355.

[36] H. Jahromi, F. A. Agblevor, *Energy* **2017**, *141*, 2186–2195.

[37] A. B. Dongil, L. Pastor-Pérez, A. Sepúlveda-Escribano, R. García, N. Escalona, *Fuel* **2016**, *172*, 65–69.

[38] E. A. Roldugina, E. R. Naranov, A. L. Maximov, E. A. Karakhanov, *Appl. Catal. A Gen.* **2018**, *553*, 24–35.

[39] H. Fang, J. Zheng, X. Luo, J. Du, A. Roldan, S. Leoni, Y. Yuan, *Appl. Catal. A Gen.* **2017**, *529*, 20–31.

[40] I. D. Mora-Vergara, L. Hernández Moscoso, E. M. Gaigneaux, S. A. Giraldo, V. G. Baldovino-Medrano, *Catal. Today* **2018**, *302*, 125–135.

[41] Z. Si, X. Zhang, C. Wang, L. Ma, R. Dong, *Catalysts* **2017**, *7*, 169.

[42] C. Boscagli, K. Raffelt, J. D. Grunwaldt, *Biomass and Bioenergy* **2017**, *106*, 63–73.

[43] N. Joshi, A. Lawal, *Chem. Eng. Sci.* **2012**, *84*, 761–771.

[44] Z. He, X. Wang, *J. Energy Chem.* **2013**, *22*, 883–894.

[45] N. T. T. Tran, Y. Uemura, S. Chowdhury, A. Ramli, *Appl. Catal. A Gen.* **2016**, *512*, 93–100.

[46] Q. Lai, C. Zhang, J. H. Holles, *Appl. Catal. A Gen.* **2016**, *528*, 1–13.

[47] Y. K. Hong, D. W. Lee, H. J. Eom, K. Y. Lee, *J. Mol. Catal. A Chem.* **2014**, *392*, 241–246.

[48] https://www.chemicalbook.com/SpectrumEN_135-98-8_13CNMR.htm

[49] T. M. Sankaranarayanan, A. Berenguer, C. Ochoa-hernández, I. Moreno, P. Jana, J. M. Coronado, D. P. Serrano, P. Pizarro, *Catal. Today* **2015**, *243*, 163–172.

[50] W. Li, L. Guo, W. Li, *Mol. Catal.* **2017**, *433*, 122–127.

[51] T. P. Maloney, K. L. Murphy, T. L. Mainsah, K. A. Nolin, *Tetrahedron Lett.* **2018**, *59*, 18–21.

[52] P. Cui, X. F. Jing, Y. Yuan, G. S. Zhu, *Chinese Chem. Lett.* **2016**, *27*, 1479–1484.

[53] M. L. Li, D. F. Chen, S. W. Luo, X. Wu, *Tetrahedron Asymmetry* **2015**, *26*, 219–224.

[54] A. Haas, D. A. Harding, J. R. D. Nee, *Microporous Mesoporous Mater.* **1999**, *28*, 325–333.

[55] H. S. Cerqueira, G. Caeiro, L. Costa, F. Ramôa Ribeiro, *J. Mol. Catal. A Chem.* **2008**, *292*, 1–13.

[56] H. Kondoh, K. Tanaka, Y. Nakasaka, T. Tago, T. Masuda, *Fuel* **2016**, *167*, 288–294.

CHAPTER 7

7. HYDRODEOXYGENATION OF AQUEOUS PHASE CATALYTIC PYROLYSIS OIL TO LIQUID HYDROCARBONS USING MULTI-FUNCTIONAL NICKEL CATALYST

1. Abstract

The liquid product of fast pyrolysis of biomass consists of organic and aqueous phases. The aqueous phase contains about 15% soluble organics and can increase the cost of wastewater treatment. In this study we investigated the hydrodeoxygenation (HDO) of aqueous phase pinyon-juniper catalytic pyrolysis oil (APPJCPO) using a new multifunctional red mud-supported nickel (Ni/RM) catalyst at different reaction temperatures and Ni loadings. Increasing the nickel content improved the activity of Ni/RM catalysts for HDO reactions but it also increased gasification. The organic liquid yield after HDO of APPJCPO using 30 wt. % Ni/RM at reaction temperature of 350 °C was 47.8 wt. % with oxygen content of 1.14 wt. %. The organic liquid fraction consisted of aliphatics, aromatics, and alkylated aromatic hydrocarbons as well as small amounts of oxygenates. The RM support catalyzed ketonization of carboxylic acids. The Ni metal catalyzed partial reduction of low molecular weight oxygenates that underwent carbonyl alkylation with aldehydes and ketones on the support material (RM). The assessment of catalyst deactivation suggested that oxidation and coke formation were main controlling factors for deactivation of Ni and RM support respectively. For comparison, commercial (~65 wt. %) Ni/SiO_2-Al_2O_3 was tested in HDO experiments. The commercial catalyst gasified the soluble organics in APPJCPO and did not produce liquid hydrocarbons.

2. Introduction

Lignocellulosic biomass is the most abundant renewable source of organic carbon on earth and the only one of low enough cost and adequate availability for large scale sustainable production of liquid fuels. Lignocellulosic biomass can be thermochemically converted into transportation fuels through three intermediate major pathways: gasification for syngas, pyrolysis or liquefaction for bio-oils, and hydrolysis of biomass to produce sugar monomer units.[1] Pyrolysis is a thermal decomposition of organic compounds in the absence of oxidizing agents. This process produces char, gas, and liquid products. The liquid product (bio-oil) can be upgraded to transportation fuel through various processes including catalytic cracking, hydrodeoxygenation (HDO), emulsification, esterification with supercritical ethanol, and steam reforming followed by Fischer Tropsch synthesis.[2] The aqueous fraction of pyrolysis oil contains about 10~30% soluble organics such as aldehydes, ketones, acids, and phenolics.[3, 4] The water-soluble organics can potentially cause corrosion of processing equipment, require wastewater treatment, and a potential source of carbon loss for the biomass conversion processes.

Low-temperature hydrogenation of the water-soluble portion of bio-oil, and reforming (to H_2) or dehydration/hydrogenation (to C_1−C_6 alkanes) are some of the methods used in processing aqueous fraction of bio-oils.[5] The hydrogenation process improves its thermal stability for further upgrading processes. Vispute and Huber showed that 15% of the carbon is lost in the solid and gas products during hydrogenation of bio-oil at 125 °C and that levoglucosan, sugars and aromatic rings were not fully converted to the corresponding alcohols at 125 °C.[6] Further, Li et al. converted an aqueous carbohydrate stream from maple wood into gasoline range products with carbon yield of

57% in a 2-step aqueous phase processing over Ru/C catalyst (1st step) and Pt/ZrP catalyst (2nd step).[7] These studies showed that the challenge with hydrogenation of water-soluble fraction of bio-oil is to minimize the H_2 consumption and carbon loss, while achieving high selectivity of the desired products. The current bio-oil HDO state of the art indicates that there is a wide range of products formed and that the associated catalytic chemistry needs to be understood in more detail.[6-8]

The structure of three major polymeric components, cellulose, hemicellulose, and lignin, are well-represented by the bio-oil components in the case of lignocellulosic biomass-derived pyrolysis oil. HDO is usually the preferred method among upgrading processes since it can produce high quality fuels. HDO can improve pyrolysis oil quality through improving oil stability and higher energy density.[9] HDO of the bio-oil involves four major classes of reactions (1) hydrogenation of C–O, C=O, and C=C bonds, (2) dehydration of C–OH groups, (3) C–C bond cleavage by retro-aldol condensation and decarbonylation, and (4) hydrogenolysis of C–O–C bonds.[1, 10, 11] In most HDO studies, guaiacol (representing the large number of mono- and dimethoxy phenols),[12-14] furfural (representing a major pyrolysis product group from cellulosics),[15-19] and acetic acid (representing a major product from hemicellulose)[20-22] have been studied as model compounds of bio-oil.[23, 24] These studies indicated that catalyst deactivation is a major challenge during HDO of bio-oil. One of the catalyst deactivation mechanisms that occur during HDO of bio-oil is carbon deposition on the catalyst surface. This deactivation represents a major limit of this technology because the catalyst has to be frequently regenerated. One approach that has been reported is to try and develop HDO catalysts

that have low acidity and hence a lower rate of coke formation.[1, 10] The synthesis of an efficient catalyst can play a crucial role in HDO process.[25]

Red mud (RM), or bauxite residue, a reddish-brown strongly alkaline solid waste, is the by-product of alumina production using the Bayer process. RM contains a diverse mixture of metal oxides, including Fe, Al, Ti, Na, Ca, and Si, as well as some trace elements, including Ga, Cr, Mn, Ni, S, Zr, K, and Co, but the actual composition depends on the process origin.[26-31] Although red mud has been investigated as a catalyst,[32-35] environmental remediation,[36] ceramics, building materials,[37] fillers, sorbents and coagulants,[38] and valuable metals recovery;[39] it is still disposed in clay-lined dams or dykes and allowed to dry naturally.

In this work, we synthesized Ni catalysts supported on RM (Ni/RM) and compared their performance with that of commercial Ni/SiO_2-Al_2O_3 in HDO of aqueous phase pinyon-juniper catalytic pyrolysis oil (APPJCPO) to produce hydrocarbons.

3. Material and methods

3.1. Material

Pinyon-juniper (PJ) biomass chips were provided by the U.S. Bureau of Land Management. Red mud (RM) was used as catalyst for fast pyrolysis of biomass. The wet red mud was dried at room temperature, reformulated and then ground and sieved to a particle size of 125−180 μm. The ground particles were calcined at 550 °C in a muffle furnace (Thermo Fisher Scientific, Waltham, MA) for 5 h before being used for the pyrolysis. The detailed characterization of the red mud has been reported by Yathavan and Agblevor.[32] Nickel on silica-alumina (~65 wt % loading Ni) catalyst powder was

obtained from Sigma-Aldrich (St. Louis, MO, USA). High purity (99%) hydrogen (Airgas, Radnor, PA, USA) was used for HDO experiments.

3.2. Pyrolysis of biomass

PJ wood chips ground to pass a 2-mm mesh were used as feedstock for production of catalytic pyrolysis oil. The pyrolysis was carried out in a pilot plant bubbling fluidized bed reactor described in detail by Mante and Agblevor.[40] At feeding rate of 0.9 kg/h (2 lb/h), catalytic pyrolysis oil was produced at 400 ° C using RM catalyst. The pyrolytic products were condensed using a series of two ethylene glycol-cooled condensers and an electrostatic precipitator (ESP) operating at 30 kV. The ESP oil contained only about 3 wt. % water while the condenser liquids contain 60 wt% water. Details of the pyrolysis pilot plant can be found elsewhere.[40] Liquid products captured by condensers were collected in centrifuge test tubes and centrifuged for 30 minutes at g-force of 2147 to separate the aqueous phase from the insoluble heavy oils. The aqueous phase was used for HDO experiments in this study.

3.3. Characterization of APPJCPO

The water content of APPJCPO was determined by Karl-Fisher titration method with Hydranal® -composite 5 solution. A Metrohm 701KF Titrino and 703 titration stand setup (Brinkmann Instruments, Riverview, FL) were used for the volumetric Karl Fischer titration. The pH was measured using Mettler Toledo pH Meter and probe (Mettler−Toledo GmbH, Switzerland). The elemental composition of APPJCPO was determined using ThermoFischer Scientific Flash 2000 organic elemental analyzer

(ThermoFisher Scientific,Waltham, MA), and the oxygen content was calculated by difference according to ASTM D5291. The GC-MS analysis of the APPJCPO was conducted by Pacific Northwest National Laboratory (PNNL) (Richland, WA, USA).

3.4. Ni/RM catalyst preparation and characterization

Ni/RM catalysts were prepared at different concentrations of nickel using wet impregnation method according to our previous studies.[41, 42] At room temperature the calculated amount of $Ni(NO_3).6H_2O$ was dissolved in 100 ml deionized water and then mixed with RM (particle size<90 μm). The mixture was heated to 70 °C and continuously stirred for 5 hours to prepare the catalyst precursor. The catalyst precursor was dried at 105 °C for 10 hours and then calcined at 620 °C for 5 hours. The catalyst precursor was reduced for 6 hours at 450 °C using a reducing gas mixture of 10% H_2 and 90% N_2 at flow rate of 20 ml/min to obtain the tested catalyst, which was designated as x wt.% Ni/RM (x= 10, 20, 30, 40).

The catalysts were characterized by thermogravimetric-temperature programmed reduction (TG-TPR), Brunauer–Emmett–Teller (BET) surface area analyzer, X-ray diffraction (XRD), inductively coupling plasma (ICP) spectroscopy, and scanning electron microscopy (SEM) as reported previously.[41, 42]

3.5. Hydrodeoxygenation (HDO) experiments

HDO reactions were carried out in a Parr Series 4560 300 mL autoclave reactor (Parr Instruments, Moline, IL). The reactor can withstand a maximum pressure of 14 MPa at 500 ° C. A Parr 4848 controller was used to control the internal temperature and

impeller speed. In a typical test, 100 g APPJCPO and catalyst (3 g) were loaded into the reactor. The reactor was flushed with hydrogen four times to purge the reactor vessel. High purity hydrogen was supplied from a reservoir tank via a pressure regulator. The reactor was then pressurized with hydrogen to 6.21 MPa (900 psi) at room temperature. A gas sample was taken from the gas sampling port for gas analysis when the reactor was at room temperature. The reactor was then heated to reaction temperature of 300, 350, or 400 °C. The reaction mixture was vigorously stirred (~1000 rpm) in order to eliminate diffusion limitations. The reaction time was recorded when the set temperature was reached. After the desired reaction time (30 minute), the reactor was cooled to room temperature using the internal cooling coil and a gas sample was collected in a tedlar bag for analysis. The reproducibility of experiments was checked and the error in all experimental measurements was found to be less than 3%. Hydrogen consumption determination, product yields distribution, and gas analysis were carried out according to our previous work.34 Conversion was calculated according to equation (1):

$$Conversion\ (\%) = \frac{(100-w_i).m_i-(100-w_f).m_f}{(100-w_{i)}.m_i} \times 100 \qquad (1)$$

Where w_i is the initial water content of APPJCPO (wt. %), m_i is the amount of APPJCPO loaded into the reactor (g), w_f is the water content of the aqueous phase after HDO (wt. %) and m_f is the amount of aqueous phase after HDO (g).

In blank experiments (without catalyst) 100 g of reaction mixture was charged into the reactor and the reactor was pressurized to 6.2 MPa (900 psi) with hydrogen and

allowed to react for 30 minutes at 350 °C to determine if the reactor walls played any role in HDO reactions. All experiments were conducted in triplicate.

3.6. Analysis of HDO products

The liquid products of HDO experiments were analyzed for their elemental composition (CHNS-O), water content by Karl-Fischer titration, HHV, density, and viscosity. Details of these analysis are described elsewhere.[34]

The organic liquid products of HDO experiments (HDO oil) were analyzed by HPLC (Shimadzu Scientific, Columbia, MD, USA) using a RID-10A detector and a Kromasil 100-5-C18 column (AkzoNobel Amsterdam, Netherlands). The HPLC was equipped with a LC-10AT pump, SCL-10Avp controller, and SIL-10A autosampler. CLASS-VP 7.3 SP1 software was used to analyze HPLC chromatograms. A CTO-10A column oven was used to maintain the column temperature at 55 °C during the analysis. The injection volume was 0.25 μl and acetonitrile at flow rate of 0.6 ml/min was used as the mobile phase. Data acquisition time was 80 minutes for all analyses. The identity of the HDO oil compounds were confirmed by GC/MS (Shimadzu GC/MS-QP5000, Shimadzu Scientific, Columbia, MD, USA).

The ^{13}C NMR spectra of the HDO oils were recorded on a BRUKER 500 MHz NMR spectrometer (Bruker Corporation, Japan). For sample preparation, about 0.3 g of the oil was dissolved in 0.9 g chloroform-d (Cambridge Isotope Laboratories, Inc., Tewksbury, MA, USA) in a 5-mm sample probe. The spectra were obtained with 3500 scans.

Thermal decomposition behavior of HDO oils were assessed by thermogravimetric analysis (TGA) using a TGA Q500 (TA Instruments, Lindon, UT, USA). Fifty milligrams of HDO oil was heated in high purity nitrogen flow from room temperature to 700 °C at a heating rate of 10 °C/min and the weight loss versus temperature was monitored. Weight loss curves were acquired by plotting the weight percent conversion versus temperature.

3.7. Catalyst deactivation

Previously we showed that three mechanisms contributed to the deactivation of Ni/RM catalyst; coke formation, oxidation, and formation of nickel iron oxide (Fe2NiO4).41, 42 Herein we assessed the degree of oxidation by conducting TG-TPR of the used catalyst after HDO experiments. Details of TG-TPR analysis and coke formation evaluation is described elsewhere.41, 42 Relative degree of oxidation (RDO) was calculated according to equation (2):

$$RDO = \frac{W_u}{W_c} \times 100 \qquad (2)$$

Where W_c is the amount of weight loss (wt. %) of fresh catalyst precursor (40%Ni/RM in calcined form) during reduction determined by TG-TPR (this value shows the maximum hydrogen uptake) and W_u is the weight loss (wt. %) of used catalyst due to reduction by TG-TPR (this value indicates the hydrogen uptake of used catalyst).

4. Results and discussion

4.1. Characterization of APPJCPO

Table 7.1 shows the pH, water content, elemental composition, and chemical composition of APPJCPO. The presence of low molecular weight carboxylic acids in aqueous phase pyrolysis oil is the main reason for the acidic nature of APPJCPO (pH 2.97). The water content of APPJCPO was about 85 wt. % indicating presence of about 15% water soluble organic compounds. GC-MS analysis of APPJCPO organics were provided by Pacific Northwest National Laboratory (PNNL) (Table 7.1). The concentration of acetic acid in APPJCPO was 15.1 wt. % (water-free basis) which was the dominant compound in the APPJCPO. Other major compounds were acetone, furfural, 1-acetoxy-2-propanone, 1-hydroxy butanone, 1-hydroxy-2-propanone, guaiacol, 2,2-dimethyl-3-heptanone, 2,3-butanedione, and 3-hydroxy-2-butanone. As discussed in our previous works, RM catalyzed ketonization reactions, which could explain the dominance of ketones in the APPJCPO compared to pyrolysis using sand as the medium.[32]

Table 7. 1: Characterization of APPJCPO.

Properties	value
pH	2.97
Water content (wt. %)	84.77
Elemental composition (wet basis)	
N	0.44
C	7.33
H	11.17
O	81.06
Chemical composition* (dry basis) (wt. %)	
Acetaldehyde	0.7
Acetic acid	15.1
Acetic anhydride	0.1
Acetone	2.4
Fructose	0.1
Furfural	6.8
Phenol	0.9
Xylose	0.3
1-acetoxy-2-propanone	2.3
1-hydroxy butanone	1.3
1-hydroxy-2-propanone	2.1
1,2-benzenediol	0.9
2-cyclopentene-1-one	0.6
2-methoxy phenol (guaiacol)	4.4

2-methyl phenol	0.2
2-methyl-1,4-benzenediol	0.3
2-methyl-2-cyclopentene-1-one	0.1
2,2-dimethyl-3-heptanone	1.2
2,3-butanedione	2.2
3-hydroxy-2-butanone	1.3
3-methyl-1,2-benzenediol	0.8
4-ethyl-1,3-benzenediol	0.4
4-methyl phenol	0.5
4-methyl-1,4-benzenediol	0.4

* Quantified ~ 45% of total carbon

4.2. HDO of APPJCPO using Ni/RM

4.2.1. Effect of Ni loading

The blank experiments showed no reactivity of the reactor walls. All results reported are therefore assumed to have no reactor wall influence. The results of HDO experiments using Ni/RM catalyst at different Ni loadings are shown in Table 7.2. RM in reduced form (RRM) was tested in HDO experiment to investigate the effect of catalyst support on the reactions. As shown in Table 7.2 the conversion of APPJCPO using RRM support was only 25.1% (Ni content of 0%) and the reaction produced 15.4% coke and 9.7% gas and a small amount of hydrogen (0.26 mol) was consumed. The liquid product consisted of one phase which had a pH of 6.11 compared to the raw feed that had a pH 2.97. The increased pH of the RRM HDO oil was attributed to ketonization of the carboxylic acids in the raw feed. The HPLC analysis of the liquid product showed reduced carboxylic acids content, especially acetic acid and increased concentrations of acetone and other ketones compared to the raw feed (see Tables 7.1 and 7.2). In addition to increased pH and ketone content and decrease in carboxylic acid concentration, the major gas produced was CO_2 which emanated from ketonization reactions.[43, 44] No hydrocarbons were detected in the reaction liquid products. We previously showed that the presence of Ni is essential to partially reduce the oxygenated compounds of APPJCPO such as furfural and guaiacol to ethers. The ethers subsequently reacted with

carbonyls on the RM support to produce linear, branched, cyclic, aromatic, and alkylated aromatic hydrocarbons. In the absence of Ni, no ethers (furan, methyl furan, and anisole) were produced and hence no carbonyl alkylation reactions occurred. Ketonization, coke formation, as well as hydrocracking were the main reactions that occurred on the RRM (Table 7.2). The gaseous products were mostly CO and CO_2 (75 mole %) and the rest were C_1-C_5 hydrocarbons in very low concentrations.

When the APPJCPO was treated with 10 wt. % Ni/RM the HDO liquid product consisted of one phase similar to the feed and its pH was 6.71. No detectable quantities of hydrocarbon liquid were produced but less coke was formed and gas yield doubled compared to 0%Ni HDO (Table 7.2). The liquid products had similar compounds as those found in the 0%Ni run and the raw feed.

The dominant gas component was methane, which was attributed to methanation of CO and CO2 on the Ni sites, because the CO2 content was relatively low compared to the 0%Ni and the water content was also higher (4.8%). The methane content of the gaseous product increased from 3.4 mole% in the 0%Ni to 58.2% in the 10%Ni (Table 7.2), while ethane increased threefold, and propane increased very slightly. The increases in ethane and propane contents were attributed to hydrodeoxygenation of acetic acid, acetaldehyde, and acetone. In contrast, butane and pentane contents decreased relative to the 0%Ni HDO probably because of the cracking of these gases on the Ni sites. It can be surmised that the dominant reactions on the 10%Ni/RM were ketonization, methanation, hydrocracking and hydrodeoxygenation. In addition to ketonization reactions on the support material, gasification of some of the acetic acid could contribute to the slight increase in pH from 6.11 at 0% Ni to 6.71 at Ni loading of 10% (Table 7.2).

The reactions on the 20%, 30%, and 30% Ni loadings showed very interesting results because unlike the 0% and 10% Ni, the liquid products formed two immiscible phases comprising water and hydrocarbons and the pH ranged from 6.83 to 6.98 (Table 7.2). The liquid product (HDO oil) yields on Ni loadings of 20%, 30%, and 40% were 54.7%, 47.8%, and 23.9% respectively with oxygen contents of 3.45 wt. %, 1.14 wt. %, and 0.17 wt. % respectively. Although the 20%Ni had the highest hydrocarbon yield, it also had the highest oxygen content and furthermore, its aqueous phase contained unreacted material. In contrast, the 30% and 40% Ni HDO aqueous phase products did not contain any detectable organic compounds and their pHs were neutral. Karl Fischer titration of these aqueous fractions showed about 99.5% water.

The HPLC and GC/MS analysis of the HDO organic liquid fraction showed a wide range of hydrocarbon compounds (Table 7.2). The formation of these liquid hydrocarbon compounds was attributed to "carbonyl alkylation" and hydrogenation reactions. The carbonyl alkylation reaction was due to the reaction of carbonyl compounds with unsaturated ethers such as anisole, furan, and methyl furan catalyzed by the reduced red mud (RRM) catalyst support. The aldehydes reacted with both furan and anisole but did not react with methylfuran, while the ketones reacted with methylfuran and anisole and not with furan. These complex reactions were catalyzed by the RRM and Ni through two pathways. First, when the concentration of the Ni on the RRM was about 20% or more, some fractions of acetic acid and other acids were reduced to aldehydes, furfural was reduced to furan and methyl furan, while guaiacol was reduced to anisole by the Ni. The RRM also catalyzed ketonization of some fraction of the acids to produce various ketones. The aldehydes and ketones then reacted with furan, methyl furan, and

anisole catalyzed by the RRM to produce various hydrocarbons. The chain length of each hydrocarbon followed very simple rules: aldehydes reacting with furan form $C_{(n+4)}$ chain length where n is the number carbon atoms in the aldehyde compound; for ketones reacting with methyl furan the carbon chain length is $C_{(n+5)}$; for anisole reactions, both aldehydes and ketones follow the same rule, $C_{(n+6)}$ where n is the number of carbons in the carbonyl compounds. These carbonyl alkylation reactions produced alkylated benzenes and long chain aliphatic compounds such as ethyl benzene, isopropyl benzene, n-hexane, 2-methylheptane etc. (Table 7.2). In Table 7.2, there are another group of hydrocarbon compound such as cyclopentane, cyclohexane, benzene, ethylcylohexane etc., which derived from hydrogenation of the carbonyl alkylation compounds and direct hydrodeoxygenation of guaiacol that were attributed to catalysis by Ni. The Ni content appears to have direct influence on the formation of these compounds and their concentrations. The 20% Ni loading is at the threshold where there is enough Ni to catalyze the carbonyl alkylation, hydrodeoxygenation, and hydrogenation reactions. Above 20% Ni, the reaction was improved but there was a penalty due to hydrocracking of hydrocarbon compounds by Ni. The Ni loading on the red mud is important because it appeared that the ketonization of the carboxylic acids was very rapid and generated large amounts of CO_2, which then underwent methanation reaction on the Ni forming H_2O, CH_4 and coke. The coke rapidly fouled and deactivated the Ni and hence the partial reduction of furfural and guaiacol did not occur. Thus, when the Ni loading was 10% or less, there were not enough active sites to produce the ethers responsible for the carbonyl alkylation reactions. However, when the Ni loading was 20% or more, there was enough active sites to catalyze the ether production. When the Ni loading is was above 30%,

there were excess sites that catalyzed hydrocracking, hydrogenation, and hydrodeoxygenation reactions.

The APPJCPO conversion on Ni loadings of 30% and 40% were similar (99.5%) but there was a considerable difference in the deoxygenation of the HDO oil. The oxygen content of 30% Ni HDO oil was 1.14 wt. % compared to 0.17 wt. % for the 40% Ni HDO oil (Table 7.2). The increase in Ni loading from 30% to 40% increased the hydrocracking of the organic compounds, which subsequently resulted in increased gas yield from 41.6% to 65.85%.

The coke yields at various Ni loadings decreased with increasing Ni loadings. The support produced the highest coke (15.4%), but as the Ni loading increased this decreased from 15.4% to 1.7% at 40% Ni loading. The coke formation reactions appeared to be influenced by two factors, the Ni content of the catalysts and the water content of the reactants. The interaction of the Ni with the support appeared to lower the char formation because when the Ni content was increased there was less exposed support material for the coke formation. The lower coke formation from HDO of APPJCPO was also attributed to the presence of about 85% water in the reaction mixture (APPJCPO), because water can moderate the coke formation. Furthermore, the chemical compounds of APPJCPO probably produced less coke compared to complicated components of ESP oil.

Table 7. 2: Effect of Ni loading on the HDO of APPJCPO using Ni/RM catalyst (the reaction temperature was 350 °C).

Parameter	Ni loading (wt. %)				
	0	10	20	30	40
H_2 consumption (mol H_2)	0.26	1.16	1.35	1.63	1.87
Conversion (%)	25.1	31.8	93.3	99.5	99.5
Products yield distribution (based on initial organic content) (wt. %)					

HDO oil	0.0	0.0	54.7	47.8	23.9
Water*	0.0	4.8	6.5	7.1	7.8
Gas	9.7	18.5	27.4	41.6	65.8
Coke	15.4	8.5	4.7	2.4	1.7
Aqueous phase HDO product properties					
Water content (wt. %)	86.25	87.65	93.35	99.95	99.95
pH	6.11	6.71	6.83	6.97	6.98
HPLC analysis of aqueous phase HDO product (dry basis) (relative concentration wt. %)					
Acetaldehyde	0.6	0.2	0	0.0	0.0
Acetic acid	0.8	0.5	0.3	0.0	0.0
Acetone	14.3	12.7	3.4	0.0	0.0
Furfural	6.8	6.6	2.4	0.0	0.0
Phenol	1.1	1	0.5	0.0	0.0
1-hydroxy-2-propanone	2.6	2.2	1.3	0.0	0.0
2-cyclopentene-1-one	1.1	1.1	0.8	0.0	0.0
2-methoxy phenol (guaiacol)	4.3	4.3	1.8	0.0	0.0
2,2-dimethyl-3-heptanone	1.4	1.1	0.3	0.0	0.0
2,3-butanedione	3.5	2.5	1.1	0.0	0.0
3-hydroxy-2-butanone	1.6	1.4	0.6	0.0	0.0
Quantified % of organics	38.1	33.6	12.5	0.0	0.0
HDO oil properties					
HPLC analysis of HDO oil (relative concentration wt. %)					
Acetone	NA	NA	8.1	3.2	0.0
Benzene	NA	NA	7.4	2.2	1.8
Butanone	NA	NA	6.4	0.4	0.0
Cyclohexane	NA	NA	1.5	2.4	3.9
Cyclopentane	NA	NA	0.0	1.9	2.2
Ethylbenzene	NA	NA	7.2	17.8	2.7
Ethylcyclohexane	NA	NA	2.5	5.3	15.5
Isopropylbenzene	NA	NA	6.8	12.7	2.9
Isopropyl cyclohexane	NA	NA	2.3	4.7	13.8
Methanol	NA	NA	1.4	3.6	1.2
n-hexane	NA	NA	0.6	3.9	5.5
n-heptane	NA	NA	0.2	1.1	2.7
n-octane	NA	NA	0.3	0.9	2.9
Sec-butylbenzene	NA	NA	0.0	10.3	2.1
Toluene	NA	NA	1.4	3.8	5.1
Tetrahydrofuran	NA	NA	4.8	1.3	0.0
Xylene	NA	NA	1.3	4.1	1.9
2-methyloctane	NA	NA	3.2	4.5	6.2
2-methyltetrahydrofuran	NA	NA	3.5	0.8	0.0
2-pentanone	NA	NA	10.7	1.1	0.0
3-methylnonane	NA	NA	5.3	7.6	12.8
Quantified % of organics	NA	NA	74.9	93.6	83.2
Elemental composition of HDO oil (wt. %)					
N	NA**	NA	0.32	0.26	0.23
C	NA	NA	80.86	81.98	82.22
H	NA	NA	15.37	16.62	17.38
O	NA	NA	3.45	1.14	0.17
HHV (MJ/kg)	NA	NA	40.15	42.12	45.62
Density (g/ml)	NA	NA	0.89	0.82	0.77
Dynamic viscosity (cP)	NA	NA	2.54	1.46	1.22
Gas composition (mol %)					
CO	8.5	5.5	4.2	3.6	2.5
CO_2	66.6	12.1	10.3	8.4	6.3
CH_4	3.4	58.2	63.8	65.4	71.3
C_2H_6	2.2	6.3	6.9	7.1	7.3
C_3H_8	7.4	8.3	7.6	6.8	6.6
C_4H_{10}	6.1	5.4	4.3	4.2	4.1
C_5H_{12}	4.2	2.3	2.8	2.6	1.6

* By difference

** Not Applicable (no HDO oil produced)

4.2.2. Effect of reaction temperature

The 30%Ni/RM catalyst was used to investigate the effect of reaction temperature on the HDO products because this catalyst produced about 48% HDO oil with relatively low oxygen content compared to 20%Ni/RM and caused significantly less gasification

than 40%Ni/RM (Table 7.2). The physicochemical properties of HDO oils, product yields distribution, and gas analysis results after HDO of APPJCPO at reaction temperatures of 300, 350, and 400 °C are shown in Table 7.3. Increasing the reaction temperature improved HDO reactions but it also increased hydrocracking. The organic liquid yield after HDO at reaction temperatures of 300, 350, and 400 °C were 51.4 %, 47.8%, and 38.7% respectively with oxygen contents of 5.35 wt. %, 1.14 wt. % and 0.11 wt. % respectively. Increasing the reaction temperature negatively affected coke formation. The coke yield increased from 1.9% at 300 °C to 4.3% at 400 °C (Table 7.3).

When the HDO reaction temperature was increased from 300 °C to 400 °C the HHV of HDO oils increased from 38.77 MJ/kg to 45.71 MJ/kg because of improved hydrodeoxygenation and formation of more hydrocarbons through the carbonyl alkylation reactions. The major gas product was methane for all reaction temperatures because of methanation of CO and CO_2. The gas analysis showed that C_3 to C_5 hydrocarbon gases possibly underwent further hydrocracking at higher temperatures to produce methane and ethane because the molar concentration of these gases decreased with increase in reaction temperature (Table 7.3).

Table 7. 3: Effect of reaction temperature on the HDO of APPJCPO using 30%Ni/RM catalyst.

Parameter	Reaction temperature (°C)		
	300	350	400
H_2 consumption (mol H_2)	1.24	1.63	1.96
Conversion (%)	88.1	99.5	99.6
Products yield distribution (based on initial organic content) (wt. %)			
HDO oil	51.4	47.8	38.7
Water*	3.3	7.1	8.3
Gas	31.5	41.6	48.3
Coke	1.9	2.4	4.3
Aqueous phase HDO product properties			
Water content (wt. %)	88.15	99.95	99.95
pH	6.02	6.97	6.98
HDO oil properties			
Elemental composition of HDO oil (wt. %)			
N	0.29	0.26	0.20

C	79.87	81.98	83.23
H	14.49	16.62	17.46
O	5.35	1.14	0.11
HHV (MJ/kg)	38.77	42.12	45.71
Density (g/ml)	0.91	0.82	0.75
Dynamic viscosity (cP)	3.67	1.46	1.20
Gas composition (mol %)			
CO	4.8	3.6	2.1
CO_2	10.2	8.4	5.5
CH_4	62.2	66.4	73.6
C_2H_6	5.8	7.1	8.3
C_3H_8	7.2	6.8	4.7
C_4H_{10}	5.4	4.2	3.1
C_5H_{12}	3.7	2.6	2.1

* By difference.

4.2.2.1. NMR of HDO oils

The ^{13}C NMR spectra of HDO at different reaction temperatures are shown in Fig 7.1. It can be clearly seen that increasing the reaction temperature influenced the chemical composition of the HDO oil. For better understanding of the process, semi-quantification of the NMR spectra shown in Fig. 7.1 was carried out by integration of different chemical shift ranges.[34, 42, 45] The semi-quantification of these spectra is presented in Table 7.4. At reaction temperature of 300 °C, carboxylic acids, aldehydes, and ketones were detected, but when the reaction temperature was increased to 400 °C, these signals disappeared. Increasing the reaction temperature also increased the amount of saturated aliphatic carbons due to saturation of double bonds and aromatic rings; consequently the amount of unsaturated aliphatic carbons and aromatic carbons decreased with increase in the reaction temperature.

The HDO oil at 350 °C had estimated research octane number (RON) of 77 and its ^{13}C NMR spectrum was similar to that of commercial gasoline[34] with the exception of a small fraction of aldehydes and ketones (1.2%, Table 7.4). The NMR results showed that at 350 °C, alcohols and methoxy phenols were converted to HDO products and carbonyl alkylation products respectively. At reaction temperature of 400 °C, the HDO oil contained only hydrocarbons and no oxygenated compounds were detected according

to NMR spectra (Fig. 7.1 and Table 7.4), thus, the 0.11% oxygen that was determined by elemental analysis (Table 7.3) was probably due to instrumental errors because the oxygen content was calculated by difference.

Table 7. 4: Functional group distribution of HDO oils from ^{13}C NMR spectral integration at different reaction temperatures.

Chemical shift region (ppm)	Dominant type of carbon	Percentage of carbon based on ^{13}C NMR analysis		
		HDO oil- 300 °C	HDO oil- 350 °C	HDO oil- 400 °C
0-28	saturated aliphatic groups	35.3	39.3	54.6
28-55	unsaturated aliphatic groups	27.5	18.3	12.4
55-95	alcohols, ethers, phenolic methoxys, anhydrosugars	11.5	0.0	0.0
95-165	aromatics, furans	10.8	41.2	33.0
165-180	carboxylic acids, esters	9.5	0.0	0.0
180-215	ketones, aldehydes	5.4	1.2	0.0

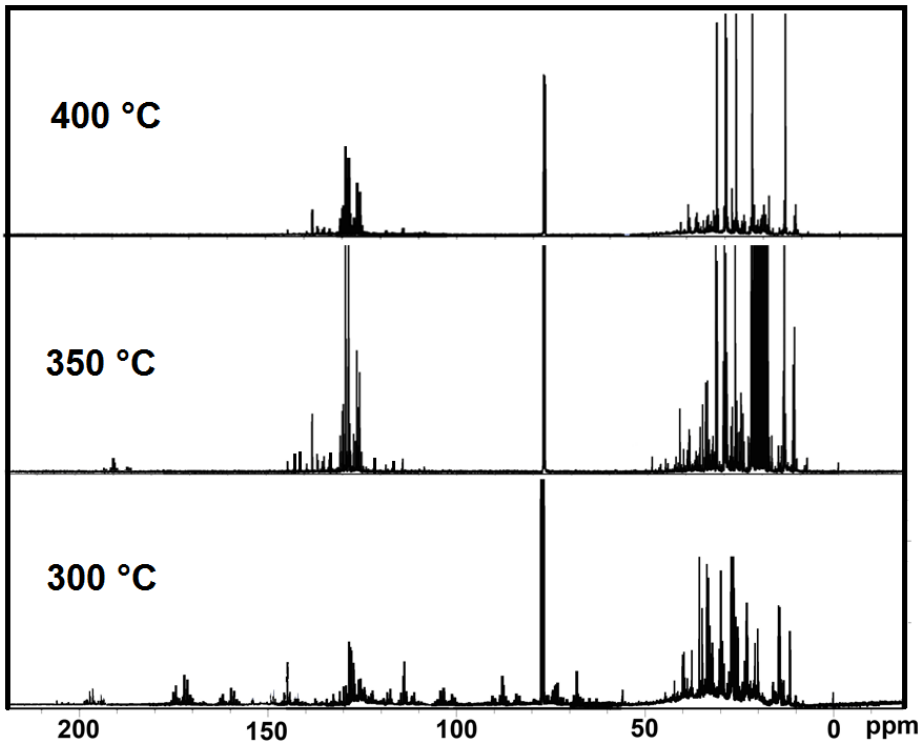

Fig. 7. 1: ^{13}C NMR spectra of APPJCPO HDO oils at different reaction temperatures.

4.2.2.2. Thermogravimetric analysis and chemical compounds of HDO oils

Fig. 7.2 shows the weight loss behavior of HDO oils during thermogravimetric analysis under nitrogen atmosphere. The weight loss temperature ranges were classified as gasoline (30-180 °C), jet fuel (180-250 °C), diesel (250-350 °C), and heavy fuel (above 350 °C).46 The HDO oil produced at reaction temperature of 300 °C had 67% gasoline range, 23% jet fuel range, and 10% diesel range hydrocarbons. The HDO oil at 350 °C contained 75% gasoline range and 25% jet fuel range hydrocarbon with no diesel range compounds. At reaction temperature of 400 °C the HDO oil was in gasoline range hydrocarbons with no jet fuel and diesel fraction (Fig. 7.2). No heavy fuel range hydrocarbons were produced after HDO of APPJCPO at these reaction temperatures.

The HDO oil obtained at 350 °C using 30% Ni/RM was further analyzed by HPLC and GC-MS. The chemical compounds were classified into five major groups; aromatics, cyclic paraffins, internal olefins, linear paraffins, and oxygenates. These results are shown in Table 7.5. From these results it is clear that nearly all of the oxygenated compounds were converted to hydrocarbons by our method.

The carbon balance on the HDO products showed that the organic (liquid), aqueous, gas and coke phases contained 59.4 wt. %, 1.5 wt. %, 35.2 wt. %, and 3.8 wt.% respectively of the carbon in the original APPJCPO. The low carbon content for the aqueous phase indicated a very high concentration of oxygenates and low concentration of hydrocarbons. In addition, the pH of the aqueous phase was neutral at 6.9 indicating absence of acids.

Table 7. 5: Classification of chemical compounds of APPJCPO HDO oil obtained at 350 °C using 30%Ni/RM.

Aromatics	Cyclic paraffins	Internal olefins	Linear paraffins	Oxygenates
Benzene	Cyclopentane	3-ethyl-non-6-ene	n-hexane	Acetone
Toluene	Cyclohexane	7-ethyl-undec-3-ene	n-heptane	2-methyltetrahydrofuran
Xylene	Ethylcyclohexane	7-isobutyl-undec-3-ene	n-octane	Tetrahydrofuran
Ethylbenzene	Isopropyl cyclohexane		2-methylheptane	Butanone
Isopropylbenzene			2-methyloctane	2-pentanone
Sec-butylbenzene			3-methyloctane	
			3-ethyloctane	
			3-methylnonane	
			3-ethylnonane	
			4-methylnonane	
			5-ethylundecane	
			5-isobutylundecane	

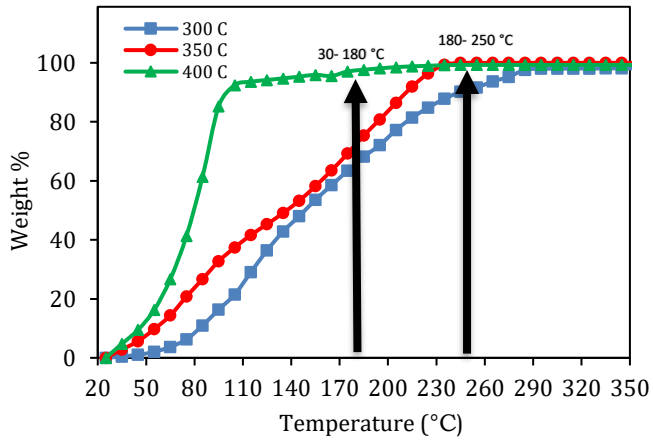

Fig. 7. 2: Petroleum equivalents of gasoline (30-180 °C), jet fuel (180-250 °C), and diesel (250- 350 °C) range hydrocarbons based on decomposition temperature weight present in APPJCPO HDO oils at different reaction temperatures.

4.3. HDO of APPJCPO using commercial Ni/SiO_2-Al_2O_3

For comparison, commercial Ni/SiO_2-Al_2O_3 (as received) which contained 63 wt.% Ni was used in HDO of APPJCPO under similar reaction conditions as the Ni/RM.[41] The APPJCPO conversions for this catalyst were 56.2%, 94.9% and 100% at reaction temperatures of 300 °C, 350 °C, and 400 °C respectively (Table 7.6). The liquid product was single phase that contained no hydrocarbon compounds, but were mostly oxygenates similar to the raw feed. The gas yield was significantly higher than that of Ni/RM catalyst (Table 7.6). Hydrogen consumption was more than twice that of Ni/RM

at all reaction temperatures. The higher activity of the commercial catalyst was attributed to higher amount of Ni loading and higher BET specific surface area.[41, 42] Unlike the RM support, the silica-alumina support did not catalyze carbonyl alkylation reactions. This catalyst deactivated more rapidly than Ni/RM when exposed to acids since it produced nearly three times more coke than Ni/RM at 350 °C. The pH of aqueous phase product at reaction temperatures of 300, 350, and 400 °C were 3.86, 5.19, and 6.97 (Table 7.6) respectively while the corresponding values for Ni/RM were 6.12, 6.97, and 6.98 respectively (Table 7.3). The commercial catalyst was less effective for the conversion of carboxylic acids because it did not catalyze ketonization reactions and only catalyzed hydrodeoxygenation reactions.

HPLC analysis of the Ni/SiO_2-Al_2O_3 aqueous phase products showed that at 300 °C, the concentration of acetic acid decreased from 15.1% to 7.8%, but the concentration of acetone did not change, which suggested that acetic acid was not ketonized to acetone. In contrast to Ni/RM, acetaldehyde concentration increased from 0.7% to 6.5 % because of the partial HDO of acetic acid. Thus, the increase in pH for the commercial catalyst was attributed to HDO of carboxylic acids on Ni metal and silica-alumina probably did not catalyze ketonization reactions. At higher reaction temperatures (350 and 400 °C), the oxygenated compounds of APPJCPO were gasified on the commercial catalyst (Table 7.6).

Table 7. 6: HDO results of APPJCPO using commercial Ni/SiO_2-Al_2O_3 at different reaction temperatures.

Parameter	Reaction temperature (°C)		
	300	350	400
H_2 consumption (mol H_2)	2.35	3.77	4.45
Conversion (%)	56.2	94.9	100
Products yield distribution (based on initial organic content) (wt. %)			

HDO oil	0.0	0.0	0.0
Water*	5.5	15.3	18.4
Gas	45.3	73.5	74.8
Coke	5.4	6.1	6.8
Aqueous phase HDO product properties			
Water content (wt. %)	90.75	95.35	99.95
pH	3.86	5.19	6.97
HPLC analysis of aqueous phase HDO product (dry basis) (relative concentration wt. %)			
Acetaldehyde	6.5	0.2	0.0
Acetic acid	7.8	2.2	0.0
Acetone	2.3	1.4	0.0
Furfural	6.1	2.3	0.0
Phenol	0.6	0.1	0.0
1-hydroxy-2-propanone	1.6	0.7	0.0
2-cyclopentene-1-one	0.4	0.0	0.0
2-methoxy phenol (guaiacol)	3.8	1.1	0.0
2,2-dimethyl-3-heptanone	0.7	0.0	0.0
2,3-butanedione	1.7	0.3	0.0
3-hydroxy-2-butanone	0.8	0.2	0.0
Quantified % of organics	32.3	8.5	0.0
Gas composition (mol %)			
CO	2.5	0.0	0.0
CO_2	6.0	0.0	0.0
CH_4	81.2	92.1	94.0
C_2H_6	4.2	4.1	3.3
C_3H_8	2.5	2.1	1.5
C_4H_{10}	2.4	1.2	0.6
C_5H_{12}	0.7	0.3	0.1

* By difference.

4.4. Catalyst deactivation and regenerability

In order to examine the deactivation of the catalyst, Ni/RM was consecutively used in HDO of APPJCPO without any catalyst regeneration between runs. These tests were performed using the 40% Ni/RM to be able to investigate the effect of feed material on catalyst deactivation and compare them with the HDO of guaiacol as bio-oil model compound,[41] and HDO of the actual bio-oil (ESP oil) using this catalyst.[42] Table 7.7 shows the results of HDO experiments after each run. During the fourth run, no hydrocarbon was produced suggesting that deactivation of Ni occurred and consequently no HDO intermediates were produced for the cross-reactions on RM support. During the fourth run, although no hydrocarbon phase was produced, the pH of the liquid product was 4.82 and the concentration of ketones were relatively high (Table 7.7) and the CO_2 (ketonization product) content was also high showing that ketonization reactions took place to some extent and the support still had some catalytic activity. There appeared to be complete deactivation of both Ni and the support during the sixth run, because the pH

of aqueous phase was 2.98 (Table 7.7). Furthermore, no CO_2 (product of ketonization) was produced during the sixth run and the reaction only produced coke (Table 7.7). Previously, we showed that the catalyst deactivation was due to oxidation of Ni, coke formation, and formation of nickel iron oxide (Fe_2NiO_4).[41, 42] Herein we focused on the effect of coke formation and oxidation on catalyst deactivation.

Because coke formation can reduce the BET specific surface area,[47, 48] the BET specific surface area (Table 7.7) was plotted against coke yield (Fig. 7.3) for HDO of APPJCPO, guaiacol,[41] and ESP oil[42] to compare the effect of feedstock on catalyst deactivation. According to Fig. 7.3, in the case of APPJCPO the data points fitted well to linear regression (R^2 of 0.99) but in the case of ESP oil and guaiacol the data points were more scattered (R^2 of 0.83 and 0.89 respectively). These results suggested that coke formation was possibly the major pathway for catalyst deactivation during HDO of APPJCPO, whereas oxidation could have a higher contribution to catalyst deactivation in the case of ESP oil and guaiacol.

Fig. 7.4 shows the TG-TPR of fresh catalyst (40%Ni/RM in reduced form), catalyst precursor (40%Ni/RM in calcined form), completely deactivated catalyst after HDO of APPJCPO (after 6 runs), and completely deactivated catalyst after HDO of ESP oil[42] (after 4 runs). The fresh catalyst did not show any reduction peaks because the catalyst was in reduced form. The catalyst precursor showed two major reduction peaks at 442°C and 583°C. The peak at 442°C appeared to have higher concentration of NiO than the 583°C peak as described previously.[42] There were no distinct peaks for RM and NiO because of interaction between NiO and the support.[41, 42] The TG-TPR profile of deactivated catalyst after HDO of ESP oil[42] showed three reduction peaks at 341°C,

477°C, and 640°C. The peak at 341°C was attributed to reduction of free NiO because its reduction temperature was close to that of NiO as reported previously.[41, 42] The other two peaks were due to the reduction of bulk phase NiO where there was interaction between NiO and RM support. The peak at 477°C was probably due to reduction of surface components of Ni/RM in the bulk phase and the peak at 640°C was possibly due to reduction of catalyst components inside the bulk phase because they had a higher reduction temperature due to mass transfer limitation to inside components. This result appeared to suggest that during HDO of ESP oil, some Ni particles lost their interactions with the support material and underwent oxidation, in addition to the oxidation of bulk phase Ni/RM.

The TG-TPR profile of deactivated catalyst after HDO of APPJCPO showed only one reduction peak at 325°C (Fig. 7.4). This peak was attributed to reduction of free NiO. This result seemed to suggest that during the HDO of APPJCPO some Ni particles lost their interactions with RM support and underwent oxidation. In contrast to HDO of ESP oil, the oxidation of bulk phase NiO did not occur because the TPR profile did not show any reduction peak between 442°C and 700°C.[42] The aqueous phase (water) appeared to inhibit the oxidation of bulk phase NiO as compared to HDO of the ESP bio-oil.[42] The RDO after complete deactivation of catalyst was 27.8% for APPJCPO compared to 76.4% in the case of ESP oil. Hence, coke formation was probably the major pathway for catalyst deactivation during HDO of APPJCPO, while oxidation and coke formation were both significant controlling factors in the deactivation of Ni/RM during HDO of ESP oil.

Table 7. 7: Catalyst deactivation during HDO of APPJCPO using 40% Ni/RM (reaction temperature of 350 °C).

Parameter	Reuse #					
	Fresh	Reuse# 1	Reuse #2	Reuse #3	Reuse #4	Reuse #5
Catalyst BET specific surface area (m^2/g)	79.3	76.6	72.7	70.4	67.6	63.1
H_2 consumption (mol H_2)	1.87	1.51	1.19	0.96	0.15	0.00
Conversion (%)	99.5	75.7	68.1	25.7	16.0	9.7
Products yield distribution (based on initial organic content) (wt. %)						
HDO oil	23.9	33.5	40.5	0.0	0.0	0.0
Water*	7.8	5.7	4.1	3.5	0.0	0.0
Gas	65.8	34.2	19.4	16.7	8.2	0.0
Coke	1.7	2.3	4.1	5.5	7.8	9.7
Aqueous phase HDO product properties						
Water content (wt. %)	99.95	94.45	91.20	88.05	86.25	84.85
pH	6.98	6.84	6.37	4.82	3.75	2.98
HPLC analysis of aqueous phase HDO product (dry basis) (relative concentration wt. %)						
Acetaldehyde	0.0	0.0	0.0	0.2	0.5	0.7
Acetic acid	0.0	0.3	0.6	3.4	8.1	15.1
Acetone	0.0	3.9	7.3	6.6	5.5	2.4
Furfural	0.0	0.0	0.0	2.7	6.2	6.8
Phenol	0.0	0.0	0.0	0.6	0.7	0.9
1-hydroxy-2-propanone	0.0	1.1	3.5	3.2	2.6	2.1
2-cyclopentene-1-one	0.0	0.0	0.9	0.7	0.6	0.6
2-methoxy phenol (guaiacol)	0.0	0.0	0.0	1.6	3.9	4.4
2,2-dimethyl-3-heptanone	0.0	0.0	2.3	1.7	1.4	1.2
2,3-butanedione	0.0	0.0	3.4	2.7	2.5	2.2
3-hydroxy-2-butanone	0.0	0.0	0.0	1.9	1.6	1.3
Quantified % of organics	0.0	5.3	18.0	25.3	33.6	37.7
HDO oil properties						
HPLC analysis of HDO oil (relative concentration wt. %)						
Acetone	0.0	0.5	1.1	NA	NA	NA
Benzene	1.8	0.7	0.3	NA	NA	NA
Butanone	0.0	5.2	9.1	NA	NA	NA
Cyclohexane	3.9	1.5	0.0	NA	NA	NA
Cyclopentane	2.2	0.7	0.0	NA	NA	NA
Ethylbenzene	2.7	1.5	0.8	NA	NA	NA
Ethylcyclohexane	15.5	9.5	4.2	NA	NA	NA
Isopropylbenzene	2.9	1.6	0.7	NA	NA	NA
Isopropyl cyclohexane	13.8	6.3	3.4	NA	NA	NA
Methanol	1.2	1.0	0.5	NA	NA	NA
n-hexane	5.5	4.2	3.5	NA	NA	NA
n-heptane	2.7	1.5	1.1	NA	NA	NA
n-octane	2.9	1.2	0.6	NA	NA	NA
Sec-butylbenzene	2.1	1.0	0.3	NA	NA	NA
Toluene	5.1	4.1	2.1	NA	NA	NA
Tetrahydrofuran	0.0	1.1	2.8	NA	NA	NA
Xylene	1.9	0.7	0.0	NA	NA	NA
2-methyloctane	6.2	3.4	1.7	NA	NA	NA
2-methyltetrahydrofuran	0.0	0.7	3.1	NA	NA	NA
2-pentanone	0.0	4.1	10.3	NA	NA	NA
3-methylnonane	12.8	7.3	3.7	NA	NA	NA
Quantified % of organics	83.2	57.8	49.3	NA	NA	NA
Elemental composition of HDO oil (wt. %)						
N	0.23	0.27	0.30	NA**	NA	NA
C	82.22	81.03	77.56	NA	NA	NA
H	17.38	15.46	13.27	NA	NA	NA
O	0.17	3.24	8.87	NA	NA	NA
HHV (MJ/kg)	45.62	40.26	33.42	NA	NA	NA
Density (g/ml)	0.77	0.85	0.92	NA	NA	NA
Dynamic viscosity (cP)	1.22	2.36	4.16	NA	NA	NA
Gas composition (mol %)						
CO	2.5	3.6	10.1	19.6	36.0	0.0
CO_2	6.3	7.8	10.3	15.8	19.4	0.0
CH_4	71.3	63.2	54.8	37.3	13.1	0.0
C_2H_6	7.3	6.7	5.4	4.0	3.8	0.0
C_3H_8	6.6	8.5	9.0	11.6	13.6	0.0
C_4H_{10}	4.1	4.8	5.5	6.3	6.9	0.0
C_5H_{12}	1.6	3.7	4.3	5.2	6.2	0.0

* By difference

** Not Applicable (no HDO oil produced)

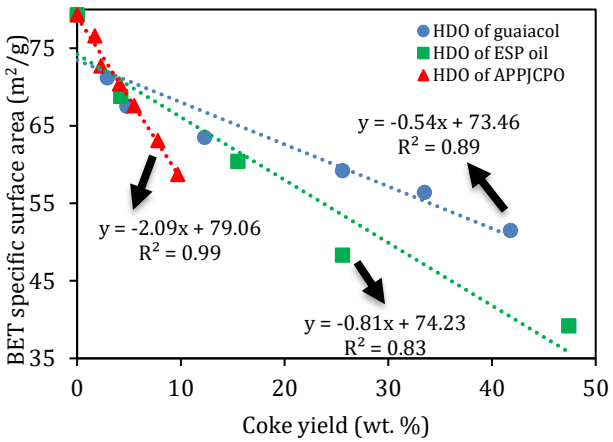

Fig. 7. 3: Catalyst BET specific surface area vs. coke yield during consecutive reuse of 40%Ni/RM without regeneration between runs for HDO of guaiacol [45], ESP oil [46], and APPJCPO.

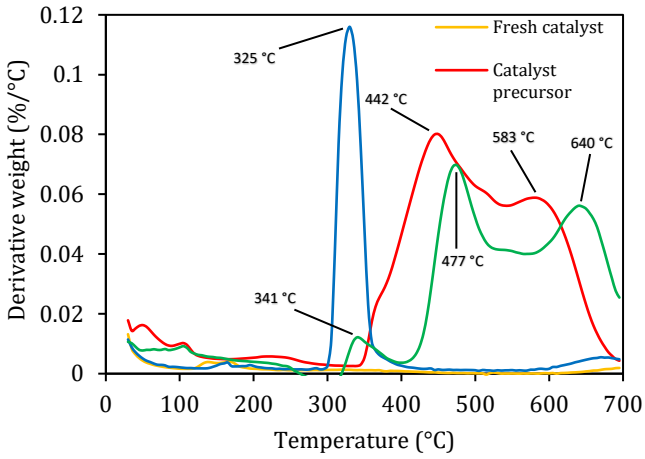

Fig. 7. 4: TG-TPR profiles of 40%Ni/RM; fresh catalyst (reduced form) (yellow), catalyst precursor (calcined form) (red), deactivated catalyst after HDO of APPJCPO (blue), and deactivated catalyst after HDO of ESP oil [46] (green).

The TG-TPR profiles of used Ni/RM after each run is shown in Fig. 7.5. It was clear that after each run more Ni particles lost their interactions with RM support and underwent oxidation because the intensity of NiO reduction peak (~325°C) increased

after each HDO experiment. In addition to coke formation, oxidation can contribute to the reduction in BET specific surface area.[49-51] The RDO of catalyst after each run showed the reduction in BET specific surface area (Fig. 7.6). The linear regression of the BET specific surface area against RDO (Fig. 7.6) showed more scatter compared to BET specific surface area versus coke yield (Fig. 7.3) suggesting that after complete deactivation of the catalyst some Ni particles were still in the bulk phase and retained their interaction with RM support. After six runs, because no bulk phase reduction peaks were observed in the TPR profile of the catalyst, this could suggest that the deactivation of Ni was mostly due to oxidation and loss of interaction with RM support, whereas the deactivation of RM support was mainly because of coke formation.

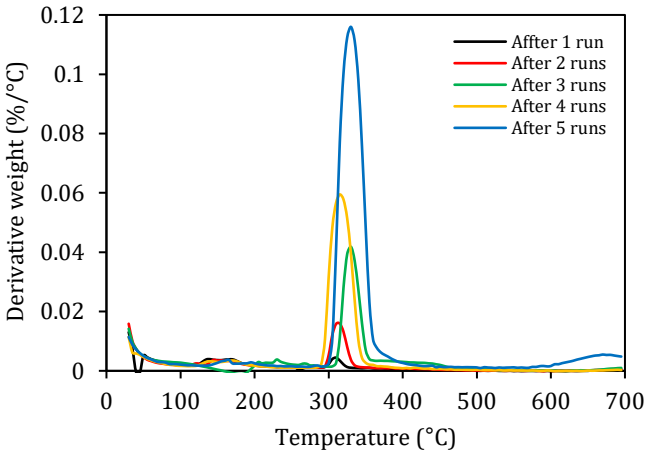

Fig. 7. 5: TG-TPR profiles of 40%Ni/RM after consecutive reuse of the catalyst without regeneration between runs after HDO of APPJCPO.

The deactivated Ni/RM catalyst (after 6 HDO runs) was regenerated by burning off the coke at 400°C in a muffle furnace followed by reduction at 450°C using a reducing gas mixture of 10% H_2 and 90% N_2 according to our previous studies.[41, 42] The

catalyst activity was completely restored after regeneration (data not provided), however the regeneration of the commercial Ni/SiO_2-Al_2O_3 was not possible following the same procedure and the catalyst did not have HDO activity after reduction (data not provided). Additionally, when exposed to air, the reduced commercial catalyst caught fire due to spontaneous oxidation, whereas the reduced Ni/RM was stable on exposure to air.

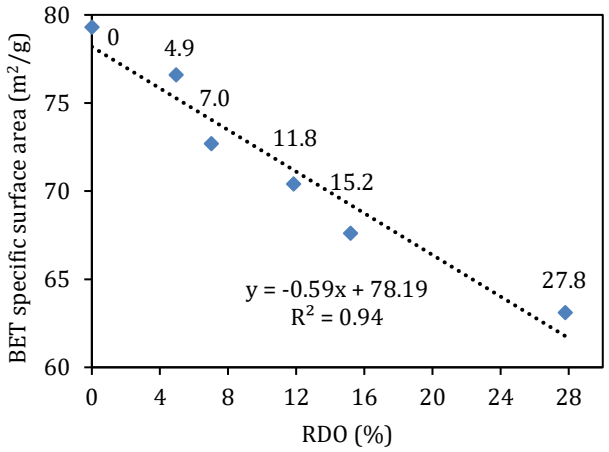

Fig. 7. 6: BET specific surface area versus RDO during consecutive HDO experiments without regeneration between runs (data labels show RDO % values).

5. Conclusion

Hydrodeoxygenation (HDO) of aqueous phase pinyon-juniper catalytic pyrolysis oil (APPJCPO) was studied using a new multifunctional Ni/RM catalyst at different Ni loadings and reaction temperatures. The HDO of APPJCPO produced liquid, gas, and solid products. The liquid product consisted of aqueous phase and organic phase (HDO oil). The HDO oil yield at reaction temperature of 350°C using 30%Ni/RM was 47.8% with oxygen content of 1.14 wt. % that consisted of 75% gasoline fraction and 25% jet

fuel fraction based on boiling point temperature ranges. For comparison, commercial Ni/SiO_2-Al_2O_3 used in HDO experiments under similar conditions gasified the organic compounds of APPJCPO and did not produce any liquid hydrocarbon. The key for the production of HDO oil on Ni/RM was the cross-reactions of HDO intermediates on the support. In the case of Ni/RM, the oxygenated compounds in APPJCPO first underwent partial reduction on Ni sites. These reduction intermediates underwent carbonyl alkylation on the support material to produce aliphatics and alkylated aromatics. Whereas in the case of the commercial catalyst, silica-alumina did not catalyze the carbonyl alkylation reactions so no liquid hydrocarbons were produced. Furthermore, RM catalyzed ketonization reactions that increased the pH of the aqueous phase to about neutral even in absence of Ni. Coke formation and oxidation appeared to be the major controlling factors for catalyst deactivation. TG-TPR results showed that some Ni particles lost their interaction with the RM support and underwent oxidation but oxidation of bulk phase Ni did not take place. Coke formation was the major cause of deactivation of the support material. This study showed that Ni/RM can serve as a multifunctional catalyst that can be used in the production of liquid hydrocarbons from low molecular weight oxygenates that are present in aqueous phase pyrolysis oils.

6. References

(1) Huber, G. W.; Iborra, S.; Corma, A. Synthesis of Transportation Fuels from Biomass: Chemistry, Catalysts, and Engineering. *Chem. Rev.* **2006**, *106* (9), 4044–4098.

(2) Xiu, S.; Shahbazi, A. Bio-Oil Production and Upgrading Research: A Review. *Renew. Sustain. Energy Rev.* **2012**, *16* (7), 4406–4414.

(3) Sanna, A.; Vispute, T. P.; Huber, G. W. Hydrodeoxygenation of the Aqueous Fraction of Bio-Oil with Ru/C and Pt/C Catalysts. *Appl. Catal. B Environ.* **2015**, *165*, 446–456.

(4) Abnisa, F.; Wan Daud, W. M. A.; Arami-Niya, A.; Ali, B. S.; Sahu, J. N. Recovery of Liquid Fuel from the Aqueous Phase of Pyrolysis Oil Using Catalytic Conversion. *Energy & Fuels* **2014**, *28* (5), 3074–3085.

(5) Jain, A. B.; Vaidya, P. D. Kinetics of Aqueous-Phase Hydrogenation of Model Bio-Oil Compounds over a Ru/C Catalyst. *Energy and Fuels* **2015**, *29* (1), 361–368.

(6) Vispute, T. P.; Huber, G. W. Production of Hydrogen, Alkanes and Polyols by Aqueous Phase Processing of Wood-Derived Pyrolysis Oils. *Green Chem.* **2009**, *11* (9), 1433.

(7) Li, N.; Tompsett, G. A.; Zhang, T.; Shi, J.; Wyman, C. E.; Huber, G. W. Renewable Gasoline from Aqueous Phase Hydrodeoxygenation of Aqueous Sugar Solutions Prepared by Hydrolysis of Maple Wood. *Green Chem.* **2011**, *13* (1), 91–101.

(8) Huber, G. W.; Chheda, J. N.; Barrett, Ch. J.; Dumesic, J. A. Production of Liquid Alkanes by Aqueous-Phase Processing of Biomass-Derived Carbohydrates. *Science* **2005**, *308*, 306–311.

(9) Zhang, X.; Wang, T.; Ma, L.; Zhang, Q.; Jiang, T. Hydrotreatment of Bio-Oil over Ni-Based Catalyst. *Bioresour. Technol.* **2013**, *127*, 306–311.

(10) Furimsky, E. Catalytic Hydrodeoxygenation. *Appl. Catal. A Gen.* **2000**, *199* (2), 147–190.

(11) Li, N.; Tompsett, G. A.; Huber, G. W. Renewable High-Octane Gasoline by Aqueous-Phase Hydrodeoxygenation of C5 and C6 Carbohydrates over Pt/zirconium Phosphate Catalysts. *ChemSusChem* **2010**, *3* (10), 1154–1157.

(12) Dongil, A. B.; Pastor-Pérez, L.; Sepúlveda-Escribano, A.; García, R.; Escalona, N. Hydrodeoxygenation of Guaiacol: Tuning the Selectivity to Cyclohexene by Introducing Ni Nanoparticles inside Carbon Nanotubes. *Fuel* **2016**, *172*, 65–69.

(13) Tran, N. T. T.; Uemura, Y.; Chowdhury, S.; Ramli, A. Vapor-Phase Hydrodeoxygenation of Guaiacol on Al-MCM-41 Supported Ni and Co Catalysts. *Appl. Catal. A Gen.* **2016**, *512*, 93–100.

(14) Mora-Vergara, I. D.; Hernández Moscoso, L.; Gaigneaux, E. M.; Giraldo, S. A.; Baldovino-Medrano, V. G. Hydrodeoxygenation of Guaiacol Using NiMo and CoMo Catalysts Supported on Alumina Modified with Potassium. *Catal. Today* **2018**, *302*, 125–135.

(15) Manikandan, M.; Venugopal, A. K.; Prabu, K.; Jha, R. K.; Thirumalaiswamy, R. Role of Surface Synergistic Effect on the Performance of Ni-Based Hydrotalcite Catalyst for Highly Efficient Hydrogenation of Furfural. *J. Mol. Catal. A Chem.* **2016**, *417*, 153–162.

(16) Xiong, K.; Wan, W.; Chen, J. G. Reaction Pathways of Furfural, Furfuryl Alcohol and 2-Methylfuran on Cu(111) and NiCu Bimetallic Surfaces. *Surf. Sci.* **2016**, *652*, 91–97.

(17) Zhang, C.; Lai, Q.; Holles, J. H. Bimetallic Overlayer Catalysts with High Selectivity and Reactivity for Furfural Hydrogenation. *Catal. Commun.* **2017**, *89*, 77–80.

(18) Wang, C.; Luo, J.; Liao, V.; Lee, J. D.; Onn, T. M.; Murray, C. B.; Gorte, R. J. A Comparison of Furfural Hydrodeoxygenation over Pt-Co and Ni-Fe Catalysts at High and Low H2pressures. *Catal. Today* **2018**, *302*, 73–79.

(19) Fu, Z.; Wang, Z.; Lin, W.; Song, W.; Li, S. High Efficient Conversion of Furfural to 2-Methylfuran over Ni-Cu/Al2O3catalyst with Formic Acid as a Hydrogen Donor. *Appl. Catal. A Gen.* **2017**, *547* (August), 248–255.

(20) He, Z.; Wang, X. Required Catalytic Properties for Alkane Production from Carboxylic Acids: Hydrodeoxygenation of Acetic Acid. *J. Energy Chem.* **2013**, *22* (6), 883–894.

(21) Onyestyák, G.; Harnos, S.; Klébert, S.; Štolcová, M.; Kaszonyi, A.; Kalló, D. Selective Reduction of Acetic Acid to Ethanol over Novel Cu2In/Al2O3catalyst. *Appl. Catal. A Gen.* **2013**, *464–465*, 313–321.

(22) Badari, A. C.; Harnos, S.; Lónyi, F.; Onyestyák, G.; Štolcová, M.; Kaszonyi, A.; Valyon, J. A Study of the Selective Catalytic Hydroconversion of Biomass-Derived Pyrolysis or Fermentation Liquids Using Propylamine and Acetic Acid as Model Reactants. *Catal. Commun.* **2014**, *58*, 1–5.

(23) Elliott, D. C.; Hart, T. R. 73 Catalytic Hydroprocessing of Chemical Models for Bio-Oil. *Energy and Fuels* **2009**, 8, 631–637.

(24) Wang, J.; Luo, Z.; Zhang, J.; Dang, Q.; Chen, W. Reactions of Furfural and Acetic Acid as Model Compounds for Bio-Oil Upgrading in Supercritical Ethanol. *Int. Conf. Electron. Commun. Control. ICECC* **2011**, *2*, 1587–1592.

(25) Si, Z.; Zhang, X.; Wang, C.; Ma, L.; Dong, R. An Overview on Catalytic Hydrodeoxygenation of Pyrolysis Oil and Its Model Compounds. *Catalysts* **2017**, *7* (6), 169.

(26) Power, G.; Gräfe, M.; Klauber, C. Bauxite Residue Issues: I. Current Management, Disposal and Storage Practices. *Hydrometallurgy* **2011**, *108* , 33–45.

(27) Wang, S.; Ang, H. M.; Tadé, M. O. Novel Applications of Red Mud as Coagulant, Adsorbent and Catalyst for Environmentally Benign Processes. *Chemosphere* **2008**, *72* (11), 1621–1635.

(28) Sushil, S.; Batra, V. S. Catalytic Applications of Red Mud , an Aluminium Industry Waste : A Review. *Appl. Catal. B Envison.* **2008**, *81*, 64–77.

(29) Hua, Y.; Heal, K. V.; Friesl-Hanl, W. The Use of Red Mud as an Immobiliser for Metal/metalloid-Contaminated Soil: A Review. *J. Hazard. Mater.* **2017**, *325*, 17–30.

(30) Liu, Y.; Naidu, R. Hidden Values in Bauxite Residue (Red Mud): Recovery of Metals. *Waste Manag.* **2014**, *34*, 2662–2673.

(31) Liu, X.; Zhang, N. Utilization of Red Mud in Cement Production: A Review. *Waste Manag. Res.* **2011**, *29*, 1053–1063.

(32) Yathavan, B. K.; Agblevor, F. A. Catalytic Pyrolysis of Pinyon-Juniper Using Red Mud and HZSM-5. *Energy and Fuels* **2013**, *27*, 6858–6865.

(33) Xu, B.; Qi, F.; Zhang, J.; Li, H.; Sun, D.; Robert, D.; Chen, Z. Cobalt Modified Red Mud Catalytic Ozonation for the Degradation of Bezafibrate in Water: Catalyst Surface Properties Characterization and Reaction Mechanism. *Chem. Eng. J.* **2016**, *284*, 942–952.

(34) Jahromi, H.; Agblevor, F. A. Upgrading of Pinyon-Juniper Catalytic Pyrolysis Oil via Hydrodeoxygenation. *Energy* **2017**, *141*, 2186–2195.

(35) Shim, W. G.; Nah, J. W.; Jung, H. Y.; Park, Y. K.; Jung, S. C.; Kim, S. C. Recycling of Red Mud as a Catalyst for Complete Oxidation of Benzene. *J. Ind. Eng. Chem.* **2018**, *60*, 259–267.

(36) Santona, L.; Castaldi, P.; Melis, P. Evaluation of the Interaction Mechanisms between Red Muds and Heavy Metals. *J. Hazard. Mater.* **2006**, *136*, 324–329.

(37) Pappu, A.; Saxena, M.; Asolekar, S. R. Solid Wastes Generation in India and Their Recycling Potential in Building Materials. *Build. Environ.* **2007**, *42* (6), 2311–2320.

(38) Li, Y.; Liu, C.; Luan, Z.; Peng, X.; Zhu, C.; Chen, Z.; Zhang, Z.; Fan, J.; Jia, Z. Phosphate Removal from Aqueous Solutions Using Raw and Activated Red Mud and Fly Ash. *J. Hazard. Mater.* **2006**, *137*, 374–383.

(39) Liu, Z.; Li, H. Metallurgical Process for Valuable Elements Recovery from Red Mud - A Review. *Hydrometallurgy* **2015**, *155*, 29–43.

(40) Mante, O. D.; Agblevor F. A. Catalytic Pyrolysis for the Production of Refinery-Ready Biocrude oils from Six Different Biomass Sources. *Green Chem.* **2014**, 16, 3364-3377.

(41) Jahromi, H.; Agblevor, F. A. Hydrotreating of Guaiacol: A Comparative Study of Red Mud-Supported Nickel and Commercial Ni/SiO2-Al2O3catalysts. *Appl. Catal. A Gen.* **2018**, *558*, 109–121.

(42) Jahromi, H.; Agblevor, F. A. Hydrodeoxygenation of Pinyon-Juniper Catalytic Pyrolysis Oil Using Red Mud-Supported Nickel Catalysts. *Applied Catal. B, Environ.* **2018**, *236* (2010), 1–12.

(43) Joshi, N.; Lawal, A. Hydrodeoxygenation of Acetic Acid in a Microreactor. *Chem. Eng. Sci.* **2012**, *84*, 761–771.

(44) Baylon, R. A. L.; Sun, J.; Martin, K. J.; Venkitasubramanian, P.; Wang, Y. Beyond Ketonization: Selective Conversion of Carboxylic Acids to Olefins over Balanced Lewis Acid–base Pairs. *Chem. Commun.* **2016**, *52*, 4975–4978.

(45) Zhang, X.; Chen, L.; Kong, W.; Wang, T.; Zhang, Q.; Long, J.; Xu, Y.; Ma, L. Upgrading of Bio-Oil to Boiler Fuel by Catalytic Hydrotreatment and Esterification in an Efficient Process. **2015**, *84*, 83–90.

(46) Tanneru, S. K.; Steele, P. H. Pretreating Bio-Oil to Increase Yield and Reduce Char during Hydrodeoxygenation to Produce Hydrocarbons. *Fuel* **2014**, *133*, 326–331.

(47) Li, Y.; Zhang, C.; Liu, Y.; Tang, S.; Chen, G.; Zhang, R.; Tang, X. Coke Formation on the Surface of Ni/HZSM-5 and Ni-Cu/HZSM-5 Catalysts during Bio-Oil Hydrodeoxygenation. *Fuel* **2017**, *189*, 23–31.

(48) Wan, Z.; Li, G. K.; Wang, C.; Yang, H.; Zhang, D. Relating Coke Formation and Characteristics to Deactivation of ZSM-5 Zeolite in Methanol to Gasoline Conversion. *Appl. Catal. A Gen.* **2018**, *549*, 141–151.

(49) Chenna, S.; Banerjee, R.; Crozier, P. A. Atomic-Scale Observation of the Ni Activation Process for Partial Oxidation of Methane Using In Situ Environmental TEM. *Chem. Cat. Chem.* **2011**, *3*, 1051–1059.

(50) Jeangros, Q.; Hansen, T. W.; Wagner, J. B.; Damsgaard, C. D.; Dunin-Borkowski, R. E.; Hébert, C.; Van Herle, J.; Hessler-Wyser, A. Reduction of Nickel Oxide Particles by Hydrogen Studied in an Environmental TEM. *J. Mater. Sci.* **2013**, *48*, 2893–2907.

(51) Coronado, I.; Stekrova, M.; García Moreno, L.; Reinikainen, M.; Simell, P.; Karinen, R.; Lehtonen, J. Aqueous-Phase Reforming of Methanol over Nickel-Based Catalysts for Hydrogen Production. *Biomass and Bioenergy* **2017**, *106*, 29–37.

CHAPTER 8

8. SUMMARY

Pyrolysis oils (bio-oils) suffer from a number of negative properties such as high acidity, poor stability, and low energy density. These properties inhibit the direct utilization of bio-oils as transportation fuels. Therefore, further processing of bio-oils is required to improve their physicochemical properties. Catalytic hydrodeoxygenation (HDO) is an effective process to overcome the negative properties of bio-oils. This process has been investigated using traditional HDO catalysts such as $CoMo/Al_2O_3$ or supported noble metal catalysts including Ru, Pd, and Pt. The former catalysts require pre-sulfidation that increases the risk of product contamination, while the latter are relatively expensive catalysts. Catalyst deactivation due to coke formation has always been a major challenge during HDO process. In addition to coke formation, hydrocracking of organic compound is another source of carbon loss during this process. Furthermore, high hydrogen consumption can potentially increase the cost of this operation. Therefore, development of new catalysts that are able to reduce hydrogen consumption, coke formation, and hydrocracking can positively impact the HDO operation.

A new multifunctional nickel catalyst for upgrading of lignocellulosic biomass-derived pyrolysis oil via HDO was developed from red mud (RM) waste. The catalyst performance was investigated in three HDO process groups; HDO of organic phase pyrolysis oil, HDO of aqueous phase pyrolysis oil, and HDO of bio-oil model compounds. The activity of the new catalyst (Ni/RM) was compared with that of commercial Ni/SiO_2-Al_2O_3.

Increasing the nickel content from 10% to 65% improved the activity of Ni/RM catalysts for HDO of organic phase pinyon-juniper (PJ) pyrolysis oil, but it also increased gasification. Maximum organic liquid yield (68.6%) was obtained when 40%Ni/RM was used. The upgraded oil had oxygen content of 1.35 wt. % and higher heating value of 45.77 MJ/kg compared to 24.88 wt. % and 28.41 MJ/kg, respectively, for the crude oil. The HDO oil properties obtained using 40%Ni/RM at reaction temperature of 400 °C was similar to that of commercial Ni/SiO_2-Al_2O_3 at reaction temperature of 450 °C. However, the organic liquid yield was much higher for 40%Ni/RM (68.6%) compared to the commercial catalyst (41.8%). The commercial Ni/SiO_2-Al_2O_3 produced more gas (27.6%) than the 40%Ni/RM (16.4%) and the coke yields for the commercial catalyst and Ni/RM catalyst were 7.3% and 4.2% respectively. Overall, application of Ni/RM improved HDO reactions, decreased hydrogen consumption, and reduced cracking and coke formation compared to commercial Ni/SiO_2-Al_2O_3.

HDO of aqueous phase pinyon-juniper catalytic pyrolysis oil (APPJCPO) produced liquid, gas, and solid (coke) products. The liquid product consisted of aqueous phase and organic phase (HDO oil). The HDO oil yield at reaction temperature of 350°C using 30%Ni/RM was 47.8% with oxygen content of 1.14 wt. % that consisted of 75% gasoline fraction and 25% jet fuel fraction based on boiling point temperature ranges. The commercial Ni/SiO_2-Al_2O_3 gasified the organic compounds of APPJCPO under similar conditions and did not produce any liquid hydrocarbon. The production of HDO oil on Ni/RM was due to the cross-reactions of HDO intermediates on the RM support. The oxygenated compounds in APPJCPO first underwent partial reduction on Ni sites. These reduction intermediates underwent carbonyl alkylation on the RM support to produce

aliphatics and alkylated aromatics. Whereas in the case of the commercial catalyst, silica-alumina did not catalyze the carbonyl alkylation reactions so no liquid hydrocarbons were produced. Furthermore, RM catalyzed ketonization reactions that increased the pH of the aqueous phase to about neutral even in absence of Ni.

HDO of guaiacol as bio-oil model compound was studied using Ni/RM and commercial Ni/SiO_2-Al_2O_3 catalysts. The major products of hydrotreating process were catechol, anisole, phenol, cyclohexane, hexane, benzene, toluene, and xylene. Complete HDO was achieved at reaction temperature of 400 °C and initial hydrogen pressure of 6.21 MPa (900 psi). Under these conditions, the selectivity to cyclohexane, benzene, toluene, and xylene over Ni/RM catalyst were 38.8, 24.5, 18.1, and 7.9% respectively, whereas these values were 62.2, 15.9, 8.4, and 4.5% respectively over Ni/SiO_2-Al_2O_3. Reaction network and the kinetics of guaiacol HDO were proposed according to analysis of the products. The Ni/RM catalyst was more effective for deoxygenation reactions than hydrogenation while commercial Ni/SiO_2-Al_2O_3 was more effective for hydrogenation than deoxygenation. Thus, hydrogen consumption per gram of bio-oil was lower for the Ni/RM catalyst compared to the Ni/SiO_2-Al_2O_3.

Cross reactivity of aqueous phase organic compounds during HDO using Ni/RM catalyst was extensively studied. These model compounds studies were carried out in two classes of reactions; furfural-based reactions, and guaiacol-based reactions. Furfural was partially reduced (on Ni sites) to furan and methyl furan. Furan reacted with aldehydes to produce linear hydrocarbons, whereas methylfuran reacted with ketones to produced branched hydrocarbons. Reactions of furan and, methylfuran with aldehydes and ketones were catalyzed on RM support. In guaiacol-based reactions, guaiacol underwent partial

reduction on Ni sites to produce anisole. Anisole further reacted with aldehydes and ketones on RM support. These reactions were called “carbonyl alkylation”. Carbonyl alkylation of C_2 to C_4 aldehydes and ketones with anisole produced alkylated aromatics, whereas C_5 to C_8 aldehydes and ketones underwent subsequent ring opening after carbonyl alkylation to produce internal olefins. Furfural reactions and guaiacol reactions produced C_6 to C_{15} linear, branched, alkylated aromatics, and internal olefins from low molecular weight oxygenated compounds in biomass pyrolysis oils. Aldehydes, ketones, and carboxylic acids are known to be responsible for poor stability and acidic nature of bio-oils. Previously, these compounds were hydrogenated or gasified in a first step mild HDO to stabilize the bio-oil for the second step severe HDO. Therefore, it was demonstrated for the first time that, through a unique catalytic activity, these compounds could be used to produce liquid hydrocarbons. The unique catalytic activity of Ni/RM prevented the carbon loss due to gasification of these low molecular weight compounds, thus, increased the overall liquid yield.

Coke formation, oxidation, and formation of nickel iron oxide appeared to be the major controlling factors for catalyst deactivation. TG-TPR results showed that some Ni particles lost their interaction with the RM support and underwent oxidation during HDO of APPJCPO. However, in contrast to HDO of ESP oil, the oxidation of bulk phase Ni did not occur. The aqueous phase (water) appeared to inhibit the oxidation of bulk phase Ni as compared to HDO of the ESP bio-oil. Coke formation was the major cause of deactivation of the support material while oxidation was more pronounced in deactivation of Ni metal. Hence, coke formation was probably the major pathway for catalyst

deactivation during HDO of APPJCPO, while oxidation and coke formation were both significant controlling factors in the deactivation of Ni/RM during HDO of ESP oil.

After deactivation, the activity of Ni/RM was completely restored by burning off the coke and reduction in hydrogen. The regeneration of the commercial catalyst was not possible following the same procedure and when exposed to air, the commercial catalyst underwent spontaneous combustion. This study showed that Ni/RM can serve as a multifunctional catalyst for upgrading of pyrolysis oils via hydrodeoxygenation and can potentially be a superior alternative to commercial Ni/SiO_2-Al_2O_3.

APPENDICES

Appendix A: Supplementary data for Chapter 3

Table A. 1: Total mass balance and carbon mass balance of HDO experiments at different initial hydrogen pressures.

P(MPa)	Total mass balance (wt.%)					Carbon balance (wt.%)				
	Organic	**Aqueous**	**Gas**	**Coke**	**SUM**	**Organic**	**Aqueous**	**Gas**	**Coke**	**SUM**
3.5	40.3	15.7	32.3	10.4	**98.7**	52.8	2.2	28.4	15.4	**98.8**
5.2	42.3	16.8	31	8.4	**98.5**	57.4	1.1	27.2	12.4	**98.1**
7	44.8	21.1	27.6	5.3	**98.8**	68.8	0	22.1	7.8	**98.7**
8.6	44.8	21.7	27.1	4.9	**98.5**	68.8	0	22.4	7.2	**98.4**
10	44.7	21.7	27.7	4.8	**98.9**	68.7	0	22.5	7.1	**98.3**

Table A. 2: H_2 consumption, physicochemical properties of the liquid products, and gas product composition at different initial H_2 pressures[*]

Properties	The reaction time and temperature were 60 min and 450 °C respectively				
	3.5 MPa	5.2 MPa	7 MPa	8.6 MPa	10 MPa
H_2 consumption (mol/kg bio-oil)	43 ± 3	48 ± 2	57 ± 4	57 ± 3	57 ± 3
Aqueous phase					
Water content (wt%)	94.77 ± 0.90	95.36 ± 0.65	99.05 ± 1.05	99.19 ±1.15	98.32 ±1.15
pH	5.02 ± 0.11	5.74 ± 0.21	6.81 ± 0.40	6.84 ± 0.31	6.86 ± 0.17
HDO oil (organic phase)					
Elemental analysis (wt%)					
N	0.34 ± 0.02	0.27 ± 0.03	0.12 ± 0.01	0.10 ± 0.01	0.06 ± 0.01
C	71.19 ± 0.51	73.82 ± 1.12	83.47 ± 1.09	83.52 ± 1.24	83.54 ± 0.95
H	10.24 ± 0.34	13.49 ±0.44	16.41 ± 0.43	16.38 ± 0.68	16.40 ± 0.61
O	18.23 ± 0.35	12.42 ± 0.51	0.00	0.00	0.00
HHV (MJ/kg)	42.72 ± 1.04	43.14 ±0.56	45.44 ± 0.84	45.56 ±0.65	45.37 ± 0.24
pH	4.88 ± 0.03	5.16 ± 0.03	NA	NA	NA
Water content (wt%)	1.07 ± 0.05	0.73 ± 0.05	<DL[**]	<DL[**]	<DL[**]
Density (g/ml)	0.88 ± 0.02	0.85 ± 0.01	0.79 ± 0.01	0.81 ± 0.01	0.81 ±0.02
Dynamic viscosity (cP)	1.54 ± 0.02	1.41 ± 0.01	1.35 ± 0.01	1.27 ± 0.02	1.26 ± 0.01
Gas composition (mole %)					
CO_2	0.61 ± 0.04	0.00	0.00	0.00	0.00
CH_4	95.71 ± 0.19	97.10 ± 0.51	85.83 ±0.19	88.53 ± 0.48	85.91 ± 0.86
C_2H_4	1.73 ± 0.01	1.39 ± 0.06	9.02 ± 0.02	6.93 ± 0.11	8.32 ± 0.04
C_3H_8	1.45 ± 0.01	1.51 ± 0.03	3.82 ± 0.03	3.09 ±0.03	3.81 ± 0.01
C_4H_{10}	0.32 ± 0.01	0.25 ± 0.02	1.18 ± 0.01	1.19 ± 0.01	1.51 ± 0.02
C_5H_{12}	0.17 ± 0.01	0.09 ± 0.01	0.15 ± 0.01	0.24 ± 0.03	0.43 0.01

[*] Errors are the standard deviation of two measurements

[**] The detection limit was 0.05%.

Table A. 3: Total mass balance and carbon mass balance of HDO experiments at different reaction times.

t(min)	Total mass balance (wt.%)					Carbon balance (wt.%)				
	Organic	**Aqueous**	**Gas**	**Coke**	**SUM**	**Organic**	**Aqueous**	**Gas**	**Coke**	**SUM**
15	53.7	17.4	25	2.6	**98.7**	78.5	0.8	15.2	4.1	**98.6**
30	51.4	17.9	26.7	2.9	**98.9**	78.1	0	15.8	4.2	**98.1**
60	44.8	21.1	27.6	5.3	**98.8**	68.8	0	22.1	7.8	**98.7**
90	37.8	18.1	34.1	8.7	**98.7**	58.1	0	27.5	12.8	**98.4**

Table A. 4: H_2 consumption, physicochemical properties of the liquid products, and gas product composition at different reaction times[*].

Properties	Temperature and hydrogen initial pressure were 450 °C and 7 MPa respectively			
	15 min	30 min	60 min	90 min
H_2 consumption (mol/kg bio-oil)	46 ± 3	50 ± 3	57 ± 3	60 ± 4
Aqueous phase				
Water content (wt%)	95.29 ± 0.79	99.21 ± 0.73	99.05 ± 1.01	99.16 ±1.33
pH	4.86 ± 0.28	6.73 ± 0.29	6.69 ± 0.11	6.84 ± 0.25
HDO oil (organic phase)				
Elemental analysis (wt%)				
N	0.21 ± 0.01	0.19 ± 0.03	0.12 ± 0.01	0.09 ± 0.02
C	78.41 ± 0.83	83.39 ± 1.23	83.47 ± 1.09	83.49 ± 1.04
H	13.27 ± 0.12	16.42 ± 0.24	16.41 ± 0.43	16.42 ± 0.31
O	8.11 ± 0.16	0.00	0.00	0.00
HHV (MJ/kg)	43.27 ± 0.44	45.58 ± 0.48	45.44 ± 0.84	45.81 ± 0.67
pH	6.19 ± 0.03	NA	NA	NA
Water content (wt%)	0.73 ± 0.15	<DL	<DL	<DL
Density (g/ml)	0.85 ± 0.01	0.81 ± 0.01	0.79 ± 0.01	0.81 ± 0.02
Dynamic viscosity (cP)	1.27 ± 0.03	1.26 ± 0.02	1.35 ± 0.01	1.11 ± 0.01
Gas composition (mole %)				
H_2	0.00	0.00	0.00	7.18 ± 19
CO_2	0.00	0.00	0.00	1.75 ± 0.09
CH_4	87.38 ± 0.78	87.71 ± 0.51	85.83 ± 0.63	80.92 ± 0.64
C_2H_4	7.46 ± 0.04	9.09 ± 0.07	9.02 ± 0.10	7.73 ± 0.04
C_3H_8	2. 96 ± 0.05	2.42 ±0.03	3.82 ±0.11	2.03 ± 0.06
C_4H_{10}	1.58 ± 0.05	0.49 ± 0.02	1.18 ±0.11	0.31 ± 0.01
C_5H_{12}	0.59 ± 0.02	0.26 ± 0.02	0.15 ± 0.01	0.06 ± 0.01

[*] Errors are the standard deviation of two measurements

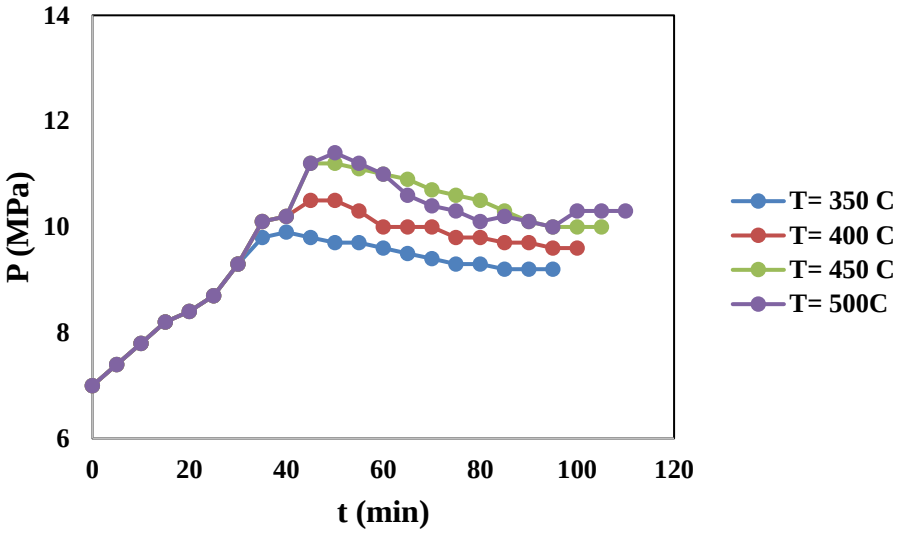

Fig. A. 1: Pressure profile during HDO experiments at different temperatures.

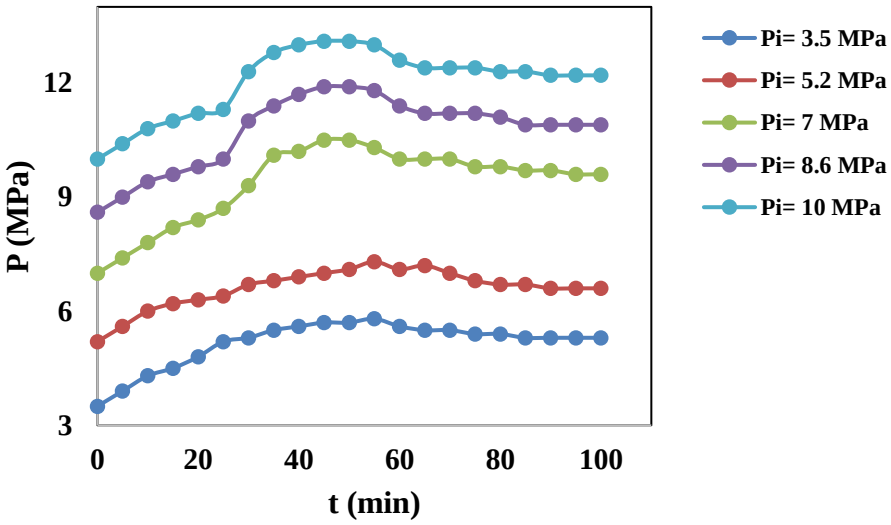

Fig. A. 2: Pressure profile during HDO experiments at different initial hydrogen pressures.

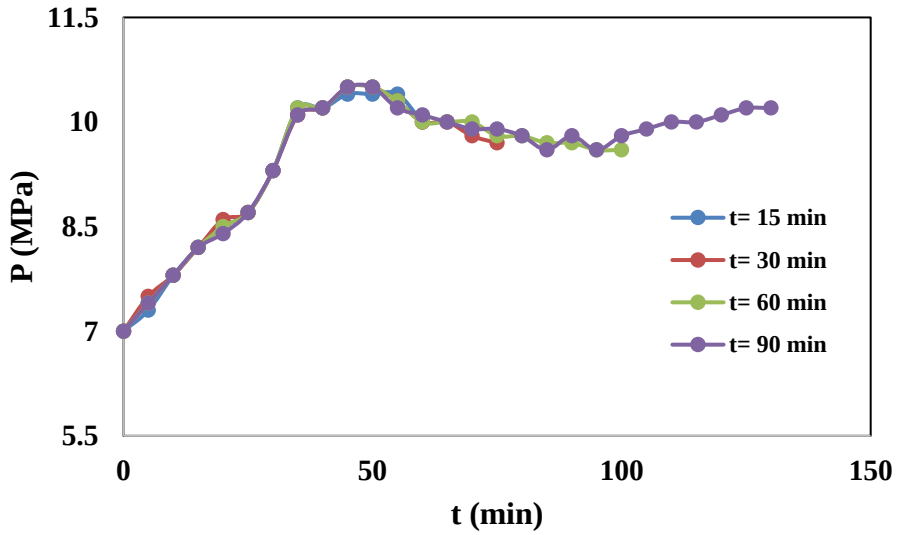

Fig. A. 3: Pressure profile during HDO experiments at different reaction times.

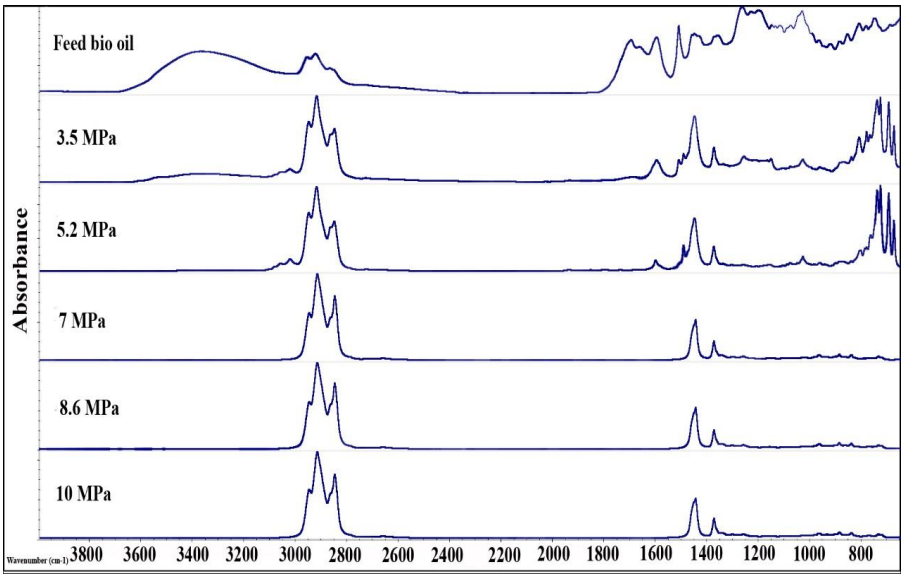

Fig. A. 4: FTIR spectra of HDO oils obtained at different H_2 initial pressures. Temperature and reaction time were 450 °C and 60 minutes respectively.

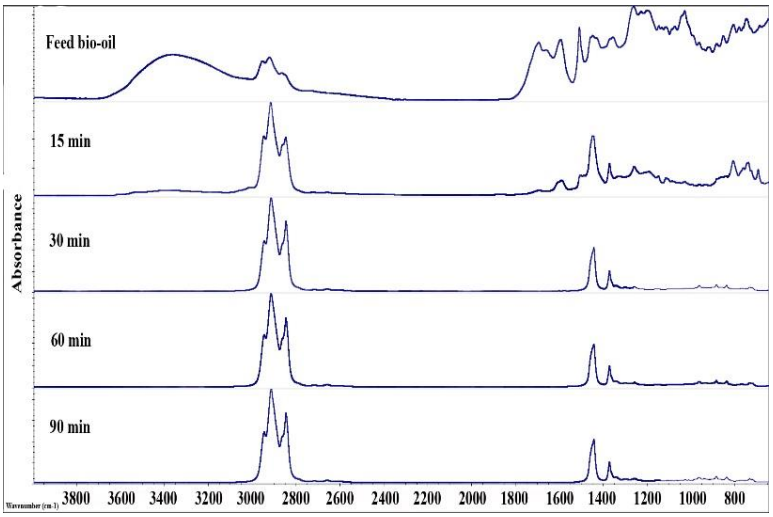

Fig. A. 5: FTIR spectra of HDO oils obtained at different reaction times. Temperature and H_2 initial pressure were 450 °C and 7 MPa respectively.

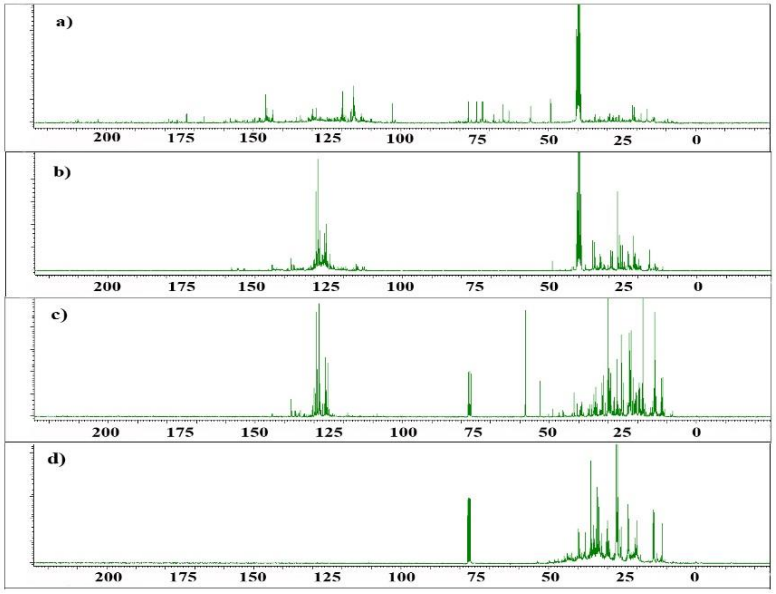

Fig. A. 6: ^{13}C NMR spectra of a) crude bio-oil b) HDO oil obtained at temperature, H2 initial pressure, and reaction time of 400 °C, 7 MPa, 60 minutes respectively c) commercial gasoline d) HDO oil obtained at temperature, H_2 initial pressure, and reaction time of 450 °C, 7 MPa, 60 minutes respectively.

Appendix B: Supplementary data for Chapter 4

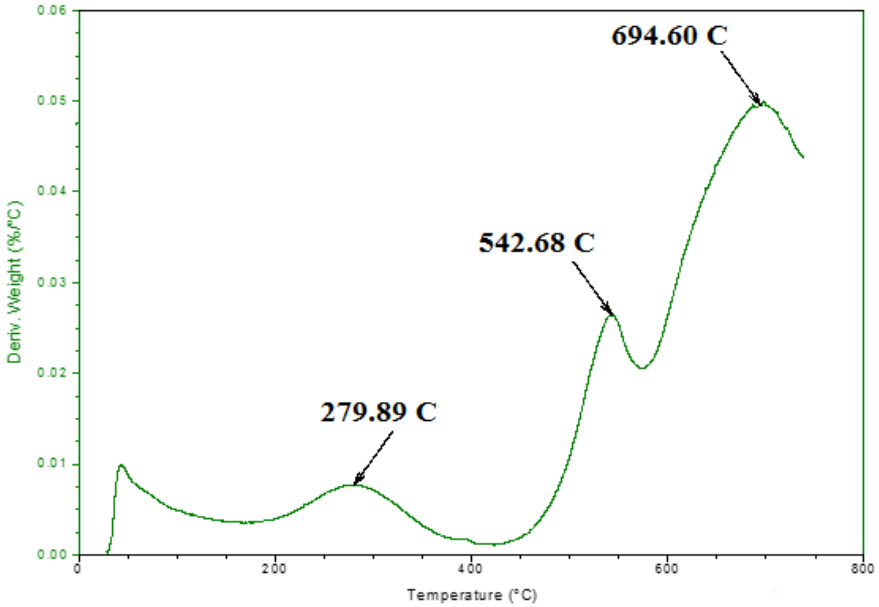

Fig. B. 1: TG-TPR profile of red mud.

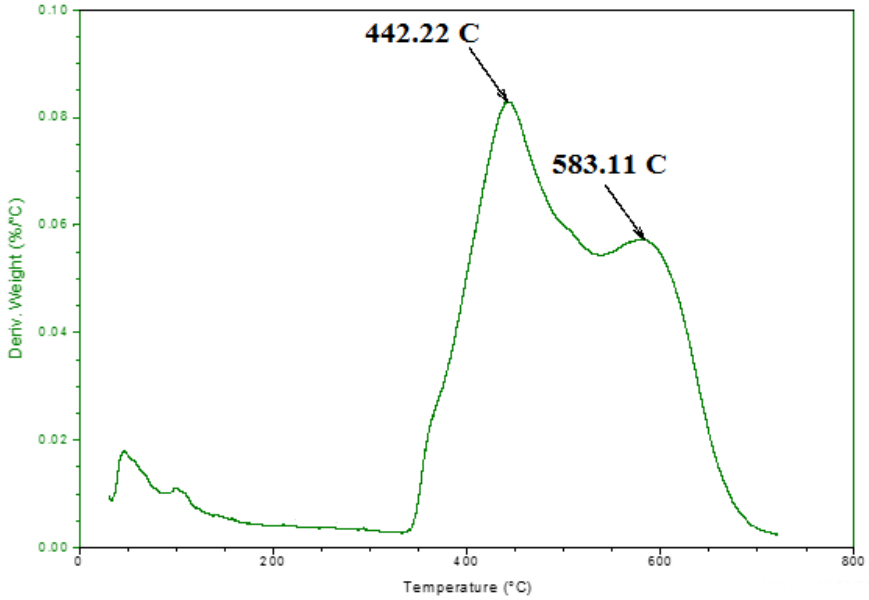

Fig. B. 2: TG-TPR profile of Ni/RM catalyst.

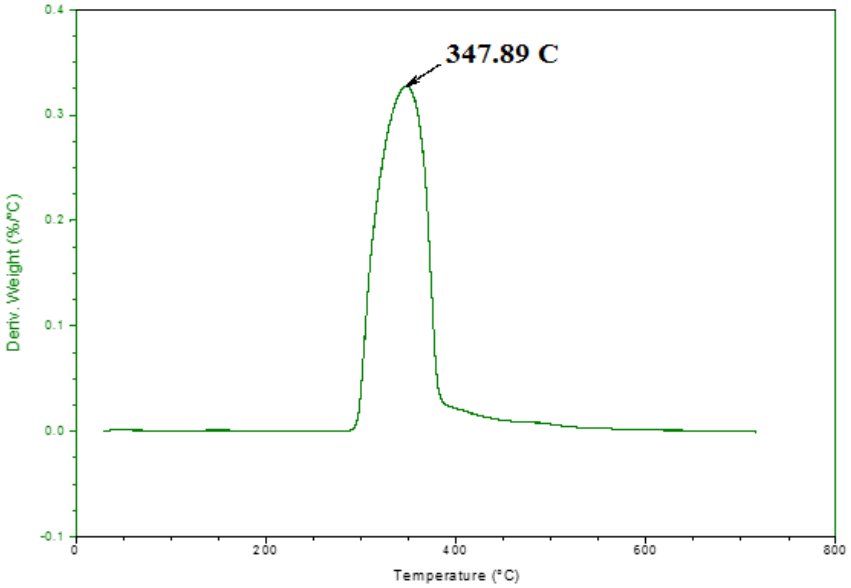

Fig. B. 3: TG-TPR profile of nickel oxide.

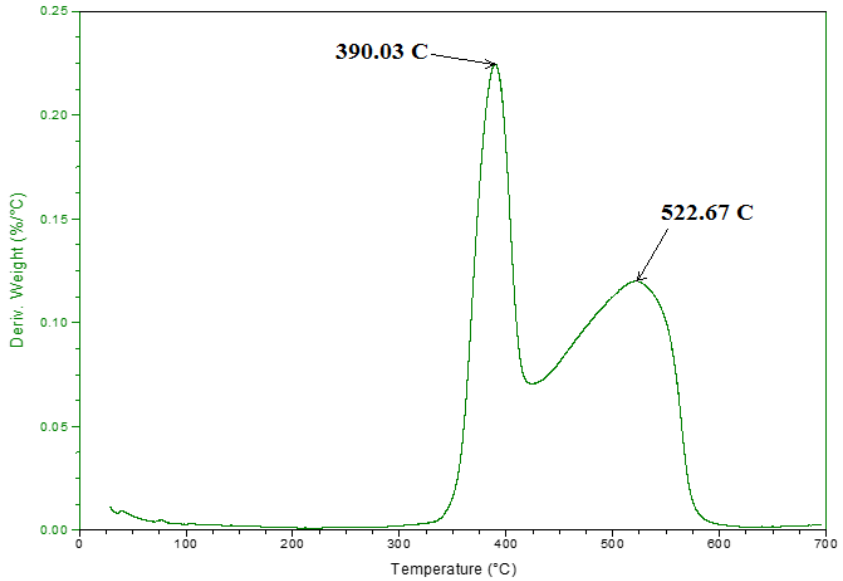

Fig. B. 4: TG-TPR profile of NiO/Fe_2O_3.

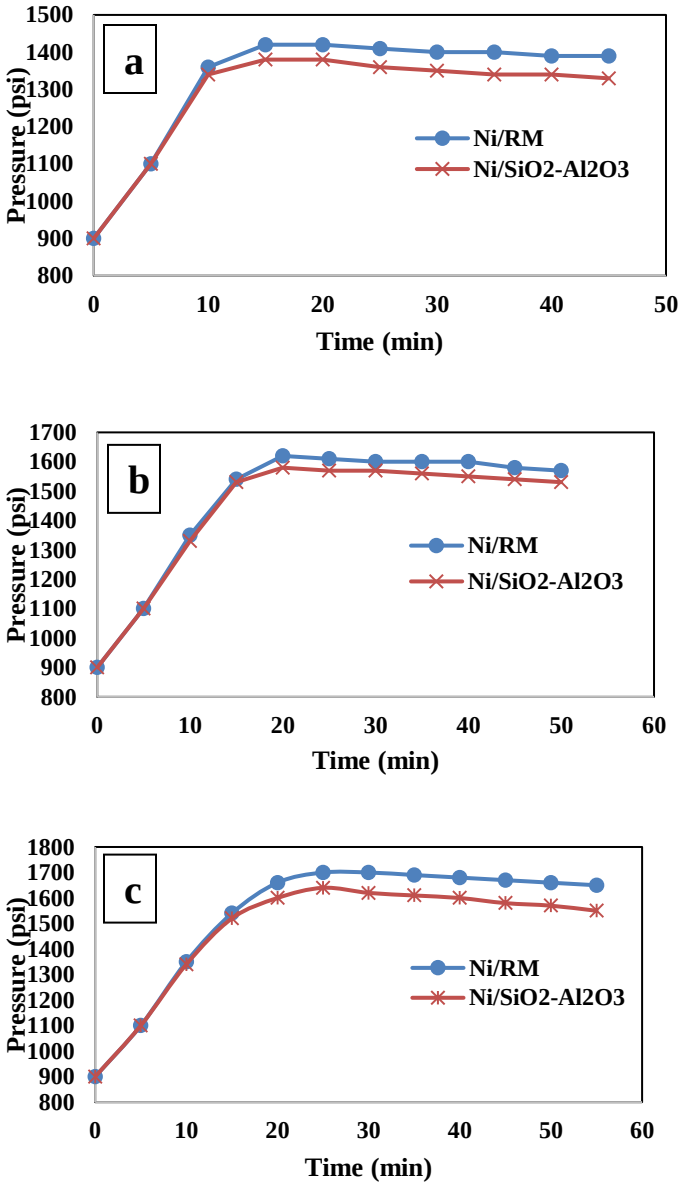

Fig. B. 5: Pressure change during HDO of guaiacol at reaction temperatures of a) 300 °C, b) 350 °C, and c) 400 °C.

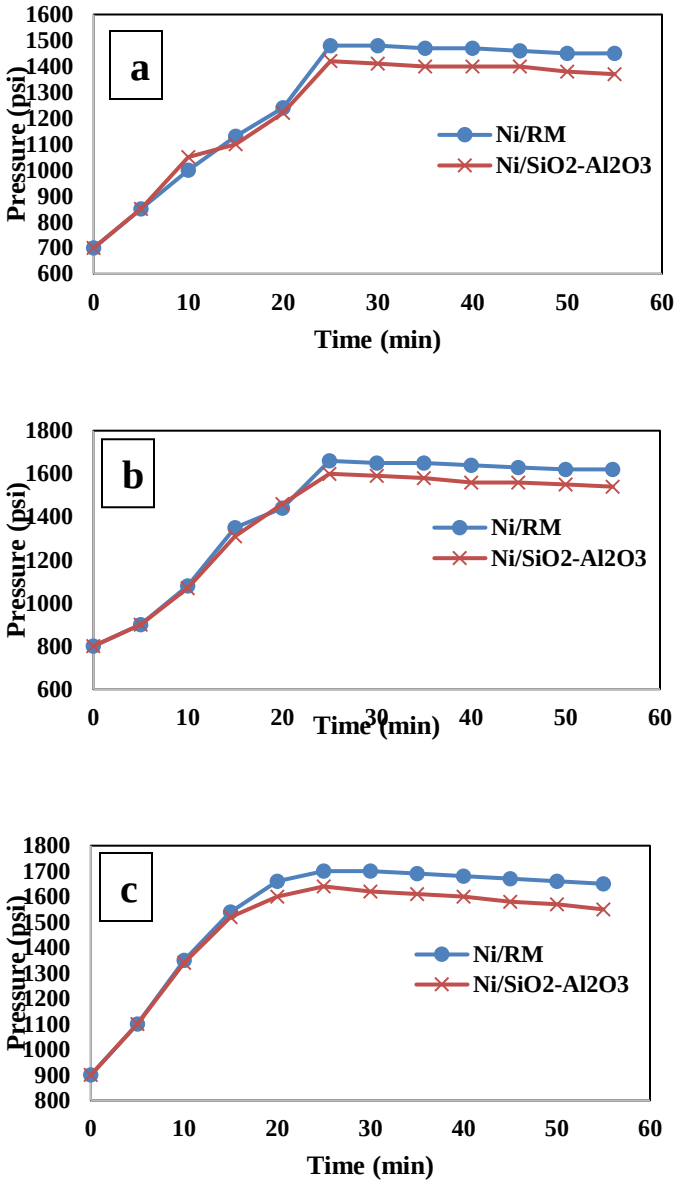

Fig. B. 6: Pressure change during HDO of guaiacol at initial H_2 pressures of a) 4.83 MPa (700 psi), b) 5.52 MPa (800 psi), and c) 6.21 MPa (900 psi).

Table B. 1: Effect of RM support on guaiacol HDO (the reaction temperature and H_2 initial pressure were 400 °C and 900 psi respectively).

Conv. (%)	H_2 Consumption (mol H_2/kg guaiacol)	**Yield (wt. %)**			
		Organic	Aqueous	Gas	Coke
2.7	0.03	75.4	0	4.7	18.3
Liquid product analysis (wt. %)					
Guaiacol		Benzene	Phenol	Anisole	Others
96.3		1.4	1.2	1.1	0
Gas product analysis (mol %)					
CO		CO_2	CH_4	C_2-C_5	
46.3		33.1	19.7	0	

Appendix C: Supplementary data for Chapter 5

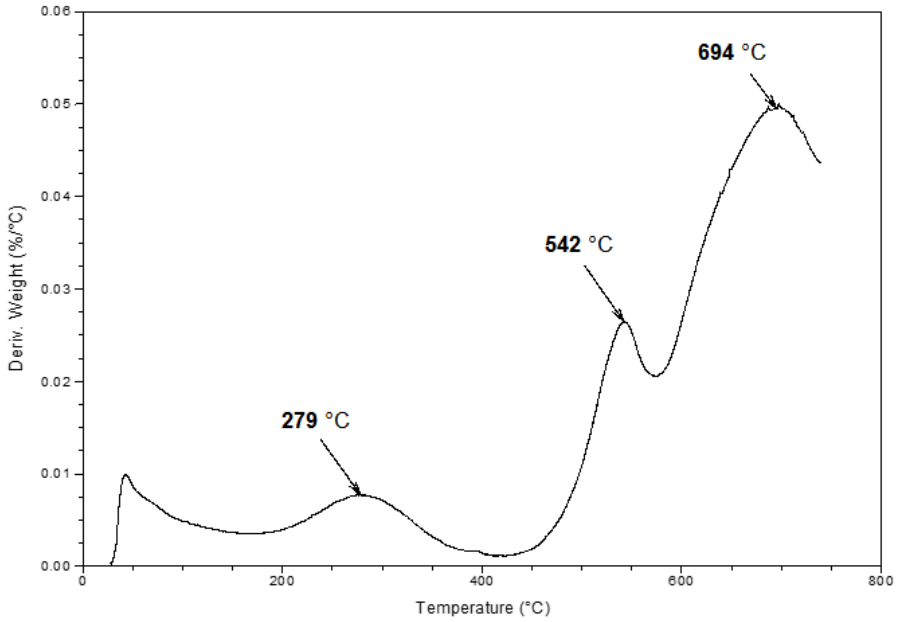

Fig. C. 1: TG-TPR profile of red mud.

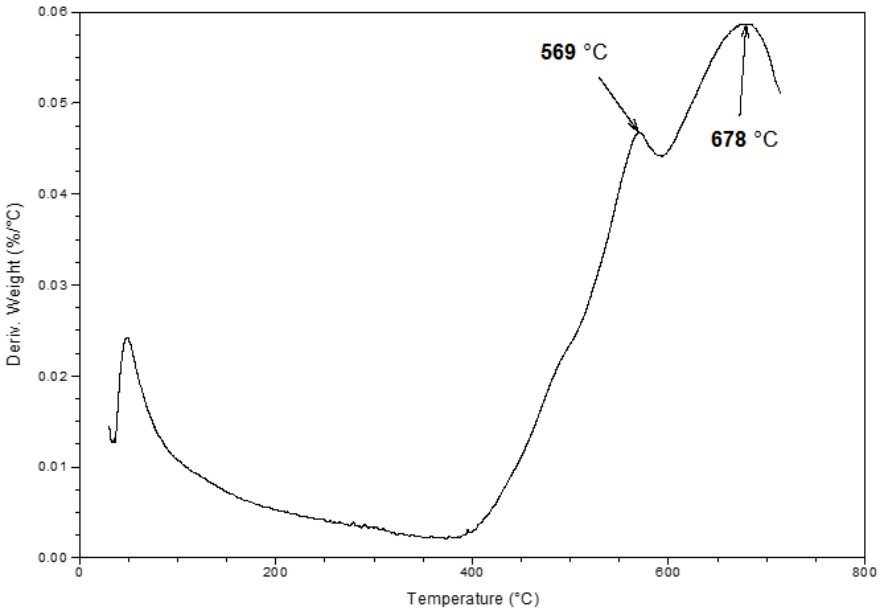

Fig. C. 2: TG-TPR profile of 10%Ni/RM.

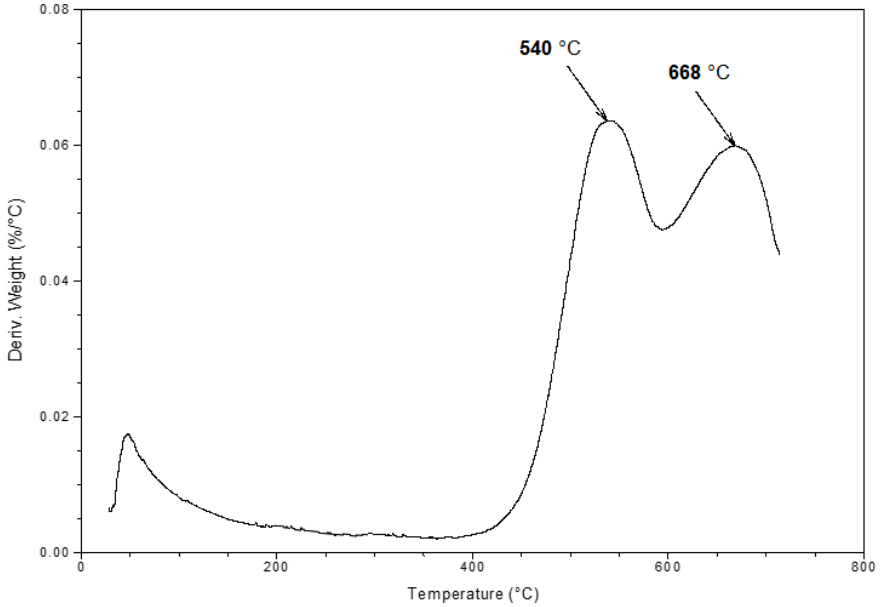

Fig. C. 3: TG-TPR profile of 20%Ni/RM.

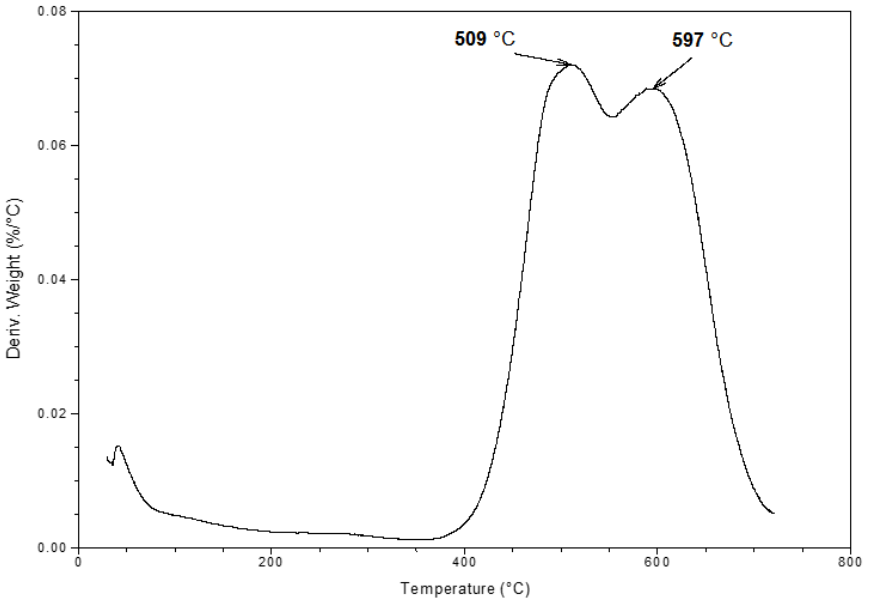

Fig. C. 4: TG-TPR profile of 30%Ni/RM.

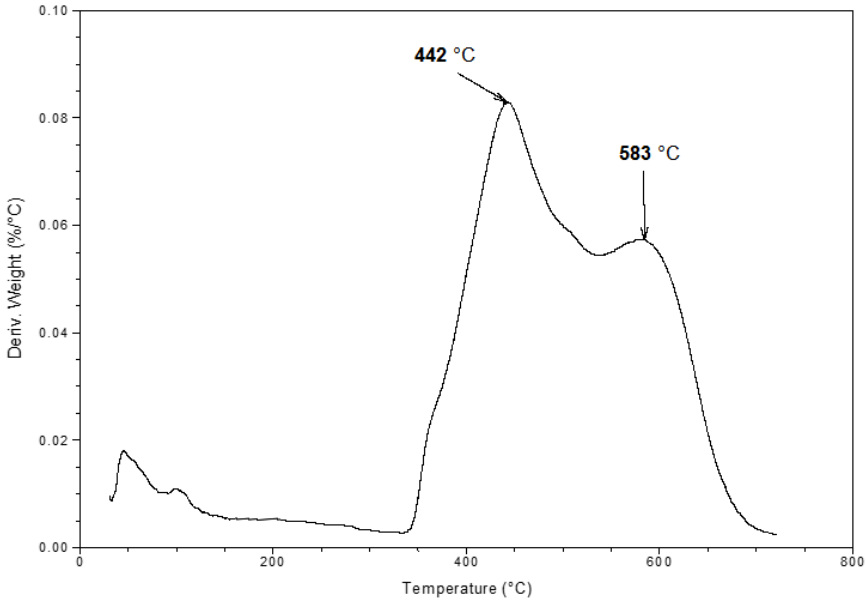

Fig. C. 5: TG-TPR profile of 40%Ni/RM.

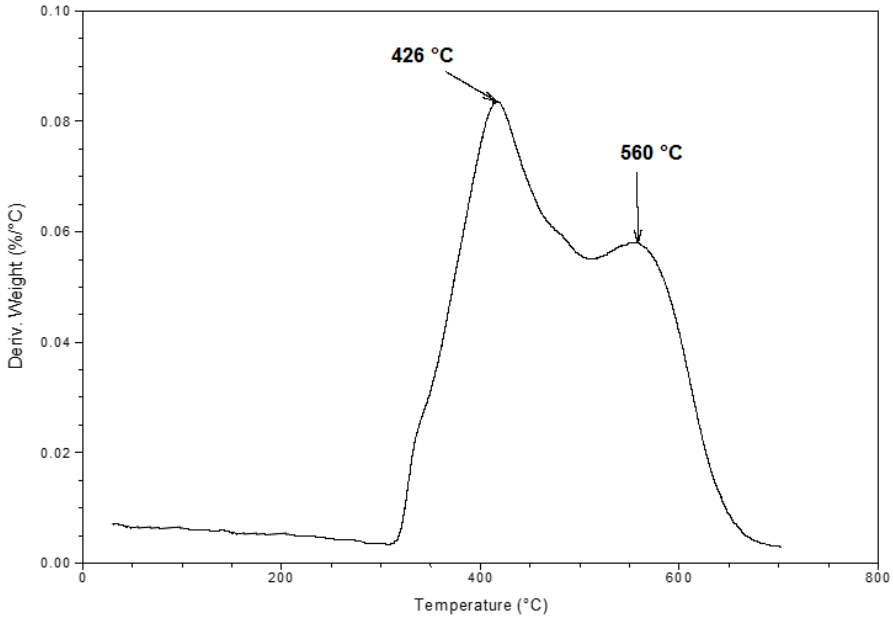

Fig. C. 6: TG-TPR profile of 50%Ni/RM.

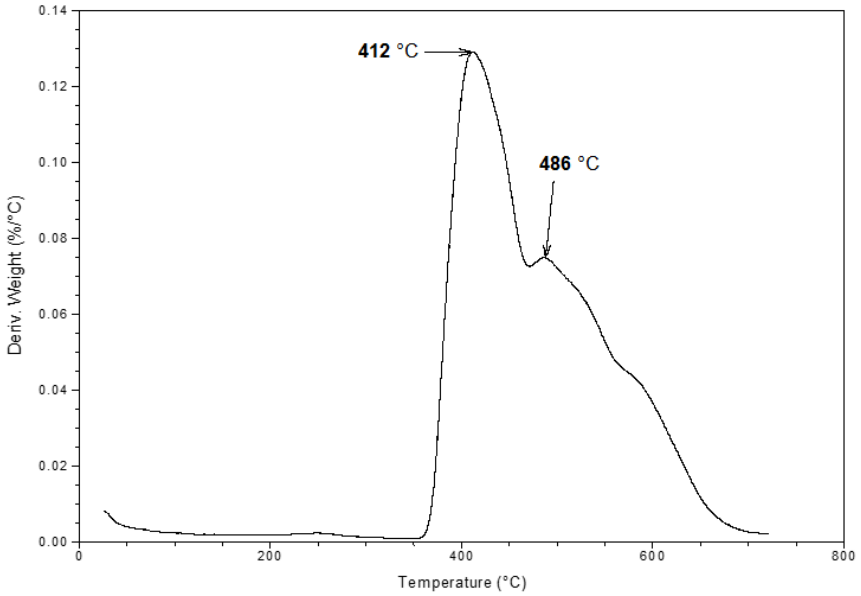

Fig. C. 7: TG-TPR profile of 65%Ni/RM.

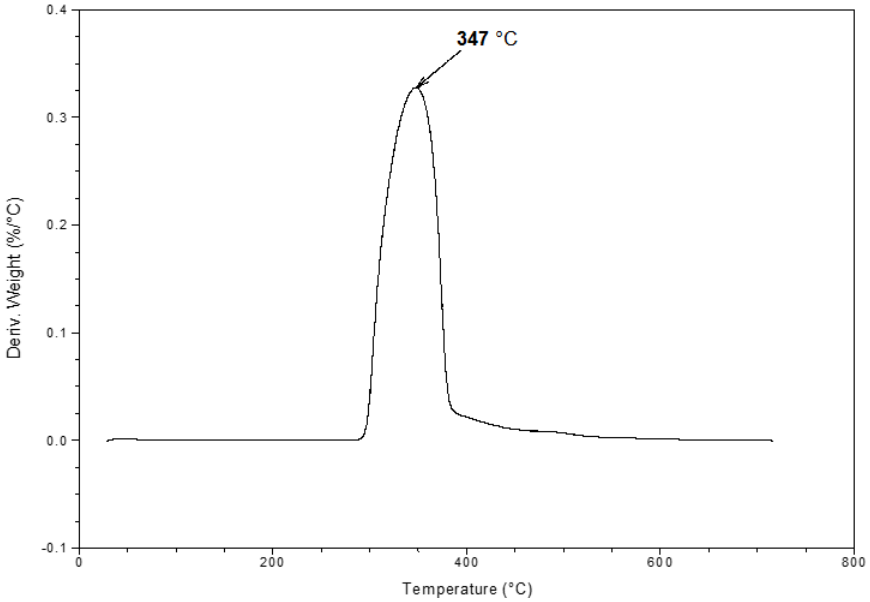

Fig. C. 8: TG-TPR profile of nickel oxide.

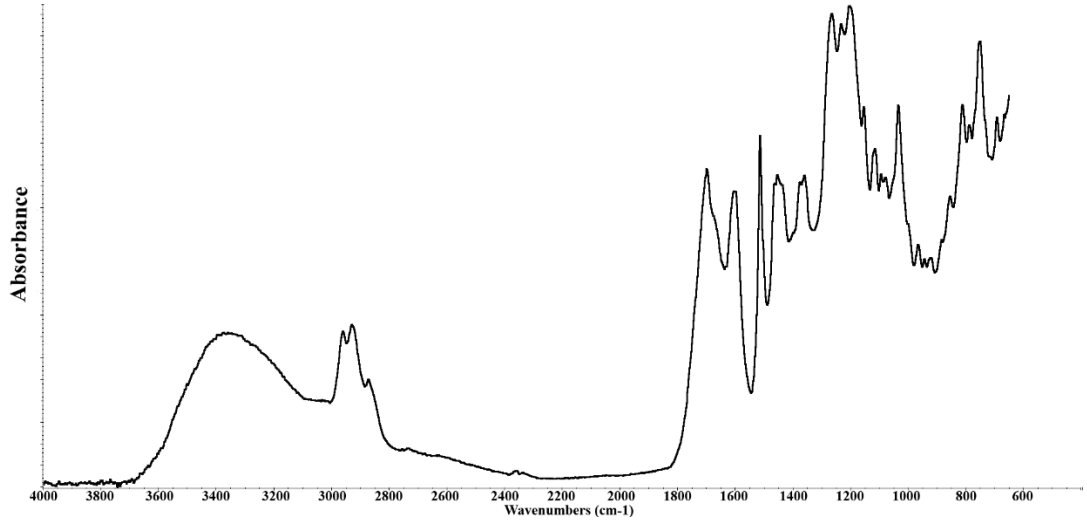

Fig. C. 9: FTIR spectrum of raw bio oil.

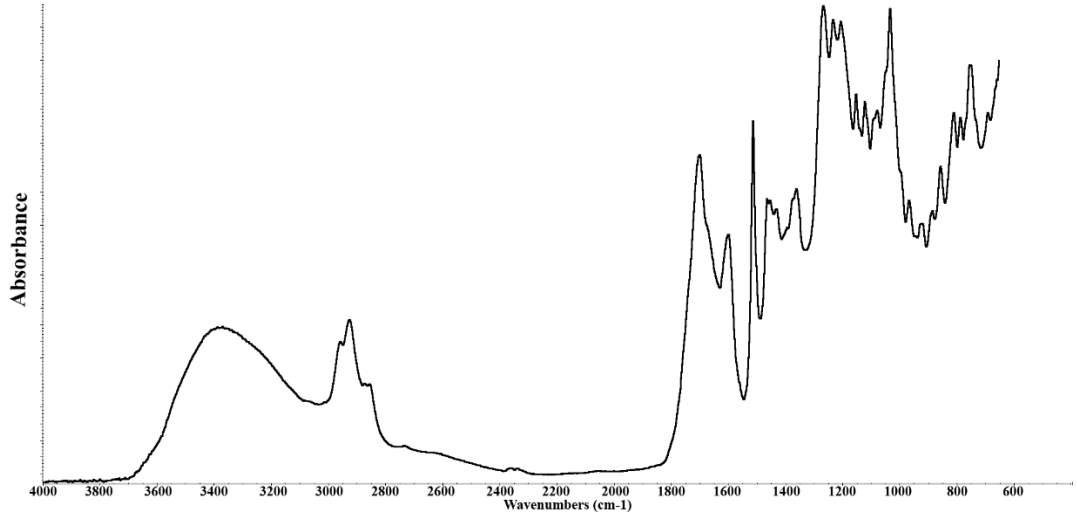

Fig. C. 10: FTIR spectrum of HDO oil using RM catalyst.

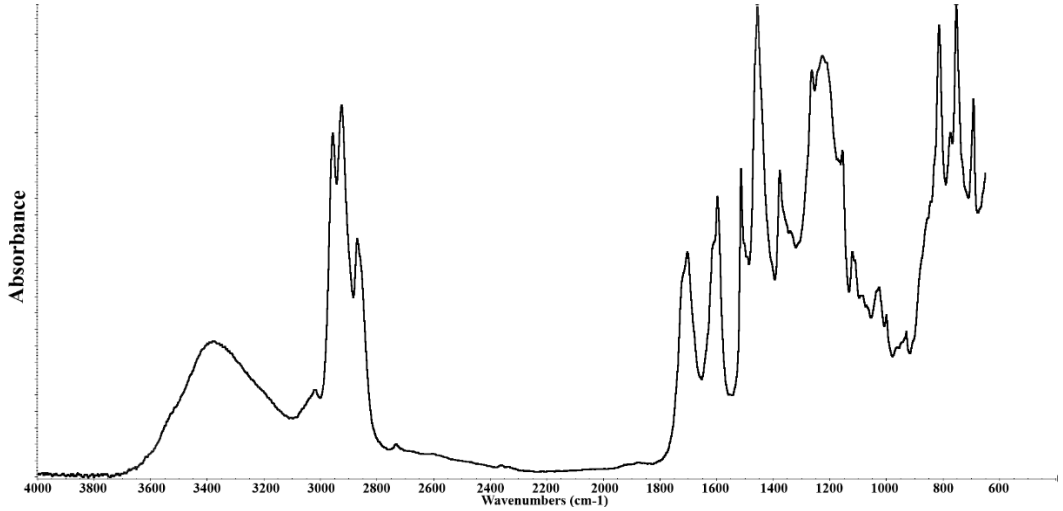

Fig. C. 11: FTIR spectrum of HDO oil using 10%Ni/RM catalyst.

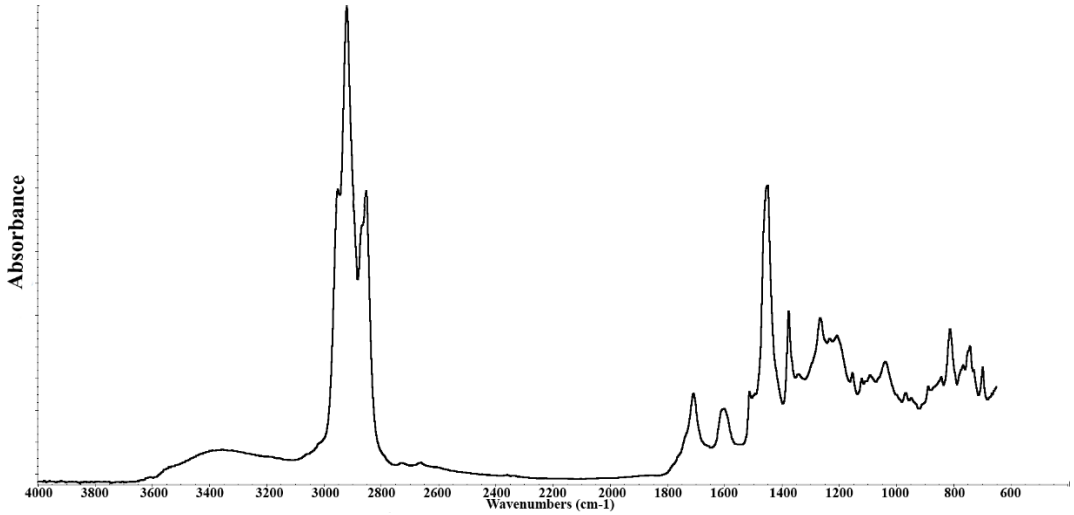

Fig. C. 12: FTIR spectrum of HDO oil using 20%Ni/RM catalyst.

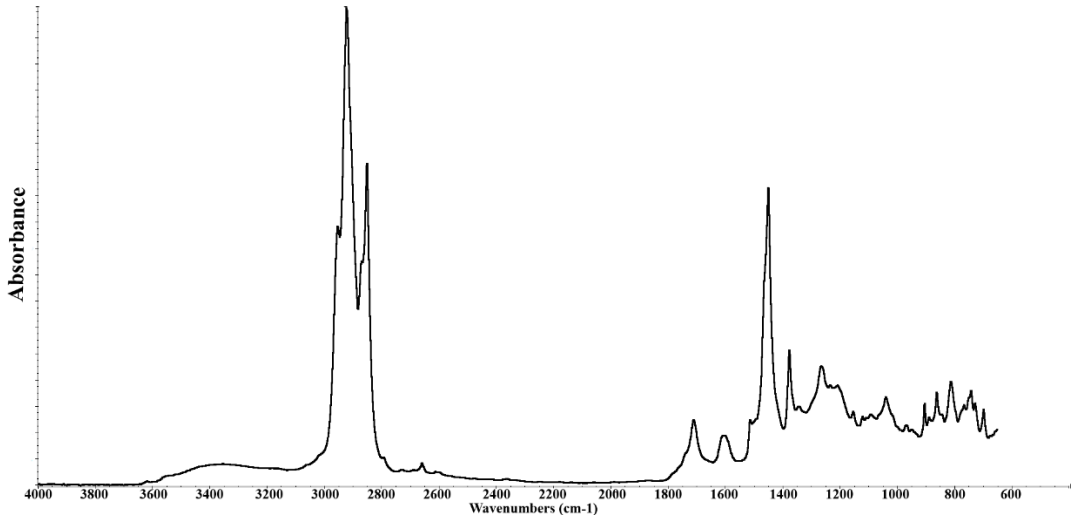

Fig. C. 13: FTIR spectrum of HDO oil using 30%Ni/RM catalyst.

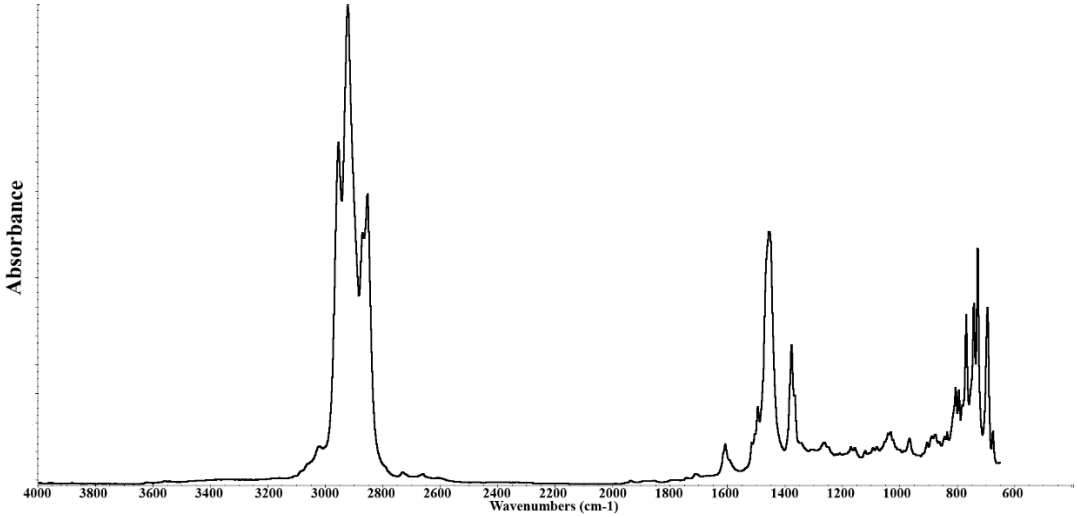

Fig. C. 14: FTIR spectrum of HDO oil using 40%Ni/RM catalyst.

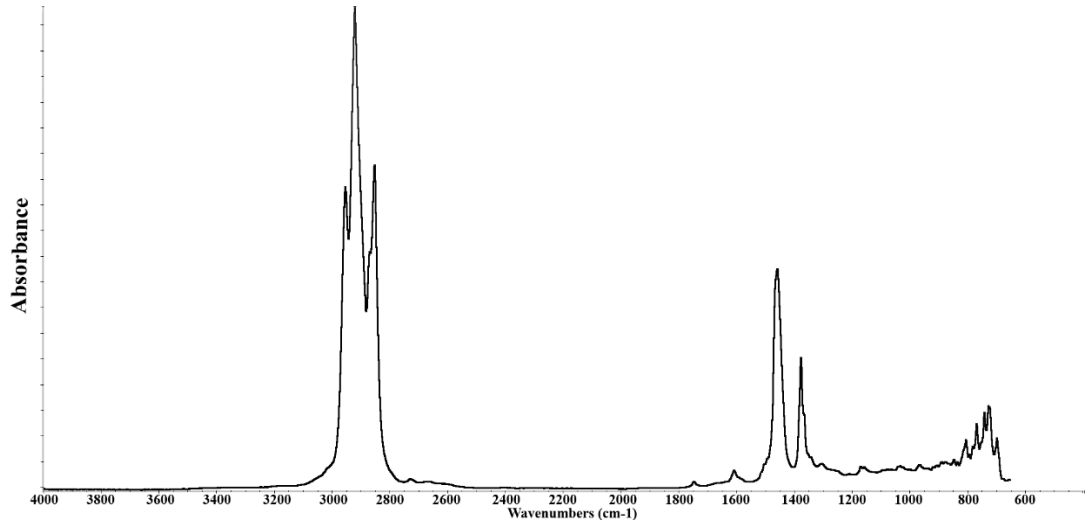

Fig. C. 15: FTIR spectrum of HDO oil using 50%Ni/RM catalyst.

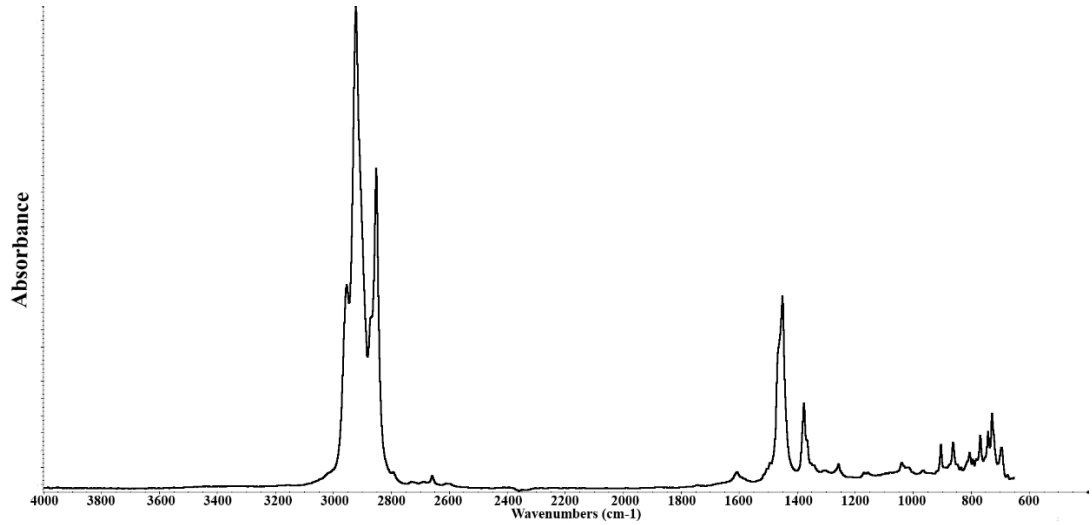

Fig. C. 16: FTIR spectrum of HDO oil using 65%Ni/RM catalyst.

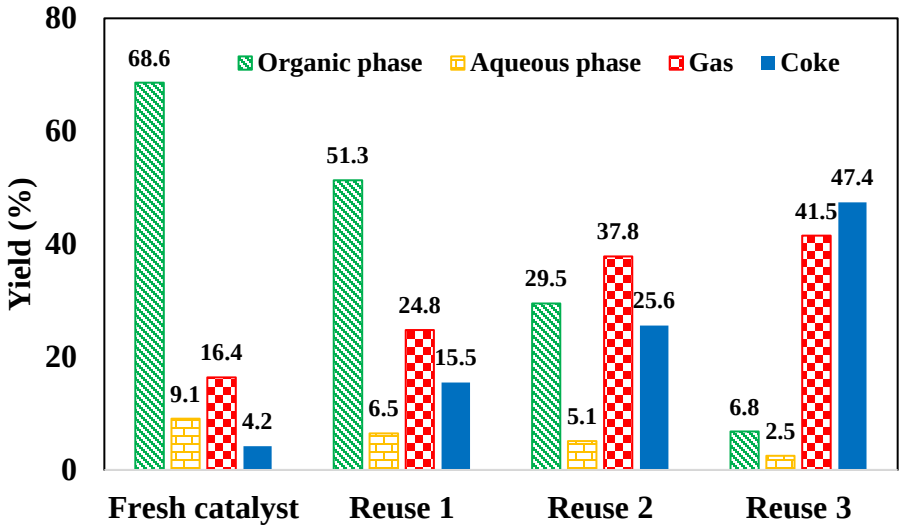

Fig. C. 17: Product yields distribution of HDO experiments reusing 40%Ni/RM catalyst consecutively without regeneration and reduction between runs.

Table C. 1: H_2 consumption, physicochemical properties of the liquid products, and gas product composition for consecutive reusing of 40%Ni/RM catalyst without regeneration and reduction between runs.

Properties	Fresh catalyst	Reuse #	Reuse # 2	Reuse # 3
H_2 consumption (mol/g bio-oil)	0.053	0.037	0.016	0.004
Aqueous phase				
Water content (wt. %)	99.45	90.55	84.15	72.45
pH	6.91	5.63	5.11	4.32
HDO oil (organic phase)				
Elemental composition (dry basis) (wt. %)				
N	0.31	0.36	0.41	0.43
C	82.52	79.45	70.18	68.83
H	15.82	12.48	9.42	8.12
O	1.35	7.71	19.99	22.62
HHV (MJ/kg)	45.77	42.35	35.61	29.46
pH	NA	5.16	4.37	4.05
Water content (wt. %)	<DL	1.56	2.63	3.11
Density (g/ml)	0.79	0.81	0.94	1.09
Dynamic viscosity (cP)	1.37	33.61	57.45	87.42
Gas composition (mole %)				
CO	3.32	5.45	8.65	11.34
CO_2	5.52	6.75	12.56	15.12
CH_4	67.34	62.75	53.38	46.68
C_2H_4	8.26	7.43	6.71	5.51
C_3H_8	7.56	7.88	8.56	9.28
C_4H_{10}	5.45	5.78	6.56	7.02
C_5H_{12}	2.47	2.76	3.15	3.81

Appendix D: Copyright permissions

Chapter 3:

Chapter 4:

Chapter 5:

CURRUCULUM VITAE

Education

- ✓ **PhD candidate, Biological Engineering**
  Utah State University, USA (2014-2018)
  Dissertation: *Hydrodeoxygenation of pinyon-juniper catalytic pyrolysis oil*

- ✓ **M.Sc., Environmental Engineering**
  Shahid Bahonar University of Kerman, Kerman, Iran (2010-2013)
  Thesis: *Investigation of the aerobic biodegradation kinetic of asphaltenes using microorganisms and comparison between biodegradability kinetic of these compounds under static and shaking conditions*

- ✓ **B.Sc., Chemical Engineering**
  Shiraz University, Shiraz, Iran (2005-2010)
  Senior project: *Experimental investigation of asphaltene precipitation on various surfaces*

Invention disclosures

- ✓ **Title:** Production of hydrogenation/hydrodeoxygenation catalyst from red mud.
  Invention ID: D18013
  Inventors: Hossein Jahromi, Foster A. Agblevor

- ✓ **Title:** Aqueous phase production of long chain hydrocarbons from low molecular weight oxygenates.
  Invention ID: D18050
  Inventors: Hossein Jahromi, Foster A. Agblevor

- ✓ **Title:** Aqueous phase synthesis of hydrocarbons from biomass oxygenates.
  Invention ID: D18051
  Inventors: Hossein Jahromi, Foster A. Agblevor

Publications

- ✓ **H. Jahromi**, F. A. Agblevor. "Hydrodeoxygenation of pinyon-juniper catalytic pyrolysis oil using red mud-supported nickel catalysts". Applied Catalysis B: Environmental. 236 (2018) 1-12.

- ✓ **H. Jahromi**, F. A. Agblevor. "Hydrodeoxygenation of guaiacol: A comparative study of red mud-supported nickel and commercial Ni/SiO_2-Al_2O_3 catalysts". Applied Catalysis A: General 558 (2018) 109-121.

- ✓ **H. Jahromi**, F. A. Agblevor. "Upgrading of pinyon-juniper catalytic pyrolysis oil via hydrodeoxygenation". Energy 141 (2017) 2186-2195.

- ✓ F. A. Agblevor, **H. Jahromi**. "Aqueous phase synthesis of hydrocarbons from furfural reactions with low molecular weight biomass oxygenates". Energy & Fuels. 32 (**2018)** 8552-8562.

- ✓ **H. Jahromi**, F. A. Agblevor. "Hydrodeoxygenation of aqueous phase catalytic pyrolysis oil to liquid hydrocarbons using multi-functional nickel catalyst". Industrial & Engineering Chemistry Research. 57 (**2018**) 13257-13268.

- ✓ F. A. Agblevor, **H. Jahromi**. "Aqueous phase synthesis of hydrocarbons from reactions of guaiacol and low molecular weight oxygenates". ChemCatChem. **2018**. ***Accepted manuscript***.

- ✓ **H. Jahromi**, M. H. Fazaelipoor, Sh. Ayatollahi, A. Niazi. "Asphaltene biodegradation under shaking and static conditions" Fuel 117(2014) 230-235.

Conference presentations

- ✓ **H. Jahromi**, F. A. Agblevor. "Hydrodeoxygenation of acetic acid as a model compound for aqueous phase pinyon juniper catalytic pyrolysis oil". Oral presentation. AIChE annual meeting. October 29 - November 3, 2017.

- ✓ **H. Jahromi**, F. A. Agblevor. "Hydrodeoxygenation of Pinyon Juniper catalytic pyrolysis oil to hydrocarbon fuels". Oral presentation. AIChE annual meeting. November 17, 2016.

- ✓ F. Agblevor, SH Beis, O. Hietsoi, **H. Jahromi**, G. Smith. "Temperature effect on Red Mud catalytic pyrolysis of various biomass species and hydrotreatment of oils". Poster presentation. TCBiomass 2017, the international conference on thermochemical conversion science. September 19-21, 2017.

- ✓ **H. Jahromi**, M. H. Fazaelipoor, Sh. Ayatollahi, S. Roozbahani. "Asphaltene biodegradation using a type of *Enterobacter* isolated from heavy crude oil". The first international conference of oil, gas, petrochemical and power plant, Tehran, Iran (July 2012).

- ✓ J. Sayyad Amin, Sh. Ayatollahi, A. Alamdari, M. Escrochi, **H. Jahromi**, and E. Nikooee, ." Bi- fractal dimension description- Inferring topography alteration of an asphaltene deposited heterogeneous surface". The 6th International Chemical Engineering Congress & Exhibition (IChEC 2009), Kish Island, Iran, (2009)

- ✓ E.Nikooee, J. Sayyad Amin, Sh. Ayatollahi, A. Alamdari, **H. Jahromi**, M. Escrochi, ."Fractal analysis of surface roughness induced by asphaltene deposits: Effect of surface topography on wettability alteration", 1st International Petroleum Conference & Exhibition Session(EAGE Conference), May 2009.